Inaugural dissertation
for
obtaining the doctoral degree
of the
Combined Faculty of Mathematics, Engineering and Natural Sciences
of the Ruprecht-Karls-University
Heidelberg

presented by
Agnieszka Seretny, M.Sc.
born in: Kraków, Poland
oral examination: June 7th 2024

From genotype to phenotype:
how *IDH1* mutations alter the landscape of intrahepatic cholangiocarcinoma

Referees:
Prof. Dr. Peter Angel
Prof. Dr. Darjus Felix Tschaharganeh

Dla Mamy

Abstract

The prognosis for intrahepatic cholangiocarcinoma (iCCA), a complex and aggressive form of primary liver cancer, is challenging due to factors such as advanced stage at diagnosis and a diverse genetic landscape. This complexity highlights the necessity of exploring and understanding the nuances of genetic mutations specific to iCCA and their potential as therapeutic targets.

Gain-of-function mutations in *Isocitrate dehydrogenase 1* (*IDH1*), leading to the production of the oncometabolite 2-hydroxyglutarate (2-HG), are particularly noteworthy in iCCA, where such mutations are common. IDH1, a key enzyme in the citric acid cycle catalyzing the oxidative decarboxylation of isocitrate to α-ketoglutarate, becomes a critical focus due to its altered role in iCCA. The detrimental effects of mutant IDH1 stem from its aberrant production of 2-HG, which competitively inhibits α-ketoglutarate-dependent oxygenases, thus affecting various biological processes including DNA and histone demethylation, hypoxic response, and collagen maturation, contributing significantly to tumorigenesis by altering epigenetic and cellular signaling pathways.

To understand the role of IDH1 in iCCA and the implications of 2-HG, a tailored mouse model was employed, using hydrodynamic tail vein injection, which allowed for the direct introduction of genetic elements into the liver. The study shows that *IDH1* mutations, in combination with other oncogenic events, significantly reduce the survival of tumor-bearing mice. The accumulation of 2-HG in tumors leads to enhanced methylation, a shift in tumor phenotype towards cholangiocytic characteristics, and changes in stromal cell infiltration. Through mass spectrometry of iCCA extracellular matrix, key elements of the 2-HG-driven phenotype were identified. This research provided extensive insights into the molecular and cellular effects of *IDH1* mutations in iCCA, revealing their impact on glycosylation, liver cell differentiation, and tumor traits.

A distinct aspect of this thesis was the investigation of immune and extracellular matrix dynamics in the context of 2-HG accumulation. This exploration highlighted the intricate relationship between immune cell infiltration, immune modulation, and *IDH1* mutations, enhancing understanding of the tumor microenvironment in iCCA. Additionally, the study introduced alternative murine iCCA models and mimicked patient-specific genomic patterns, enriching the research spectrum. A significant breakthrough was the identification of a novel immunogenic peptide, targeting IDH1 mutant cholangiocarcinoma cells, paving the way for mutation-specific immunotherapy.

In conclusion, this thesis demonstrates the critical role of mutant IDH1 in modulating the tumor microenvironment and cell differentiation in iCCA. It significantly advances our knowledge of iCCA pathology and lays the groundwork for innovative, targeted treatment strategies and personalized medicine.

Zusammenfassung

Die Prognose für intrahepatische Cholangiokarzinome (iCCA), eine komplexe und aggressive Form von Leberkrebs, stellt aufgrund von Faktoren wie einem fortgeschrittenen Stadium bei der Diagnose und einer diversen genetischen Landschaft eine Herausforderung dar. Diese Komplexität zeigt die Notwendigkeit, die Nuancen von genetischen Mutationen, die spezifisch für iCCA sind, zu erforschen und zu verstehen, sowie ihr Potenzial für therapeutische Zwecke zu nutzen.

Mutationen, die eine Funktionszunahme in Isocitrat-Dehydrogenase 1 (IDH1) verursachen und zur Produktion des Onkometaboliten 2-Hydroxyglutarat (2-HG) führen, sind bei iCCA besonders auffällig. IDH1 ist ein Schlüsselenzym im Zitronensäurezyklus, das die oxidative Decarboxylierung von Isocitrat zu α-Ketoglutarat katalysiert. Aufgrund seiner veränderten Rolle in iCCA wird IDH1 zu einem wichtigen Faktor. Die schädlichen Effekte von mutiertem IDH1 ergeben sich durch seine fehlerhafte Produktion von 2-HG, welches kompetitiv α-Ketoglutarat-abhängige Oxygenasen hemmt. Somit werden verschiedene biologische Prozesse, einschließlich DNA- und Histondemethylierung, sowie auch hypoxische Antwort und Kollagenreifung, beeinflusst. Dies trägt erheblich zur Tumorigenese bei, indem es epigenetische und zelluläre Signalwege verändert.

Um die Rolle von IDH1 in iCCA und die Implikationen von 2-HG zu verstehen, wurde ein maßgeschneidertes Mausmodell verwendet, das durch hydrodynamische Schwanzveneninjektion direkte genetische Veränderungen in die Leber ermöglicht einzuführen. Die Forschung zeigt, dass die IDH1-Mutationen in Kombination mit anderen onkogenen Ereignissen die Überlebensrate von tumorbelasteten Mäusen signifikant reduziert. Die Anhäufung von 2-HG in Tumoren führt zu verstärkter Methylierung, einer Verschiebung des Tumorphänotyps in Richtung cholangiozytischer Merkmale und auch Veränderungen in der Infiltration von Stromazellen. Durch Massenspektrometrie der extrazellulären Matrix von iCCA wurden Schlüsselelemente des durch 2-HG veränderten Phänotyps identifiziert. Diese Forschung lieferte umfassende Einblicke in die molekularen und zellulären Effekte von IDH1-Mutationen in iCCA und zeigte ihre Auswirkungen auf Glykosylierung, Leberzelldifferenzierung und Tumorcharakteristika.

Ein Schwerpunkt dieser Arbeit war die Untersuchung der Dynamik des Immunsystems und der extrazellulären Matrix im Kontext der 2-HG-Anhäufung. Diese hob die komplexe Beziehung zwischen Immunzellinfiltration, Immunmodulation und IDH1-Mutationen hervor und verbesserte das Verständnis der Tumormikroumgebung in iCCA. Darüber hinaus wurden durch alternative iCCA-Mausmodelle und imitierte patientenspezifische genomische Muster der Forschungsspektrum erweitert. Ein signifikanter Durchbruch war die Identifizierung eines neuartigen immunogenen Peptids, das auf IDH1-mutierte Cholangiokarzinomzellen abzielt und den Weg für eine mutationspezifische Immuntherapie ebnet.

Zusammenfassend zeigt diese Arbeit die wichtige Rolle von mutiertem IDH1 bei der Regulierung der Tumormikroumgebung und der Zelldifferenzierung in iCCA. Sie erweitert unser Wissen über die Pathologie von iCCA erheblich und legt den Grundstein für innovative, zielgerichtete Behandlungsstrategien und personalisierte Medizin.

Table of contents

List of figures

List of tables

List of abbreviations

abbreviation	full meaning
2-HG	2-hydroxyglutarate
AHCYL1	Adenosylhomocysteinase hydrolase-like protein 1
AML	acute myeloid leukemia
ABC	ammonium bicarbonate
ACTB	Actin beta
ALP	alkaline phosphatase
ARID1A	AT-rich interactive domain-containing protein 1A
BAP1	BRCA1 associated protein-1
BCA	bicinchoninic acid assay
bp	base pair
BSA	bovine serum albumin
CAFs	cancer-associated fibroblasts
Cas9	CRISPR-associated protein 9
CCA	cholangiocarcinoma
CCL17	C-C motif chemokine ligand 17
CD	Cluster of differentiation
CMCP	Center for Model Systems and Comparative Pathology Heidelberg
CMV	human cytomegalovirus immediate-early enhancer and promoter
CRISPR	Clustered regularly interspaced short palindromic repeats
cDNA	complementary DNA
DAB	3,3′-diaminobenzidine
ddH2O	double-distilled water
ddNTP	dideoxynucleotide
DES	Desmin
DKFZ	Deutsches Krebsforschungszentrum, eng. German Cancer Research Center
DMMB	1,9-dimethylmethylene blue
DMEM	Double modified Eagle's medium
DMSO	dimethyl sulfoxide
DNA	deoxyribonucleic acid
DNP	2,4-dinitrophenol
DMR	differentially methylated region
dNTP	deoxynucleotide
DTT	dithiothreitol

eCCA	extrahepatic CCA
EF1a	Elongation factor 1-alpha 1
EDTA	ethylenediaminetetraacetic acid
ECM	extracellular matrix
et al.	et alia, and others
EtOH	ethanol
EV	empty vector
FBS	fetal bovine serum
FGFR	Fibroblast growth factor receptors
FOXP3	Forkhead box P3
GAGs	glycosaminoglycans
G-CSF	Granulocyte colony-stimulating factor
GEMMs	genetically engineered mouse models
GFP	Green fluorescent protein
GM-CSF	Granulocyte-macrophage colony-stimulating factor
Gnd-HCl	guanidine hydrochloride
H3	histone H3
H3K27me3	tri-methylation of lysine 27 on histone H3
H3K9me3	tri-methylation of lysine 9 on histone H3
H&E	haematoxylin and eosin stain
HCC	hepatocellular carcinoma
HES1	Hairy and enhancer of split-1
HIF	Hypoxia-inducible factor
HRP	horseradish peroxidase
HS-GAGs	heparan sulfate-GAGs
HSCs	hepatic stellate cells
HTVi	hydrodynamic tail vein injection
IDH1/IDH2	Isocitrate dehydrogenase 1/2
IFN-γ	Interferon-γ
IHC	immunohistochemistry
IL	Interleukin
IPA	Ingenuity Pathway Analysis
IRES	Internal ribosomal entry site
ITGAV	Integrin alpha V
ITGB5	Integrin subunit beta 5
KRT19	Cytokeratin 19
LFQ	label free quantification

LY6G	Lymphocyte antigen 6 complex locus G6D
MHC	Major histocompatibility complex
mMCP-counter	Microenvironment Cell Populations-counter
MOG	Myelin oligodendrocyte glycoprotein
mRNA	messenger RNA
MS	mass spectrometry
myr-Akt	myristoylated Akt
NEB	New England Biolabs
NETs	neutrophil extracellular traps
NICD	Notch intracellular domain
OS	overall survival
PCA	principal component analysis
PCR	polymerase chain reaction
PDGFR-α	Platelet-derived growth factor receptor alpha
PEI	polyethylenimine
PFS	progression-free survival
PBS	phosphate-buffered saline
PDX	patient-derived xenografts
PMA	phorbol myristate acetate
PTEN	Phosphatase and tensin homolog
phospho-H2A.X	phospho-histone H2A.X
phospho-H3	phospho-histone H3
RNA	ribonucleic acid
RNA-seq	RNA sequencing
RT	room temperature
Rosa26	Reverse Oriented Splice Acceptor, Clone 26
RPA3	Replication protein A3
SB	Sleeping Beauty
SDS	sodium dodecyl sulfate
SDS-PAGE	sodium dodecyl sulfate polyacrylamide gel electrophoresis
SMAD4	SMAD family member 4
SOX9	SRY-box transcription factor 9
sGAGs	sulfated glycosaminoglycans
sgRNA	single guide RNA
TET	Ten-eleven translocation
TBST	Tris-buffered saline with Tween20
TNS3	Tensin 3

Tm	melting temperature
TME	tumor microenvironment
TP53	Tumor protein P53
Tregs	T regulatory cells
TSS	transcription start sites
v/v	volume/volume
qPCR	quantitative reverse transcription PCR
WB	Western blot
WT	wild-type
w/v	weight/volume
α-KG	alpha-ketoglutarate
α-SMA	Alpha-smooth muscle actin

1. Introduction

1.1. Liver anatomy and function

The liver holds a paramount position in the human body, functioning as the largest internal organ and playing a crucial role in various physiological processes [1], [2], [3]. Its distinctive reddish-brown color and lobulated structure are easily recognizable. However, the liver's pivotal role extends far beyond its physical attributes. Its importance to human health and life is underscored by its multifaceted functions in digestion [4], metabolism [6], [7], immunity [7], [8], detoxification [9], [10], and regulation of numerous biochemical reactions [11].

Histologically, the liver is composed of hepatocytes - the primary parenchymal liver cell type - which contribute to approximately 80% of the organ's mass [12]. These cells are responsible for most of the liver's metabolic activities [13], [14], including metabolism of lipids [15], [16], carbohydrates [17], and proteins [18], [19], [20]. Hepatocytes also play an essential role in the production and excretion of bile, aiding in digestion and absorption of dietary fats [21], [22].

The second parenchymal cell type in the liver is cholangiocytes, which are epithelial cells lining the biliary tract, and they play essential roles in bile formation [21], [22]. Initially, hepatocytes have been recognized as the primary parenchymal cells of the liver. However, recognizing cholangiocytes as parenchymal cells is significant because it underscores their pivotal role in maintaining liver health and function. Cholangiocytes have unique properties that distinguish them from other liver cell types and can undergo transdifferentiation into hepatocyte-like cells under certain conditions [23], [24].

In the dynamic landscape of liver cell plasticity, both hepatocytes and cholangiocytes display exceptional adaptability, playing pivotal roles in liver function and regeneration. Hepatocytes not only transdifferentiate into cholangiocytes but also into other cell types when faced with liver injury, highlighting their versatility and resilience [25], [26], [27]. Similarly, cholangiocytes are capable of transdifferentiating into hepatocyte-like cells, further underscoring their significance in the liver's regenerative processes [28]. This bidirectional plasticity is vital in maintaining liver homeostasis and in response to damage, offering promising therapeutic potentials for liver diseases [29].

The liver's intricate cellular landscape extends beyond its non-parenchymal cells like Kupffer cells, stellate cells, and endothelial cells, to include a host of immune cells that play crucial roles in its defense mechanisms [7], [30], [31], [32], [33], [34]. Neutrophils, for instance, are rapidly mobilized to the liver in response to infection or injury, where they engage in the elimination of pathogens and contribute to tissue repair processes [35], [36], [37]. Meanwhile, T cells within the liver, are integral to the organ's immune surveillance and tolerance. They not only mediate responses to viral infections and tumors but also help in dampening excessive inflammation to prevent chronic liver diseases [36], [38], [39], [40]. These immune cells,

alongside the detoxification and immune functions primarily orchestrated by Kupffer cells, collectively fortify the liver's capability to protect the body from harmful substances and manage the immune response to inflammation or injury [13], [14], [41].

Liver can regenerate after surgical resection or chemical injury, underscoring its resilience and indispensability [42], [43]. However, the liver's crucial roles also render it vulnerable to a range of diseases, including viral hepatitis, liver cirrhosis, and liver cancer [31], [44], [45], [46]. Consequently, understanding the liver's physiology and pathology is critical in mitigating these health threats. Therefore, a comprehensive understanding of liver physiology and pathology is imperative for mitigating these health challenges.

In conclusion, the liver's complexity, significance, and vast array of functions underscore its paramount importance in the human body, necessitating ongoing scientific exploration to enhance human health and address liver-associated diseases.

1.2. Model systems in liver research

The advancement in understanding the pathogenesis of liver cancer and the development of novel therapeutic strategies hinge significantly on the utilization of robust and representative tumor models. These models serve as indispensable tools that can simulate the disease in a controlled environment, allowing for mechanistic studies, drug testing, and the development of therapeutic strategies.

The *in vitro* models, including liver cell lines and organoids derived from different liver diseases, provide a foundational step in investigating the biological behavior of liver diseases [37], [47], [48]. These models have been instrumental in identifying key molecular pathways involved in liver pathologies, including fibrosis, cirrhosis, and tumor formation [49], [50]. However, these cell lines often lack the heterogeneity seen in the diverse spectrum of liver diseases [47]. Recently, three-dimensional culture systems such as organoids have been developed, offering a more accurate representation of the liver tissue architecture and disease microenvironment [48], [51], [52].

Patient-derived xenografts (PDX) are another powerful tool for studying liver-associated diseases [53]. These involve the implantation of patient tumor tissues into immunodeficient mice, preserving the histological and genetic features of the original tumor [48], [54], [55]. PDX models are particularly useful for studying tumor heterogeneity and for preclinical testing of therapeutic strategies [53], [56], [57], [58].

Genetically engineered mouse models (GEMMs) of liver cancer are invaluable for studying the sequential events of liver-associated diseases [59], [60]. By manipulating the expression of genes involved in liver function and disease, GEMMs allow for the study of the role of specific genetic alterations in disease development [61], [62], [63], [64]. Additionally, these models can be exposed to various diets and pathogens to better understand the environmental and infectious contributors to liver diseases. Different dietary conditions, such as high-fat or alcohol-rich diets, can be introduced to mimic diseases like non-alcoholic fatty liver disease [65], [66] or alcoholic liver disease [66], [67], respectively. Likewise, pathogens

that affect liver function, such as the hepatitis C virus, can be introduced to study their impact and the body's immune response [68], [69]. However, GEMMs can be time-consuming and expensive to develop and maintain [70], [71].

Hydrodynamic tail vein injection (HTVi) is a unique and powerful tool for generating mouse models of liver cancer [72]. This technique enables the rapid introduction and expression of genetic material in the liver, allowing researchers to study the effects of specific genetic changes on liver function and disease progression [73], [74]. HTVi allows for the modeling of multiple genes at the same time [75], [76], and up to 40% of hepatocytes can take up DNA following injection [74], [77]. This provides a fast alternative to the development of GEMMs, and the heterogeneity introduced through HTVi closely mirrors that seen in liver diseases, providing a platform for studying the clonal evolution and genetic diversity of liver-associated diseases [49], [78]. However, it's important to note that while HTVi enables the study of tumor heterogeneity and the rapid introduction of genetic material, it does not recapitulate the gradual accumulation of genetic alterations seen in human liver diseases [79]. Despite this limitation, the HTVi method has greatly enhanced our ability to model liver-associated diseases cancer in mice, and concurrently, it has proven to be invaluable in deciphering the genetic intricacies and progression of liver cancers.

1.3. Overview of primary liver cancer

Primary liver cancers, notably hepatocellular carcinoma (HCC) and cholangiocarcinoma (CCA), pose significant public health challenges globally, significantly influencing morbidity and mortality rates [46]. Historically, it has been believed that primary liver malignancies stem directly from liver cells, with HCC originating from hepatocytes and CCA from cholangiocytes [80], [81]. Beyond these predominant types, there are less common forms of primary liver cancer such as fibrolamellar HCC, mixed HCC-CCA tumors, and hepatoblastoma, the latter being the main form of liver cancer in children [82].

The global burden of primary liver cancer is heavy, with it being the sixth most commonly diagnosed cancer and the fourth leading cause of cancer-related deaths worldwide [83], [84]. The incidence of these cancers varies widely across regions, with the highest rates in East and Southeast Asia, and Africa. This variation correlates closely with the prevalence of chronic hepatitis B infection, a major risk factor for HCC [46].

HCC and CCA, the primary forms of liver cancer, predominantly manifest in contexts of chronic liver disease and sustained inflammatory conditions. HCC, accounting for about 75% to 85% of cases, typically develops in settings of cirrhosis due to chronic hepatitis, alcohol abuse, or non-alcoholic steatohepatitis related to metabolic syndrome [31], [44], [46], [81], [85]. In parallel, CCA, making up approximately 10% to 15% of cases, often arises in similar environments of chronic liver inflammation, with additional risks stemming from specific conditions like primary sclerosing cholangitis, liver fluke infections, and certain hereditary liver disorders [22], [86], [87], [88], [89], [90].

Both cancer types, HCC and CCA, are not only linked to chronic liver inflammation and pathogen exposure but also to the remarkable plasticity and transdifferentiation abilities of liver cells. The cell of origin for these primary liver cancers can be either hepatocytes or cholangiocytes, which, due to their plasticity, have the potential to transdifferentiate, thus blurring the lines of cell-of-origin categorization [91], [92], [93]. This cellular adaptability, when combined with diverse genetic mutations, underscores the complexity of liver cancer pathogenesis. A deeper understanding of these processes is essential for the development of targeted interventions that address the underlying liver diseases and reduce the risk of these serious malignancies.

1.4. Deep dive into cholangiocarcinoma

1.4.1. Classification and characteristics

CCA is a particularly aggressive form of liver cancer [94] and the second most common primary liver cancer after HCC. Despite its relatively lower incidence compared to other liver cancer, CCA poses a considerable health burden [95], [96].

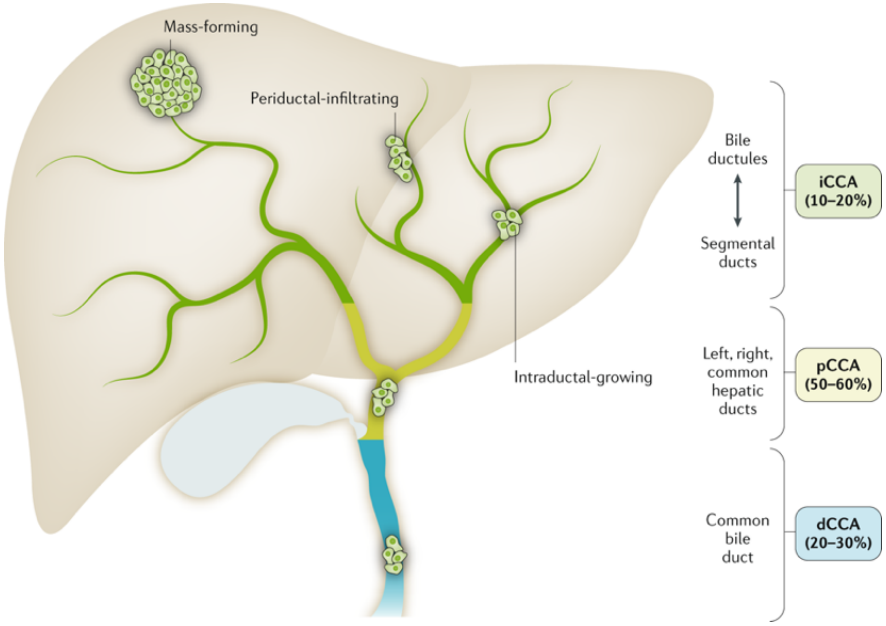

Figure 1. Anatomical classification of cholangiocarcinoma.
Unmodified from Banales et al. Nat. Rev. Gastroenterol. Hepatol. 2020 [96].

CCA can be further classified into intrahepatic (iCCA), perihilar (also known as hilar), and distal subtypes based on its anatomical site of origin within the biliary tree (**Figure 1**) [96]. Each subtype presents unique characteristics and clinical challenges [97]. Perihilar and distal CCAs, often collectively referred to as extrahepatic CCAs (eCCA), emerge from the bile ducts outside the liver [98]. In contrast, iCCA arises within the liver from small bile ducts and is categorized as a form of primary liver cancer [99].

Epidemiologically, the incidence of CCA has been increasing globally over the past few decades [100]. There are several recognized risk factors, including chronic biliary tract inflammation due to liver fluke infection (*O. viverrini* and *C. sinensis*) [97], primary sclerosing cholangitis [101], exposure to specific toxins [102], congenital biliary cystic diseases [103], and certain genetic aberrations [104], [105]. However, a considerable number of CCA cases occur in the absence of these risk factors [106], [107], indicating the involvement of other pathogenic elements. Interestingly, unlike eCCA, iCCA can develop in both cirrhotic and non-cirrhotic livers [105], [108].

Histopathologically, most CCAs are well to moderately differentiated adenocarcinomas with glandular morphology and often exhibiting a desmoplastic stromal reaction [109]. The tumors can display various growth patterns, including mass-forming, periductal infiltrating, and intraductal, each with different clinical and prognostic implications [96]. iCCA can present as a solitary mass, multifocal lesions, or a diffusely infiltrating disease, often accompanied by a fibrous stroma that contributes to the tumor's desmoplastic nature [110], [111], [112].

1.4.2. Clinical presentation and treatment options

From clinical perspective, CCA tends to be asymptomatic in its early stages [113], which contributes to its typically late diagnosis and poor prognosis [80]. When symptoms manifest, they often include non-specific complaints such as abdominal discomfort [114], and weight loss [115]. Jaundice, while more commonly associated with eCCA, may also present in iCCA, particularly when larger intrahepatic bile ducts are involved [116], [117].

Treatment options for CCA are largely dependent on the stage of the disease at diagnosis [90], [118], [119]. Surgical resection offers the best chance for cure in early-stage disease [109], [120]. However, given the often late-stage diagnosis, many patients are ineligible for surgery at presentation, necessitating alternative therapies such as chemotherapy, radiotherapy, and targeted therapies [121], [122], [123].

Exploration of molecular mechanisms in cholangiocarcinogenesis has advanced substantially in the past decade, bringing forth novel therapeutic targets and tailored treatment approaches [122], [124], [125]. Nevertheless, CCA continues to have a poor prognosis, emphasizing the urgent need for improved early detection techniques, a deeper understanding of the disease's origins, and the creation of more potent treatments [120], [126], [127]. A thorough investigation into the genetic landscape of CCA is pivotal. This effort is key to unlocking the potential of precision medicine and could pave the way for breakthroughs in both diagnosis and treatment.

1.4.3. Mutational landscape

At the genomic level, CCA is characterized by a high degree of heterogeneity, exhibiting a broad spectrum of gene mutations, copy number alterations, and changes in gene expression [105], [128], [129], [130]. Recent advances in high-throughput sequencing technologies have

provided unprecedented insights into the genetic architecture of CCA, unveiling several recurrently mutated genes and key oncogenic pathways (**Figure 2**) [124], [131].

One of the most frequently mutated genes in iCCA is *Isocitrate dehydrogenase 1* and *2* (*IDH1* and *IDH2*), with mutations observed in about 20% of iCCA cases [132], [133]. IDH mutations result in the production of an oncometabolite which promotes tumorigenesis [134]. Importantly, the presence of IDH mutations has implications for targeted therapy, as IDH inhibitors have shown promise in clinical trials [118], [135].

Epigenetic alterations, such as changes in DNA methylation and histone modification, also play a significant role in iCCA's pathogenesis [136], [137], [138]. For instance, mutations in *BRCA1 associated protein-1* (*BAP1*), a gene encoding for a protein involved in histone deubiquitination, have been associated with an aggressive iCCA phenotype and poorer patient outcomes [129], [139], [140].

Fusions and rearrangements of *Fibroblast growth factor receptor 2* (*FGFR2*) are another significant genetic event in iCCA, occurring in approximately 10-15% of cases [129], [141]. These fusions lead to constitutive activation of the FGFR pathway, driving cellular proliferation and survival [141]. Several FGFR inhibitors are currently under investigation as potential therapeutic options for patients with FGFR alterations [141], [142], [143].

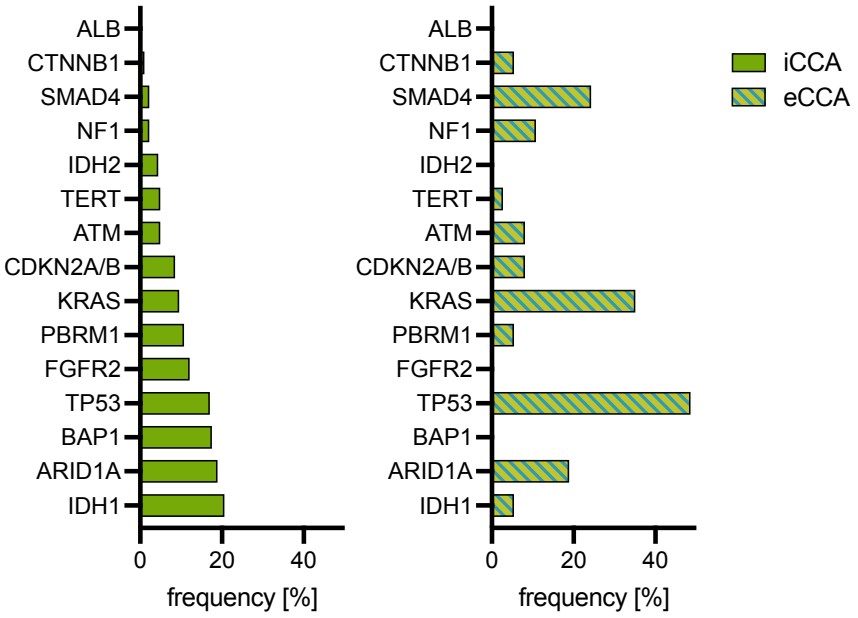

Figure 2. Comparative mutation prevalence in iCCA and eCCA.
Mutation frequencies in 412 iCCA and 37 eCCA cases, derived from Boerner et al. Hepatology 2021 [144] and Cheng et al. J Mol Diagn. 2015 [145], respectively.

Other genes recurrently mutated in iCCA include *Tumor protein p53* (*TP53*), *KRAS*, and *SMAD family member 4* (*SMAD4*), among others [100], [142], [146], [147], [148]. These mutations impact various cellular pathways, including cell cycle regulation, signal transduction, and DNA repair mechanisms, all of which contribute to the malignant transformation [129], [148], [149].

In contrast, eCCA tends to have a different mutational profile, with a higher prevalence of *KRAS*, *TP53* and *SMAD4* mutations and fewer *IDH* and *FGFR* alterations [96], [130], [150]. This distinction highlights the necessity of understanding the unique genetic underpinnings of each subtype to develop effective targeted therapies.

Nevertheless, despite these advances, the mutational landscape of CCA is far from fully mapped [136], [142], [151], [152]. Furthermore, the clinical implications of many identified mutations remain to be fully elucidated, underscoring the need for further research.

The integration of genomic data and clinical practice is vital, as it could pave the way for more personalized and effective therapeutic strategies, ultimately improving patient outcomes.

1.5. IDH mutations: molecular insights and oncogenic implications

1.5.1. Variants and functions of IDH isozymes

As previously highlighted, IDH mutations hold a significant prevalence in iCCA, making a detailed exploration of their roles and implications crucial. IDH enzymes play a pivotal role in cellular metabolism, specifically within the Krebs cycle. They catalyze the oxidative decarboxylation of isocitrate to α -ketoglutarate (α-KG) [153]. There are three isozymes of IDH in human cells, namely IDH1, IDH2, and IDH3. IDH1 is localized in the cytoplasm and peroxisomes, while IDH2 and IDH3 are found in the mitochondria (**Figure 3**) [154].

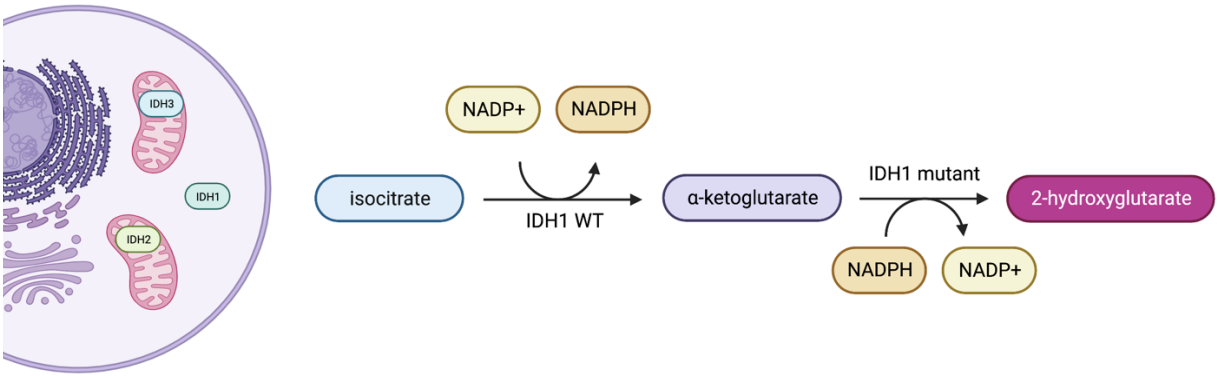

Figure 3. Function of IDH mutations in cancers.
Created with Biorender.

Both IDH1 and IDH2 are NADP+-dependent enzymes that serve dual purposes: they generate NADPH, aiding in cellular defense against oxidative damage [155], and produce α-KG, essential for the Krebs cycle and various cellular processes [156], [157].

IDH3, on the other hand, is a NAD+-dependent enzyme primarily involved in the Krebs cycle, converting isocitrate to α-KG in the mitochondria [158]. This reaction is a regulatory point and is considered one of the rate-limiting steps in the Krebs cycle, ensuring proper

cellular energy production [159]. Unlike IDH1 and IDH2, mutations in IDH3 are rare in cancers. Nevertheless, any alterations in IDH3 activity could potentially have implications for cellular energy balance and metabolic homeostasis [160].

While IDH1 and IDH2 are tightly regulated, they are not typically considered the primary rate-limiting steps of the Krebs cycle [158], [159]. However, mutations in these enzymes, result in aberrant activity which can contribute to cancer development and progression, distinguishing them from IDH3 in the context of cancer [160].

1.5.2. IDH1 mutations patterns across cancers

IDH1 mutations present a complex landscape, manifesting with striking variations in frequency across different malignancies. This inconsistency raises intriguing questions about the underlying mechanisms and the factors influencing the distribution of these mutations (Figure 4).

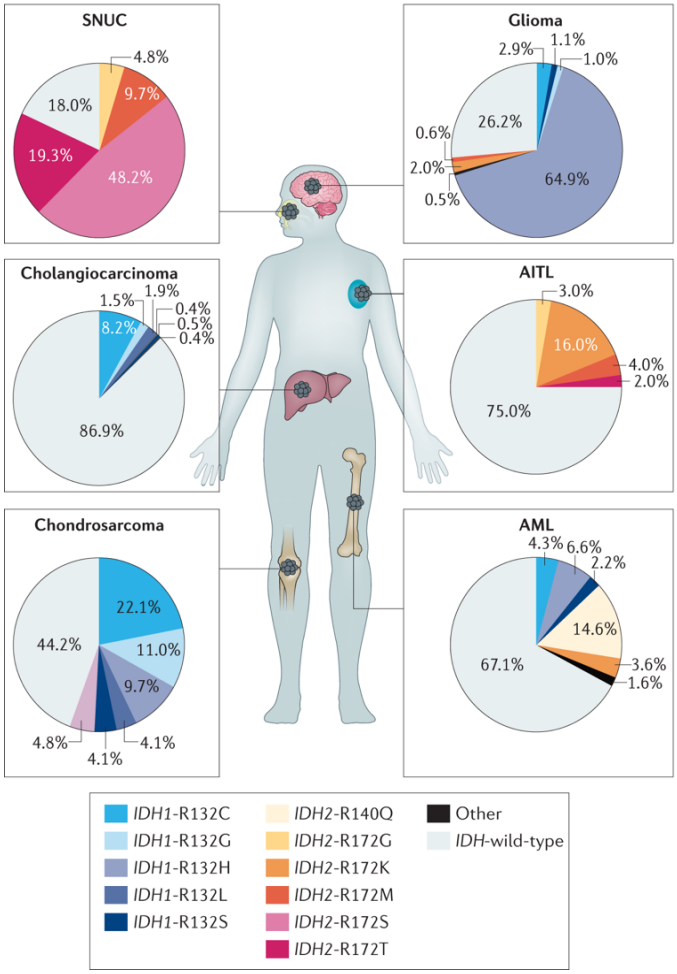

Figure 4. Prevalence of IDH mutations in cancers.
Unmodified from Pirozzi et al. Nat Rev Clin Oncol. 2021 [132].

One of the first malignancies where IDH1 mutations were identified is glioma, specifically lower-grade gliomas and secondary glioblastomas [161], [162], [163]. These mutations occur in approximately 70-80% of these tumors, usually involving the R132 residue [132], [156]. IDH1 mutations in gliomas have been shown to results in epigenetic dysregulation [164], [165], impaired cell differentiation [166], [167], and the promotion of tumorigenesis [163], [168], while paradoxically being associated with a better prognosis and a distinct response to therapy [162].

In iCCA, the IDH1 mutations are predominantly found at the R132 residue [132], similar to gliomas. The most common IDH1 mutation in iCCA is the R132C substitution, although other variants such as R132G, R132L, and R132S, and R132L are also present [169], [170]. The frequency of IDH1 mutations in iCCA varies across studies but is generally observed in approximately 10% to 23% of cases, making it a significant molecular subset of this cancer type [150], [171], [172], [173]. The presence of these mutations not only has profound implications for the biology and clinical management of iCCA but also correlates with distinct clinical outcomes. These genetic alterations are linked to specific pathogenic processes, including extensive epigenetic remodeling, which can influence the immune response to the tumor and affect the efficacy of therapeutic interventions. [174], [175].

Acute myeloid leukemia (AML) is another malignancy where IDH1 mutations play a significant role, with a prevalence of around 15-20% [132]. These mutations in AML are associated with specific clinical and biological characteristics, such as older age, normal karyotype, and concurrent mutations in *Nucleophosmin 1* [176], [177], [178]. IDH1-mutated AML also shows susceptibility to IDH inhibitors, leading to clinical responses and, in some cases, complete remissions [179].

In chondrosarcomas, IDH1 and IDH2 mutations are found in a significant number of cases [132], impacting the tumor's molecular characteristics and clinical behavior [156], [180], [181], [182], [183]. These mutations are associated with specific histological subtypes and contribute to altered epigenetic regulation and cell differentiation [181], [184], [185]. Similarly, in iCCA, IDH1 mutations play a parallel role to other malignancies [60], [134], [186], [187].

Interestingly, IDH1 mutations are relatively rare in other cancers, such as colorectal, breast, and lung cancers [132]. The reasons behind this differential prevalence across various malignancies remain a subject of active research and debate, with several theories proposed to explain the observed patterns.

One theory proposes a link between IDH mutations and tissue-specific factors, particularly the developmental origin and lineage of cells. Supporting this hypothesis, gliomas and AML, which frequently harbor IDH mutations, arise from cells of the neuroectodermal and hematopoietic lineage, respectively [188]. IDH mutations in these malignancies are thought to induce a block in cell differentiation, supporting the self-renewal and uncontrolled proliferation of immature cell types [189], [190]. This theory suggests that IDH mutations may confer a selective growth advantage to certain cell lineages, thereby contributing to tumorigenesis in a context-dependent manner.

Another theory posits that IDH mutations may be a response to specific oncogenic stresses or environmental exposures that vary across different tissue types [191], [192]. For instance, a chronic inflammatory milieu, as observed in iCCA, may provide a setting conducive to the selection of IDH mutations. This concept is supported by evidence that IDH mutations can be associated with specific risk factors in iCCA, such as liver fluke infection [170], [193].

A third hypothesis is based on the principle of mutational heterogeneity, suggesting that the varied prevalence of IDH mutations across cancers could simply be a reflection of the inherent genetic diversity and mutational processes operating within different tumor types [194], [195]. This theory posits that the overall mutational landscape of a tumor, shaped by factors such as DNA repair capacity, replication errors, and exposure to mutagens, ultimately determines the likelihood of acquiring specific mutations, including those in IDH.

A fourth perspective considers the cellular context, including factors such as metabolic status. In this view, certain cells may be more vulnerable to the effects of IDH mutations due to their metabolic requirements for either α-KG or NADP+ [167], [196], [197], [198], [199], [200], [201].

Additionally, the presence of other genetic alterations may act synergistically with IDH mutations to promote tumorigenesis [202]. For example, gliomas with the IDH1 R132H mutation often harbor concurrent alterations in *TP53* and *ATRX* chromatin remodeler, which may contribute to an amplified oncogenic impact [146], [180].

Lastly, there are studies suggesting a dynamic role of IDH1 mutations in cancer progression. For instance, in gliomas, mutant IDH1 expression initially drives tumor formation, it can rapidly transition from a driver to a passenger role in the tumor's development [203], [204]. This implies that the impact of IDH1 mutations may evolve over time, potentially influencing the tumor's response to therapy and its overall behavior.

These diverse theories, while not mutually exclusive, collectively contribute to the complex landscape of IDH mutations observed across cancers.

1.5.3. Consequences of 2-HG production and accumulation

Mutations in IDH1/2 are highly relevant in the context of oncogenesis, particularly in central nervous cancers [154], [205], [206]. These mutations observed in cancers are gain-of-function mutations, typically occurring at arginine residues in the active site (R132 in IDH1 and R172 in IDH2) [176], [206], [207], [208], [209]. These mutations confer a neomorphic activity to IDH1/2, allowing the mutated enzyme to catalyze the reduction of α-KG to 2-hydroxyglutarate (2-HG), an oncometabolite, which can alter cellular functions [134], [153].

2-HG has a transformative effect on cellular function, which can be largely attributed to its ability to competitively inhibit a class of enzymes that rely on α-KG as a cofactor [156], [187], [210]. The perturbation of these α-KG-dependent enzymes leads to a broad range of cellular changes that contribute to the malignant phenotype [60] (**Figure 5**).

The affected α-KG-dependent enzyme group includes a variety of dioxygenases that are involved processes such as DNA and histone demethylation [210], hypoxia-inducible factor (HIF) regulation [211], DNA damage repair [212], and collagen biosynthesis [212].

Specifically, prolyl hydroxylases, which stabilize HIF, are inhibited by 2-HG [156], [213]. This inhibition leads to activation of hypoxia-responsive genes that promote angiogenesis, metabolic adaptation, and survival in hypoxic conditions [211], [213], [214]. Each of these processes has a significant influence on tumorigenesis, shaping the phenotype of the resultant cancer.

Moreover, DNA and histone demethylases, including the Ten-eleven translocation (TET) family of DNA demethylases and the Jumonji C domain-containing histone demethylases, are critical for maintaining the cell's epigenetic landscape [215], [216], [217]. Inhibition of these enzymes by 2-HG, leads to aberrant methylation patterns that can alter gene expression, impacting cellular processes such as differentiation, proliferation, and apoptosis [134], [164], [167], [217], [218]. Additionally, 2-HG has been found to interfere with the function of DNA damage repair proteins [212], potentially leading to genomic instability and an increased risk of mutations, which could have significant ramifications in the context of cancer development and progression [219], [220], [221], [222], [223].

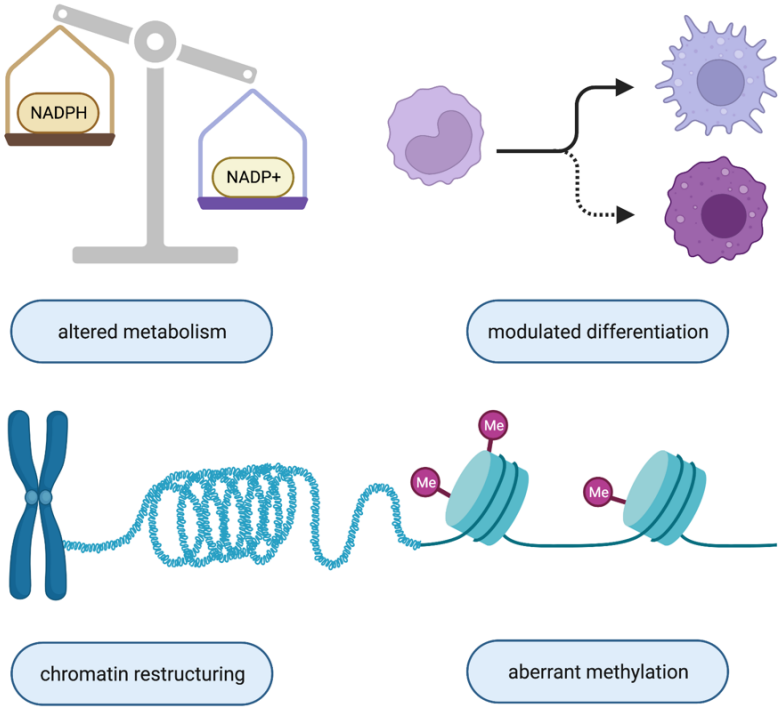

Figure 5. Downstream effects of 2-HG accumulation.
Created with Biorender.

Lastly, the 2-HG-induced inhibition of α-KG-dependent enzymes involved in collagen biosynthesis can disrupt the extracellular matrix, affecting cell adhesion, migration, and tissue

integrity. These processes are crucial in the context of cancer metastasis [212], [224], [225], [226].

Understanding the role of α-KG-dependent enzymes and their inhibition by 2-HG provides a unique perspective on the phenotypic changes induced by IDH mutations. This knowledge not only helps elucidate the molecular pathogenesis of IDH-mutated cancers but also opens avenues for potential therapeutic interventions.

1.5.4. Enzymatic traits of IDH1 mutants

Delving deeper into 2-HG's influence, it is crucial to explore the variations in 2-HG production capabilities among different IDH1 mutants. These variations, influenced by the type of mutation and its location within the protein structure, lead to distinct oncogenic impacts. By dissecting these catalytic traits, light is shed on how they contribute to the heterogeneity of IDH1 mutations and their consequences in cancer.

As mentioned above, mutations in IDH predominantly at active site arginine residues (R132 in IDH1, R172 in IDH2) [161], [169], [176], [179], [206], [207], [209], [227], [228], [229], giving rise to mutants which exhibit considerable variation in terms of 2-HG production capabilities. These variations are influenced by the type of mutation and its location within the protein structure [228], [230], leading to subtle differences in the active site configuration influencing substrate affinity and product release. For example, IDH1 R132C mutants produce higher 2-HG levels than R132H counterparts [228], [231]. This differential 2-HG production can profoundly influence cellular processes, including epigenetic regulation and tumor metabolism.

Less common mutations within IDH1, such as R132S, R132G, and R132L, result in 2-HG production, suggesting neomorphic capabilities, that are yet to be fully understood [169], [208], [228], [232], [233], [234]. IDH2 mutations, such as R172K, R172M, and R140, are predominantly identified in hematological malignancies [169], [176], [206], [227], [229], [235]. These mutants similarly produce 2-HG and induce tumorigenesis, although they are less extensively characterized in comparison to IDH1 R132H mutation.

Emerging evidence suggests that the quantity and perhaps the isoform-specificity of 2-HG production could influence the cellular consequences of IDH mutations and thereby their likelihood of contributing to the development of specific cancers. Notably, mutations in IDH1, typically found in gliomas, iCCA, and AML, primarily result in the production of D-2HG, while the less common IDH2 mutations can produce both D- and L-2HG [157], [236], [237].

Early studies have indicated that the D- and L- isoforms of 2-HG exert distinct effects on cellular function [238]. As mentioned earlier, D-2HG is a competitive inhibitor of α-KG-dependent enzymes, leading to widespread effects. In contrast, the impact of L-2HG, while less studied, appears to involve somewhat distinct cellular pathways, such metabolic stress and hypoxia response pathways [217], [238], [239], [240], [241].

Factors like cellular localization and metabolic context, in addition to structural differences, likely contribute to the differential 2-HG production. For example, IDH1, localized

mainly in the cytosol and peroxisomes [153], [162], [242], [243], and IDH2, found in mitochondria, may interact differently with cellular metabolism [132], [162], [243].

These mutations, while leading to 2-HG production, may have differential effects on enzyme activity, stability, cellular localization, and protein interactions, contributing to their distinct oncogenic impacts. Moreover, cellular contexts such as the developmental lineage, microenvironment, and metabolic status can modulate the effects of 2-HG and IDH mutations. This differential 2-HG production, influenced by IDH mutation type and location, highlights the complex landscape of IDH mutational heterogeneity. IDH with higher catalytic capabilities potentially has more potentially more pronounced effect on α-KG-dependent dioxygenases. Consequently, this can influence the epigenetic landscape, cellular differentiation, and tumor metabolism in distinct ways.

1.6. Current approaches in IDH1-targeted therapies

It is becoming increasingly clear that nuanced and comprehensive understanding of mutations is crucial for developing effective treatments. Advances in molecular oncology have led to targeted therapies for cancer, shifting from broad-spectrum agents to more specific drugs. This is particularly promising for IDH1 mutations, where therapies aimed at inhibiting 2-HG production, a key driver of tumorigenesis, demonstrate significant potential [164].

The development of small molecule inhibitors targeting the mutated IDH1 enzyme, such as the first-in-class IDH1 inhibitor ivosidenib (AG-120), represents a primary strategy in this domain. These inhibitors have demonstrated significant efficacy, particularly in clinical trials for AML, and are currently being tested in other IDH1-mutated cancers, including gliomas and CCAs [118], [148], [207], [244].

Besides directly inhibiting mutant IDH1, another therapeutic approach involves targeting the downstream consequences of 2-HG accumulation. Agents such as DNA methyltransferase inhibitors and histone deacetylase inhibitors are being explored to counteract the epigenetic changes induced by 2-HG, with ongoing investigations in both clinical and preclinical settings [245], [246], [247], [248], [249], [250].

While IDH1-targeted therapies have shown promise, they also face significant challenges. For instance, some patients do not respond to these therapies, or they eventually develop resistance [174]. This indicates a need for the development of combination therapies that target multiple aspects of the pathogenesis of IDH1-mutated cancers [64], [187], [245], [249], [251]. Furthermore, the potential toxicities of long-term inhibition of IDH1, a crucial enzyme in cellular metabolism, remain a critical concern that warrants careful monitoring and research [252].

The future of IDH1-based therapies is likely to involve a more precise understanding of the biological consequences of *IDH1* mutations, allowing for the design of highly specific and potent inhibitors [253], [254]. It may also involve the development of biomarkers to predict response to therapy and monitor treatment effectiveness [131], [255], [256], and the use of combination therapies to prevent or overcome resistance.

1.7. Understanding the IDH1-driven phenotype in iCCA

As we navigate through the intricacies of iCCA and its association with IDH1 mutations, the necessity to explore and hypothesize about the potential unique phenotype driven by these genetic alterations becomes increasingly evident. The presumed IDH1-driven phenotype in iCCA is suggested to present a distinct landscape, potentially characterized by specific metabolic, epigenetic, and cellular alterations. However, it is important to acknowledge that our current understanding of this landscape is limited, and much remains to be discovered and confirmed. By attempting to dissect these characteristics, we aim to glean invaluable insights into the tumor's behavior on a molecular and mechanistic level, its interaction with the microenvironment, and its potential response to therapeutic interventions.

The need for a comprehensive exploration and understanding of the IDH1-driven phenotype extends beyond academic curiosity; it holds tangible implications for patient care. Patients with iCCA harboring IDH1 mutations may potentially exhibit different clinical courses, responses to treatment, and overall prognoses compared to those with wild-type IDH1. Therefore, a thorough exploration and characterization of the IDH1-driven phenotype is not just a scientific endeavor, but a clinical necessity.

2. Study objectives

The objective of this thesis was to explore the role and implications of *IDH1* mutations in iCCA, with a particular focus on the molecular and cellular effects of these mutations and the subsequent accumulation of the oncometabolite 2-HG produced by mutant IDH1. The study sought to enhance our understanding of how these genetic alterations contribute to the pathogenesis of iCCA and to investigate potential therapeutic strategies targeting these specific mutations and their metabolic consequences.

Firstly, the thesis aimed to develop and validate a reliable IDH1 mutant iCCA model. This involved employing HTVi techniques to establish a foundational model for studying the effects of these mutations in liver cancer. The goal was to provide a comprehensive view of how distinct IDH1 mutants could potentially differentially impact tumor development and progression.

Next, focus was placed on providing molecular and cellular insights into the effects of 2-HG accumulation stemming from activity of mutant IDH1. This involved investigating how these mutations influence liver cell differentiation, tumor microenvironment characteristics, and the overall metabolic and epigenetic landscape in iCCA. The study utilized various *in vivo* and *in vitro* methodologies, offering a detailed understanding of the mutational impacts. Additionally, examination was extended to the effects on the tumor microenvironment, focusing on stromal deposition, immune infiltration, and modulation, which are critical aspects in the progression and treatment response of iCCA.

Lastly, an exploration was targeted towards novel approaches to leverage 2-HG-driven vulnerabilities, particularly from immunotherapeutic and genetic perspectives. These novel approaches provide potential alternatives to current IDH1 inhibitor treatments, offering a fresh perspective in the management of iCCA.

The study emphasized the importance of a nuanced understanding of *IDH1* mutations for developing effective treatments and highlighted potential avenues for future research in this area.

3. Material and methods

3.1. Animal experiments

3.1.1. Mice

All animal experiments were approved by regional authorities (Karlsruhe, Germany) and performed in compliance with their regulations.

C57BL/6N female mice were obtained from Janvier. HLA-A*0201 HLA-DRA*0101 HLA-DRB1*0101 transgenic mice devoid of mouse MHC (referred to as A2.DR1 mice) C57BL/6-Tg(HLA-DRA*0101,HLA-DRB1*0101)1Dmz-Tg(HLA-A2.1-beta2M)1Bpe-IAbetabtm1Doibeta2mtm1Doi-H-2Dbtm1Bpe-IAalphatm1Bpe-IEbetatm1Bpe were provided by in-house breeding at the DKFZ.

3.1.2. Hydrodynamic tail vein injection (HTVi)

Hydrodynamic injections were kindly performed by Lio Boese, Kai Volz or Prof. Darjus Tschaharganeh (Tschaharganeh lab, DKFZ). Briefly, C57BL/6N female mice, aged 7-8 weeks were administered a sterile 0.9% saline solution containing the relevant plasmids. The solution, equivalent to 10% of the mouse's body weight (approximately 2 mL), was rapidly injected into the tail vein within a span of 5 to 7 seconds. This method, contingent on the specific vector utilized, facilitated efficient *in vivo* transfection of hepatocytes, leading to targeted liver gene knock-outs and/or overexpression.

The dosage of each plasmid for each mouse was established as follows: 20 µg of the pX330-based plasmid was used for gene knock-out purposes, and 10 µg of all pT3-EF1a-based plasmids for transposon-mediated gene overexpression, except for pT3-EF1a-myrAkt for which only 5 µg was used. The CMV-SB, instrumental in enabling genomic integration of the transposon, was incorporated into the injection mix at a volume equal to one-fifth of the total pT3-EF1a plasmids injected. Plasmids used in this study are collected in (**Table 1**). Vectors containing *Idh1* sequences were kindly provided by Dr. Stefan Pusch (Clinical Cooperation Unit Neuropathology, DKFZ).

3.1.3. Handling of mouse tissue

Mice were monitored twice a week and euthanized via cervical dislocation in accordance with the termination criteria defined in the animal permit. Immediately following euthanization, tissue samples were rinsed in PBS (Sigma-Aldrich), photographed using a stereomicroscope (Leica, MZ10F, MC170) or simple camera, and rapidly frozen on dry ice for subsequent protein, mRNA, and gDNA extraction and then stored at -80°C until further processing. The remaining the tissue was processed for (immuno-)histochemistry analyses.

Portion of it was encased in Tissue-Tek OCT (Sakura) and frozen, while the remainder was preserved in 4% paraformaldehyde for at least 24 hours at 4°C before embedding. If applicable, a small piece of tissue was also saved for derivation of primary tumor cell line.

Table 1. List of plasmids used for HTVi

name	description	origin
CMV-SB13	Sleeping beauty transposase expression vector	AG Tschaharganeh, DKFZ, Heidelberg
pX330-U6-Chimeric_BB-CBh-hSpCas9	Human codon-optimized SpCas9 and chimeric guide RNA expression plasmid	Addgene, #42230
pT3 EF1a-KrasG12D-IRES-IDH1	Transposon-based $KRas^{G12D}$ and IDH1 (WT or mutant) expression plasmid	Tschaharganeh Lab, DKFZ, Heidelberg
pT3 EF1a-GFP-IRES-IDH1	Transposon-based GFP and IDH1 (WT or mutant) expression plasmid	Tschaharganeh Lab, DKFZ, Heidelberg
pT3-EF1a-NICD-IRES-IDH1	Transposon-based Notch Intracellular Domain (NICD) and IDH1 (WT or mutant) expression plasmid	Tschaharganeh Lab, DKFZ, Heidelberg
pT3-EF1a-myrAkt	Transposon-based myristoylated AKT expression plasmid	Tschaharganeh Lab, DKFZ, Heidelberg

3.1.4. Isolation of tumor-derived cell lines

Using sterile surgical tools, liver tumors were surgically excised and immediately washed with sterile PBS. A scalpel was used to mechanically dissect approximately 10-100 mg of the resected tissue, which was then submerged in solution containing Collagenase D and Dispase® II (4 mg/ml in DMEM, both Sigma Aldrich) for 30 min at 37°C with gentle shaking. The resulting dissociated cells were washed with complete DMEM and plated on previously pre-coated dishes (30 µg/ml, PureCol., Advanced BioMatrix). After undergoing 2-3 passages, the isolated cells were free from other contaminating cells of non-tumor origin. At this stage, derived cell lines were subjected to a mycoplasma test.

3.1.5. Peptide vaccination and tumor cell inoculation

Protocol established by Schumacher *et al.* [257] was followed. Briefly, male A2.DR1 mice, aged 8-15 weeks, were immunized with 100 µg IDH1 R132G peptide in Montanide-ISA51 (Seppic). Montanide-ISA51 emulsions were prepared by mixing equal volume of peptide in PBS to 1 mg/ml or DMSO in PBS (as sham control) and mice received 2 subcutaneous injections of 50 µl each into the lateral pectoral regions. Subsequently, an injection of 300 ng recombinant murine GM-CSF (Immunotools) in PBS was administered subcutaneously between injection sites, and Aldara cream containing 5% imiquimod (Meda Pharma) was applied at the shaved

injection site. Mice were boosted after 10 and 21 days. Recombinant murine GM-CSF (rmGM-CSF) was not applied during the boost vaccinations. Vaccination were performed with great help of Julius Michel and Khwab Sanghvi (Clinical Cooperation Unit Neuroimmunology and Brain Tumor Immunology, DKFZ).

3.1.6. Tumor cell inoculation

On day 25 following initial peptide vaccination, 0.5×10^6 tumor-derived cells resuspended in 100 µl PBS were subcutaneously injected into the shaved right and left flanks of A2.DR1 mice. In order to track tumor growth, mice were anesthetized with isoflurane (Zoetis) with the following settings for the isoflurane flow: air pressure 1-1.5 bar, flowmeter 2-2.5 L/min, isoflurane vaporizer 3-3.5 vol%, scavenger 45-50. Measurements were performed with a caliper and tumor volume was measured with the following formula: tumor volume = (length x width^2)/2. Once allografted tumors reached a diameter of 1 cm were observed, animals were euthanized by cervical dislocation.

3.1.7. Isolation of splenocytes and IFN-γ ELISpot

Spleens were excised from vaccinated and sham-treated A2.DR1 mice. Organs were mashed through a 40 µm cell strainer. Erythrocytes were lysed with ACK Lysing Buffer (Thermo Fisher Scientific), and cells were washed before culturing in RPMI1640 containing 10% fetal bovine serum (FBS; Gibco) and 100 U/mL penicillin and 100 µg/mL streptomycin (Sigma Aldrich). For splenocytes, medium was supplemented with 1 mM sodium-pyruvate, 2 mM glutamine (both PAA Laboratories), 100 µM non-essential amino acids (Lonza), and 50 µM β-mercaptoethanol (Sigma-Aldrich).

ELISpot white bottom multiwell plates (MAIPSWU10, Millipore) were coated with anti-mouse IFN-γ (AN18, Mabtech) and blocked with RPMI1640 containing 10% FBS and 100 U/mL penicillin and 100 µg/mL streptomycin. Mouse splenocytes were seeded at 5×10^5 per well and stimulated with 10 µg/mL peptide. As negative controls, Myelin oligodendrocyte glycoprotein (MOG) peptide was used at equal concentrations and peptide diluent PBS 10% DMSO (vehicle) was used at equal volume. The positive control was 20 ng/mL phorbol myristate acetate (PMA, Sigma-Aldrich) with 1 µg/mL ionomycin (Sigma-Aldrich). After 36 h, IFN-γ-producing cells were detected with biotinylated anti-mouse IFN-γ (R4-6A2), streptavidin-ALP (all Mabtech) and ALP colour development buffer (Bio-Rad) and quantified using an ImmunoSpot Analyzer (Cellular Technology Ltd).

3.2. (Immuno-)histochemistry (IHC)

Tissue samples were collected, fixed in 4% paraformaldehyde for at least 24 hours at 4°C, and then embedded in paraffin wax according to standard procedures. The paraffin-embedded tissues were sectioned into 3 µm thick slices using a microtome. Sections

underwent deparaffinization with xylene, followed by rehydration through using a descending alcohol series and finally, a washing step with distilled water.

For, immunohistochemistry (IHC), antigen retrieval was achieved by boiling the tissue sections in a pressure cooker for 8 minutes using citrate buffer (10 mM trisodium citrate dihydrate, 0.5 %(v/v) TWEEN® 20, pH 6.0), which was followed by cooling period of 5 minutes under running water. Following this, endogenous peroxidase activity was inhibited by treating the sections with 3% hydrogen peroxide for 10 minutes and subsequently washed 1 min under running water and twice with PBS for 2 min each.

Table 2. List of antibodies used for IHC

antibody	Supplier and catalog number	dilution
primary antibodies		
CCL17	abcam ab182793	1:50
CD3	Epredia RM-9107-S1	1:100
CD31	Cell Signaling Technology 77699S	1:100
CD4	abcam abcam183685	1:500
CD8a	Invitrogen 14-0808-82	1:100
KRT19	abcam 133496	1:400
cleaved Caspase 3	Cell Signaling Technology #9664	1:400
DES	Cell Signaling Technology #5332S	1:50
ERG	Cell Signaling Technology #97249	1:150
FOXP3	Thermo Fisher Scientific 14-5773-82	1:50
H3K27me3	Cell Signaling Technology 9733S	1:100
H3K9me3	abcam ab8898	1:400
HNF4α	abcam ab181604	1:1000
LY6G	Invitrogen 13-9668-82	1:100
phospho-H2A.X	Cell Signaling Technology #9718	1:500
phospho-H3	Cell Signaling Technology #9701	1:200
SOX9	EMD Millipore AB5535	1:250
αSMA	Cell Signaling Technology #19245	1:400
secondary antibodies		
ImmPRESS HRP goat anti-rabbit	Vector Laboratories, Inc. MP-7451	
ImmPRESS HRP goat anti-mouse	Vector Laboratories, Inc. MP-7452	

Non-specific antibody binding was prevented by incubating the sections with a blocking solution consisting of 5% BSA with 0.05 % Triton X-100 for 1 hour at room temperature (RT) and incubated with the primary antibody diluted in blocking buffer overnight at 4°C. Post-incubation, the sections were washed three times with PBS/Triton X-100 (0.05 %) for 5 min and subsequently incubated with the appropriate horseradish peroxidase (HRP)-conjugated

secondary antibody for 30 minutes at RT, followed by three washing steps with PBS/Triton X-100 (0.05 %). The specific antibodies used for this study and their dilution are listed in **Table 2**.

Subsequently, slides were stained with ImmPACT DAB Peroxidase (HRP) Substrate (Vectorlabs) according to manufacturer's instructions and observed under the microscope until desired staining intensity was achieved.

Counterstaining was performed using hematoxylin for a duration of 1-2 min, washed with tap water. Once counterstained, slides prepared for chromogenic detection were dehydrated through a series of graded alcohols, cleared in xylene, and mounted with a permanent mounting medium using Surgipath Micromount Mounting Medium (Leica). Finally, images were captured using a light microscope for chromogenic detection – slides were scanned using the Hamamatsu NanoZoomer Digital Pathology system and analyzed using QuPath (Quantitative Pathology & Bioimage Analysis).

Processes involved in (immuno-)histochemistry stainings were kindly performed by Luise Butthof (Tschaharganeh Lab, DKFZ) and members of the CMCP (Institute of Pathology, University Clinic Heidelberg).

3.3. Molecular analysis techniques

3.3.1. DNA analysis

3.3.1.1. Methylation analysis

DNA isolation from tumor tissue was performed with QIAmp Mini (Qiagen) according to manufacturer's instructions, including the optional step of RNAse treatment (Qiagen). Obtained samples were processed by Microarray Core Facility at DKFZ.

Genome-wide screening of DNA methylation patterns was performed by using the Infinium MouseMethylation285k BeadChips (Illumina, San Diego, US), allowing the simultaneous quantitative measurement of the methylation status at >285,000 CpG sites. By combining Infinium I and Infinium II assay chemistry technologies, the BeadChip provides a balanced coverage of CpG islands, translation start sites, enhancers, imprinted loci, and other regions.

DNA concentrations were determined using PicoGreen (Molecular Probes Inc., Eugene, USA). The quality of genomic DNA samples was checked by agarose-gel analysis, and samples with an average fragment size > 3kb were selected for methylation analysis.

500 ng genomic DNA from each sample was bisulfite converted using the EZ-96 DNA Methylation Kit (Zymo Research Corporation, Orange, US) according to the manufacturer recommendations. Bisulfite treatment leads to the deamination of non-methylated cytosines to uracils, while methylated cytosines are refractory to the effects of bisulfite and remain cytosine.

Each sample was whole genome amplified and enzymatically fragmented following the instructions in the Illumina Infinium HD Assay Methylation Protocol Guide. The DNA was

applied to Infinium MouseMethylation285k BeadChip and hybridization was performed for 16-24h at 48°C. During hybridization, the DNA molecules annealed to locus-specific DNA oligomers linked to individual bead types. One or two probes were used to interrogate CpG locus, depending on the probe design for a particular CpG site.

Allele-specific primer annealing was followed by single-base extension using DNP- and biotin-labeled ddNTPs. Infinium II uses only one bead type with a unique type of probe allowing detection of both alleles. The methylated and unmethylated signals are generated respectively in the green and the red channels.

After extension, the array was fluorescently stained, scanned, and the intensities at each CpGs were measured. Microarray scanning was done using an iScan array scanner (Illumina). DNA methylation values, described as beta values, were recorded for each locus in each sample. DNA methylation beta values were continuous variables between 0 and 1, representing the percentage of methylation of a given cytosine corresponding to the ratio of the methylated signal over the sum of the methylated and unmethylated signals.

In this study, the analysis of genome-wide DNA methylation data was conducted using the RnBeads package for R. RnBeads is a comprehensive tool designed for the analysis of methylation data, particularly suitable for bead array platforms like the Illumina Infinium HumanMethylation450K BeadChip.

The package facilitates several key steps: data import and preprocessing, which includes normalization, background correction, and handling missing values; differential methylation analysis for identifying differentially methylated regions and positions; and extensive annotation of methylation sites. Moreover, RnBeads generates detailed reports and interactive visualizations, aiding in the interpretation of epigenetic data. This tool's integrative analysis capability also allows for the combination of methylation data with other genomic data types, offering a holistic view of the epigenetic landscape. The flexibility and scalability of RnBeads make it an ideal choice for handling and analyzing large-scale methylation datasets. Additional analysis was performed with Reactome package.

Analysis was performed with great help of Iva Buljan and dr. Pavlo Lutsik (Computational Cancer Epigenomics, DKFZ).

3.3.1.2. T7 endonuclease I assay

Genomic DNA isolation from tissue was performed using the Puregene Core Kit A (Qiagen) according to the manufacturer's protocol following Puregene Tissue Kit. Briefly, Proteinase K (0.4 mg/ml, Sigma Aldrich) was added to the tissue in submerged in lysis buffer. Next, the sample was incubated for 1 h with gentle shaking at 55°C. To inactivate Proteinase K, the sample was incubated at 95°C for 5 min, which was followed by addition of RNase A solution (60µg/ml, Qiagen) and incubated for 5 min at 37°C before cooling samples on ice for 1 min. The proceeding steps involved protein precipitation, alcohol precipitation in 70% EtOH and 1 h DNA rehydration at 65°C.

The quality and concentration of the isolated DNA were evaluated using a NanoDrop ND-1000 Spectrophotometer (Thermo Scientific). Extracted DNA was stored at -20°C until needed for downstream applications.

In order to detect CRISPR-mediated gene modifications and test for the effectiveness of sgRNAs, T7 endonuclease I assays were performed. For that, gDNA isolated from modified cells was used to amplify the target region via PCR.

PCR reactions were set up using Q5 Hot Start High-Fidelity (New England Biolabs, NEB) according to manufacturer's protocol with 200-400 ng gDNA template and primers listed in Table 3. Primers specific to the guide of interest were designed and tested for the alignment temperature, leading to a ~300-800 bp product with a single specific band. Ten percent of the resulting amplicons were run on agarose gel while the rest were PCR purified with QIAquick PCR Purification Kit (Qiagen) according to manufacturer's instructions.

PCR products were denatured and reannealed to form heteroduplexes, after which T7 endonuclease I (NEB) was added and incubated at 37°C for 30 min. The final mix was loaded on 2% agarose gel or 10% polyacrylamide gel to verify the editing.

Table 3. Overview of PCR primers used for T7 Endonuclease I assay

name		sequence (5'-3')
Tet1	forward	TTTGAGAATTCACATCCATTGC
	reverse	GCTTTGTGTTCTTTGCAACAAG
Tet2	forward	AACATAGCCAATACCTGATGGG
	reverse	TCTGGAGGTAAGGTAGCCTTTG

3.3.2. RNA analysis

3.3.2.1. RNA isolation

Tissue samples were placed on dry ice, and fragments approximately 2-5 mm^3 in size were cut using a disposable scalpel. The tissue resuspended in lysis buffer (RNeasy Mini Kit, Qiagen) was then homogenized BeadBlaster tubes (Biozym) in homogenizer (Precellys 24, Bertin Instruments), and the lysate was transferred directly into QIAshredder tubes (Qiagen). Tissue shredding was carried out according to manufacturer's instruction.

In following step RNA was isolated from the collected samples following the protocol of the RNeasy Mini Kit (Qiagen). The yield and purity of the RNA were assessed using a NanoDrop ND-1000 Spectrophotometer (Thermo Scientific) and the samples were immediately utilized for downstream applications and subsequently stored at -80°C.

3.3.2.2. Reverse transcription and quantitative real-time PCR (qRT-PCR)

Isolated RNA was reversely transcribed into cDNA with the TaqMan®Reverse Transcription Reagents (Thermo Fisher Scientific) in a 20 µl reaction with minor adjustments to master mix composition from manufacturer's protocol (**Table 4**).

Table 4. Reverse transcription reaction

	per 1 reaction
10x RT buffer	2 µl
Random hexamer (50 µM)	1 µl
$MgCl_2$ (25 mM)	4.4 µl
RNase inhibitor (20 U/µl)	0.4 µl
dNTP mix (10 mM)	4 µl
MultiScribe™ Reverse Transcriptase (50 U/µl)	1 µl

Obtained cDNA was diluted 1:20 and used for qPCR analysis. It was conducted using the PowerUp SYBR Green Master Mix (Thermo Fisher Scientific). Reactions were prepared according manufacturer's protocol for 20 ul volume (**Table 5**) and carried out with fact cycling program on QuantStudio 3 Real-Time PCR System (Applied Biosystems).

Table 5. Overview qPCR reaction

	per 1 reaction
PowerUp SYBR Green Master Mix (2X)	10 µl
Primer forward (10 µM)	0.8 µl
Primer reverse (10 µM)	0.8 µl
cDNA (1:20 diluted)	1 µl
H_2O	17.4 µl

Each sample was analyzed in triplicate with primers either specific for the genes of interest or for the reference housekeeping gene (**Table 6**). The quantification of relative gene expression of each sample triplicate was calculated using the ΔΔCT method.

Table 6. Overview qPCR primers

name		sequence (5'-3')
murine qPCR primers		
Ccl17	forward	TACCATGAGGTCACTTCAGATGC
	reverse	GCACTCTCGGCCTACATTGG
Actb	forward	GCTTCTTTGCAGCTCCTTCGT
	reverse	ACCAGCGCAGCGATATCG

3.3.2.3. RNA sequencing and differential gene expression analysis

For RNA sequencing, total RNA from tumor tissue samples was isolated as described above. Library preparation and RNA sequencing was performed by the Genomics and Proteomics Core Facility at the DKFZ. 50 bp single-read sequencing was performed using a NovaSeq 6K PE 50 SP (Illumina). Sequence alignment was performed using STAR (Version 2.5.3a) and GRCm38mm10_PhiX as reference genome. For further analysis, data was processed using HTSeq-count to generate readcount tables and FPKM files, and DESeq2 to identify differentially expressed genes. Final analysis was performed with the help of the Ingenuity Pathway Analysis (IPA) software.

3.3.3. Protein analysis

3.3.3.1. Protein isolation for Western blot

Tissue samples were placed on dry ice, and fragments approximately 3-8 mm^3 in size were cut using a disposable scalpel. The tissue resuspended in lysis buffer was then homogenized with BeadBlaster tubes (Biozym) in homogenizer (Precellys 24, Bertin Instruments), and the lysate was transferred to a fresh 1.5 mL tube. Subsequently, it was and incubated on ice for 30 min, and sonicated for 5 minutes on ice (Transsonic T460/H, Elma). The composition of the lysis buffer is shown in **Table 7** and **Table 8**. Post-lysis, tubes were centrifuged at 13,000 rpm for 10 min at 4°C. At the end, supernatants were transferred to fresh 1.5 mL tubes and stored at -20°C.

To obtain cell lysates, the cell pellets were first submerged in lysis buffer, initiating the incubation process on ice. Subsequently, the same protocol was followed.

Table 7. Cell lysis buffer for protein extraction

reagent	volume
10x cell lysis buffer (Cell Signaling Technology)	100 µl
10x protease inhibitor (cOmplete™ Mini, Sigma Aldrich)	100 µl
50x phosphatase inhibitor	20 µl
ddH_2O	780 µl

Table 8. Phosphatase inhibitor cocktail

reagent	concentration
sodium fluoride	250 mM
sodium orthovanadate	50 mM
sodium pyrophosphate	50 mM
β-glycerophosphate	50 mM

3.3.3.2. Protein isolation for histone quantification

Histone isolation was performed with Histone Extraction Kit (abcam) according to manufacturer's instructions.

3.3.3.3. Protein quantification

Protein concentrations were quantified using the BCA protein assay kit according to manufacturer's instructions (Pierce Biotechnology) based on BSA (molecular biology grade, NEB) standard curve using microplate reader (FLUOstar Omega, BMG LABTECH).

3.3.3.4. SDS-PAGE and Western blot

Protein concentrations in samples for Western blot were adjusted to 1 µg/µl in 5x Laemmli buffer (100 mM Tris-HCl pH 6.8, 5 %β-mercaptoethanol, 5% glycerol, 2 %SDS) and samples were denatured for 5 min at 95°C. Following denaturation, lysates were used for SDS-PAGE. Briefly, equal amounts of proteins (20-50 µg per lane for protein lysates, 1-5 µg per lane for histone extracts) were separated by SDS-PAGE on an 8-15% polyacrylamide gel under reducing conditions, for approximately 2 hours at 120V. Then, the separated proteins were transferred to an equilibrated polyvinylidene difluoride membrane (Carl Roth) using wet transfer system (Bio-Rad) at 90V for 2 hours.

Table 9. Overview of antibodies used for immunoblotting

antibody	source	dilution
primary antibodies		
H3K27me3	Cell Signaling Technology #9733S	1:5000
H3K9me3	abcam ab8898	1:5000
H3	Cell Signaling Technology #4499S	1:10 000
HES1	Cell Signaling Technology #11988	1:1000
IDH1	Dianova W09	1:500
KRAS	SantaCruz F234	1:500
NOTCH	Cell Signaling Technology #3608	1:1000
Actin-HRP	Sigma-Aldrich, A3854	1:20 000
secondary antibodies		
Goat polyclonal anti-mouse HRP-conjugated secondary antibody	Jackson Immuno Research, 115-035-008	1:20 000
Goat polyclonal anti-rabbit HRP-conjugated secondary antibody	Jackson Immuno Research, 111-035-003	1:20 000

The membrane was blocked with 5% non-fat dried milk in Tris-buffered saline with Tween-20 (TBST) for 1 hour at RT to prevent non-specific binding. The membrane was then incubated overnight at 4°C with primary antibodies of interest, diluted appropriately in 5% non-fat milk in TBST. After washing thrice with TBST, the membrane was incubated with HRP-conjugated secondary antibodies for 1 hour at RT. The overview of all antibodies used in this study is shown in Table 9.

The membrane was again washed three times with TBST and developed using the Clarity Western ECL Substrate (Bio-Rad Laboratories) according to manufacturer's instructions using FluorChem M (ProteinSimple).

3.3.3.5. Mass spectrometry

3.3.3.5.1. Sample preparation

Tumor tissue samples were turned into a fine, homogenous powder using cryoPREP® dry tissue pulverizer. For the purpose of separating cellular from extracellular fractions, a protocol established by McCabe *et al.* [258] was followed with minor alterations.

Briefly, approximately 100 mg of pulverized tumor tissue was homogenized with the help of BeadBlaster tubes (Biozym) in homogenizer (Precellys 24, Bertin Instruments) on program 2 in 200 µl of high salt buffer (50 mM Tris-HCl, 0.25% CHAPS, 25 mM EDTA, 3 M NaCl, pH 7.4) supplemented with 10 µl/mL fresh protease inhibitor (Halt Protease Inhibitor Cocktail, Thermo Scientific). Homogenate was vortexed at 4 °C for 20 min. Homogenized tissue was spun at 17,000 × g (4°C) for 15 min.

The resulting supernatant was saved as intracellular fraction. The pellet was further extracted with 1 mL high salt buffer two times with homogenization after each buffer addition. Cellular extracts were pooled into a single soluble fraction.

ECM-enriched pellets were homogenized in 6M Gnd-HCl, 100 mM ammonium bicarbonate (ABC) at BeadBlaster tubes (Biozym) in homogenizer (Precellys 24, Bertin Instruments) and vortexed at RT overnight. Homogenate was spun at 18,000 × g (4°C) for 15 min, and the supernatant was collected as the Gnd-HCl fraction.

Remaining pellets were reduced and alkylated by incubating in 10 mM DTT, 100 mM ABC pH 8.0 for 30 min at 37 °C before adding 2.5× molar excess of IAM (over DTT) and incubating in the dark for 15 min. Samples were spun at 18,000 × g (4°C) for 15 min, and the supernatant was discarded. Pellets were then treated with freshly prepared HA buffer (1 M NH_2OH-HCl, 4.5 M Gnd–HCl, 0.2 M K_2CO_3, pH adjusted to 9.0 with NaOH) at 200 µl/mg of the starting tissue dry weight. Each tube was placed under a stream of nitrogen gas and sealed before being homogenized BeadBlaster tubes (Biozym) and incubated at 45 °C with shaking (1000 rpm) for 4 h. Following incubation, the samples were spun for 15 min at 18,000 × g, and the supernatant was removed and stored as the extracellular fraction at −80 °C until further proteolytic digestion with trypsin.

Following steps were kindly performed by MS-Based Protein Analysis Core Facility at the DKFZ. Protein samples (10 µg for the intracellular samples; extracellular matrix preparation started from 100 mg and resulting protein amounts were used) were run for 0.5 cm into an SDS-PAGE and the entire piece was cut out and digested using trypsin according to Shevchenko *et al.* [259] adapted to on a DigestPro MSi robotic system (INTAVIS Bioanalytical Instruments AG).

3.3.3.5.2. LC/MS method

A LC-MS/MS analysis was carried out on an Vanquish Neo UPLC system (Thermo Fisher Scientific) directly connected to an Orbitrap Exploris 480 mass spectrometer (Thermo Fisher Scientific) for a total of 120 min. Peptides were online desalted on a trapping cartridge (Acclaim PepMap300 C18, 5µm, 300Å wide pore; Thermo Fisher Scientific) for 3 min using 30 ul/min flow of 0.1% TFA in water. The analytical multistep gradient (300 nl/min) was performed using a nanoEase MZ Peptide analytical column (300Å, 1.7 µm, 75 µm x 200 mm, Waters) using solvent A (0.1% formic acid in water) and solvent B (0.1% formic acid in acetonitrile).

For 102 min the concentration of B was linearly ramped from 4% to 30%, followed by a quick ramp to 78%, after two minutes the concentration of B was lowered to 2% and a 10 min equilibration step appended. Eluting peptides were analyzed in the mass spectrometer using data depend acquisition mode.

A full scan at 120k resolution (380-1400 m/z, 300% AGC target, 45 ms maxIT) was followed by up to 2 seconds of MS/MS scans. Peptide features were isolated with a window of 1.4 m/z, fragmented using 26% NCE. Fragment spectra were recorded at 15k resolution (100% AGC target, 54 ms maxIT). Unassigned and singly charged eluting features were excluded from fragmentation and dynamic exclusion was set to 35 s.

3.3.3.5.3. Data analysis

Data analysis was carried out by MaxQuant (version 2.1.4.0) [260] using an organism specific database extracted from Uniprot.org under default settings (mouse containing 55341 entries from 03.01.2022; construct sequences with 2 entries (KrasG12D_(567aa) and IDH1_Mm_(1245aa))). Identification FDR cutoffs were 0.01 on peptide level and 0.01 on protein level. Match between runs option was enabled to transfer peptide identifications across Raw files based on accurate retention time and m/z.

Quantification was done using a label-free quantification (LFQ) approach based on the MaxLFQ algorithm [261]. The LFQ normalization was applied separately for intra- and extracellular via parameter grouping. A minimum of 2 quantified peptides per protein were required for protein quantification. The initial data processing was executed independently, albeit with coding assistance from ChatGPT. Subsequent analysis was carried out using Reactome and IPA platforms.

3.3.4. Biochemical analysis

3.3.4.1. DMMB assay

For sample preparation, liver tissue samples were thawed and fixed in 4% paraformaldehyde and subsequently weighed and then minced into small pieces with a tissue homogenizer (Precellys 24, Bertin Instruments). The tissue fragments were placed in Proteinase K digestion buffer (2 mg/mL Proteinase K, 0.5% SDS, 100 mM Tris pH 8.0) and incubated at 65°C overnight until complete digestion in order to extract GAGs. Following incubation, the samples were centrifuged at 10,000 x g for 10 minutes to separate debris. The supernatant, which contained the GAGs, was collected for further analysis.

For the 1,9-dimethylmethylene blue (DMMB) assay, 20 µl of each sample supernatant was pipetted into a 96-well microplate. To each well, 200 µl of DMMB (16 mg/L DMMB, 3 g/L glycine, 1.6 g/L NaCl and 95 ml/L of 0.1 M acetic acid, pH 3.0) was added. Absorbance was read immediately at 525 nm using microplate reader (FLUOstar Omega, BMG LABTECH).

3.3.4.2. 2-HG assay

Protein isolation itself was performed as in **3.3.3.1**, but a different lysis buffer was applied. The composition of the buffer can be found in **Table 10**.

Table 10. Cell lysis buffer for biochemical assays

reagent	volume
2x NP-40 lysis buffer (300 mM NaCl, 2% NP-40, Tris-HCl 100 mM, pH 8.0)	500 µl
10x protease inhibitor (cOmplete™ Mini, Sigma Aldrich)	100 µl
50x phosphatase inhibitor	20 µl
ddH_2O	380 µl

Deproteinization involved introducing 25 µl of ice-cold 2 M PCA into followed by 100 µl of the sample (serum, protein lysate). After a brief 2-minute period on ice, samples were centrifuged at 4000 rpm for 20 minutes at RT. The supernatant from the centrifugation was added fresh tubes already containing 5 µl of ice-cold 1 M KOH and the samples were placed on ice for 2 minutes. This was followed by another round of centrifugation at 4000 rpm for 20 minutes at RT. The resulting supernatant was used for the assay.

The master mix contained 10x HEPES at 1M, pH 8, 10 mM NAD+, 0.1 µg/µl D-2-hydroxyglutarate dehydrogenase, 0.1 U/µl Diaphorase, 125 µM resazurin, and the balance of ddH_2O; and 75 µl was aliquoted into each well of a black 96-well plate. Next, 25 µl of the sample was introduced into each well.

The plate was then incubated at RT in the dark. The duration of incubation was dependent on the nature of the sample: for serum samples incubation lasted approximately 30 minutes, while tissue lysates required an approximate 15-minute incubation period. The measurement was carried in a microplate reader (FLUOstar Omega, BMG LABTECH) at $\lambda_{excitation}$ = 540 nm and $\lambda_{emmission}$ = 590 nm. The concentration of 2-HG in the samples was quantified against a standard curve.

3.3.4.3. Carbohydrate estimation

Carbohydrate estimation was performed with Pierce™ Glycoprotein Carbohydrate Estimation Kit (Thermo Fischer Scientific) according to manufacturer's instructions following desalting of samples initially utilized for DMMB assay facilitated by Zeba™ Spin Desalting Columns (Thermo Fischer Scientific).

3.4. Cloning and plasmid generation

3.4.1. Molecular cloning

3.4.1.1. Generation of CRISPR/Cas9 guide plasmids

sgRNAs were designed using the online tool CHOPCHOP. To generate oligonucleotides suitable for cloning into a CRISPR/Cas9 vector, the target sequence was converted into reverse complementary DNA oligonucleotides. To the original sequence as well as the resulting sequence, 5' overhangs were added CACC and CAAA, respectively, thus generating overhangs complementary to BbsI or BsmbI restriction sites of the respective target vectors (pX330 or lentiCRISPR v2). The sgRNA sequences used in this study are shown in **Table 11**.

Table 11. sgRNA sequences used in this study

name	sequence (5' – 3')
murine sgRNAs	
sgRPA3_top	CACCGCTGGCGTTGACGCGCGCTT
sgRPA3_bot	AAACAAGCGCGCGTCAACGCCAGC
mAHCYL_1top	CACCGAATTACAACGTCCACCTGC
mAHCYL_1bot	AAACGCAGGTGGACGTTGTAATTC
mAHCYL_2top	CACCGTGGGAGCGTGTACGTTCTC
mAHCYL_2bot	AAACGAGAACGTACACGCTCCCAC
mITGAV_1top	CACCGCATGGACCGAGGTTCCGAT
mITGAV_1bot	AAACATCGGAACCTCGGTCCATGC
mITGAV_2top	CACCGAGTTACTTCGGATTCGCCG
mITGAV_2bot	AAACCGGCGAATCCGAAGTAACTC

name	sequence (5‘ – 3‘)
mITGB5_1top	CACCGCCCAATACACGGATTGGTC
mITGB5_1bot	AAACGACCAATCCGTGTATTGGGC
mITGB5_2top	CACCGCCGTGGATTGCCAAAGTAC
mITGB5_2bot	AAACGTACTTTGGCAATCCACGGC
mTNS3_1top	CACCGCATCCGCTCCCGATCGTAA
mTNS3_1bot	AAACTTACGATCGGGAGCGGATGC
mTNS3_2top	CACCGGGCTTCGTAAGCTGAGCAT
mTNS3_2bot	AAACATGCTCAGCTTACGAAGCCC
mITGAV_1top	CACCGCATGGACCGAGGTTCCGAT
mITGAV_1bot	AAACATCGGAACCTCGGTCCATGC
mAHCYL_1top	CACCGAATTACAACGTCCACCTGC
mAHCYL_1top	AAACGCAGGTGGACGTTGTAATTC
mAHCYL_2top	CACCGTGGGAGCGTGTACGTTCTC
mAHCYL_2top	AAACGAGAACGTACACGCTCCCAC
mTET1_top	CACCGATTAATCACATCAACGCCG
mTET1_bot	AAACCGGCGTTGATGTGATTAATC
mTET2_top	CACCGAGTGCTTCATGCAAATTCG
mTET2_bot	AAACCGAATTTGCATGAAGCACTC
human sgRNAs	
AHCYL_1top	CACCGCAAATTGAGTAGACGACCC
AHCYL_1bot	AAACGGGTCGTCTACTCAATTTGC
AHCYL_2top	CACCGATGTCGTAATAACTTGCAC
AHCYL_2bot	AAACGTGCAAGTTATTACGACATC
ITGAV_1top	CACCGCATTAGTGGTAACCTATCG
ITGAV_1bot	AAACCGATAGGTTACCACTAATGC
ITGAV_2top	CACCGCACCTCTCTTCATGGATCG
ITGAV_2bot	AAACCGATCCATGAAGAGAGGTGC
ITGB5_1top	CACCGTTTCAGAGCGAGCGATCCA
ITGB5_1bot	AAACTGGATCGCTCGCTCTGAAAC
ITGB5_2top	CACCGTTTCTCCTACACGGCACCG
ITGB5_2bot	AAACCGGTGCCGTGTAGGAGAAAC
ITGB5_1top	CACCGTTTCAGAGCGAGCGATCCA
TNS3_1top	CACCGGTACGACAACGATGCTGGG
TNS3_1bot	AAACCCCAGCATCGTTGTCGTACC
TNS3_2top	CACCGCGAGTCCCAGCGTATCAGT
TNS3_2bot	AAACACTGATACGCTGGGACTCGC

The oligonucleotides were phosphorylated using T4 Polynucleotide Kinase (PNK, 10,000 U/ml, NEB) according to the manufacturer’s protocol and subsequently annealed. After

conclusion of annealing and phosphorylation, samples were diluted 1:250 making the insert ready for ligation.

The vectors for sgRNAs delivery were digested over the course of 5 hours and dephosphorylated with recombinant shrimp alkaline phosphatase (rSAP, NEB) for 45 minutes at 37°C and purified using the QIAquick PCR Purification Kit (Qiagen) in order to obtain the backbone for cloning. Both steps were performed according to manufacturer's instructions. The pX330 was subjected to digestion using BsmBI (NEB) at 37°C and the lentiCRISPR v2 with BsmBI (NEB) at 55°C.

The insert was ligated to the digested plasmid with the T4 DNA Ligase (400,000 U/ml, NEB) for 1 h at RT and subsequently used for transformation.

3.4.1.2. HiFi Assembly

In order to create expression plasmids, respective DNA sequences was introduced to respective backbones using the NEBuilder® HiFi DNA Assembly Master Mix (NEB) according to manufacturer's instructions.

Briefly, primers partially complementary (ranging from 15 to 40 nucleotides) to both the target amplicon and the vector were employed to amplify the NICD from the donor plasmid (PT3 EF NICD IRES mCherry). Primers used to amplify the insert are shown in Table 12.

Post-amplification, the insert underwent purification using column PCR (QIAquick PCR Purification Kit, Qiagen), followed by the quantification of DNA concentration with NanoDrop ND 100 Spectrophotometer (Thermo Fisher Scientific). The assembly reaction involved the combination of the digested vector backbone (pDEST6.2/V5-DEST) with the purified amplicon in a 1:2 molar ratio. The amounts of vector and fragments were calculated with the NEBioCalculator.

Assembled mixture was further supplemented with 10 µl of NEBuilder HiFi DNA Assembly Master Mix, and the volume was adjusted to 20 µl using ddH_2O. The reaction was then incubated at 50°C for one hour and subsequently used for transformation.

Table 12. Primer sequence for HiFi Assembly

name	sequence (5' – 3')	Tm
plenti_NICD_IRES_IDH1_F	AAATAACACTAGTCCAGTGTGGTGGTATCGCGCGTAAGCGGCCGCTAGAA	62°C
plenti_NICD_IRES_IDH1_R	TGTACAAACTTGTTGATATCTGCAGCTGTAAGATGAACACAGTGGGGCTC	

3.4.2. Transformation of heat competent E. coli

For transformation of bacteria with ligated plasmids, 25 µl of NEB® Stable Competent *E. coli* (High Efficiency) bacteria (NEB) was incubated with 3 µl of the ligation reaction on ice

for 10 min, which was followed by heat shock at 42°C for 45 sec, and again incubation on ice for 1 minute. The bacteria were then plated on carbenicillin-containing agar plates (100 µg/ml) and incubated upside down overnight at 32°C. The resulting bacterial clones were picked and used for further downstream applications.

3.5. Plasmid DNA purification

Purification of plasmid DNA depending on the desired amount was carried out with either the QIAprep Spin Miniprep Kit or with the QIAGEN Plasmid Plus Midi Kit (Qiagen), according to manufacturer's protocols. Plasmid concentration was measured using a NanoDrop ND 100 Spectrophotometer (Thermo Fisher Scientific) and stored -20°C until needed for downstream applications. Validation of plasmids was performed via sequencing by Microsynth Seqlab GmbH (Switzerland).

3.6. Cell culture

3.6.1. Cultivation

The cell lines used for this study were maintained in a humidified incubator at 37°C with 5% CO_2 in sterile conditions. The cells were cultured in Dulbecco's Modified Eagle Medium (DMEM, Sigma) supplemented with 10% fetal bovine serum (FBS; Gibco) and 1% penicillin/streptomycin (10,000 U/ml penicillin and 10 mg/ml streptomycin, Sigma Aldrich), which from here on out will be called complete medium. Upon reaching near full confluency cells were split after trypsinization using Trypsin-EDTA solution (0.25%, sterile-filtered, Sigma Aldrich). Tumor-derived cell lines were cultivated in the same manner on dishes or plates pre-coated with 30 µg/ml collagen solution (PureCol®, Advanced BioMatrix). Cell lines used in this study can be found in Table 13.

For cryopreservation, cells were resuspended in freezing medium (45% FBS, 45% complete medium, 10% DMSO) and frozen on -80°C in cryogenic vials.

Table 13. Cell lines

cell line	tumor entity	origin
SNU1079	intrahepatic cholangiocarcinoma	AG Roessler, University Clinic Heidelberg
RBE	intrahepatic cholangiocarcinoma	AG Roessler, University Clinic Heidelberg
HT1080	chondrosarcoma	AG Pusch, DKFZ, Heidelberg
murine tumor-derived cell lines	HTVi-induced liver tumorigenesis	AG Tschaharganeh, DKFZ, Heidelberg

3.6.2. Virus production

Lentivirus was produced using HEK293T cells, which were plated on 10 cm plates a day prior to transfection. The transfection mix consisted of 1 mL DMEM, 8 µg psPAX2, 2.5 µg pMD.2G, 10 µg of the chosen vector (**Table 14**), and 60 µL of polyethylenimine (PEI, 1 µg/µL in ddH2O, Polysciences). After brief vortexing for 5 seconds, the mixture was left to incubate at RT for 30 minutes, then carefully added dropwise to the HEK293T cells, which were 80% confluent at the time of transfection.

The medium was replaced 24 hours post-transfection with fresh complete medium, and the viral supernatant was collected and filtered through 0.45 µm cellulose acetate membrane filters (VWR) 48 hours post-transfection and stored at -20°C for short period of time, until usage.

Table 14. List of plasmids used for *in vitro* experiments

plasmid	description	origin
plasmids used for production of viral particles		
psPAX2	2nd generation lentiviral packaging plasmid	Addgene #12260
pMD.2G	VSV-G envelope expression plasmid	Addgene #12259
plasmids used for CRISPR-mediated gene knock-out *in vitro*		
lentiCRISPR v2	lentiviral backbone expressing SpCas9 and puromycin resistance from EFS promotor and sgRNA from U6 promotor	Addgene #52961
pLKO.U6-EFs-GFP-P2A-Blasticidin	lentiviral backbone expressing SpCas9 and sgRNA under U6 promoter	Tschaharganeh lab, DKFZ, Heidelberg
plasmids used for stable gene expression *in vitro*		
pLenti6.2/V5-DEST	lentiviral expression vector under CMV promoter	Thermo Fisher, V36820
pLenti6.2/V5-DEST-NICD	lentiviral NICD expression vector under CMV promoter	AG Tschaharganeh, DKFZ, Heidelberg

3.6.3. Stable transduction of tumor-derived cell lines

Target cells were plated in 6-well plates the day prior to transduction. On the following day, cells were transduced with viral supernatants in the presence of polybrene (4 µg/mL, Sigma Aldrich). Two days post-transduction, cells were selected with antibiotic matching produced viral particles (puromycin dihydrochloride (2 µg/mL) or blasticidin S HCl (10 µg/mL), both Thermo Fisher Scientific).

3.6.4. Competition assay

The assessment of the impact of gene alterations on cell proliferation and viability was conducted through competition assays. Cell lines derived from murine tumors, underwent transduction to express Cas9. Following this, a selection process was implemented, post which the cells were subjected to a second round of transduction to express sgRNA, with GFP serving as an expression marker. For controls, sgRosa was employed as a negative control, while sgRpa3 was utilized as a positive control. Subsequently, these transduced and edited cells were mixed at a 70:30 ratio with their unedited parental cell counterparts. The acquisition and analysis were performed using the guava easyCyte HT system.

3.6.5. Colony formation assay

The clonogenic capacity of cells was assessed with colony formation assay (CFA). The number of cells seeded for the colony formation assay varied according to the growth rate of each cell line. Specifically, for mouse cell lines, 500 cells per well were seeded, whereas for human cell lines, 1000 cells per well were seeded. The cells were seeded in 12-well plates and allowed to grow for a period of 10-14 days. After that time, the assay was terminated by performing crystal violet staining (0.05 % (w/v) crystal violet, 1 % (v/v) formaldehyde, 1% (v/v) methanol in PBS). For the staining with crystal violet, wells were first washed with PBS and then incubated with crystal violet staining solution for 20 min with gentle shaking at RT. After the staining period, the solution was removed and the plates were first rinsed with water to remove excess dye, then air dried.

3.6.6. Proteome Profiler Mouse XL Cytokine Array

The experiment was conducted following the manufacturer's instructions. Subsequently, the analysis was performed using a macro developed in-house for Fiji, which was created with the assistance of ChatGPT.

3.7. Internet resources

resource	website
BioRender	https://app.biorender.com/
CellMarker 2.0	https://ngdc.cncb.ac.cn/databasecommons/database/id/6110
CHOPCHOP	http://chopchop.cbu.uib.no/
DepMap	https://depmap.org/portal/
NEBioCalculator	https://nebiocalculator.neb.com/#!/ligation
PubMed	https://pubmed.ncbi.nlm.nih.gov/
Uniprot	https://www.uniprot.org/

3.8. Software

software	source
ChatGPT	OpenAI
Fiji	open source
Ingenuity Pathway Analysis	Qiagen
Microsoft Office	Microsoft
Mendeley Desktop	Elsevier
Prism 8	GraphPad
RStudio	open source
SnapGene	GSL Biotech LLC
QuPath	open source

3.9. Statistical analysis

The statistical analysis was performed with GraphPad Prism 8. The type of statistical analysis employed is specified in the figure caption. Significance levels are depicted as *: $p < 0.05$, **: $p < 0.01$, ***: $p < 0.001$, ****: $p < 0.0001$.

4. Results

4.1. Establishing and validating IDH-mutant iCCA model

4.1.1. Development of an IDH-mutant iCCA model using HTVi

Given the significant prevalence of *IDH1* mutations in cholangiocarcinomas, my research focused on understanding how these mutations specifically contribute to iCCA development and progression. Expanding on the approach of O'Dell *et al.* for inducing iCCA through tissue-specific conditional activation of KRAS(G12D) and inactivation of *Tp53* [262], I aimed to incorporate *Idh1* mutations in this genetic background.

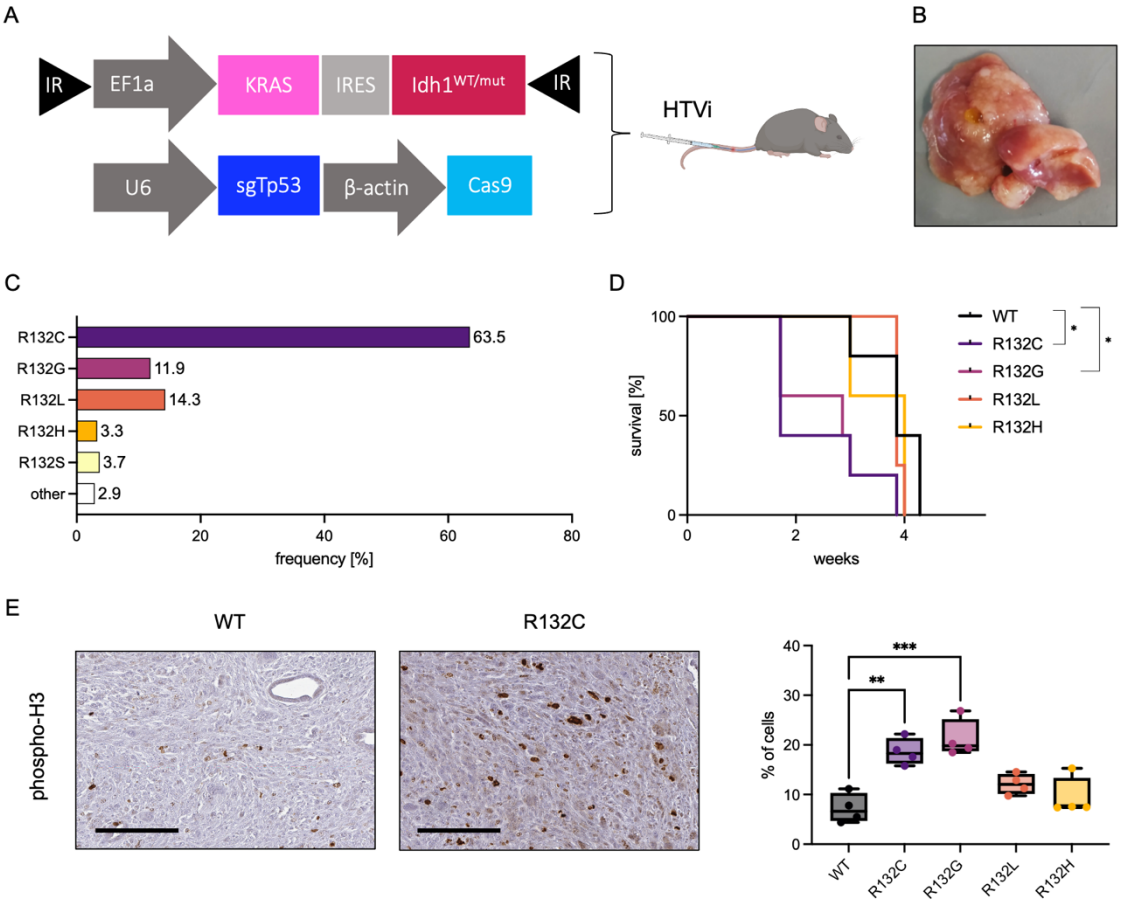

Figure 6. Dissecting the impact of *Idh1* mutations on iCCA progression and survival within HTVi framework.
A. Schematic representation of the HTVi experimental setup. B. Representative macroscopic image of obtained KRAS;TP53;IDH1 tumor. C. Prevalence of *IDH1* mutations in iCCA, adapted from Boscoe AN et al., J Gastrointest Oncol, 2019 [263]. D. Kaplan-Meier survival curve of mice bearing KRAS;TP53;IDH1 tumors, p-value: *=p≤0.05 (log-rank (Mantel-Cox) test), N=3. E. Immunohistochemical evaluation of phospho-H3 in KRAS;TP53;IDH1 tumors; left: representative images of tumor samples, scale bar: 300 µm; right: corresponding quantification. Each data point signifies an individual mouse, **=p≤0.01 and ***=p≤0.001 (one-way ANOVA with post hoc Tukey's test).

For this, I employed the HTVi, Sleeping Beauty Transposon system [264], and generated vectors, which allowed overexpression of oncogenic KRAS(G12D) (which will be referred to as KRAS) in combination with specific *Idh1* mutations and combined them with *Tp53* deletion (Figure 6A&B). This approach enabled simultaneous introduction of KRAS and either *Idh1* wild-type (WT) or a selected *Idh1* mutation (R132C/R132G/R132H/R132L) into hepatocytes *in vivo*, along with CRISPR/Cas9-mediated gene disruption of the *Tp53* gene. Furthermore, this setup allowed to investigate differences of individual *Idh1* mutations on tumor biology as well as common traits of mutant IDH1 in iCCA.

Informed by the prevalence of human *IDH1* mutations [263], the selection of point mutations in the *Idh1* gene — which lead to the amino acid substitutions R132C, R132G, and R132L on the protein level — was based on their observed frequency in human iCCA cases (Figure 6C). All of these mutations are present in at least 10% cases of human iCCA, with IDH1 R132C occurring in over 60% of these instances. Additionally, I included the less frequent IDH1 R132H mutation as a control within my experimental framework. Even though IDH1 R132H mutation is relatively rare in iCCA (found in less than 4% of cases) it can be frequently found in other malignancies, particularly in gliomas where its prevalent in up to 65% of cases [132]. This provided a comparative benchmark in my experimental approach.

After injection of respective plasmid cocktails, I witnessed rapid tumor growth in the livers and all groups had to be euthanized roughly 4 weeks after injection. Remarkably, even in this highly aggressive tumor model IDH1 R132C and R132G mutants adversely affected survival of tumor-bearing mice in comparison to the IDH1 WT counterparts by 2 weeks (Figure 6D).

To examine this phenomenon further, I conducted immunohistochemistry (IHC) staining for phospho-H3 staining, which is a recognized marker for mitosis [265], [266]. The staining results showed more than one-fold increase in phospho-H3 expression in IDH1 R132C and R132G mutants (Figure 6E), consistent with accelerated tumor progression of these KRAS;TP53;IDH1 mutants in the survival study. This suggests that different IDH1 mutants could differentially affect tumor cell proliferation.

These results serve as a stark illustration of the potent oncogenic potential of specific *IDH1* mutations when combined with other genetic alterations such as KRAS activation and *Tp53* deletion. It emphasizes the critical need for timely intervention in the treatment of iCCA and validates the relevance of this model in studying the rapid progression and lethal nature of this disease.

4.1.2. KRAS;TP53;IDH1 iCCA model validation

Next, my investigation sought to validate the iCCA model by confirming overexpression of KRAS and IDH1, as well as the disruption of *Tp53*. To achieve this, I conducted Western blot (WB) analysis, which revealed marked overexpression of KRAS and IDH1 in the KRAS;TP53;IDH1 tumor tissue compared to normal tissue control, indicating successful genetic manipulation (Figure 7A). Additionally, the T7 endonuclease I assay was instrumental in demonstrating *Tp53* disruption, with distinct bands corresponding to the expected sizes confirming the mutations

at the *Tp53* gene locus (**Figure 7B**). These results collectively confirmed that the tumor tissue exhibited the desired genetic alterations, setting a solid foundation for subsequent functional analyses.

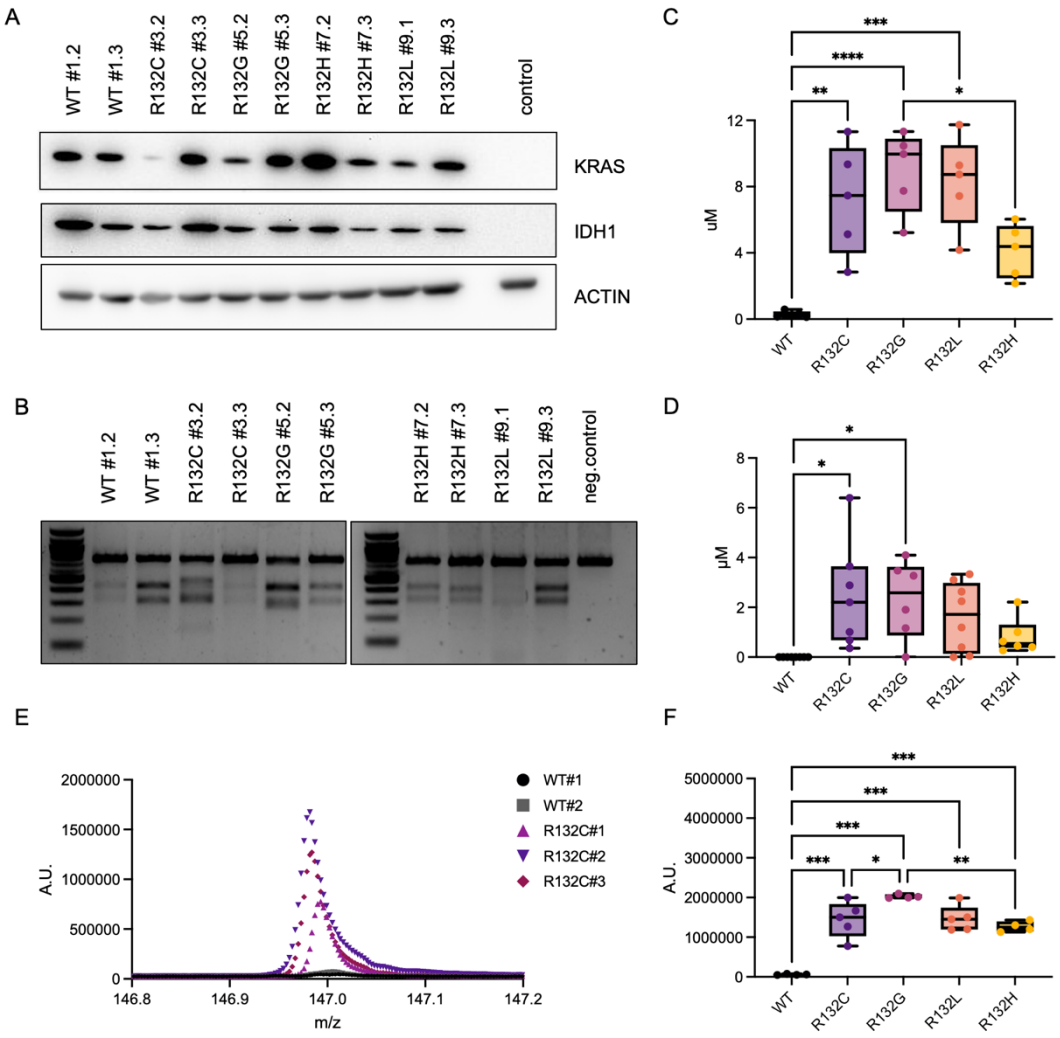

Figure 7. Validation and quantification of KRAS expression, *Tp53* disruption, and 2-HG accumulation in KRAS;TP53;IDH1 tumor samples.

A. Western blot analysis of KRAS;TP53;IDH1-tumor-derived samples, B. agarose gel showing the disruption of *Tp53* using the T7 endonuclease I assay, arrows indicate expected cleavage products. C. intracellular levels of 2-HG in tumor-derived samples, each sign represents one mouse, p-value: *=p≤0.05 and **=p≤0.01, ***=p≤0.001, ****=p≤0.0001 (one-way ANOVA with post hoc Tukey's test). D. 2-HG levels in serum samples from tumor-bearing mice, each sign represents one mouse, p-value: *=p≤0.05. E. MALDI-TOF spectra showing m/z values from 146.8 to 147.2 of IDH WT and IDH mutant tissue. Peaks at m/z 147 represent 2-HG. F. 2-HG levels measurement by MALDI-TOF in tumor sections, each sign represents one mouse, p-value: *=p≤0.05 and **=p≤0.01, ***=p≤0.001, ****=p≤0.0001 (one-way ANOVA with post hoc Tukey's test).

A critical aspect of this validation was the measurement of the oncometabolite 2-HG, which serves as a link between genetic alterations and their phenotypic manifestations. To thoroughly assess this, I applied both biochemical and biophysical methods. The former

confirmed the presence of 2-HG not just within the tumor tissues but also in the serum of the tumor-bearing mice.

Interestingly, the level of 2-HG in iCCA-specific mutants (R132C, R132G, and R132L) was ten-fold increased in comparison to IDH1 WT samples, while the IDH1 R132H mutant exhibited only five-fold increase in the level of 2-HG accumulated in the tissue (**Figure 7C**). Moreover, in terms of serum samples, while an increase for both IDH1 R132L and R132H was noticeable, it was only significant for the IDH1 R132C and R132G mutants when compared to IDH1 WT, amounting to approximately 2 µM (**Figure 7D**).

Quantification of 2-HG in tumor samples was further confirmed by MALDI-TOF mass spectrometry of frozen tissue sections [230], demonstrating a significant increase in 2-HG levels in the IDH1 mutant samples in comparison to their IDH1 WT counterparts (**Figure 7E&F**). This biophysical method appeared to be the more sensitive than the biochemical assay, distinguishing even minor differences between 2-HG levels. Here, the IDH1 R132G mutant exhibited the highest levels of 2-HG, followed by R132L, R132C, and finally R132H presenting moderate levels of production of the oncometabolite. Furthermore, the 2-HG levels produced by IDH1 R132G in the tissue samples were also significantly increased in comparison to IDH1 R132C and R132H.

Overall, the R132G IDH1 mutant consistently exhibited the highest levels of 2-HG accumulation across all techniques and sample types, followed by either R132C or R132L, with the R132H mutation showing the lowest level of 2-HG among these IDH1 mutants. This finding is consistent with the observed behavior of these IDH1 mutants *ex vivo* and their documented activity in other types of cancer [228], thereby reinforcing the validity of the model in reflecting the alterations caused by presence of different *Idh1* mutations.

4.2. Molecular and cellular insights into *Idh1* mutations

4.2.1. Investigation of glycosylation in mutant IDH1 tumors

In the next step, I focused on the histological examination of samples from KRAS;TP53;IDH1. The analysis delineated a clear distinction in morphology of tumor nodules; those with more pronounced glandular structures and a robust stromal presence were predominantly found in IDH1 mutant samples, as opposed to the less pronounced glandular and stromal features observed in nodules from IDH1 WT tumors (**Figure 8A**).

The striking desmoplastic reaction in mutant IDH1 tumors suggested a potential alteration in the production of stromal components, such as glycoproteins and glycosaminoglycans (GAGs). Upon performing Alcian Blue staining, which selectively binds to acidic polysaccharides and proteins, and some types of GAGs in tissue samples [267], I found that the structural changes observed in the histological analysis were indeed found to be closely associated with glycosylation processes (**Figure 8B**). The presence of these molecules in IDH1 R132C and R132G mutants was notably enhanced, showing a marked increase in comparison to not only IDH1 WT, but also IDH1 R132H.

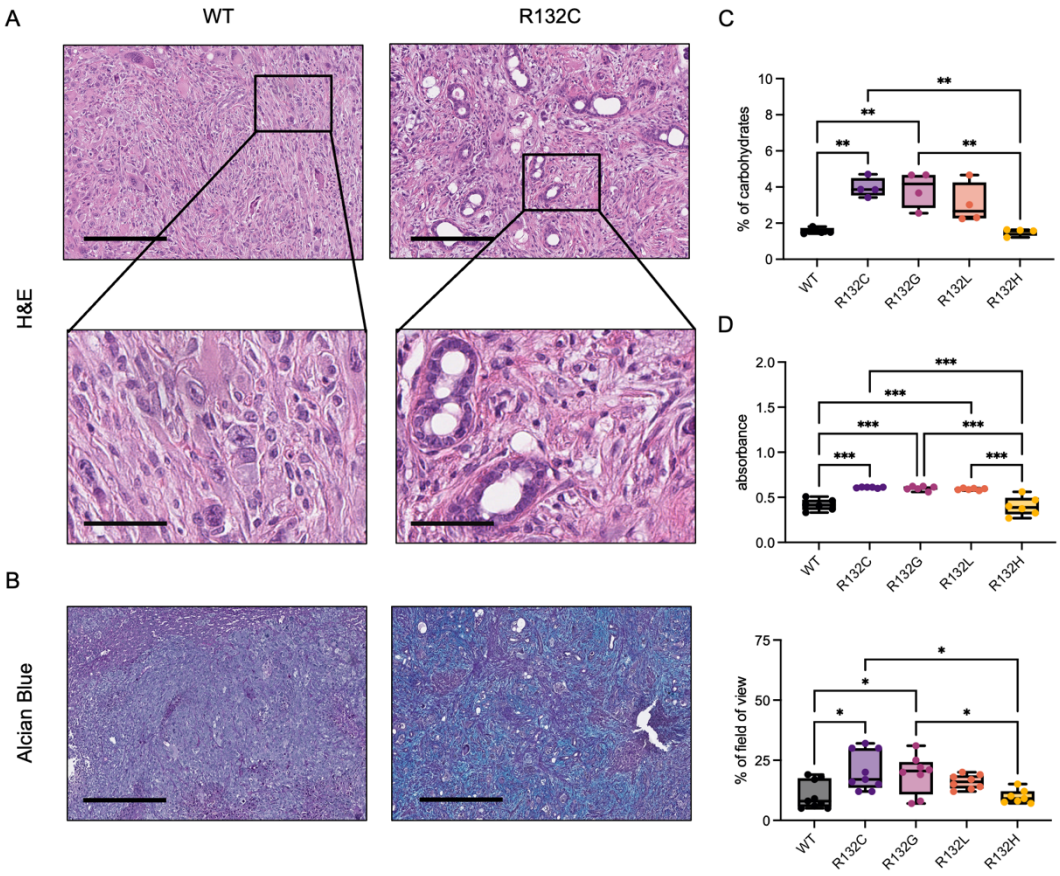

Figure 8. Evaluating the glycosylation spectrum of KRAS;TP53;IDH1 tumor samples.

A. H&E staining of tumor samples with representative images of KRAS;TP53;IDH1 tumors, at 10x magnification (top, scale bar: 300 µm) and 40x magnification (bottom, scale bar: 75 µm). B. Alcian Blue staining of tumor samples with representative images (left, scale bar: 300 µm) and quantification results (right). C. Carbohydrate content quantification in tumor samples. D. Determination of sGAG levels using the DMMB assay. B, C and D. each data point represents an individual mouse sample, *=p≤0.05, **=p≤0.01, ***=p≤0.001 (one-way ANOVA with post hoc Tukey's test).

To further investigate this observed increase, I conducted detailed biochemical analysis with two distinct assays. The first, glycoprotein carbohydrate estimation assay, was employed to assess the overall glycoprotein levels, confirming a one-fold increase in glycoprotein content among the iCCA-specific IDH1 mutant samples (**Figure 8C**). Additionally, the 1,9-dimethylmethylene blue (DMMB) assay (**Figure 8D**) specifically quantified sulfated glycosaminoglycans (sGAGs), revealing an increase in iCCA-specific IDH1 mutant samples in comparison to IDH1 WT counterparts and IDH1 R132H. The DMMB assay, by binding to the sulfate groups of GAGs, provided a more focused quantification of these acidic polysaccharides visualized by Alcian Blue.

Notably, my findings revealed that only the iCCA-specific IDH1 mutants were associated with heightened glycosylation levels, whereas in contrast the IDH1 R132H mutant exhibited glycosylation patterns that were indistinguishable from those of the IDH1 WT samples, suggesting a mutation-specific impact on the glycosylation pathways. Thus, this data

demonstrates that the marked stromal response in mutant IDH1 tumors is at least in part caused by increased deposition of glycoproteins and (sulfated) GAGs.

4.2.2. *Idh1* mutations and their implication on liver cell differentiation and identity

Given marked differences in tumor morphology, I further focused on the effect of *Idh1* mutations on cellular differentiation and identity.

By applying IHC on tumor samples, I found out that all IDH1 mutant tumor cells displayed higher levels of Cytokeratin 19 (KRT19) (**Figure 9A**), a marker for cholangiocytic differentiation [268], and SOX9 (**Figure 9B**), a marker associated with progenitor cells and hepatic regeneration [269]. Of note, IDH1 R132G mutant tumors not only exhibited the highest expression of KRT19, this expression level was also notably higher in comparison to the IDH1 R132H mutant.

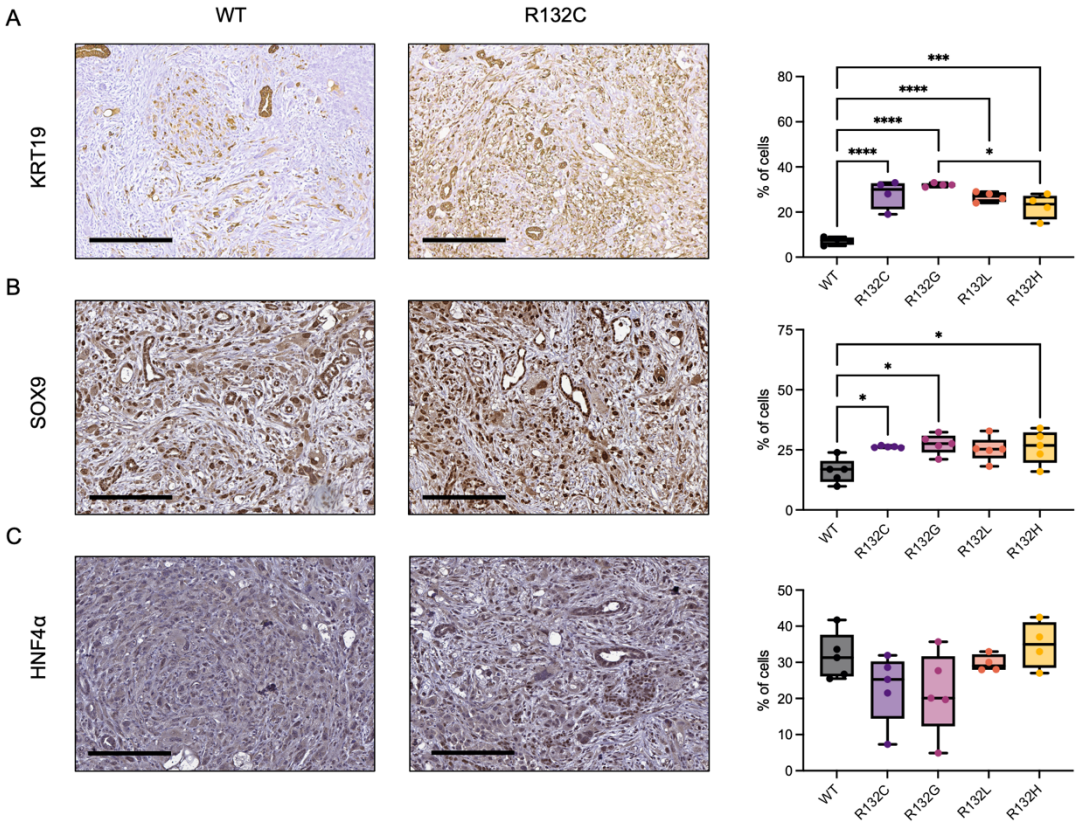

Figure 9. Immunohistochemical profiling of key liver markers in KRAS;TP53;IDH1 tumors.
IHC analysis of KRAS;TP53;IDH1 tumors, left: representative images of tumor samples, scale bar: 300 µm; right: corresponding quantification. A. KRT19, B. SOX9, and C. HNF4α staining. A, B, C. Each data point represents an individual mouse, *=p≤0.05, ***=p≤0.001, ****=p≤0.0001 (one-way ANOVA with post hoc Tukey's test).

However, the expression of HNF4α, a transcription factor fundamental to hepatocyte identity [270], did not show a significant change, although there was a noticeable trend

towards decreased expression and inverse correlation with increased 2-HG levels (Figure 9C).

The increased cholangiocytic markers in IDH1 mutant tumors suggest a shift towards a cholangiocytic phenotype, underscoring 2-HG's role in influencing cellular identity in iCCA. This finding highlights how *Idh1* mutations can impact tumor cell identity and progression.

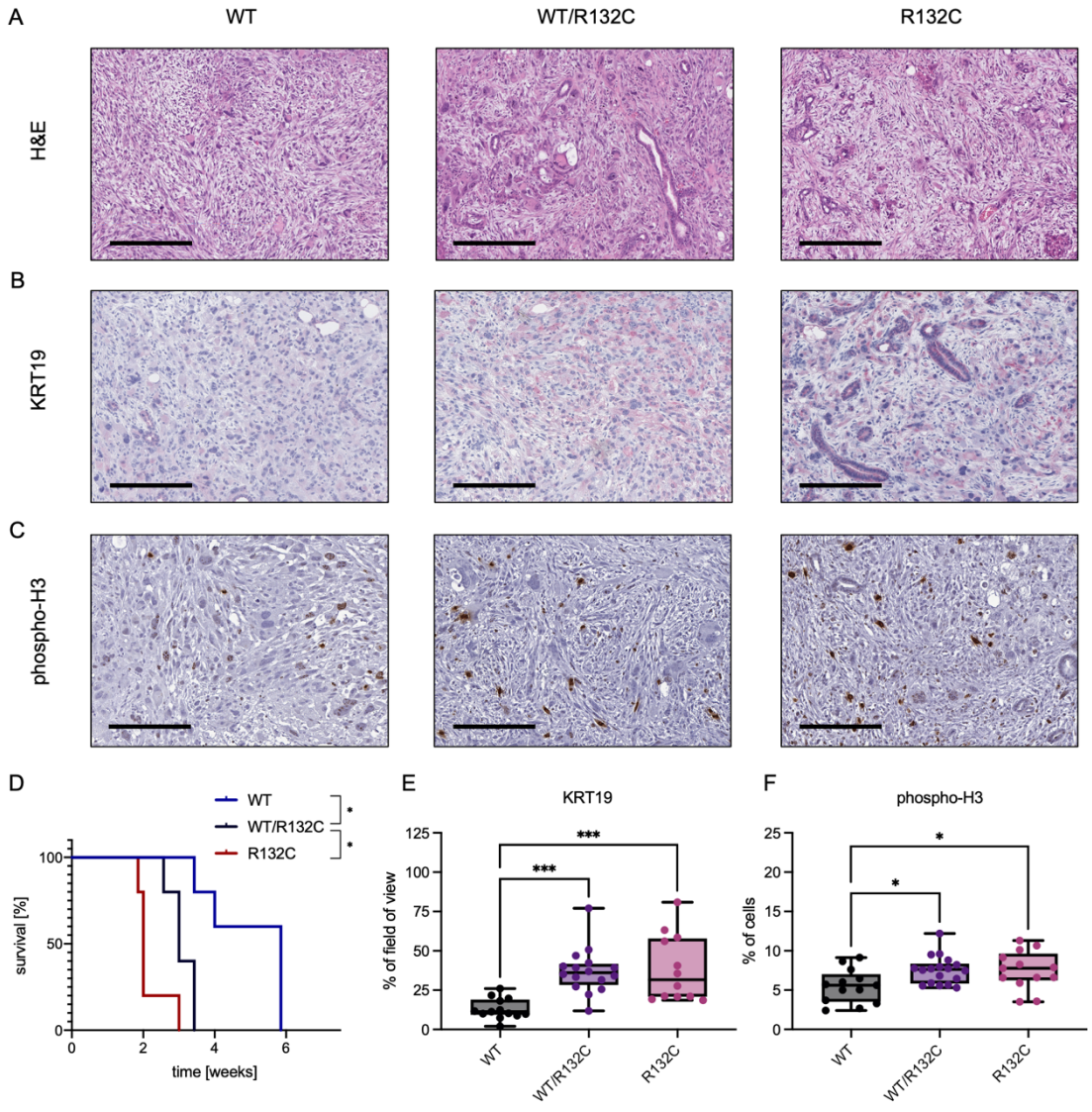

Figure 10. Correlation of histological characteristics with survival in KRAS;TP53;IDH1-tumor-bearing mice.
A. H&E staining of tumor samples showcasing representative histological features. B&C. IHC analysis of KRAS;TP53;IDH1 tumors, representative images of tumor samples, scale bar: 300 µm. B. KRT19, C. SOX9, D. Kaplan-Meier survival analysis of KRAS;TP53;IDH1-tumor-bearing mice, p-value: *=p≤0.05 (log-rank (Mantel-Cox) test) E. and F. Quantification corresponding to B. and C., respectively. Each data point represents a field of view, *=p≤0.05, ***=p≤0.001 (one-way ANOVA with post hoc Tukey's test).

4.2.1. Exploring the impact of IDH1 expression balance on tumor characteristics in KRAS;TP53;IDH1 mice

Building on the observed phenotypic variations, I aimed to elucidate the relationship between IDH1 expression levels and phenotypic diversity in KRAS;TP53;IDH1-tumor-bearing mice. The central inquiry focused on whether the phenotypic differences were indeed a direct outcome of the variable IDH1 WT and mutant expression levels and the consequent 2-HG production.

To address the concern of overexpression of the IDH1 mutant compared to the IDH1 WT, I designed an experiment where mice were administered either IDH1 WT (referred to as "WT"), a 1:1 mixture of IDH1 WT and IDH1 R132C ("WT/R132C"), or IDH1 R132C alone ("R132C"), along with a KRAS;TP53 plasmid mixture through HTVi. This approach allowed for a controlled variation in equilibrium of IDH1 WT and mutant expression and 2-HG levels, enabling a detailed observation of their impact on tumor development.

In line with my previous findings, the IDH1 WT/R132C group exhibited an intermediate phenotype, serving as a bridge between the characteristics of WT and R132C groups. Histological analysis confirmed that the presence of the IDH1 mutant was essential for the observed increase in glandular morphology and stromal presence (**Figure 10A**). A similar trend was evident in IHC analyses. Markers such as KRT19 and phospho-H3 indicated almost 2-times increase in expression levels when comparing WT group to WT/R132 group, and to R132C group (**Figure 10B&E and C&F**), reflecting an upward shift in cholangiocytic phenotype and proliferation rate, respectively.

Moreover, the survival rate of mice in the WT/R132C group, though not reaching the longevity of up to 6 weeks seen in the WT group, was notably greater than the roughly 2-week survival span of the R132C group (**Figure 10D**).

In summary, the presence of mutant IDH1 emerges as the key determinant in influencing tumor phenotype through 2-HG production. Meanwhile, the level of expression of IDH1 mutant plays a crucial role in dictating survival outcomes. These findings underscore the significant impact of this equilibrium in shaping tumor dynamics and their underlying molecular mechanisms.

4.3. Epigenetic alterations: exploring histone and DNA methylation dynamics

IDH1 mutations are widely recognized for their profound epigenetic effects, notably affecting DNA and histone methylation, a conclusion supported by extensive research [134], [164], [167], [217], [218]. Additionally, I explored how these mutations through elevated 2-HG levels might alter methylation and affect gene expression and cellular behavior in the context of KRAS;Tp53;IDH1. This exploration into the epigenetic ramifications of *IDH1* mutations within this specific oncogenic context underscores the intricate molecular mechanisms driving tumor formation and progression.

4.3.1. Mapping methylation: differences between IDH1 WT and mutant tumors

To investigate the epigenetic changes associated with *Idh1* mutations, I first examined their influence on DNA methylation. Recognizing that dot blot assays lack the sensitivity to detect nuanced differences in methylation, I chose to use a methylation array method.

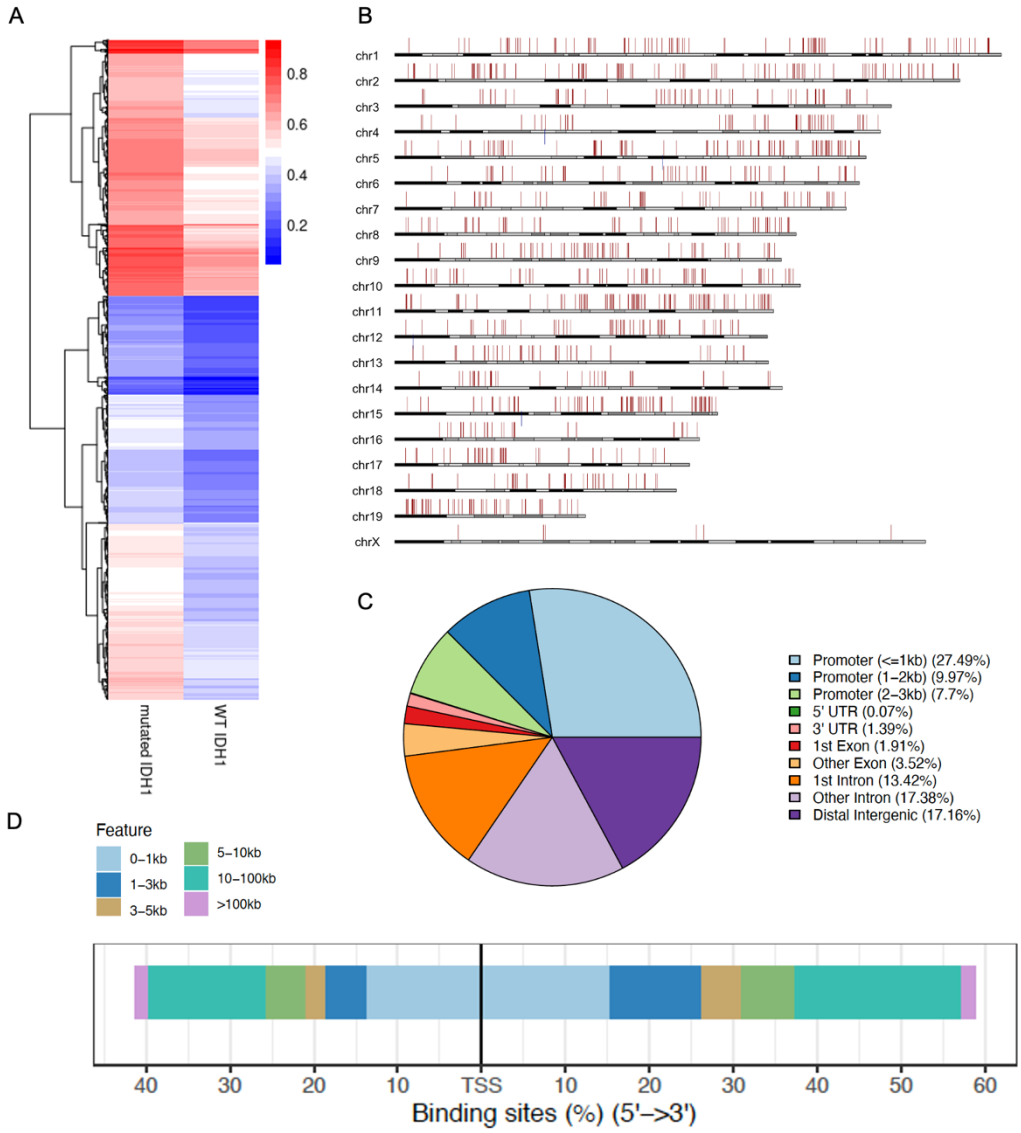

Figure 11. Comparative analysis of methylation in KRAS;TP53;IDH1 tumors.

A. Heatmap visualization of DMRs between IDH1 mutant and IDH1 WT tumor samples. The heatmap shows row z-scores for all identified DMRs (p-value threshold: ≤0.05, $\log_2$ of the mean quotient in means across all sites in a region threshold: ≥|1.5|) B. Spatial distribution of DMRs on chromosomes. C. Overview of hypermethylation alterations in IDH1 mutants vs. IDH1 WT. D. Analysis of hypermethylation distribution proximal to TSS in IDH1 mutants.

This technique permitted a thorough examination of the genome-wide methylation status in KRAS;TP53;IDH1 tumor tissue samples, with a particular focus on differentially methylated regions (DMRs) that could impact gene expression.

The analysis revealed distinct methylation patterns between IDH1 WT and mutant tumors. With a p-value threshold of < 0.05 and a $\log_2$ of the mean quotient in means across all sites in a region set to ≥|1.5|, 1361 DMRs were identified as hypermethylated, while 4 DMRs were hypomethylated. A heatmap visualization of DMRs indicated a trend towards hypermethylation in mutant samples in comparison to their IDH1 WT counterparts (**Figure 11A**). Mapping these DMRs across chromosomes showed a widespread distribution (**Figure 11B**), underscoring the extensive impact of *Idh1* mutations on the epigenetic landscape.

The interpretation of these methylation changes can be approached from two analytical perspectives: by examining the location of DMRs (such as promoter, exon, intron, UTR, distal intergenic) or by assessing their proximity to transcription start sites. Each perspective offers valuable insights into the epigenetic consequences of *Idh1* mutations.

A considerable proportion of the identified DMRs, approximately 45%, are situated within *Promoter* regions, indicating potential effects on gene transcription initiation due to hypermethylation in IDH1 mutants (**Figure 11C**). DMRs in *Distal intergenic* regions (17.2%) and within gene bodies – *Other exons* (3.5%), *Other introns* (17.4%) – suggest varied impact on gene expression and possibly splicing patterns. Methylation in the *First intron* (13.4%) might disrupt promoter and splicing regulation [271].

Close to TSS, 30% of hypermethylated DMRs could directly influence transcriptional activity, while 45% of DMRs in the 5-100 kb range from TSS may modulate regulatory element activity in a context-dependent manner (**Figure 11D**).

Further comparative analysis focused strictly on differences between IDH1 R132C and WT tumors. Firstly, heatmap visualization of DMRs indicated hypermethylation in IDH1 mutant samples when compared to WT tumors (**Figure 12A**). In the next step, Reactome analysis highlighted differential methylation patterns affecting cellular pathways.

An increase in methylation within cell death pathways suggested a possible mechanism for enhanced tumor cell survival (**Figure 12B**). Such a pattern could lead one to hypothesize that tumors with the KRAS;TP53;IDH1 mutations may possess enhanced survival properties, effectively evading the usual cell death mechanisms. Yet, when I tested this theory using a biological marker – staining with cleaved Caspase 3, which indicates apoptosis or programmed cell death [272] – the results did not support this hypothesis (**Figure 12C**), indicating that the relationship between methylation and *Cell death* pathways might be more complex than anticipated in this case.

When examining the enrichment in *Extracellular matrix* (ECM) pathways, the results were somewhat unexpected. Reflecting on prior experiments, one might have envisioned an opposing methylation trend – specifically, that the ECM-related pathways might exhibit a methylation dip, not a surge (**Figure 12D**). This unexpected trend could suggest that the methylation differences I observed are inherently dynamic in nature, rather than rigidly deterministic within this experimental context.

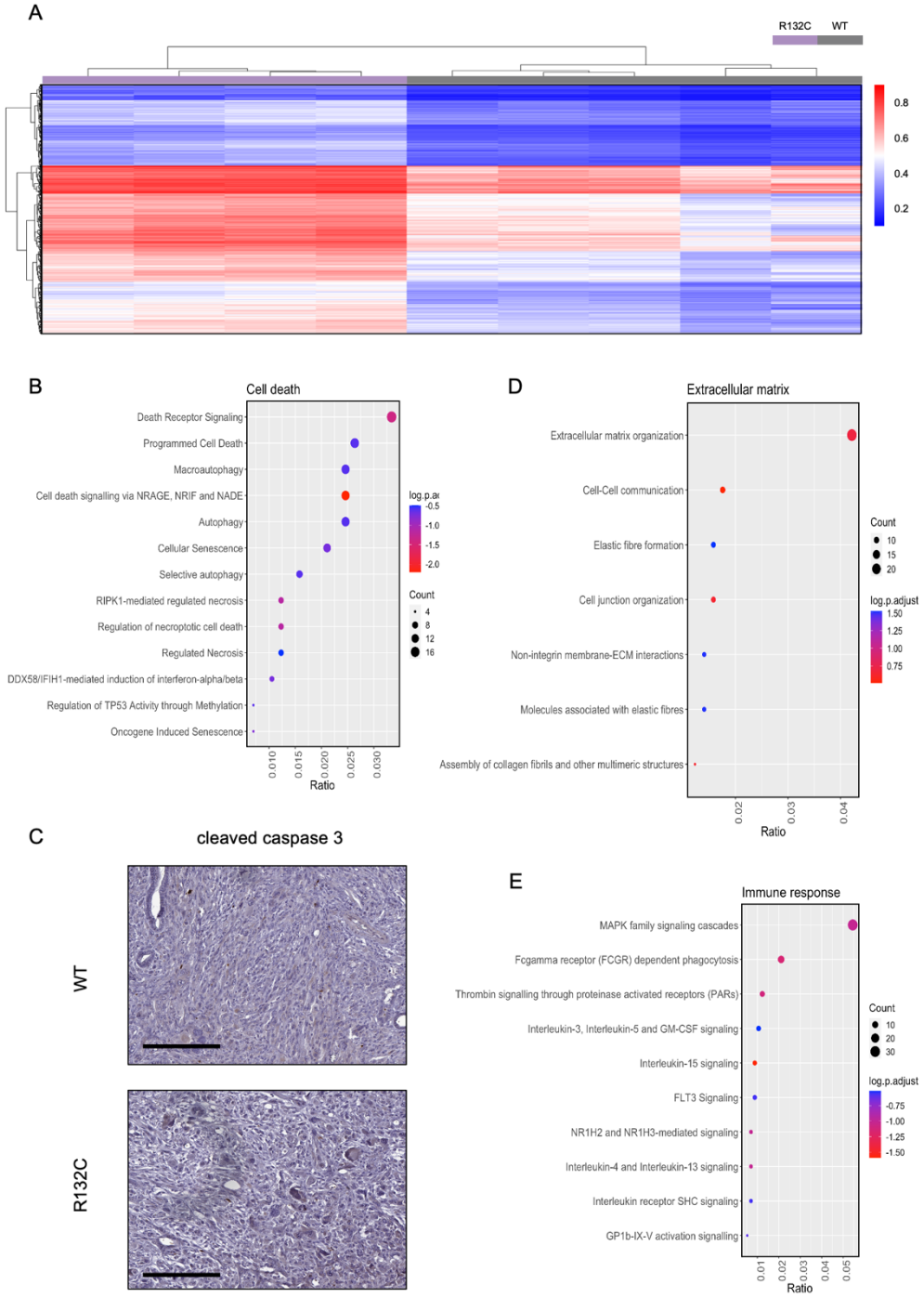

Figure 12. Differential methylation patterns and pathway enrichment in IDH1 R132C mutant tumors.
Heatmap representation of DMRs between IDH1 R132C mutant tumor samples and their IDH1 WT counterparts. The heatmap shows row z-scores for all identified DMRs (p-value threshold: ≤0.05, $\log_2$ of the mean quotient in means across all sites in a region threshold: ≥|1.5|). B, D, & E. Functional pathway enrichment analyses: B. Cell death, D. Extracellular matrix, and E. Immune response pathways. The depth of the color for each pathway signifies the log of the p-value adjusted for multiple comparisons. Horizontal graph length denotes the gene ratio, while circle area indicates gene counts within each pathway. C. Immunohistochemical analysis of cleaved Caspase 3 in KRAS;TP53;IDH1 tumors, representative images of tumor samples, scale bar: 300 µm.

This data also underscores a significant increase in methylation across *Immune response*-related pathways, potentially steering the tumor microenvironment towards immune suppression (**Figure 12E**) [62], [273], [274], [275]. Accurately gauging the exact ramifications calls for a granular exploration of each pathway's role within the tumor microenvironment.

Subsequent chapters will explore the dynamics of immune response and ECM in iCCA, building on the established connection between 2-HG accumulation and the tumor microenvironment (**Chapter 4.4**). The key takeaway from these findings is that the accumulation of 2-HG in IDH1 mutant tumors is associated with DNA hypermethylation, which could have significant implications for gene expression and tumor behavior.

4.3.2. Understanding the link between 2-HG accumulation and DNA methylation patterns

Building on the established link between 2-HG and increase in methylation via TET enzyme inhibition [273], I next aimed to explore the potential mechanistic link between this interaction to the phenotypic alterations observed KRAS;TP53;IDH1 tumor development. I hypothesized that the 2-HG-mediated inhibition of TET enzymes could be a pivotal factor driving the observed phenotypic changes.

To test this hypothesis, I utilized CRISPR/Cas9 technology to disrupt the *Tet1* or/and *Tet2* genes, aiming to replicate the hypermethylation and phenotypic changes induced by 2-HG accumulation, along with a KRAS;TP53 plasmid mixture through HTVi. The disruption of *Tet1* or/and *Tet2* was confirmed using the T7 endonuclease I assay, as visualized by distinct bands on agarose gel electrophoresis (**Figure 13A&B**). However, contrary to the hypothesis, the histological analysis did not reveal the anticipated stromal or glandular morphology changes akin to those caused by 2-HG accumulation in KRAS;TP53;IDH1 tumor upon disruption of *Tet* genes (**Figure 13C**).

Further histological examination showed a one-fold increase in KRT19 expression in the *Tet1*/*Tet2* knock-out tumors in comparison to the KRAS;TP53 control tumors (**Figure 13D&F**). This was not observed in tumors with individual knock-outs, suggesting that a significant reduction in TET activity is necessary to drive the phenotypic changes seen with 2-HG accumulation.

Nonetheless, no significant differences between the groups were noted in phospho-H3 staining (**Figure 13E&G**), and survival rates of tumor-bearing mice from different groups remained unchanged (**Figure 13H**).

The findings indicate that simply disrupting *Tet1* or/and *Tet2* does not fully replicate the phenotypic alterations induced by 2-HG accumulation in iCCA, nor does it affect tumor survival in this context. This suggests that the path from 2-HG accumulation to the observed tumor phenotype in this iCCA model is not solely dependent on the inhibition of TET enzymes and points to a more complex network of (epigenetic) regulation at play.

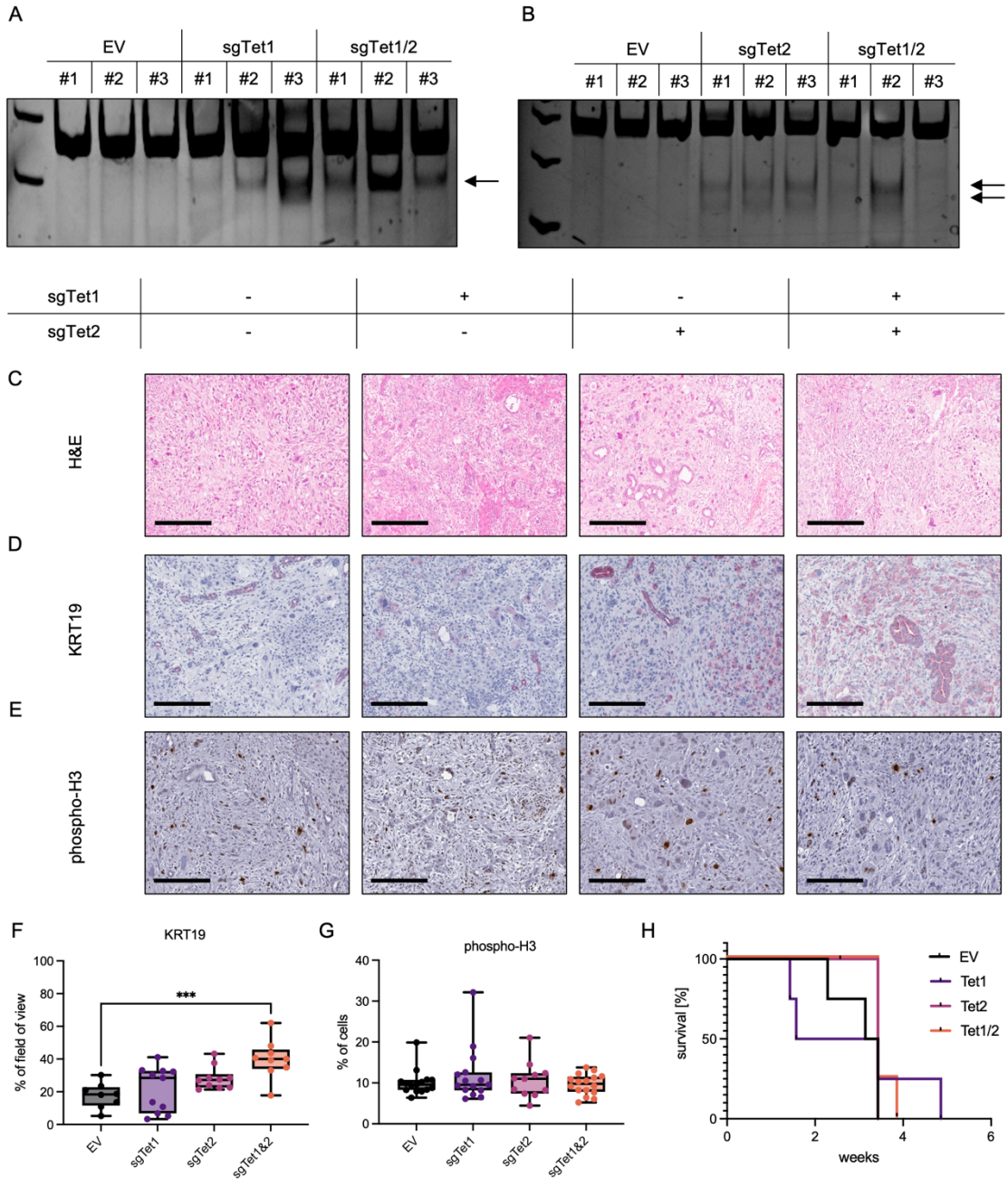

Figure 13. Exploring the effects of *Tet1/2* gene disruption in KRAS;TP53-driven tumors.

Agarose gel electrophoresis demonstrating A. *Tet1*, and B. *Tet2* disruption using the T7 endonuclease I assay, arrows indicate expected cleavage products. C. H&E staining of tumor samples showcasing representative histological features. Immunohistochemical analysis of KRAS;TP53;IDH1 tumors, representative images of tumor samples, D. KRT19, and E. phospho-H3, F. and G. corresponding quantification. Each data point represents a field of view, ***=p≤0.001 (one-way ANOVA with post hoc Dunnett's test). C, D, E. scale bar: 300 µm. H. Kaplan-Meier survival analysis of KRAS;TP53;TET1/TET2-tumor-bearing mice (log-rank (Mantel-Cox) test).

4.3.1. Probing the effects of 2-HG on histone methylation patterns

Building on these insights, the next phase of the investigation turned its focus to the effects of 2-HG on histone methylation patterns. Specifically, the focus was on histone methylation marks that are pivotal in gene expression regulation and have been previously associated with increased levels of 2-HG [217], [274], [275], [276], [277].

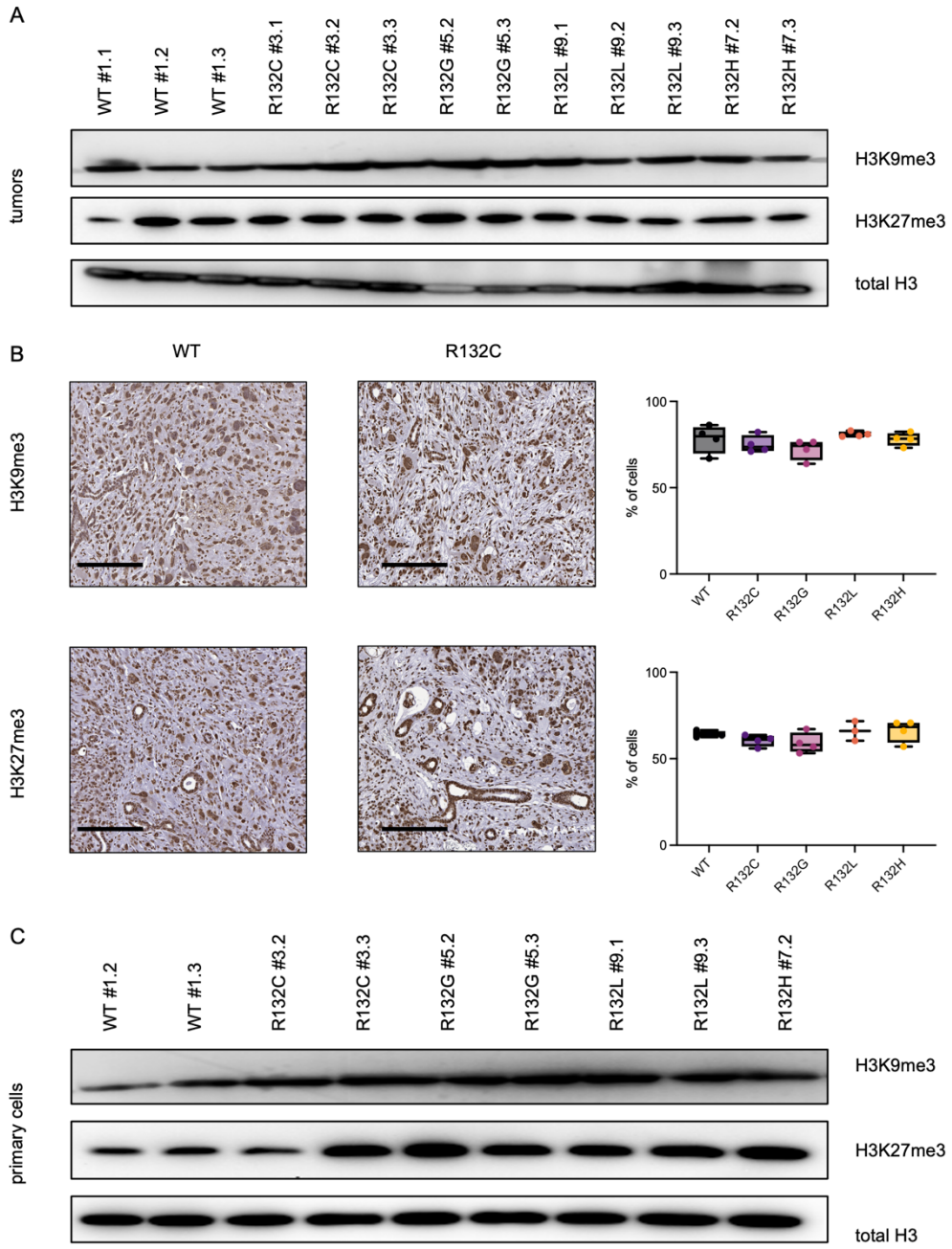

Figure 14. Analysis of histone methylation in context of 2-HG accumulation.

Western blot analysis of total H3K9me3 and H3K27me3 in KRAS;TP53;IDH1 A. tumor samples, and C. tumor-derived primary cell lines. B. Immunohistochemical analysis of KRAS;TP53;IDH1 tumors; top: H3Kme3, bottom: H3K27me3. Left: representative images of tumor samples, scale bar: 300 µm; right: corresponding quantification. Each data point signifies an individual mouse.

To explore this, I utilized WB analysis which indicated a modest increase in total H3K9me3 levels in IDH1 R132C and R132G mutants, whereas there were no differences in total H3K27me3 between tumor tissue samples (**Figure 14A**). IHC analysis corroborated these findings, showing no significant differences in the levels of H3K9me3 and H3K27me3 in KRAS;TP53;IDH1 tumors (**Figure 14B**).

However, when examining histone methylation in the more homogeneous environment of tumor-derived primary cell lines, a clearer pattern emerged. There was a notable increase in both H3K9me3 and H3K27me3 total levels in the IDH1 mutant cell lines in comparison to IDH1 WT samples, with a particularly evident trend for H3K9me3 (**Figure 14C**).

The takeaway from these observations is that while very subtle, if any, 2-HG-associated changes are detectable in histone methylation patterns in KRAS;TP53;IDH1 tumor samples, more pronounced alterations are evident in tumor-derived primary cell lines. In the *in vitro* setting, I was able to observe a connection between *Idh1* mutation and increase in total H3K9me3 and H3K27me3 levels. This suggests that 2-HG can indeed influence the epigenetic landscape, potentially affecting gene expression and cellular behavior in this iCCA model.

4.3.2. Transcriptional insights into IDH1 mutant tumor progression

To decode transcriptional changes in IDH1 mutant tumors, I employed RNA-seq analysis. This powerful tool allowed me to scrutinize the gene expression profiles of tumor tissues, aiming to uncover the specific transcriptional changes occurring in IDH1 mutant tumors and how these alterations could drive tumor development and progression.

The comparative analysis between IDH1 WT and individual IDH1 mutants showed that IDH1 R132C mutant exhibited the most distinct transcriptional profile (data not shown), prompting a focused subsequent examination between IDH1 WT and the R132C mutant.

With a p-value threshold of <0.05 and $\log_2$fold change threshold value set at > |1.5|, 108 genes were identified as downregulated, while 168 genes were upregulated, as depicted in the volcano plot (**Figure 15A**). Ingenuity Pathway Analysis (IPA) was utilized to interpret the data, focusing on the identification of any significant changes in signaling pathways.

The results from the RNA-seq revealed an increase in kinetochore metaphase signaling (**Figure 15B**), a critical indicator of cell cycle progression, which could imply a state of rapid cellular division [278], [279]. A corresponding decrease in G2/M damage checkpoint regulation was also observed, pointing towards a potential mechanism for the tumors to bypass DNA damage control, thereby promoting genomic instability [221]. Delving deeper into this observation, I looked into abundance of phospho-H2A.X, a known sensitive molecular marker of DNA damage [280], in KRAS;TP53;IDH1 tumors. This analysis revealed that there is an upward trend in level of this marker in the IDH1 mutant tumors, but it is only significant for IDH1 R132C tumors (**Figure 15C**).

These findings indicate that the accumulation of 2-HG in IDH1 mutant tumors leads to a change in the tumor microenvironment (TME), marked by rapid cell proliferation and the

evasion of DNA damage checkpoints. These factors underscore the profound impact of IDH1 mutant activity and 2-HG levels on tumor behavior.

Additionally, IPA highlighted a notable upregulation in the biosynthesis of GAGs, specifically chondroitin and heparan sulfates (**Figure 15B**), which are key components of ECM in liver cancer.

Overall, the RNA-seq results not only corroborate earlier observations (**Chapter 4.1**) but also strengthen the link between 2-HG accumulation and phenotypic changes in IDH1 mutant tumors, suggesting a consistent and coherent mechanistic thread where 2-HG in promotes rapid tumor growth and alters the TME, thus contributing to the aggressive phenotype observed in IDH1 mutant tumors.

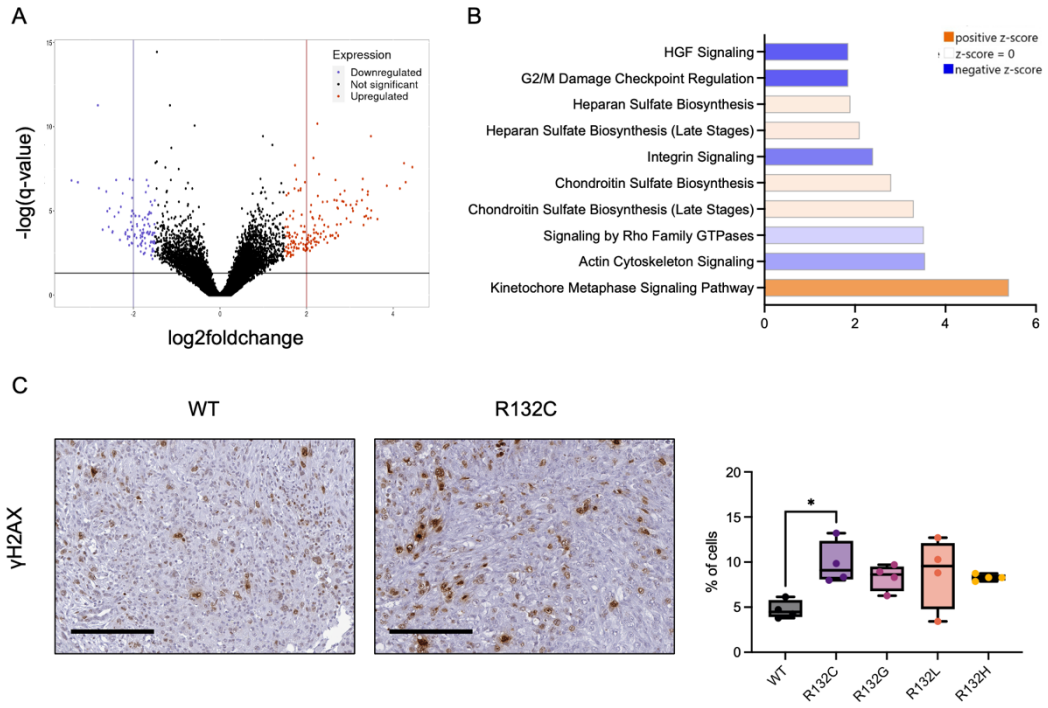

Figure 15. Evaluating transcriptional differences between IDH1 R132C mutant and IDH1 WT KRAS;TP53 tumors.
A. Volcano plot highlighting genes differentially expressed between IDH1 R132C mutant and IDH1 WT (p-value threshold: ≤0.05, black line; log_2foldchange threshold: ≥1.5, red data points; log_2foldchange threshold: ≤-1.5, blue data points, log_2foldchange = 2, red line; log_2foldchange = -2, blue line). B. IPA (employing a 1.75-fold change threshold) of differentially expressed genes. C. IHC evaluation of phospho-H2A.X in KRAS;TP53;IDH1 tumors; representative tumor images on the left with associated quantification on the right. Each data point signifies an individual mouse, *=p≤0.05 (one-way ANOVA with post hoc Tukey's test), scale bar: 300 µm.

4.4. Immune, stromal, and ECM interactions in iCCA context of 2-HG accumulation

My previous results implicated a marked remodeling of the tumor stroma due to 2-HG accumulation. Thus, I further analyzed changes in the TME, particularly effects on immune and

stromal cell interactions, and the resulting implications for cancer progression and treatment response.

4.4.1. Unveiling the impact of 2-HG on the cellular underpinnings of the tumor stroma

To gain first insights into changes in the TME, I employed the murine Microenvironment Cell Populations-counter (mMCP-counter), a robust method for quantifying immune and stromal cell populations in murine bulk RNA-seq samples [281]. The analysis highlighted marked differences, particularly in *Fibroblasts* representing stromal cells, as well as in *Vessels* and *Lymphatics*, which are indicative of the tumor's vasculature (**Figure 16A**).

Increased presence of Desmin (DES) and alpha-Smooth muscle actin (α-SMA), markers of myofibroblasts and activated fibroblasts, respectively [282], [283], suggests that the TME of iCCA-specific IDH1 mutant tumors are densely populated with these cells (**Figure 16B&C**).

The expression levels of DES and α-SMA were significantly elevated in these IDH1 mutants compared to WT counterparts. Specifically, DES expression in IDH1 R132C and R132G mutants showed a three-fold increase, while α-SMA expression was three-fold higher in IDH1 R132C and R132L mutants. In IDH1 R132G mutants, α-SMA expression was even more elevated, exhibiting a five-fold increase. In contrast, the IDH1 R132H mutant displayed expression levels that was not significantly different in comparison to IDH1 WT counterparts.

I further examined vascular changes by staining for CD31 (Cluster of differentiation 31, also known as Platelet/endothelial cell adhesion molecule-1) and ETS-related gene (ERG), both markers for endothelial cells indicative of blood vessels [284], [285] (**Figure 16C&D**). While there was a trend toward increased vessel prevalence in the IDH1 mutant tumors in comparison to IDH1 WT tumors, it was not statistically significant, except in the IDH1 R132C tumors when stained for ERG. Furthermore, I did also not observe significant differences in abundance of lymphatic vessels (data not shown).

The accumulation of' 2-HG in iCCA leads to a notable enrichment of activated fibroblasts in the tumor microenvironment, suggesting a shift toward a fibrotic stroma, potentially impacting the ECM composition. Despite this stromal activation, the data does not demonstrate a corresponding increase in blood or lymphatic vessel formation, suggesting a selective effect of 2-HG on the stromal cell components within the TME in the context of KRAS;TP53;IDH1 tumor formation.

4.4.2. Elucidating ECM dynamics in IDH1 mutant iCCA via mass spectrometry

Next, my study investigated the impact of *Idh1* mutations on the structure and composition of the ECM within the TME, utilizing mass spectrometry for detailed insights. I adopted a method outlined by McCabe *et al.* [286], extracting both intracellular fractions and those enriched in ECM components from KRAS;TP53;IDH1 tumor tissue samples (**Figure 17A**).

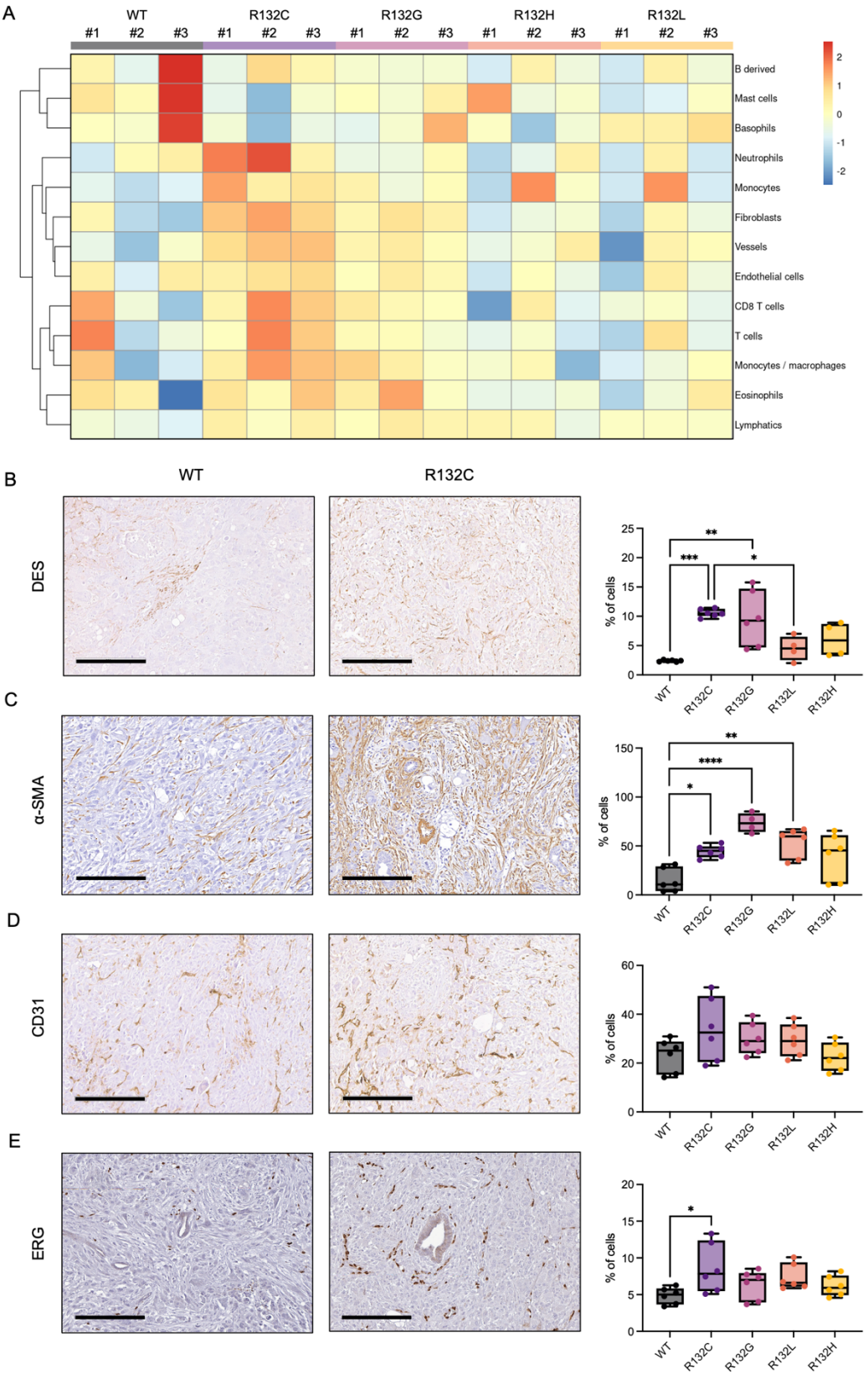

Figure 16. Immune and stromal cell landscape in KRAS;TP53;IDH1 tumors.

A. Heatmap showing scores for immune and stromal cell populations calculated with mMCP-counter. The heatmap illustrates row Z-scores for all included cell populations. Immunohistochemical analysis of

KRAS;TP53;IDH1 tumors, left: representative images of tumor samples, scale bar: 300 µm; right: corresponding quantification. B. DES, C. α-SMA, D. CD31, E. ERG, Each data point signifies an individual mouse. *=p≤0.05 and **=p≤0.01, ***=p≤0.001, ****=p≤0.0001 (one-way ANOVA with post hoc Tukey's test).

The ensuing proteomic analysis discerned between intracellular and extracellular samples, revealing a distinct, less complex composition in the ECM-enriched samples (**Figure 17B**). Subsequent analysis was then directed towards comparing ECM-enriched fractions from IDH1 WT and IDH1 R132C samples.

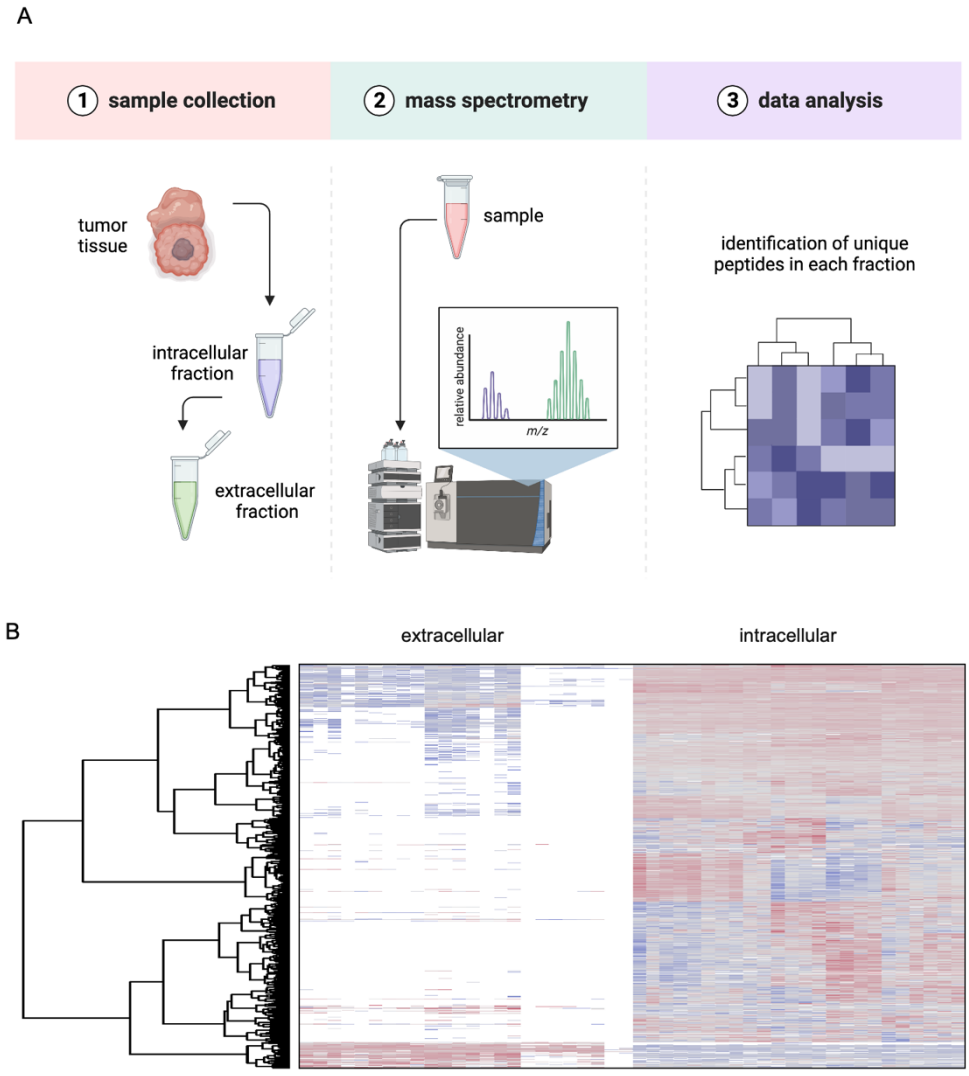

Figure 17. Proteomic profiling: intracellular vs. ECM components in KRAS;TP53;IDH1 samples.
A. Schematic illustrating the isolation process for ECM-enriched samples from KRAS;TP53;IDH1 tumors. B. Heatmap visualization of isolated intracellular and ECM-enriched components showcasing differential protein expressions based on intensity-based absolute quantification, and highlighting contrasts between intracellular and ECM-enriched fractions.

First, I used IPA which showed the upregulation of the *Integrin signaling pathway* in the IDH1 R132 ECM-enriched samples, which is critical for cell-ECM communication and adhesion [287], [288], and indicates an ongoing matrix reconfiguration (**Figure 18A**). Enhanced *Leukocyte extravasation* pointed to a robust immune response, directing white blood cells from circulation into the tumor [289], [290]. Additionally, the presence of *Neutrophil extracellular traps* (NETs), intricate structures formed by neutrophils to trap and neutralize pathogens [291], added another layer of complexity to the immune dynamics.

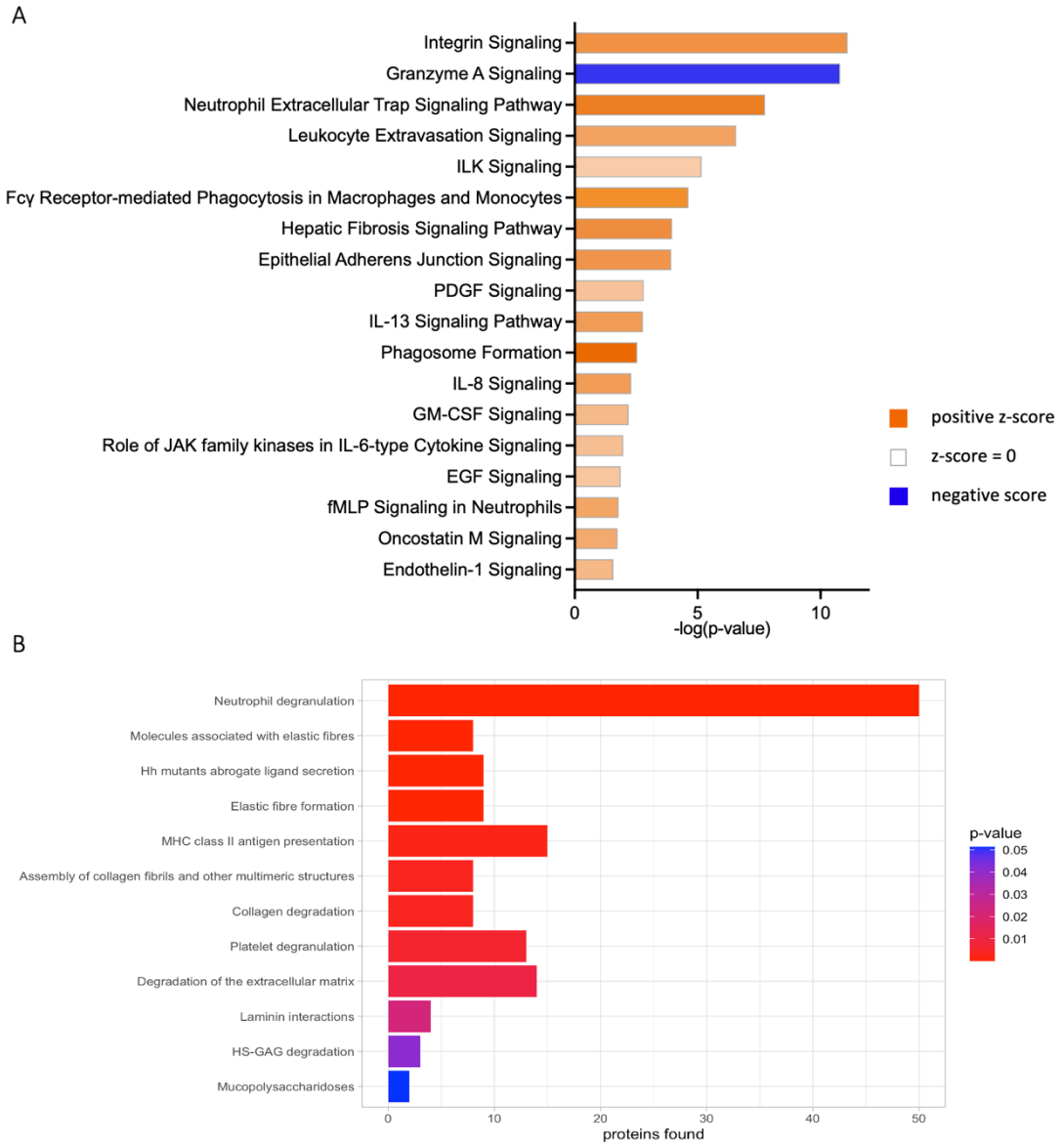

Figure 18. Dynamic alterations in the ECM composition and immune response in IDH1 mutant tumors.
Comparison between IDH1 mutant ECM-enriched samples and IDH1 WT counterparts. A. IPA (p-value threshold: ≤0.05, $\log_2$foldchange threshold: ≥|1.5|). B. Reactome analysis (p-value threshold: ≤0.05).

Furthermore, this seeming increase in immune activity is accompanied by a noticeable decrease in granzyme A signaling, a mechanism critical for cytotoxic T-cells and NK cells to

initiate target cell apoptosis [292]. This observation suggests a potential compromise in the TME's immune surveillance capabilities.

The Reactome analysis further revealed a significant increase in *Neutrophil degranulation* activities in IDH1 R132C mutant samples (**Figure 18B**). This process, involving the release of granules packed with antimicrobial and signaling molecules [293], suggests an intensified inflammatory response, potentially exerting a profound influence on the ECM [291]. This process is often tied to pronounced matrix remodeling as these immune cells release enzymes and reactive species that degrade and transform ECM components [291], [293].

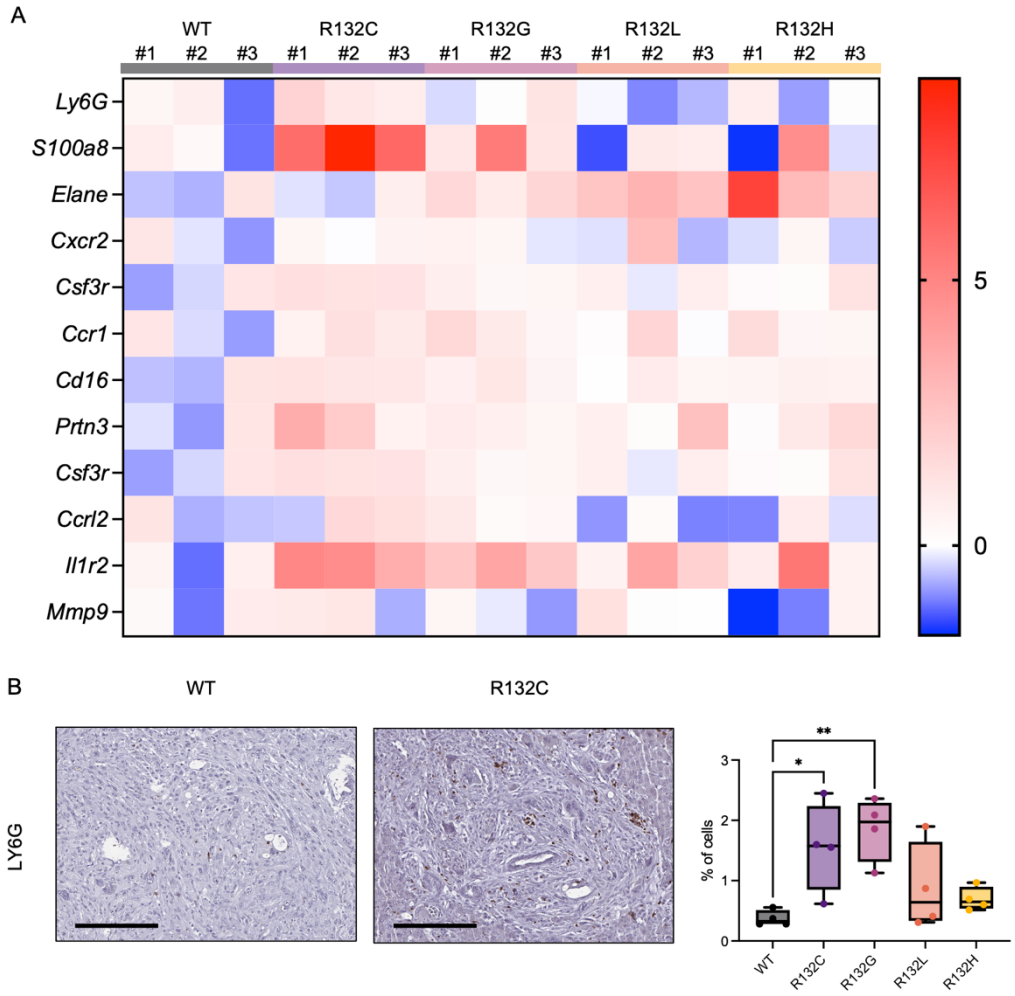

Figure 19. Neutrophil infiltration in KRAS;TP53;IDH1 mutant tumors.

A. Heatmap representation of gene expression profiles for liver neutrophil markers. The color gradient within the heatmap denotes row Z-scores for each cluster gene marker, offering a comparative view of their expression levels. B. Immunohistochemical evaluation demonstrates LY6G presence in KRAS;TP53;IDH1 tumor samples. Left: representative images of tumor samples, scale bar: 300 µm; right: corresponding quantification. Each data point represents a field of view, *=p≤0.05, **=p≤0.01 (one-way ANOVA with post hoc Dunnett's test).

In the next step, I focused on examining the neutrophil infiltration into KRAS;TP53;IDH1 tumors. For this purpose, I employed liver neutrophil markers identified through CellMarker 2.0, database of manually curated cell markers in human/mouse, supplemented by web tools

based on single cell RNA-seq data. This analysis indicated a trend of upregulation of these markers in IDH1 R132C and R132G mutants compared to IDH1 WT counterparts (**Figure 19A**). Delving deeper into this phenomenon, IHC staining revealed an increase in LY6G-positive cells, typically indicative of neutrophil presence on the protein level [294], in the same IDH1 mutant samples from the KRAS;TP53;IDH1 cohort (**Figure 19B**). Specifically, R132G and R132C mutants demonstrated an elevated expression of neutrophil markers on mRNA and protein level.

Additionally, the observed upregulation of *Elastic fiber formation* and *Assembly of collagen fibril and other multimeric structures* suggests a structurally reinforced ECM (**Figure 18B**). Yet, this reinforcement is countered by the concurrent *Collagen degradation* and *Heparan sulfate proteoglycans (HS-GAGs) degradation*, implying a dynamic equilibrium between ECM strengthening and breakdown, characteristic of a TME with rapid turnover.

On the cytokine front, as revealed by IPA, the surge in *IL-6-type*, *IL-8*, *IL-13* and *GM-CSF signaling* underscored a multifaceted immune response in TME (**Figure 18A**). These interleukins are implicated in a range of processes, from collagen synthesis and neutrophil recruitment to fibrosis, highlighting their central roles in both immune responses and ECM dynamics [295], [296].

In summary, this thorough analysis has exposed a sophisticated network of immune modulation, potential evasion tactics, and extensive ECM remodeling within IDH1 mutant context. These findings do more than just delineate the molecular complexities of IDH1 mutant tumors and the dynamic shifts of the ECM; they underscore the imperative to dissect these alterations at a mechanistic and molecular level to fully grasp their implications in tumor progression and therapy.

4.4.3. Delineating immune cell infiltration in IDH1 mutant tumors

In an effort to discern the differences in immune cell infiltration between IDH1 mutant and IDH1 WT tumors, I drew initial insights from mMCP-counter (**Figure 16A**). Given the ambiguous results from this method, I then applied the CCA-specific matrix, established by Nishida *et al.* [297], to more accurately classify the interactions of immune cells within the TME of this tumor type, based on bulk RNA-seq findings.

While in this case again the RNA-seq results did not yield starkly distinct patterns, they provided tentative insights into the immune landscape of IDH1 mutant tumors (**Figure 20**). I observed a downregulation of *Immune checkpoint molecules* within IDH1 mutant tumors in comparison to IDH1 WT tumors, which could potentially alter the therapeutic landscape, particularly affecting the efficacy of immune checkpoint blockade therapies [298].

Additionally, there was a downregulation of genes linked to MHC class I presentation and processing (*H2-K1*, *H2-D1*, *B2m*, *Tap1*) a pattern that could effectively render the tumor cells less visible to immune surveillance by cytotoxic T cells [299], promoting a state conducive to immune evasion. Conversely, the upregulation of genes involved in MHC class II antigen presentation (*H2-DMb2*, *H2-DMb1*, *H2-Dma*, *H2-Ob*, *H2-Oa*) could represent a compensatory mechanism or an attempt to enhance helper T cell responses [299]. However, this may also

lead to an immunosuppressive environment if regulatory T cells (Tregs) are preferentially activated, which play known role in dampening immune responses [300]. Furthermore, the inconsistent pattern observed in the expression of *Cytolytic markers*, crucial for understanding the immune system's engagement and efficacy against tumor cells, underscores the complexity and variability of the tumor immune landscape in IDH1 mutant tumors.

This analysis also unveiled an increase in signaling and activation-related markers, suggesting a TME that is perhaps on high alert or primed for action. This activated state, however, is counterbalanced by an increased presence of markers tied to Tregs. This increased presence of Treg markers suggests a tumor environment skilled in disguising itself, effectively hindering the host's immune response.

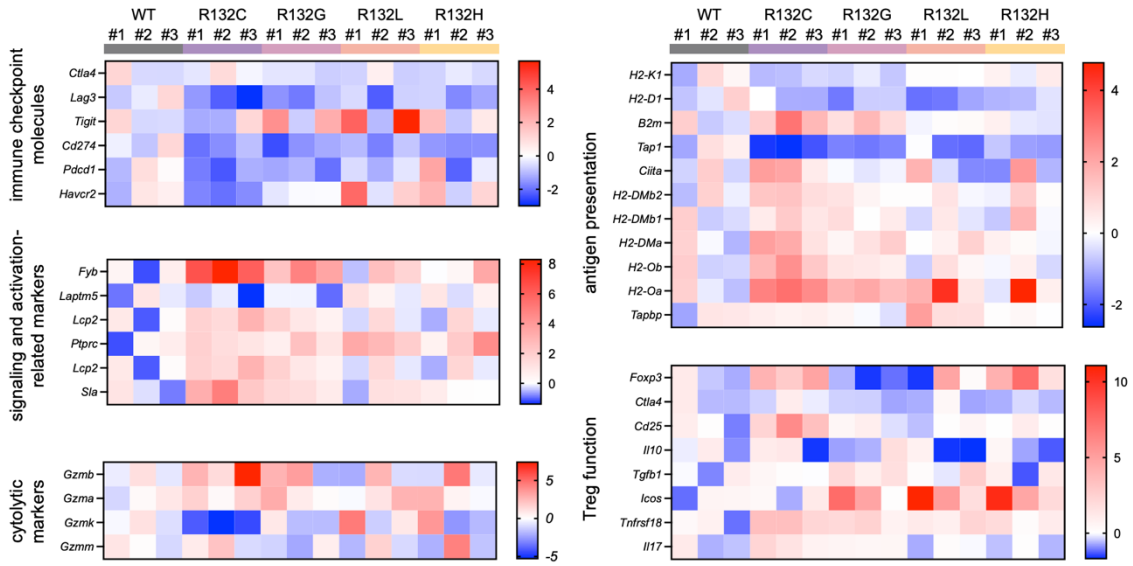

Figure 20. Gene expression landscape in KRAS;TP53;IDH1 tumors: a glimpse into inflammation signatures.
Heatmap representation of gene expression profiles for T cell associated gene sets. The color gradient within the heatmap denotes row Z-scores for each cluster gene marker, offering a comparative view of their expression levels.

To validate these insights, I turned to IHC stainings. I began with CD3 staining, a marker of T-cells [301]. This revealed at least a one-fold increase in T-cell infiltration in nearly all IDH1 mutant tumors (**Figure 21A**).

Next, I examined infiltration of CD4-positive cells, with CD4 being the marker for helper T-cells [301]. The results followed a similar pattern to data obtained from CD3 staining, showing a one-fold increase in CD4-positive cells in almost all IDH1 mutant samples (**Figure 21B**). Notably, for both CD3 and CD4 staining, all IDH1 mutants, with the sole exception of IDH1 R132L group, demonstrated an increase in these markers. This pointed towards a TME in IDH1 mutant tumors which is potentially rich in immune activity, which could be either pro-tumoral or anti-tumoral.

Considering earlier insights from CCA-specific matrix, and the data obtained from methylation array and mass spectrometry analysis which hinted at inflammation in TME as well

as immunosuppression, I next assessed the infiltration of CD8-positive cells. CD8 is a marker of cytotoxic T-cells (also known as CTLs), which when activated are key players in targeting and killing tumor cells [302]. Interestingly, the only IDH1 mutant to show an increase in this marker was IDH1 R132L (**Figure 21C**), which might suggest a shift towards anti-tumoral immune activity and tumor growth inhibition in this group.

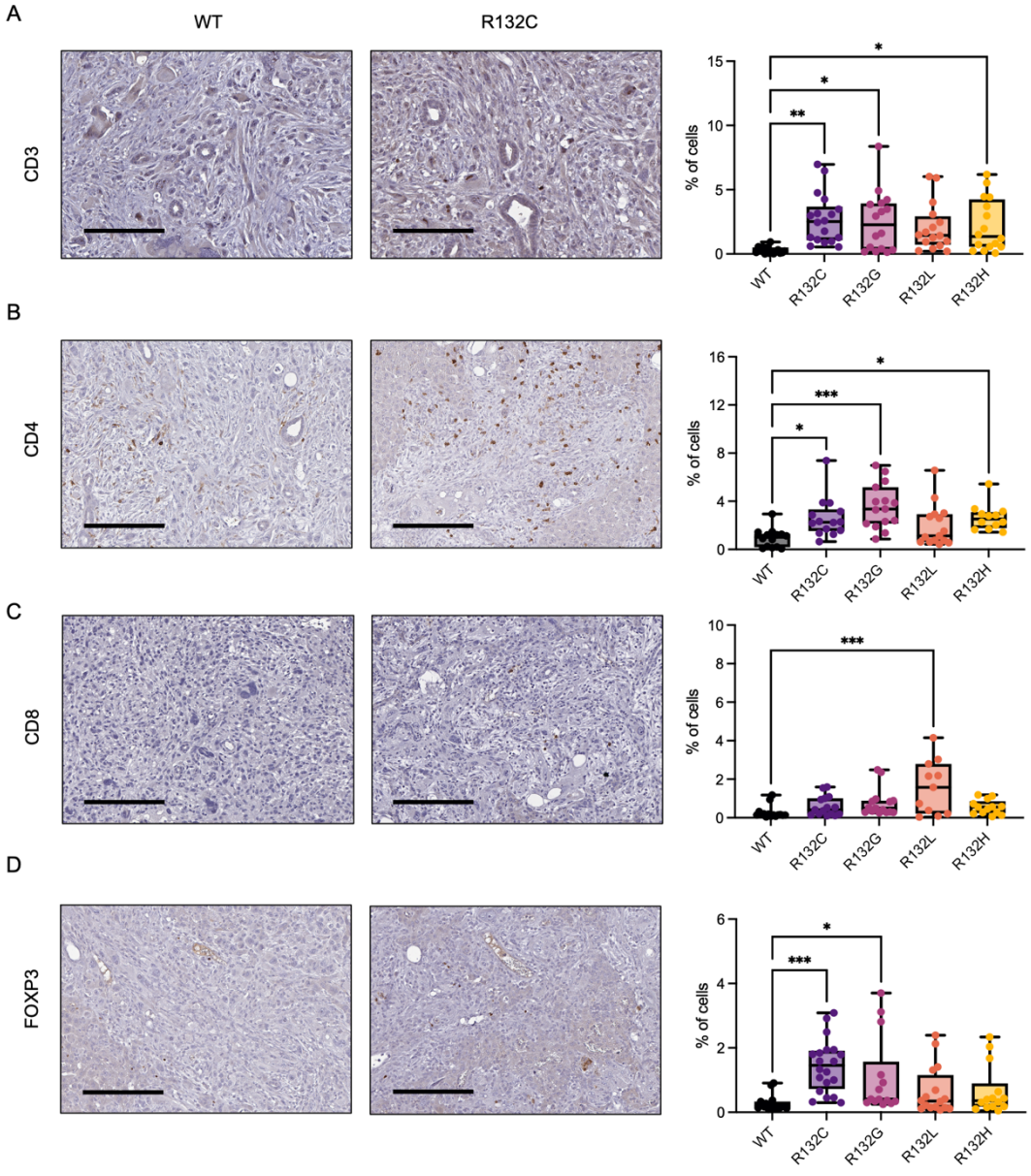

Figure 21. Immunohistochemical profiling of key T cell markers in KRAS;TP53;IDH1 tumors.
IHC analysis of KRAS;TP53;IDH1 tumors, left: representative images of tumor samples, right: corresponding quantification. A. CD3 staining, B. CD4 staining, C. CD8, and D. FOXP3 staining. A, B, C, D. each data point represents a field of view, *=p≤0.05, **=p≤0.01, ***=p≤0.001 (one-way ANOVA with post hoc Tukey's test).

Subsequently, I explored the possibility of the IDH1 mutant TME being immunosuppressed in the T-cell context. The staining for Forkhead box P3 (FOXP3), a marker

for Tregs [301], presented intriguing results (**Figure 21D**). Notably, the IDH1 R132C and R132G mutant displayed, respectively, a two-fold and a one-fold increase in FOXP3 expression compared to both the IDH1 WT tumors.

Overall, these findings suggest a markedly immunosuppressive environment within IDH1 R132C and R132G mutant tumors. Given that no significant differences were observed for CD8 and FOXP3 for IDH1 R132H tumors indicates that different *Idh1* mutations have vastly divergent effect on the immune landscape in the context of KRAS;TP3;IDH1 tumors.

These intricate immune profiles could critically inform the development of targeted therapies, highlighting the nuanced interplay between tumor cells and the immune system in the context of IDH1 mutant-driven tumorigenesis.

4.4.4. Immune modulation in IDH1 mutant tumors

Having established a structurally and immunologically altered TME, I concentrated my efforts on identifying the specific molecular signals that recruit and influence immune cells within the TME.

To this end, with the help of a cytokine array, I compared supernatants obtained from KRAS;TP53;IDH1 tumor-derived cell lines. This step was critical in linking the observed ECM alterations with potential changes in cytokine expression of tumor cells, which could be driving the immune cell dynamics within the TME.

The results accentuated an upregulation of certain cytokines in the conditioned media harvested from primary tumor-derived IDH1 R132C cells in comparison to their IDH1 WT counterparts (**Figure 22A**). Interestingly, the IDH1 mutant supernatants displayed significantly elevated levels of CCL7. Likewise, a similar pattern could be observed for CCL20 and G-CSF.

The question at hand was whether these cytokines are upregulated in IDH1 mutant tumors and, if so, what implications this might have for the tumor TME. To address this, I first turned to bulk RNA-seq data from KRAS;TP53;IDH1 tumors. The analysis revealed a consistent upward trend for *Ccl17* and *G-Csf* gene expression in the IDH1 R132C mutant tumors, but not for *Ccl20* (**Figure 22B**).

Considering the high expression of C-C motif chemokine ligand 17 (CCL17) observed in tumor-derived cell lines and tumor samples, it continued to be the focus of the experiments. To validate these findings, I employed qPCR to measure *Ccl17* expression levels in the KRAS;TP53;IDH1 samples. The qPCR results confirmed an increasing trend of *Ccl17* in the IDH1 mutant tumors (**Figure 22C**), aligning with the sequencing data and correlating with the level of 2-HG produced in the IDH1 mutant. However, it is noteworthy that this trend was significant only for the R132G IDH1 mutant.

Next, I performed IHC to visualize the presence of CCL17 in the tumor samples. The IHC staining provided a clear visual confirmation of trend for increased CCL17 in the IDH1 mutant samples (**Figure 22D**), corroborating the molecular data, with the all of the iCCA-specific IDH1 mutants exhibiting an upregulation of this cytokine.

The integration of proteomic, genomic, and histological data points to a definitive upregulation of CCL17 in IDH1 mutant tumors. Given the earlier noted increase in FOXP3-positive Tregs in IDH1 R132C and R132G tumors and the known function of CCL17 in recruiting Tregs to tissue sites [303], [304], it is plausible that the upregulation of CCL17 contributes to the immunosuppressive milieu in this context by significantly enhancing Treg recruitment.

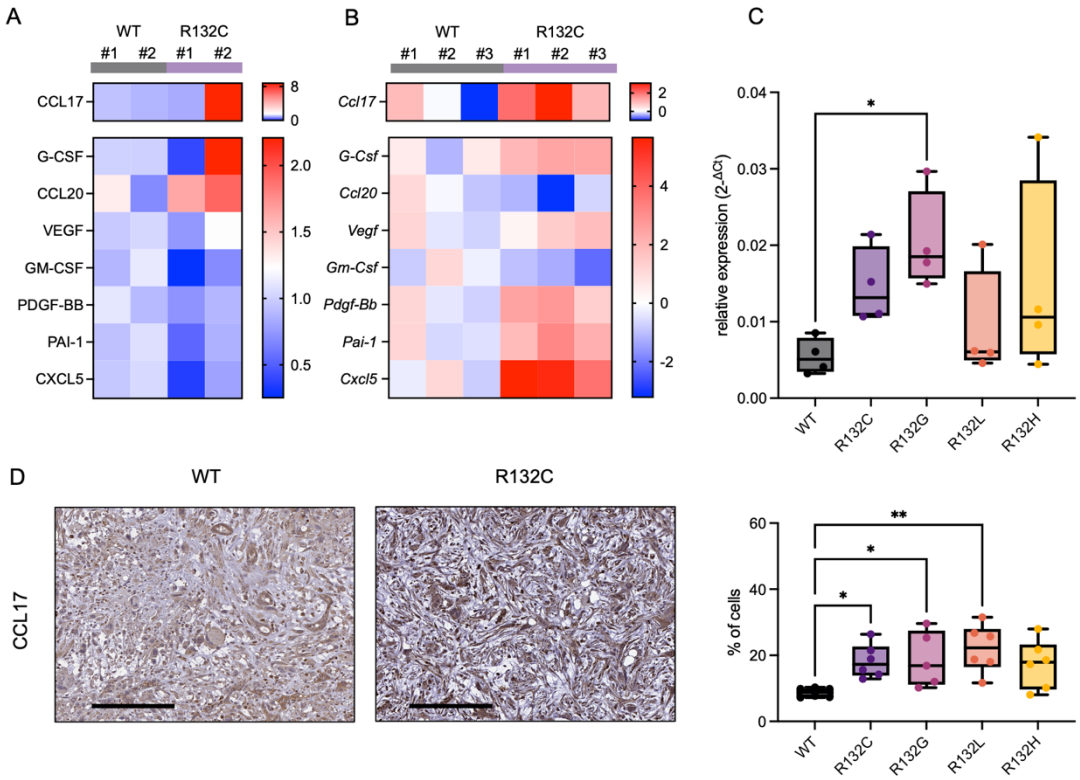

Figure 22. Immune modulation mediated by IDH1 mutants in TME of KRAS;TP53;IDH1 tumors.
Z-score based heatmap illustrating the differences between IDH1 mutant samples and IDH1 WT counterparts. A. Analysis using Proteome Profiler Mouse Cytokine Array on supernatants from KRAS;TP53;IDH1-tumor-derived cell lines, B. RNA-seq results derived from samples from KRAS;TP53;IDH1-tumor. C. Assessment of *Ccl17* level evaluation via qPCR from KRAS;TP53;IDH1 samples. Each data point signifies an individual mouse. *=p≤0.05 (one-way ANOVA with post hoc Tukey's test). D. IHC evaluation highlighting CCL17 presence in KRAS;TP53;IDH1 tumor samples, left: representative images of tumor samples, right: corresponding quantification. Each data point represents a field of view, *=p≤0.05, **=p≤0.01 (one-way ANOVA with post hoc Dunnett's test).

The take-home message from this section of the study is the identification of CCL17 as a potentially key player in the immunosuppressive environment of IDH1 mutant tumors, which could be a target for therapeutic intervention.

Such detailed analysis is essential to unveiling novel treatment strategies by delving into the therapeutic vulnerabilities driven by 2-HG. This approach not only opens the door to innovative therapies but also emphasizes the nuanced interplay between genetic mutations and the immune environment, paving the way for precision medicine in iCCA treatment.

4.5. *IDH1* mutations in tumorigenesis: genomic to functional insights

4.5.1. Beyond major players: IDH1 and its partners in iCCA

My research also focused on unraveling how *IDH1* mutations interact with other genetic alterations in driving or modulating iCCA progression, thereby dissecting their roles in 2-HG driven tumorigenesis. To this end, I utilized the cBioPortal, an open-access platform for exploring multidimensional cancer genomics data. This resource aggregates data from consortium projects and individual studies, enabling analysis of genetic correlations and patient outcomes.

The analysis conducted on patient data through cBioPortal revealed an expected co-occurrence between *KRAS* and *TP53* mutations [305], which are also well-established drivers of iCCA in murine models [262]. However, in human datasets, *IDH1* mutations appeared to be mutually exclusive with these, suggesting a potential functional redundancy (**Table 15**). Additionally, *IDH1* mutations showed a tendency to co-occur with mutations in *AT-rich interactive domain-containing protein 1A* (*ARID1A*), *BAP1*, and *Protein polybromo-1* (*PBRM1*) (**Table 15** and **Figure 23A**), indicating potential cooperative roles in iCCA progression [305].

Table 15. Genomic associations: decoding the interactions in iCCA.
Analysis based on data from cBioPortal based on query combining available iCCA cases (collectively 782): JHU, Nat Genet 2013; MSK, Clin Cancer Res 2021; MSK, Hepatology 2021; Mount Sinai 2015; Shanghai, Nat Commun 2014.

		log2 odds ratio	p-value	q-value	tendency
KRAS	TP53	1.378	0.001	0.006	co-occurrence
IDH1	TP53	-1.175	0.007	0.021	mutual exclusivity
IDH1	KRAS	-0.595	0.383	0.466	mutual exclusivity
IDH1	ARID1A	0.734	0.054	0.102	co-occurrence
IDH1	BAP1	0.371	0.392	0.466	co-occurrence
IDH1	PBRM1	0.414	0.404	0.466	co-occurrence

Addressing the discrepancies between mouse model findings and human genomic signatures, my study has evolved from solely focusing on the KRAS;TP53 model to developing models that more accurately mirror the genomic traits seen in human iCCA cases with *IDH1* mutations. This involves integrating *IDH1* mutations with oncogenic events from human datasets or those known to drive iCCA in mice, thereby enhancing the insights gained from the KRAS;TP53 model.

4.5.2. Mimicking patient-specific genomic patterns

With the goal of mimicking the genetic landscape of human iCCA, I created models that combined IDH1 (either WT or R132C) with alterations in *Pbrm1*, *Arid1a*, and *Bap1* utilizing

CRISPR/Cas9 system via HTVi. Surprisingly, this combination did not lead to any tumor formation within an 18-month period (data not shown).

In an attempt to increase the oncogenic potential, I introduced additional mutations, namely disruption of either *Tp53* or *Pten (Phosphatase and tensin homolog)*. Notably, *Pten* disruption resulted in hepatomegaly which emerged after about 40 weeks, overshadowing any discernible effect of *Idh1* mutation (**Figure 23B**), which was evidenced by the lack of difference in survival of tumor-bearing mice and the histology of livers from these animals.

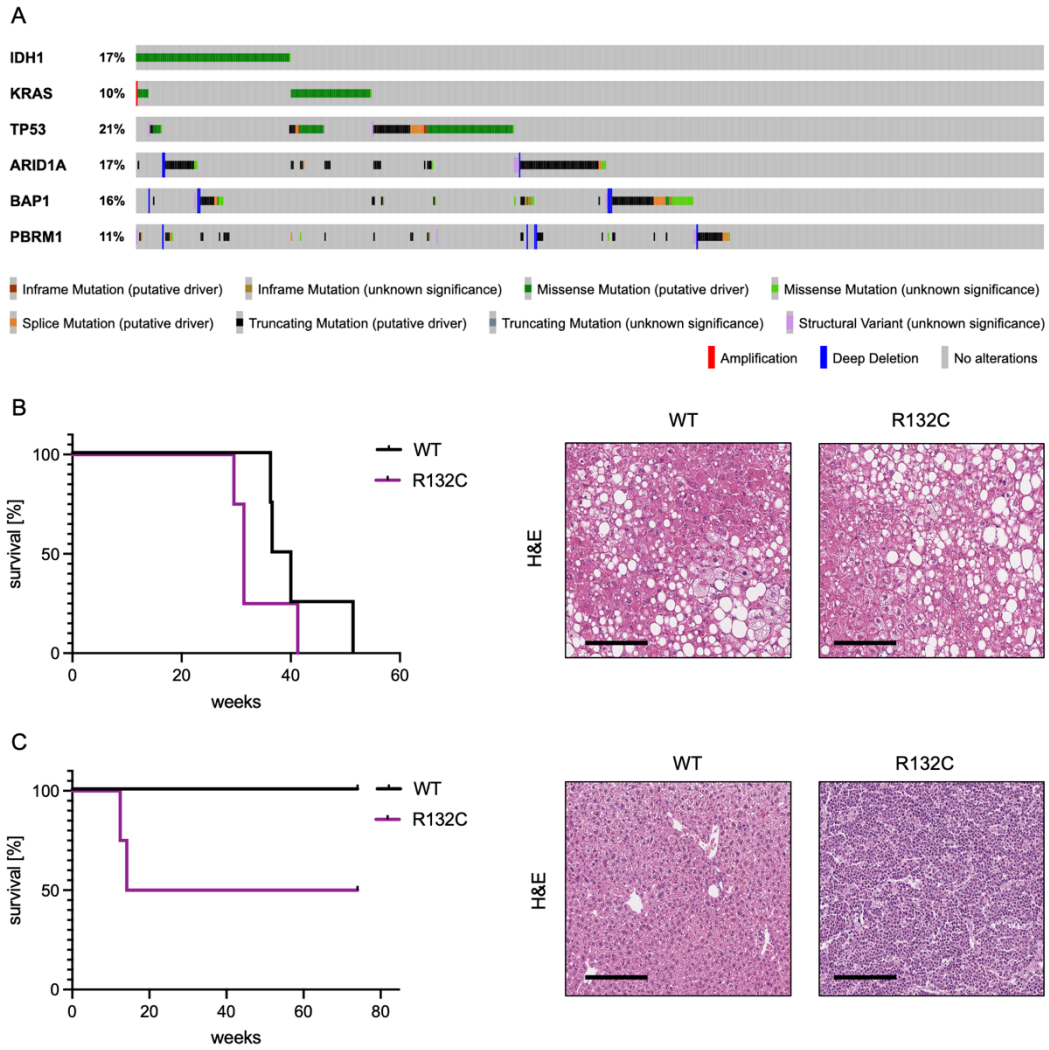

Figure 23. Comparative analysis of survival and histopathology in distinct iCCA mutations.

A. Mutation prevalence in selected genes associated with iCCA, cBioPortal, iCCA cohort (MSK, Hepatology 2021), 412 samples. B. Left: Kaplan-Meier survival curve for ARID1A;BAP1;PBRM1;PTEN;IDH1 tumor-bearing mice, right: representative histopathological H&E images from the cohort, scale bar: 300 µm. C. Left: Kaplan-Meier survival curve for ARID1A;BAP1;PBRM1;TP53;IDH1 tumor-bearing mice, right: representative histopathological H&E images from the cohort, scale bar: 300 µm.

Introducing the *Tp53* gene disruption resulted in tumor growth after roughly 20 weeks, but these tumors, specific to the IDH1 R132C condition, presented in the lumbar region and

resembled chondrosarcoma (**Figure 23C**). While the role of IDH1 R132C in chondrosarcoma is established [132], this was not the primary focus of my iCCA-centered research.

The results highlighted the unpredictability of genetic interactions in oncogenesis. Despite advanced genetic tools, replicating the complex interplay of mutations found in human cancer remains a challenging endeavor. This underscores the need for continuous refinement of experimental models to better understand and mimic the genomic landscape of iCCA.

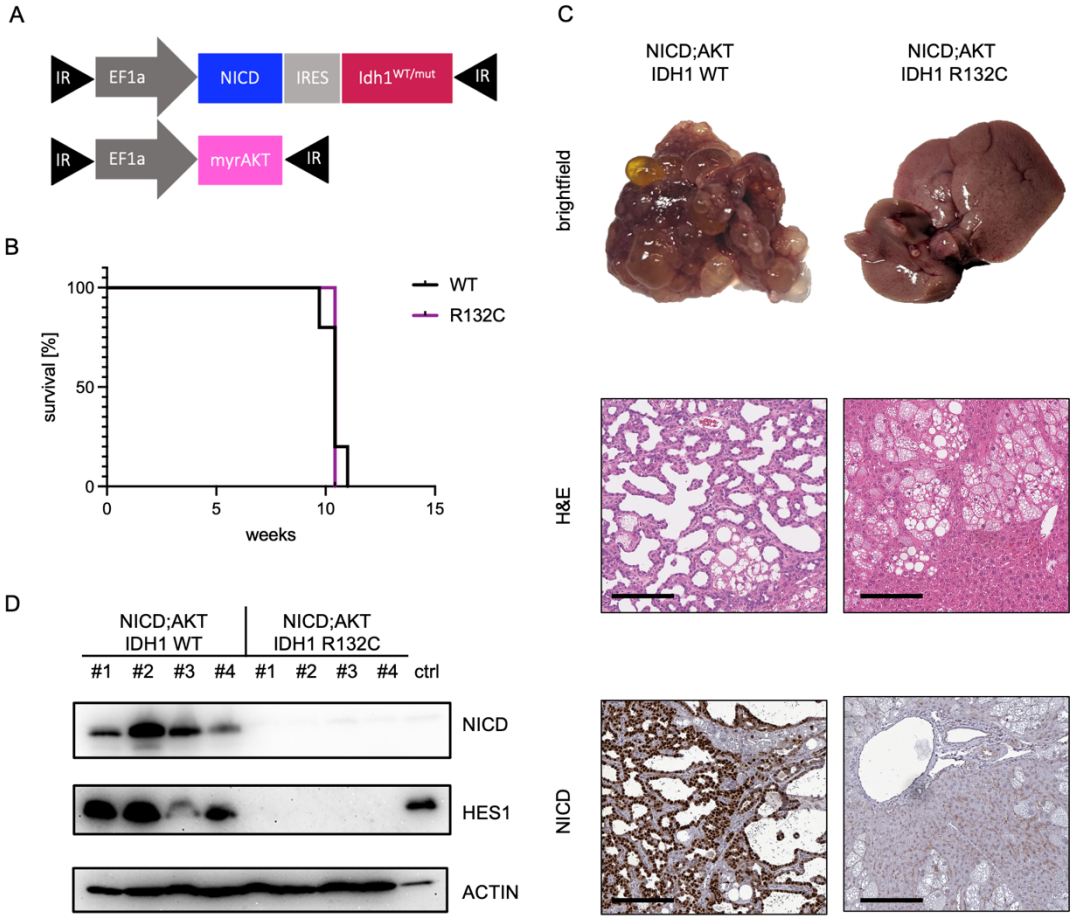

Figure 24. Disruption of expected cyst formation in mice bearing NICD;AKT;IDH1 tumors.
A. Schematic representation of the HTVi experimental setup. B. Survival rates of mice bearing NICD;AKT;IDH1 tumors. C. Representative images of obtained tumors. Top: brightfield, middle: H&E, bottom: NICD; scale bar: 300 µm. D. Western blot analysis of NICD;AKT;IDH1 tumor tissue samples.

4.5.3. Investigating alternative murine iCCA models *in vivo* beyond KRAS;TP53

To further explore the role of *IDH1* mutations in iCCA, I investigated their interplay with the NOTCH and AKT pathways, well-established oncogenic precursors to CCA in mouse models [306]. The method involved using a HTVi to introduce a combination of Notch Intracellular Domain (NICD), the constitutively active form of AKT, myristoylated AKT, and either IDH1 (either WT or R132C) into mice (**Figure 24A**). This combination was expected to induce cyst formation, a precursor to tumor development. There was no difference in survival rates

between mice with IDH1 WT and IDH1 R132C when combined with NICD and AKT, as all of them were sacrificed 10 weeks after HTVi (Figure 24B).

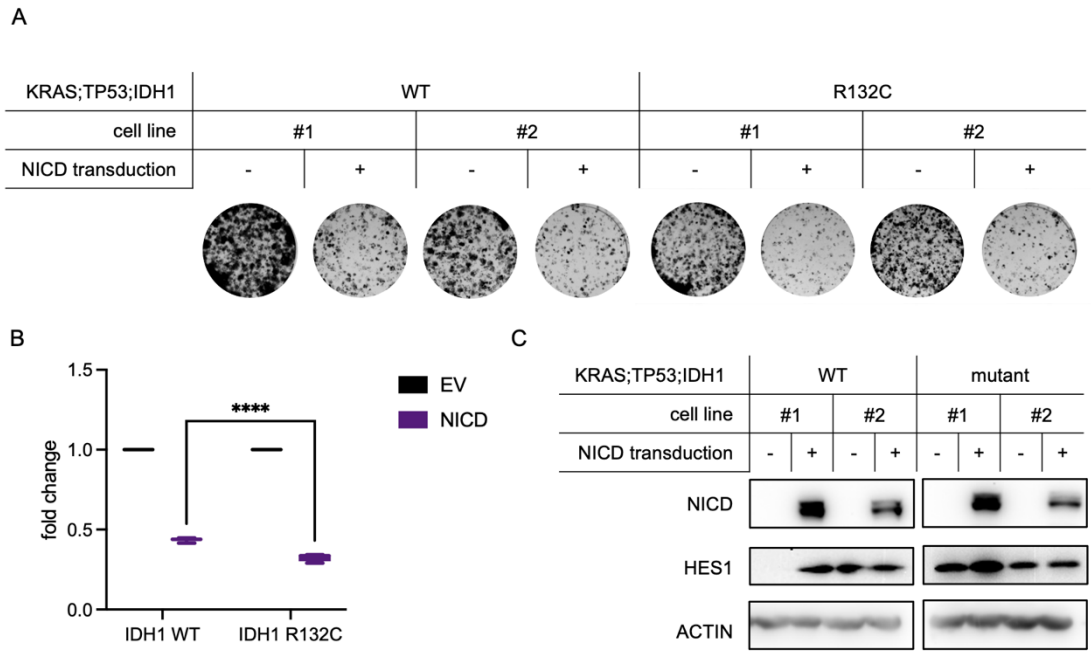

Figure 25. Influence of NICD overexpression on KRAS;TP53;IDH1 tumor derived cells.
A. Representative images portraying viability of KRAS;TP53;IDH1 tumor-derived cell lines upon NICD overexpression. B. Quantitative assessment of cell viability, denoted as a fold change relative to the baseline set by empty vector (EV) transduction. C. WB analysis highlighting NICD and HES1 expression shifts following NICD overexpression in KRAS;TP53;IDH1 cell lines.

A notable finding in this model was the unexpected tumor morphology. The NICD;AKT;IDH1 WT tumors developed as anticipated, with the liver being populated by cysts. In contrast, the NICD;AKT;IDH1 mutant tumors exhibited a morphology resembling that typically seen in AKT-only tumors. This was particularly striking as the histological analysis revealed a complete absence of cyst formation in the NICD;AKT;IDH1 mutant group (Figure 24B&C).

To further understand these results, I validated the expression of NICD. IHC and WB analyses showed that NICD, and its downstream target HES1 [307], were absent in the NICD;AKT;IDH1 R132C tissue samples. This finding suggests that the expression of IDH1 R132C and/or the accumulation of 2-HG may be mutually exclusive with NICD expression (Figure 24C&D), which could explain the absence of the cyst formation.

Moreover, I attempted to replicate the *in vivo* conditions *in vitro* by acquiring tumor-derived cell lines from NICD;AKT;IDH1 tumors. However, this proved unsuccessful, as the unique cystic morphology was only observed in the context of IDH1 WT, leaving no comparative baseline for the mutant condition.

Adapting to these challenges, I utilized KRAS;TP53;IDH1 tumor-derived cell lines, transducing them with a vector carrying the NICD overexpression cassette. This experiment

focused on the comparison between IDH1 WT and IDH1 R132C. The results were revealing: KRAS;TP53 cells with *Idh1* mutation showed a reduced ability to form colonies upon NICD overexpression compared to their IDH1 WT counterparts (**Figure 25A&B**).

While NICD overexpression's impact was evident in this context, and NICD overexpression was validated in all KRAS;TP53 cell lines, discerning a consistent pattern of NICD target expression proved challenging. For instance, HES1, used as a representative example, did not show a clear expression pattern (**Figure 25C**). This suggests the possibility of compensatory mechanism or a disruption in the NOTCH signaling pathway.

Overall, these results indicate an unforeseen and complex interaction between IDH1 mutations and key oncogenic pathways, influencing tumor morphology and cellular behavior, and potentially altering the course of iCCA progression.

4.6. Exploring vulnerabilities of IDH1 mutant iCCA

Recognizing the hallmark characteristics of *IDH1* mutations in certain iCCAs, there exists a strategic opportunity to target this unique genetic signature in tumor cells, while aiming to preserve normal tissue. Driven by this hypothesis, I designed a series of experiments to address this from different angles.

4.6.1. Decoding 2-HG-driven genetic dependencies

To understand the unique vulnerabilities introduced by *IDH1* mutations in iCCA, I sought to decode the genetic dependencies driven by the 2-HG. Utilizing the DepMap portal database, a repository of large-scale genetic datasets, I identified genes whose suppression or loss leads to detrimental effects on cancer cell viability specifically present or notably intensified in the presence of 2-HG.

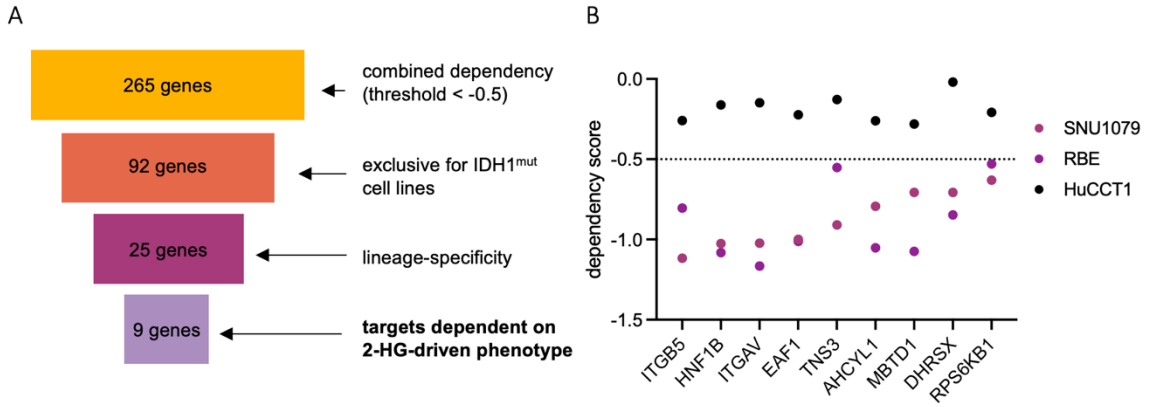

Figure 26. Unraveling 2-HG driven genetic dependencies in iCCA cell lines.
A. Schematic representation of the experimental process employed to uncover genetic dependencies influenced by the presence of 2-HG. B. Comparative analysis of dependency scores in iCCA cell lines harboring IDH1 mutations (SNU1079 and RBE) in comparison to the IDH1 WT control (HuCCT1).

The study focused on two human iCCA cell lines, SNU1079 and RBE, each harboring distinct *IDH1* mutations (IDH1 R132C and IDH1 R132S, respectively). These mutations endow the cells with the capability to produce 2-HG, rendering them perfect subjects for this investigation [308].

Dependency scores in CRISPR/Cas9 loss-of-function screens signify the importance of genes for cell survival or growth. A negative score indicated a gene's critical role, with a threshold of -0.5 marking significant cell dependency (**Figure 26A**). This filtering criterion narrowed the gene list to 265, which was further refined to 92 after excluding genes also essential to the iCCA IDH1 WT cell line (HUCCT1) [309].

A pivotal criterion in this selection was the enrichment of these genes in liver-associated lineages, which ensured that the candidate targets were pertinent to liver tumors, thus enhancing the translational potential of my findings. This rigorous process spotlighted nine primary candidate genes for deeper exploration (**Figure 26B**). Experimental validations prompted a particular focus on *AHCYL1* (*Adenosylhomocysteinase hydrolase-like protein 1*), *TNS3* (*Tensin 3*), *ITGAV* (*Integrin alpha V*), and *ITGB5* (*Integrin subunit beta 5*).

To place these genetic dependencies in the context of gene expression, RNA-seq data was analyzed, which revealed an upregulation of the candidate genes in KRAS;TP53; IDH1 R132C tumors (**Figure 27A**). To determine if this analysis could be applicable to a murine *in vivo* system and to further elucidate the functional consequences of these genes within the context of the KRAS;TP53;IDH1 model, competition assays were conducted.

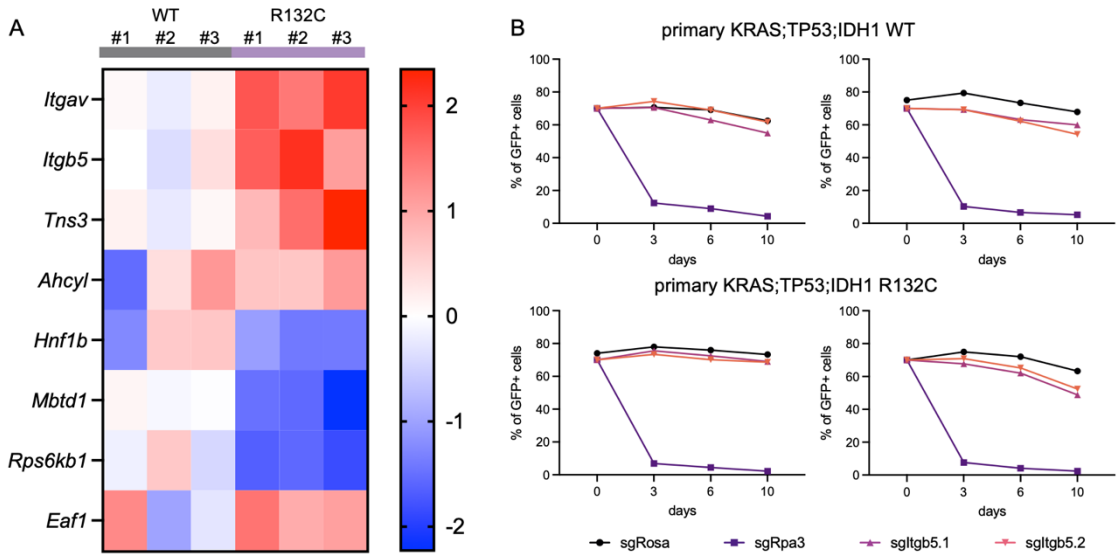

Figure 27. Insight into gene expression patterns and perturbation effects in KRAS;TP53;IDH1 tumors.
A. Z-score heatmap visualization of expression patterns of nine candidate genes in KRAS;TP53;IDH1 WT and mutant tumors. B. Representative competition assay results following the CRISPR/Cas9-mediated disruption by two independent sgRNAs targeting a specific candidate, assays are performed in two distinct KRAS;TP53;IDH1 WT (top) and IDH1 R132C (bottom) primary tumor-derived cell lines; sgRosa26 and sgRpa3 are used as negative and positive controls, respectively.

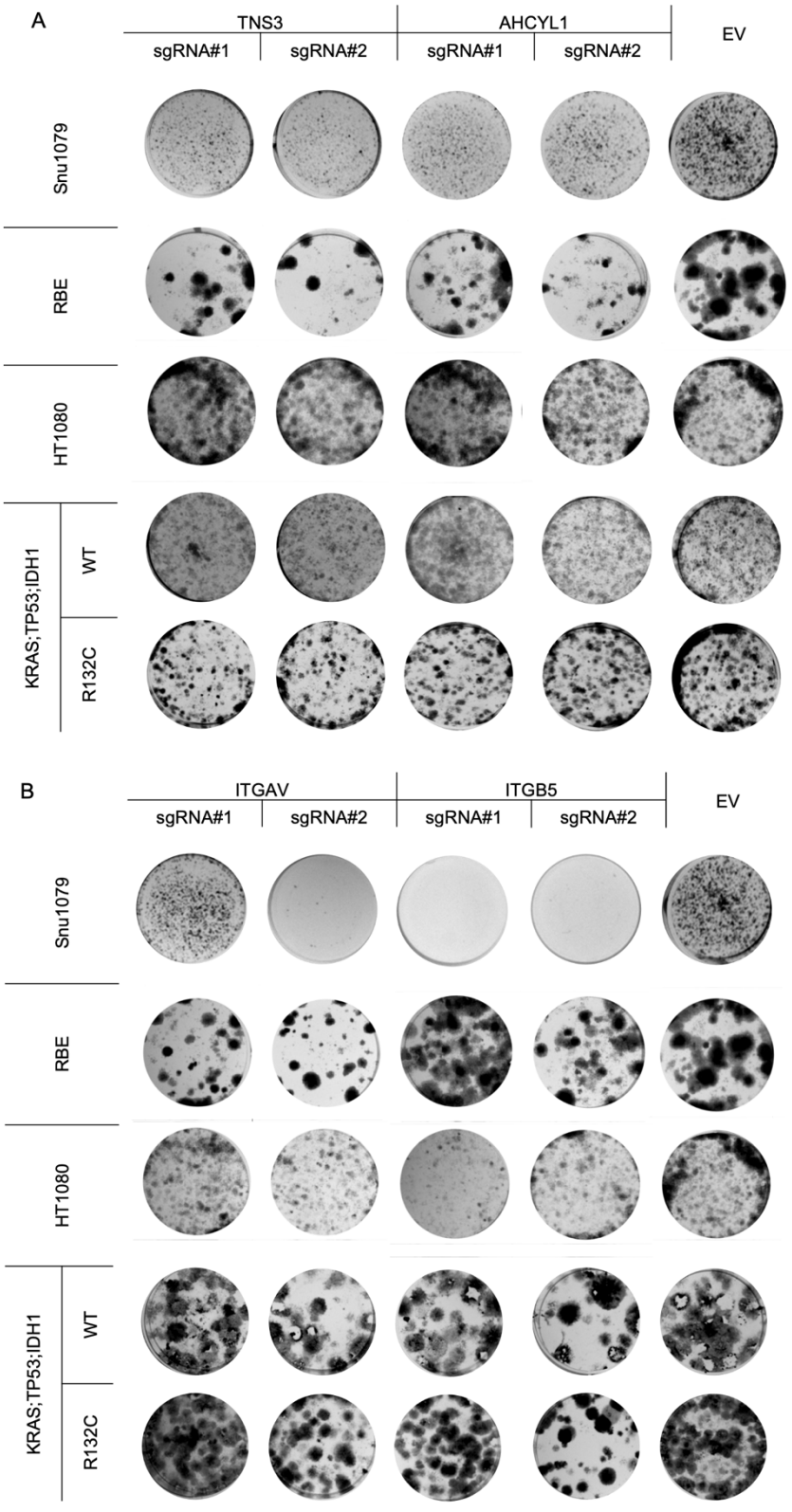

Figure 28. Assessing genetic dependencies: effects of candidate gene deletion on viability of 2-HG producing cells. Colony formation assay results for SNU1079, RBE, HT1080 and primary tumor-derived KRAS;TP53;IDH1 WT and R132C cells upon CRISPR/Cas9-mediated knock-out of A. *TNS3* and *AHCYL1 (Tns3* and *Ahcyl1* for murine cell lines*)*, B. *ITGAV* and *ITGB5 (Itgav* and *Itgb5* for murine cell lines*)*.

These assays entailed mixing GFP-positive CRISPR/Cas9-edited tumor-derived cells with unedited parental cells to track competitive growth dynamics. However, these assays did not demonstrate significant growth differences between primary tumor-derived IDH1 R132C cell lines and their IDH1 WT counterparts (**Figure 27B**).

Seeking to reconcile these findings with the DepMap analysis, I proceeded to evaluate the impact of gene disruptions on cell viability of established human cell lines whose data was used for the initial analysis, SNU1079 and RBE, through colony formation assays. Additionally, I incorporated HT1080, a chondrosarcoma cell line with the same IDH1 mutation as SNU1079 [155] to provide insights into the broader implications of 2-HG accumulation beyond just iCCA. Furthermore, murine tumor-derived iCCA cell lines from KRAS;TP53;IDH1 tumors were also maintained in this experiment.

Intriguingly, CRISPR/Cas9-mediated knock-outs of *TNS3* and *AHCYL1* led to reduced viability in both SNU1079 and RBE cell lines, underscoring their potential as therapeutic targets (**Figure 28A**). Conversely, for *ITGAV* and *ITGB5* I noted reduced viability of SNU1079 but not RBE cells (**Figure 28B**). I found that HT1080 remained unaffected by the disruption of *TNS3* and *AHCYL1* but exhibited sensitivity to disruption of *ITGAV* and *ITGB5*. This suggests that, despite sharing the IDH1 mutation with SNU1079, HT1080 cells may have distinct cellular mechanisms or pathways influenced by these genes.

Furthermore, when considering all four candidate genes (*Tns3*, *Ahcyl1*, *Itgav*, and *Itgb5*), it became evident that there were no marked differences in the effects of gene knock-outs when comparing IDH1 R132C cell lines with IDH1 WT counterparts.

These experiments emphasize that the presence and accumulation levels of 2-HG in different cellular contexts can lead to varied effects, influenced by a complex interplay of genetic, epigenetic, and metabolic factors. This variability points to the intricate and nuanced nature of cellular responses to 2-HG, highlighting the necessity for a thorough investigation into how these factors collectively shape the biological outcomes in different cell types and conditions.

In summary, my research into iCCA cell lines highlights *AHCYL1*, *TNS3*, *ITGAV*, and *ITGB5* as potential therapeutic targets, underlining the importance of cellular context in refining cancer therapy strategies and advancing targeted treatment development.

4.6.2. Immunotherapeutic potential: harnessing IDH1 mutants in iCCA

This study phase focused on the potential of immunotherapy to target *IDH1* mutations in iCCA, specifically exploring the use of IDH1 mutants' unique neoantigen properties for developing cancer vaccines.

Collaborating with Michael Platten's team at the DKFZ, I employed synthetic peptides to activate dendritic cells [310], aiming to produce T- and B-cells targeting cancer cells [311], building on previous work on IDH1 R132H mutant tumors of central nervous system [231], [312].

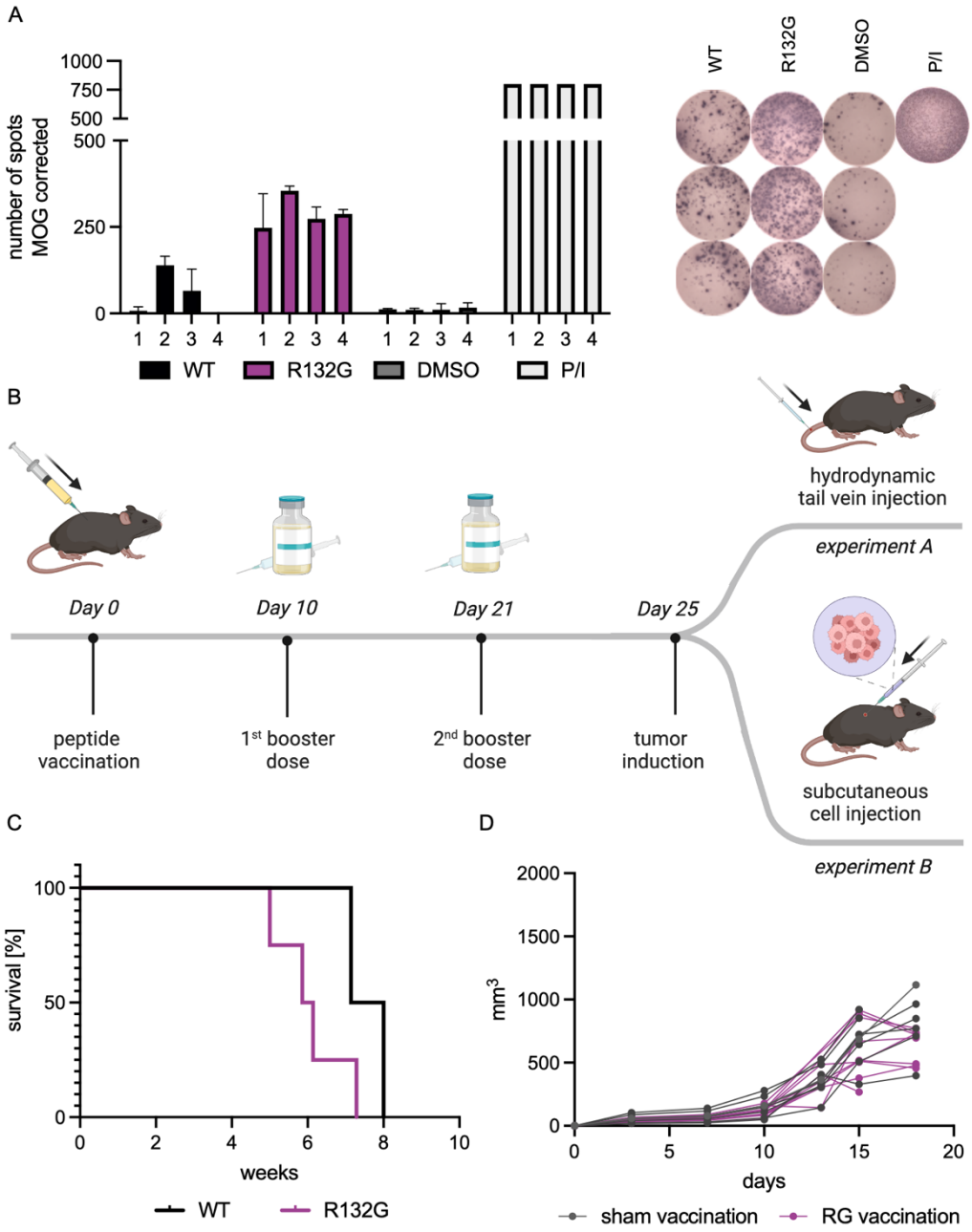

Figure 29. Assessing the efficacy and impact of R132G vaccination on IDH1 mutant tumors.

A. Analysis of mutation-specific IFN-γ response to IDH1 peptides post-vaccination of A2.DR1 mice with R132G peptide. Splenocytes were restimulated with indicated peptides (black: IDH1 WT, purple: IDH1 R132G, grey: DMSO as a vehicle control, and light grey: PMA with ionomycin as a positive control). Left: quantification of ELISpot analysis, normalized against MOG control, an unspecific peptide. Each bar represents a single mouse. Error bars represent mean + standard deviation from technical replicates, right: visualization of representative results from ELISpot of an A2.DR1 R132G vaccinated mouse. B. Experimental workflow for preventive vaccination with the R132G peptide vaccination, followed in experiment A: by HTVi injection of the KRAS;TP53;IDH1 WT or KRAS;TP53;IDH1 R132G cocktail, and in experiment B: by subcutaneous injection of A.2DR1 KRAS;TP53;IDH1 tumor-derived cells. C. Kaplan-Meier survival curve for R132G-vaccinated KRAS;TP53;IDH1-tumor bearing mice. D. Growth curves of flank tumors of R132G- and sham-vaccinated KRAS;TP53;IDH1 R132G-tumor bearing mice. Each line represents an individual flank tumor.

In this experimental model, A2.DR1 mice, which express human-like MHC I and II molecules, were immunized with iCCA-specific IDH1 peptides exhibiting structural resemblance to the IDH1 R132H prototype, because they only differed in the amino acid sequence at the R132 position, aligning with target mutations. These peptides were administered in a Montanide-ISA51 emulsion to enhance the immune response [313], followed by booster doses to fully prime the immune system. The immune response was measured using the ELISpot assay, which quantifies IFN-γ production by splenocytes after *ex vivo* stimulation with the peptides.

Among the tested peptides, the R132G peptide emerged as particularly notable, eliciting a strong, consistent and specific immune response compared to stimulation with the IDH1 WT peptide, suggesting its potential as an iCCA-specific immunogenic epitope (

Figure 29A).

Following the protocol established by Schumacher *et al.* [231], I tested the efficacy of the R132G peptide in a preventive vaccination setup combined with the HTVi model (

Figure 29B, experiment A). However, the peptide did not confer the expected protection to mice bearing KRAS;TP53;IDH1 R132G tumors after preventive vaccination, despite its promising *ex vivo* efficacy. The survival of both IDH1 mutant and WT tumor-bearing mice was approximately 7 weeks (

Figure 29C).

Acknowledging the liver's unique immune-privileged status [314], which could have dampened the immune response and affect the efficacy of immunotherapy [315], I adapted the experimental approach. Instead of the HTVi method, I administered KRAS;TP53;IDH1 R132G tumor-derived cells from A2.DR1 subcutaneously after the preventive vaccination protocol (

Figure 29B, experiment B). This modification, however, did not alter the outcome; the R132G peptide still did not demonstrate the anticipated *in vivo* immunogenicity and was not able to prevent or inhibit tumor growth of KRAS;TP53;IDH1 R132G in comparison to the sham control (

Figure 29D).

In summary, the investigation into the immunotherapeutic potential of IDH1 mutants in iCCA revealed a promising avenue through the R132G peptide's immunogenic response. Yet, the complexity of the liver's (immune) environment and the challenges of translating *ex vivo* efficacy to *in vivo* effectiveness became apparent. These findings, while not conclusive, provide direction for future research and underscore the need for continued exploration and refinement of strategies.

5. Discussion

IDH1 mutations are pivotal in several cancer types, notably in iCCA [132]. These mutations are the most prevalent genetic alteration in iCCA, leading to the abnormal production of 2-HG [316], which has been shown to play a significant role in cancer development and progression [132]. While iCCA is relatively rare, occurring in a limited number of individuals annually [317], its incidence is increasing [318], [319], [320]. Despite it, treatment options for iCCA remain limited [120], [123], underscoring the critical need for targeted therapies and further research in this area.

5.1. Influence of *Idh1* mutations on iCCA histopathology

Examining various *IDH1* mutations in a background of altered *KRAS* and *Tp53* genes, I found that iCCA-specific mutations (R132C, R132G, R132L) led to high 2-HG production, while the R132H mutation yielded moderate levels of this oncometabolite. This finding is crucial as increasing 2-HG levels seemed to dictate the phenotype in KRAS;TP53;IDH1 cohort.

Firstly, high level of 2-HG in IDH1 R132C and R132G mutant tumors were correlated with shorter survival times in mice, in contrast to their IDH1 WT counterparts. Conversely, the R132H mutation, which resulted in moderate 2-HG levels, was not associated with such drastic survival reduction.

This pattern of 2-HG production was observed in both serum and tumor protein extracts, consistent with previous research on mutant IDH1 catalytic activity [228]. The literature also supports the association between *IDH1* mutations in iCCA and the detection of 2-HG in plasma [321] and serum [322], where its levels are indicative of early disease progression.

The clear link between the increased production of 2-HG and reduced survival in the KRAS;TP53 cohort, highlights the importance of 2-HG as a potential biomarker for iCCA. Further, it suggests that monitoring 2-HG levels in blood could be a less invasive, yet practical approach for early detection, continuous monitoring, and evaluating therapeutic responses.

Furthermore, my results pointed to enhanced kinetochore metaphase signaling in IDH1 mutants, as identified through RNA-seq analysis, suggesting a potential mechanism for the aggressive nature of these tumors. This finding is consistent with the known characteristics of rapidly proliferating tumors [278], [279]. Moreover, the elevated expression level of proliferation marker observed in IDH1 R132C and R132G mutants via phospho-H3 staining underscore the pivotal role of 2-HG in influencing tumor behavior and survival outcomes in these tumors characterized by high 2-HG accumulation.

Interestingly, IDH1 R132C mutants, in comparison to IDH1 WT, exhibited increased levels of phospho-H2A.X, highlighting a significant difference in DNA damage response between the IDH1 mutant and WT forms in this context. The decrease in G2/M damage checkpoint regulation observed in the RNA-seq data may indicate a mechanism through which

IDH1/2 mutations contribute to tumor aggressiveness and poor prognosis, hinting at possible DNA damage checkpoint evasion, genomic instability, and accelerated proliferation of DNA-damaged cells [221], [323]. This aspect is particularly noteworthy as it aligns with previous results regarding the contribution of these mutations to genomic instability in iCCA [324]. Additionally, *IDH1/2* mutations are linked with enhanced hypermethylation at specific genomic loci, potentially contributing to the genomic instability observed in iCCA [325].

Overall, the impact of *IDH1* mutations on cancer proliferation and progression is complex and highly context-dependent. While Wang *et al.* [173] demonstrated that *IDH1/2* mutations correlate with better outcomes in iCCA, this may be misleading due to the grouping of IDH1 and IDH2 mutations. In contrast, other studies [130], [326], [327], [328], [329], [330] and Molenaar *et al.*'s meta-analysis [331] strongly suggest the necessity of analyzing *IDH* mutations independently, revealing no significant correlation between IDH1 mutations alone and clinical outcomes like overall survival (OS) and progression-free survival (PFS). Additionally, the frequency of *IDH1* mutations differs in fluke-infected versus non-infected iCCA patients, further indicating environmental factors' role in disease outcomes [128], [332].

In case of chondrosarcomas, both *IDH1* and *IDH2* mutations, particularly the prevalent *IDH1* R132C mutation, are consistently associated with worse OS compared to WT IDH [333], [334]. This fact underlines the importance of differentiating between *IDH1* and *IDH2* mutations in cancer studies to accurately assess their impact.

In contrast, *IDH* mutations in gliomas are associated with better patient outcomes, with longer OS and PFS, regardless of the tumor grade [167], [211], [335], [336], [337], [338], [339], [340], [341], [342], [343], [344]. However, it is particularly notable that secondary glioblastoma, a more aggressive brain tumor, often develops from lower-grade gliomas that frequently harbor *IDH* mutations [345]. This difference could be attributed to the specific IDH1 R132H mutant in gliomas, which is known for lower 2-HG production compared to iCCA-specific mutations, thus emphasizing the distinctive and nuanced role of 2-HG levels.

It is important to note that the influence of IDH1 R132C and R132G mutant effects on iCCA progression might be more straightforward to assess in the KRAS;TP53 model, as this model reduces the number of confounding factors such as external risk factors or preexisting inflammatory conditions. This focus on a direct comparison of mutations provides clarity in understanding their individual impacts, but it also means that it might not be capturing the full complexity of iCCA progression. Considering the various factors that can influence disease outcomes in iCCA underscores the complexity of its progression, particularly in relation to *IDH1* mutations.

In conclusion, broadly generalizing different *IDH1* mutations in iCCA could potentially obscure their individual impacts on tumor progression, as aptly emphasized by Grassian *et al.* [346]. Differentiating between mutation types (R132C, R132G, R132L, etc.) is imperative for understanding their specific effects and developing effective treatments.

5.2. *Idh1* mutations and the induction of hypermethylation state in iCCA

The role of 2-HG in inhibiting α-KG-dependent dioxygenases, impacting TET enzymes and histone demethylases [156], [316], [210], [347], [348], leads to hypermethylation in both histones and DNA [156], [210]. This process is crucial, as it can alter regions governing cellular functions.

In the KRAS;TP53 cohort, IDH1 mutants showed marked hypermethylation, where almost all DMRs showed increased methylation. This finding aligns with Wang *et al.*, who found that *IDH1* mutations in iCCA are correlated with hypermethylation patterns. They also observed that methylation patterns in iCCA are similar to those found in gliomas [349], speculating that the divergent target genes in "different tumor types may reflect differences in chromatin modifications or accessibility to TET dioxygenases between distinct mature cell lineages".

The distribution of DMRs across chromosomes in KRAS;TP53 IDH1 mutant tumors illustrates a global epigenetic alteration, a common feature in many cancers [350]. These changes can simultaneously affect multiple genes and pathways, adding to cancer's complexity and heterogeneity.

Promoter region methylation, making up 45% of DMRs, typically suppresses gene transcription, impacting various cellular processes [351], [352] and tumor progression via silencing of tumor suppressor genes [353], [354], [355]. Conversely, the remaining 55% of DMRs outside promoter regions, including 17% in distal intergenic areas, may shape chromatin architecture and affect gene expression over large genomic areas [356]. Gene body methylation, representing almost 21% of DMRs, can modulate gene expression and splicing patterns, leading to diverse mRNA and protein isoforms [357], [358], [359], [360]. Additionally, over 13% of DMRs in the first intron may interfere with promoter functionality and splicing, adding complexity to gene regulation and expression outcomes [356], [359], [360], [361]. These methylation patterns suggest a complex impact on gene expression and functionality in IDH1 mutants, ranging from direct transcriptional repression to subtler effects on gene functionality.

The influence of 2-HG influence extends also to histone methylation, affecting key epigenetic markers like H3K9me3 and H3K27me3 [276], [277], as they are pivotal for cell fate decisions and differentiation, are known to be affected by 2-HG accumulation [217], [274], [275]. I observed H3K9me3 and H3K27me3 accumulation in IDH1 mutant tumor-derived primary cells, but no differences in tumor samples from KRAS;TP53;IDH1 tumors. The differences between *in vivo* and *in vitro* highlight the challenges of studying oncometabolites in the tumor microenvironment.

While I have identified distinct methylation landscapes in mutant IDH1 versus WT IDH1 tumors, further research is necessary to fully grasp these changes and their impact on cellular pathways and tumor behavior. Nonetheless, this supports existing knowledge about 2-HG-induced hypermethylation and underscores potential therapeutic strategies targeting these epigenetic alterations.

5.3. The role of 2-HG as differentiation modulator in iCCA

Using HTVi and the Sleeping Beauty Transposon, my study expanded upon O'Dell *et al.*'s iCCA model [262], highlighting the role of IDH1 mutants in liver cancer. Of note, the HTVi approach targets primarily hepatocytes [74], [77] which is a crucial aspect especially when considering the cellular origin of iCCA.

Examining KRAS;TP53;IDH1 tumors created using this method, I have observed notable histological changes in IDH1 mutant tumors compared to IDH1 WT counterparts, particularly in glandular structures and stromal responses. These changes correlate with increased KRT19, indicating a shift towards cholangiocytic characteristics in all IDH1 mutant tumors. This supports the notion that 2-HG impairs cellular differentiation, leading to neoplasms from dysfunctional precursor cells [362], [363], [364]. It also contributes to the growing body of knowledge challenging the traditional view that only hepatocytes lead to HCC and cholangiocytes to iCCA [91], [93], [365].

Furthermore, notable upregulation of not only KRT19 but also SOX9 suggests significant cellular reprogramming, indicative of hepatic lineage switching where hepatocytes may transform into cholangiocytic-like cells, leading to iCCA [366], [367], [368]. This also aligns with existing research indicating that liver cancer can initially form as undifferentiated tumors which, upon specific perturbations such as modifying expression of APC and NICD, can evolve into forms like HCC or iCCA, respectively [365].

Thus, the presence of IDH1 mutants and the subsequent accumulation of 2-HG appear to be key drivers in the cellular transformation from hepatocytes to the cholangiocytic lineage, offering insight into the development process of iCCA. Of note, this phenomenon was observed in all mutant IDH1 tumors independently of the specific type of *Idh1* mutation they possessed, suggesting that even moderate levels of that oncometabolite can introduce a phenotype switch towards cholangiocytes.

While there was a significant correlation between the presence of 2-HG and the upregulation of KRT19 and SOX9 in all KRAS;TP53;IDH1 tumors, an inverse trend was noted for HNF4α, albeit it was not significant. This partially aligns with a previous study demonstrating that IDH2 and 2-HG inhibit liver progenitor cell differentiation and promote tumor metastasis [186]. It is important to note that this paper primarily analyzed the effects of the IDH2 R140Q mutant, which has been shown to be less catalytically active than even IDH1 R132H [369]. The latter is known for producing moderate levels of 2-HG compared to iCCA-specific mutations.

These observations hint at a complex interplay of 2-HG with cellular processes, with its concentration dictating divergent paths in cancer development. A gradient effect could be postulated – where lower concentrations of 2-HG potentially inhibit hepatocytic differentiation, but as the levels of 2-HG escalate beyond a certain threshold, the inhibition of hepatocytic differentiation diminishes due to the robust upregulation of cholangiocytic lineage expression markers.

Building on research linking 2-HG-induced methylation to cellular differentiation [204], [346], [370], I also explored the potential mechanistic link between 2-HG accumulation, DNA

hypermethylation, and phenotypic changes in KRAS;TP53;IDH1 tumor development. Despite 2-HG being a known inhibitor of TET2 activity [371], my study using CRISPR/Cas9 disruption of *Tet2* and/or *Tet1* in combination with KRAS;TP53 background did not reveal strong interactions between *Idh1* mutations, *Tet* gene disruption, and tumor phenotypes, challenging the initially hypothesized mimicking of 2-HG-induced phenotype in such a context.

Notably, the only significant phenotypic change was in *Tet1*&*Tet2*-disrupted tumors where KRT19 expression was increased, suggesting a shift towards a cholangiocytic trait. This implies that increased DNA methylation alone may not fully replicate the 2-HG-driven phenotype.

Additionally, literature indicates that 2-HG and mutant IDH expression can enhance repressive histone methylation, hindering cellular differentiation or triggering dedifferentiation in cancer models [33], [44], [61]. This mechanism might explain the hepatocytic characteristics observed in this study, though significant differences related to methylation marks associated with 2-HG accumulation were noticeable primarily in the context of primary tumor-derived cell lines and not in tumor tissue itself. It is essential to recognize that the specific process of transdifferentiation in the setting of IDH mutation is still not fully understood.

Interestingly though, mutant IDH1 R132C has been shown to promote cartilage differentiation in mesenchymal stem cells but inhibits osteogenic properties, potentially contributing to the lack of osteosarcomas with this mutation, preferentially forming chondrosarcomas [372].

This research underscores the importance of understanding tumor-driven cellular differentiation changes for therapeutic applications [373], [374], [375], [376] and reveals how mutant IDH1 and/or 2-HG accumulation disrupt cellular differentiation in liver cancer, indicating that 2-HG-induced hepatocytes can undergo transformation into cholangiocytic-like tumor cells *in vivo*. The dual impact of 2-HG on both hepatocytic and cholangiocytic marker expression highlights its complex and pivotal role in cancer progression, where its concentration-dependent effects have far-reaching implications for tumor development and behavior, specifically by focusing on the underlying mechanisms of cellular transformation and lineage determination.

5.4. 2-HG accumulation and its effects on the glycosylation landscape in iCCA

In the KRAS;TP53;IDH1 model, significant morphological differences between IDH1 WT and mutant tumor samples, particularly robust stromal reactions and complex glandular morphologies, are linked to altered glycosylation processes. I have observed consistent upregulation of glycosylation-related molecules such as carbohydrates, mucins, GAGs, and particularly sulfated GAGs in mutant IDH1 samples.

Glycosylation, a crucial post-translational modification, involves the attachment of carbohydrates to proteins or lipids, leading to the formation of glycoproteins and proteoglycans, such as mucins and GAGs, respectively [377], [378]. These complex molecules

play pivotal roles in various cellular functions, including signaling, adhesion, and facilitating cell-cell and cell-matrix interactions, processes crucial for tumor growth and metastasis [187], [378], [379], [380], [381], [382], [383], [384], [385], [386], [387], [388], which are potentially upregulated in IDH1 mutant tumors.

RNA-seq data supports this, indicating an increase in GAG biosynthesis, especially chondroitin and heparan sulfates. These sulfates are essential components of the ECM in context of liver cancer and play critical roles in cell signaling, adhesion, growth, and the remodeling of the TME [389], [390].

Interestingly, the upregulation of glycosylation-associated processes was observed only in iCCA-specific IDH1 mutants (R132C, R132G, R132L) but not IDH1 R132H which points to mutation-specific effects on glycosylation pathways, potentially due to variations in enzymatic activity or metabolic byproducts of these mutations. While specific research linking 2-HG directly to glycosylation changes in iCCA is limited [391], the well-documented influence of 2-HG on metabolic pathways in cancer [392], [393], [394], and of metabolic changes on glycosylation [395], [396], [397], [398] suggests a possible indirect association.

The impact of 2-HG on glycosylation processes could potentially explained by its capability to inhibit α-KG-dependent enzymes. Specifically, Fe(II)/α-KG-dependent-hydroxylases, as referenced in the work of Simmons *et al*., may influence glycosylation by modulating nucleotide sugar metabolism [399]. This modulation affects the availability of sugar substrates for glycosylation, indirectly influencing glycosylation processes in cells. On the other hand, α-KG-dependent dioxygenases, as explored by Jia *et al*., may also modulate glycosylation through protein hydroxylation, affecting protein structure and function, thus altering glycosylation patterns and related enzymatic activities [400].

The altered enzymatic function of mutant IDH1 may also have broader metabolic repercussions, hypothetically increasing the availability of metabolic intermediates necessary for glycosylation processes. Grassian *et al.* highlight the role of *IDH1* mutations in shifting citric acid cycle dynamics, potentially impacting glycosylation via altered energy states and precursor availability [401]. Elevated glucose metabolism in mutant IDH1 cells, as shown by Fujiwara *et al.*, suggests an increased substrate availability for glycosylation due to a surplus of glucose-derived sugar moieties [402].

Furthermore, the disruption of NADPH homeostasis due to the synthesis of 2-HG by IDH1 mutants, as noted by Gelman *et al.*, could affect the pentose phosphate pathway, crucial for nucleotide sugar metabolism and thus essential for glycosylation processes [403]. Concurrently, alterations in glutamine metabolism, as indicated by Reitman *et al.*, could influence glycosylation substrate pools, particularly affecting UDP-N-acetylglucosamine synthesis [404]. These metabolic effects could be the underlying cause of altered glycosylation processes in iCCA-specific IDH1 mutant samples.

In conclusion, these findings highlight a clear link between IDH1 mutants and emergence of aberrant glycosylation processes in this iCCA model, affecting the tumor's architectural features. This underscores the potential role of glycosylation in shaping both biochemical and physical aspects of the TME, impacting cellular functions, and influencing

tumor growth and metastasis. These insights emphasize the importance of glycosylation patterns as critical diagnostic and prognostic markers [388], [405], [406], [407], underscoring their potential utility in IDH1-mutant iCCA.

5.5. *Idh1* mutation affects tumor microenvironment

5.5.1. 2-HG as driver of fibrotic stroma formation

One of the striking findings is the marked increase in stromal populations in the KRAS;TP53 tumors with IDH1 iCCA-specific mutations compared to their IDH1 WT counterparts. This is evidenced firstly by the elevated abundance of fibroblastic signature on the RNA level and further confirmed by a significant upregulation in the expression of markers of activated fibroblasts and myofibroblasts, α-SMA [283] and DES [282], respectively.

Research indicates that hepatic stellate cells (HSCs) in the liver, when activated, can differentiate into fibroblasts, leading to a proliferation of contractile and fibrogenic cells that significantly impact cancer progression [408]. Further studies attributed an important role to HSCs in promoting cholangiocarcinoma cells through cytokine-dependent pathways, also indicating their potential transition into activated fibroblasts [409], [410]. Additionally, the interplay between HSCs and myofibroblasts in promoting tumorigenesis in the liver has been documented [411]. In KRAS;TP53 IDH1 mutant tumors, an increased presence of α-SMA- and DES-positive cells suggests HSC differentiation into fibroblasts, highlighting TME complexities in iCCA.

Furthermore, the transformation of fibroblasts into cancer-associated fibroblasts (CAFs) within iCCA is significant, marked by α-SMA and PDGFR-α expression [412]. Co-culturing fibroblasts with iCCA cells can induce this transformation, promoting tumor growth [413]. The presence of CAFs contributes to increased proliferation, migration, and invasion of iCCA cells, and promotes tumor growth in mouse models [414], [415]. This transformation process is a key aspect of the iCCA TME, affecting disease progression and therapeutic outcomes, offering another perspective on the observed stromal phenotype in mutant IDH1 tumors.

The enhanced expression of DES also points to an increase in myogenic fibroblasts. It has been shown that bile duct isolates can differentiate into myofibroblasts [416]. The increase in α-SMA and DES suggests a shift towards a more fibrotic stroma in the TME, which contributes to tumor stiffness [417]. In the liver environment, stiffness activates HSCs, driving their differentiation into myofibroblasts and in turn exacerbating liver fibrosis [418]. Additionally, fibrosis stimulates mesothelial cells to differentiate into myofibroblasts, adding another layer to the complexity of TME interactions [419].

Considering the stronger α-SMA increase compared to DES in terms of fold-increase in IDH1 mutant KRAS;TP53 tumors in comparison to their IDH1 WT counterparts, one could speculate that 2-HG triggered upregulation of α-SMA-positive cells which leads to increased DES-positive cells as TME stiffness and fibrosis escalate.

Notably, the upregulation of α-SMA and DES was observed in iCCA-specific IDH1 mutant tumors, but not in those with IDH1 R132H mutant. The divergent effects of 2-HG might be contingent on the cell of origin in the TME [420], or alternatively, a certain threshold of 2-HG accumulation might be required to trigger the fibrotic stroma phenotype, a threshold not reached in IDH1 R132H mutants that produce only moderate levels of this oncometabolite.

While the general influence of 2-HG on the TME has been documented in various cancers, and there is abundant evidence of fibrotic stroma development in iCCA, the specific link of 2-HG to the stromal phenotype in iCCA represents a novel finding. The enrichment of activated fibroblasts and myofibroblasts, combined with increased fibrosis, emphasizes the potential of targeting these stromal components. Targeting agents that can modulate the activity of fibroblasts or degrade fibrotic components may augment the effectiveness of other therapies, including immunotherapy [421].

A unique aspect in the KRAS;TP53;IDH1 model is the selective activation of stromal cells without increased vascularization, suggested by unchanged endothelial markers in the context of mutant IDH1. This highlights a distinct pathophysiological aspect of iCCA, where 2-HG affects TME without vascular changes. Understanding this selective activation could inform targeted treatments focusing on stromal components. However, the absence of angiogenesis might also be attributed to rapid tumor formation in the KRAS;TP53;IDH1 model.

This research emphasizes the nuanced understanding of the TME in iCCA, particularly the role of 2-HG, and the potential of targeting stromal cells to improve therapeutic outcomes. Future studies should explore the long-term effects of stromal activation on angiogenesis and investigate targeted therapies disrupting fibroblasts' pathological contributions to iCCA progression.

5.5.2. The role of 2-HG in extracellular matrix remodeling

Proteomic analysis of ECM-enriched KRAS;TP53;IDH1 tumor samples revealed significant ECM composition changes in IDH1 mutant tumors. These alterations include notably upregulated pathways related to integrins, leukocyte extravasation, neutrophil activity, particularly in releasing NETs, and various interleukins when compared to IDH1 WT counterparts.

A marked increase in neutrophil degranulation activities in these KRAS;TP53;IDH1 mutant tumors along with the augmented presence of LY6G-positive cells suggests an intensified inflammatory response with profound effects on the ECM [422]. Notably, neutrophils can form NETs, which play a pivotal role in suppressing T-cell responses within the TME, thus promoting tumor growth via metabolic and functional exhaustion of these cells [423].

NETs also contribute to tumor cell proliferation, migration, and increased metastatic burden, particularly in hepatic metastases [424], [425], [426], [427]. The elevation in GM-CSF in IDH1 mutant tumors, associated with granulocyte differentiation [62],

potentially contributing to this observed phenotype. Additionally, IPA revealed an increase in immune activity in IDH1 mutant tumors, evidenced by a surge in interleukins such as IL-6, IL-8, and IL-13, which are known to play roles in inflammation and immune modulation [291], [295], [428], and a decrease in granzyme A signaling indicating impaired immune surveillance [429].

This inflammatory response, coupled with immunosuppression, mirrors dynamics seen in other cancers [430]. Chronic inflammation can also trigger HSCs to differentiate into myofibroblast-like cells [431], potentially explaining the fibrotic stromal phenotype exhibited by KRAS;TP53;IDH1 mutant tumors.

Beyond that, 2-HG is also known to disrupt collagen maturation via inhibiting α-KG-dependent enzymes, leading to upregulated collagen isoforms and ECM remodeling [432], [433]. This results in ECM strengthening and simultaneous breakdown, characteristic of a rapidly evolving TME [434] which is notably evident in the KRAS;TP53;IDH1 mutant tumors as well. Additionally, the neutrophil degranulation can contribute to ECM remodeling through specific matrix-remodeling enzymes and NETs [435].

Ultimately, ECM fortification exhibited by collagen fibril assembly, an effort to introduce rigidity to the matrix [436], can be counterbalanced by the degradation of collagen and HS-GAGs, facilitated by enzymes present in the ECM [436], [437], [438], which creates spaces exploitable by migrating tumor cells [439]. Beyond that, the upregulated integrin signaling pathway, crucial for cell-ECM communication and adhesion, underscores this continuous matrix reconfiguration. These cited studies could explain the outcomes observed in proteomic analysis of KRAS;TP53;IDH1 tumor samples, highlighting the intricate balance between ECM fortification and degradation as a pivotal aspect of tumor progression and metastasis.

Furthermore, CAFs, whose possible presence was observed in IDH1 mutant KRAS;TP53 tumors, play a role in regulating the collagen biosynthetic pathway, impacting tumor growth and promoting drug resistance in cancer cells [440]. These fibroblasts within iCCA secrete high levels of IL-6 [441], [442], possibly explaining the increased abundance observed in the proteomic analysis.

Interestingly, the findings from this study contrast with those of Amankulor *et al.*, who described that IDH1 R132H mutation leads to downregulation of leukocyte chemotaxis and suppression of the tumor-associated immune system in gliomas [443]. Conversely, the iCCA-specific IDH1 mutants in this study demonstrated an enhanced effect on leukocyte extravasation. This divergence suggests that varying tissue concentrations of 2-HG can result in different downstream effects, despite a similar overarching outcome of immunosuppression.

In summary, these experiments demonstrate a complex interplay between *IDH1* mutations, ECM dynamics, and immune modulation in the liver cancer TME. These mutations in the context of KRAS;TP53 foster an environment conducive to cellular adhesion, matrix deposition, structural reconfiguration, and immune evasion, highlighting the need for further research into the molecular mechanisms driving these alterations in tumor progression and therapy.

5.5.3. 2-HG as immune infiltration modulator

This study provides a detailed examination of immune cell infiltration in IDH1 mutant tumors within a KRAS;TP53-driven tumor development context, revealing distinct patterns of immune modulation compared to IDH1 WT counterparts.

Using CCA-specific matrix, established by Nishida *et al.* [297], I observed downregulation of immune checkpoint molecules and genes linked to MHC class I presentation in IDH1 mutant tumors, indicating potential immune evasion. This finding aligns with the work of Amankulor *et al.*, who demonstrated similar effects of *IDH1* mutations on the repression of the tumor-associated immune system in gliomas [443].

Increased T-cell infiltration, indicated by CD3 and CD4 staining, suggests a more active immune environment in IDH1 mutant tumors, except for those with the IDH1 R132L mutant, which exhibited increase only in the abundance of CD3 marker. While CD3 and CD4 are markers for T-cells and helper T-cells, respectively [301], the specific role and impact of this infiltration in the context of IDH1 mutant tumors remains unclear, highlighting a gap in current literature.

Upregulation of genes associated with MHC class II antigen presentation in the IDH1 mutant tumors' RNA-seq data could indicate either a compensatory mechanism or an effort to enhance helper T-cell responses. However, this might lead to an immunosuppressive environment, especially if Tregs are preferentially activated, which are known for their role in suppressing immune responses [444].

It is particularly noteworthy to highlight the increased Treg signatures and FOXP3 staining, in the KRAS;TP53 IDH1 R132C and R132G mutants. In stark contrast, tumors with the IDH1 R132L mutation showed a significant increase in infiltration by CD8-positive cell populations. Prominence of CD8-positive cells, known as key players in combating tumors [302], indicates a more aggressive immune response against R132L mutant tumors, suggesting that this IDH1 mutant may create a TME more favorable for immune-mediated tumor suppression. This could explain the delayed tumorigenesis in KRAS;TP53;IDH1 R132L mutant-bearing mice compared to those with IDH1 R132C and R132G mutations.

Conversely, IDH1 R132H mutant tumors showed increased CD3 and CD4 markers, suggesting a more active or primed TME in relation to helper T-cell infiltration. Especially since it was observed without notable differences in CD8 and FOXP3 levels. Similarly to IDH1 R132L, IDH1 R132H tumors also exhibited survival rate comparable to IDH1 WT tumors. This similarity could be attributed to the helper T-cell infiltration and the probable activation of anti-tumoral functions [445], [446], [447].

Furthermore, as explained earlier, iCCA-specific IDH1 mutant tumors have altered glycosylation, which is known to contribute to immune responses [383], [384]. Specific glycosyltransferases modify cell surface glycosylation, enabling cancer cells to either evade immune detection [448], [449] or engage it [450], [451], [452]. This potentially contributes to the immunosuppressive phenotype exhibited by Treg abundance in case of IDH1 R132C and

R132G mutant tumors. Conversely, there is an immunostimulatory response characterized by the presence of CD8-positive or CD4-positive T-cells in case of IDH1 R132L and R132H mutant tumors, respectively.

In contrast, some studies suggest that IDH1/2 mutant gliomas typically exhibit lower immune infiltration compared to WT tumors [453], [444], [454], [455], [456], with a notably low representation of Tregs [457]. This includes a study by Ren *et al.*, reporting a positive prognosis correlation with increased NK cell infiltration in these gliomas [458]. Furthermore, Wang *et al*. found that IDH1 mutant glioblastomas are characterized by increased tumor-associated macrophages/microglia infiltration and CD8-positive T-cell enrichment [459], while in KRAS;TP53;IDH1 tumors abundance of CD8-positive T-cells was affected exclusively in IDH1 R132L tumors.

Despite variations between some studies, overall, in IDH mutant gliomas 2-HG generally acts as immunosuppressive agent posing a significant challenge to immunotherapeutic approaches in these tumors [460], [461], contributing to the so called 'immune-desert' microenvironment [462], [463]. The discrepancy between gliomas and IDH1 mutant KRAS;TP53 tumors in this context might be attributed to differences in tumor types or stages, as discussed by Bindea *et al.* [464], and specific mutations within the *IDH* genes.

Collectively, these findings suggest that there is a gradient of immune responses where IDH1 R132H and IDH1 R132L might stimulate anti-tumoral immune response, while IDH1 R132C and IDH1 R132G conversely trigger pro-tumoral immune response.

This variability underscores the importance in distinguishing between specific type of amino acid substitution in the *IDH1* gene, as each mutation leads to distinct downstream effects on the immune landscape. Furthermore, these immune dynamics imply that IDH1 mutant tumors may respond variably to immunotherapies, highlighting the need for personalized treatment strategies based on specific *IDH1* mutations. However, it is crucial to acknowledge that these observations require further validation and exploration. The complexity of tumor-immune interactions, influenced by diverse *IDH1* mutations, necessitates extensive research to confirm these findings and to understand their implications fully in clinical setting.

Additionally, the elevated levels of CCL17 in KRAS;TP53 IDH1 R132C and R132G mutant tumors, suggest a role for this cytokine in shaping the immune dynamics within the TME, with tumor cells likely responsible for its production. The observed increase in FOXP3-positive Tregs, especially in IDH1 R132C and R132G mutant tumors, further underscores an immunosuppressive environment. This environment is likely facilitated by the tumor-derived CCL17's recruitment of Tregs [465], [466], [467].

In conclusion, this study contributes to understanding the unique immune landscape shaped by individual *IDH1* mutations, particularly the role of CCL17 in the immunosuppressive environment of IDH1 mutant tumors. These insights highlight complex changes in immune dynamics and gene expression patterns and underscore the potential for novel treatment strategies targeting factors like 2-HG and CCL17.

5.6. Exploiting *IDH1* mutation-induced vulnerabilities in iCCA

5.6.1. Leveraging *IDH1* mutations for their neoantigen properties

This study explores the immunotherapeutic potential of targeting IDH1 mutations in iCCA, particularly for cancer vaccine development leveraging IDH1 mutant neoantigen properties. Our novel approach in iCCA treatment strategies, which was inspired by the work of Schumacher *et al.* [231], involved synthetic peptides to target iCCA cells with *IDH1* mutations.

The focus was on peptide R132G, chosen for its strong immunogenic response in preliminary assays. However, translating this *ex vivo* efficacy to *in vivo* models proved challenging. Despite the R132G peptide's promising immune response *in vitro*, its effectiveness in a preventive vaccination setup was less pronounced. The survival outcomes in the KRAS;TP53;IDH1 HTVi mouse model did not reflect the anticipated protective effect of the R132G vaccine for the IDH1 R132G tumor-bearing mice. This observation is pivotal, considering the liver's unique immune-privileged status, formidable challenge for immunotherapy [468], [469], [470], [471] and is known for reducing effectiveness of immune-based cancer treatments [7], [471], [472].

In order to circumvent the potential confounding factors stemming from the liver's immune-privileged status and more effectively address the question of the R132G peptide's immunogenic capacity *in vivo*, I transitioned from HTVi to a subcutaneous injection approach using tumor-derived KRAS;TP53;IDH1 R132G cells. Even with this altered model, the modest success of the preventive vaccination protocol with R132G peptide suggests inherent barriers posed by this setup. A contributing factor to this limited efficacy might be 2-HG, known for its potential role in immune evasion [473], [474], [475].

This challenge is exacerbated by the fact that cells employed for the allograft, possessing a KRAS;TP53 background in the tumor model, might intrinsically promote tumor growth, a factor that could undermine the tested immunotherapy's effectiveness. KRAS, a genetic enhancer of cellular proliferation, resistance to apoptosis, and metabolic adaptations, contributes to tumor growth [476], [477]. Similarly, the knock-out of *Tp53*, a critical regulator of genomic stability, further complicates matters by enabling uncontrolled cell division, evasion from apoptosis, and increased DNA-damage tolerance [478].

In conclusion, while the study successfully demonstrated the immunogenicity of the R132G peptide variant *in vitro*, its efficacy *in vivo* in the KRAS;TP53 context was limited. Despite these limitations, the findings do not undermine the potential of IDH1 mutants as viable targets for cancer vaccines in iCCA. Instead, they underscore the complexities and challenges inherent in developing effective immunotherapies. This is particularly pertinent given that IDH1 inhibitors are already being utilized in clinical settings [207], [244], [479].

The unique immune environment of the liver and the difficulties in translating *in vitro* findings to effective *in vivo* treatments are significant obstacles that need to be addressed.

Therefore, further research and refinement of immunotherapeutic approaches are essential to fully exploit the therapeutic potential of targeting *IDH1* mutations in iCCA.

5.6.2. 2-HG-driven genetic vulnerabilities

Investigation into the genetic dependencies in IDH1 mutant iCCA cells reveals significant insights into the vulnerabilities conferred by the oncometabolite 2-HG. By utilizing the DepMap portal database, critical genes impacting cell viability in a 2-HG-dependent manner were identified. These genes, including *AHCYL1*, *TNS3*, *ITGAV*, and *ITGB5*, are potential therapeutic targets in the IDH1 mutant context.

AHCYL1 senses intracellular SAH levels, a molecule pivotal in methylation and cellular signaling, influencing autophagy and broader cellular functions [480], while TNS3 is associated with cellular processes such as migration, which is integral for tumor metastasis [226], [481]. The integrin subunits, ITGAV [482] and ITGB5 [483], on the other hand, represent gatekeepers of cellular interactions, mediating cell-to-matrix interactions, a key factor in tumor invasiveness and angiogenesis.

The integration of CRISPR/Cas9 screening data from Depmap with KRAS;TP53;IDH1 RNA-seq results provided a comprehensive perspective on the role of these genes in iCCA cell survival. The observed upregulation could therefore present a strategic target; speculatively, by selectively inhibiting the expression and function of these genes, it could be possible to induce a detrimental effect on the cancer's progression. Such targeted approaches could potentially disrupt key survival pathways in iCCA cells, offering a novel avenue for therapeutic intervention in this challenging cancer type.

However, the competition assay using KRAS;TP53 tumor-derived cells did not show significant differences between IDH1 mutant and IDH1 WT cells upon knock-out of individual genes of interest. This result countering the hypothesis, might be, as explained before, attributed to the overexpression of KRAS and disruption of *Tp53*. This background which intrinsically promotes proliferation could makes it challenging for 2-HG presence to significantly influence these already hyperactive cells, obscuring phenotypic differences both *in vitro* and *in vivo*.

In the next step, I shifted focus from murine cell lines to established human cell lines. This shift enabled examination of the differential responses of iCCA cell lines SNU1079 and RBE to CRISPR/Cas9-mediated gene knock-outs, providing valuable insights.

The reduced viability in both cell lines following *TNS3* and *AHCYL1* knock-outs suggests these genes are crucial for cell survival across different cell types, highlighting their potential as broad-spectrum therapeutic targets. Conversely, the distinct responses to *ITGAV* and *ITGB5* knock-outs – reducing viability in SNU1079 but not in RBE – underscore the unique cellular pathways specific to each cell line. This variation emphasizes the necessity of a nuanced approach in targeting these genes, considering the specific cellular context of each cancer type.

Responses in HT1080 cells, a chondrosarcoma line with the expression of IDH1 R132C mutant, further demonstrate that cellular responses can vary significantly even with common genetic mutations. This cell line displayed lack of sensitivity to *TNS3* and *AHCYL1* knock-outs and decreased viability upon *ITGAV* and *ITGB5* disruption. This variation points to the unique molecular pathways in different cancer types and the influence of co-existing mutations or epigenetic modifications.

This part of the study sheds light on how 2-HG affects genetic dependencies in IDH1 mutant iCCA, identifying key genes for potential targeted therapies. Further research is needed to understand their roles and develop effective treatments, opening new paths for precision medicine in iCCA with *IDH1* mutations.

5.7. IDH mutations in iCCA: partnerships with oncogenic pathways

The critical involvement of *IDH1* mutations in iCCA is evident through comprehensive genomic data from sources like cBioPortal. These mutations are mutually exclusive with established iCCA drivers like *KRAS* and *TP53* in human datasets, suggesting a unique tumorigenesis pathway in IDH1-mutated iCCA, contrasting with murine models. This highlights a potential functional redundancy and the importance of human-centric models in understanding iCCA pathogenesis. Additionally, the co-occurrence of *IDH1* mutations with *ARID1A*, *BAP1*, and *PBRM1* mutations indicates possible synergistic effects in tumorigenesis, underlining the need for a comprehensive understanding of genetic interplays in cancer.

5.7.1. Replicating patient-specific genomic patterns in iCCA research

The development of mouse models incorporating human iCCA-specific genetic patterns, particularly the combination of IDH1 (WT or R132C) with *Pbrm1*, *Arid1a*, and *Bap1* mutations, aimed to provide a more accurate representation of the human disease. This approach, however, served as a reminder of the complexity and unpredictability of genetic interactions when no cancer development was observed upon introduction of *Pbrm1*, *Arid1a*, and *Bap1* knock-outs in combination with IDH1 WT or IDH1 R132C via HTVi even after 18 months.

The introduction of additional CRISPR/Ca9-mediated mutations such as *Tp53* or *Pten* deletions in order to improve the tumorigenicity led to divergent outcomes like chondrosarcoma-like tumors or hepatomegaly, respectively, both of which deviate from the typical iCCA phenotype.

These results illustrate the challenges in replicating the intricate genetic landscape of human cancers in animal models [484], [485], [486] and highlight the need for ongoing refinement of these models to achieve more predictive insights into iCCA pathogenesis, particularly in the context of *IDH1* mutations.

5.7.2. Challenges in mimicking iCCA with IDH1 mutations in mouse models

The alternative to exploring the genetic patient-specific genomic patterns in iCCA involves employing additional to KRAS;TP53 iCCA *in vivo* mouse models to investigate the role of *Idh1* mutations in this tumor type. Utilizing the HTVi, NICD and constitutively active AKT were introduced, a technique widely recognized for simulating iCCA features [487]. This approach combined NICD;AKT with either the IDH1 WT or R132C, ultimately providing valuable insights into the interplay between *IDH1* mutations and the NOTCH and AKT signaling pathways.

The NOTCH and AKT pathways are recognized as oncogenic drivers in CCA models [487] and play crucial roles in cell differentiation, proliferation, and survival [488], [489], [490], [491], [492], [493], [494]. Synergistic overexpression of NICD and constitutively active form of AKT [495], disrupts hepatic cell dynamics, leading to early tumorigenic events such as cyst formation, a key precursor in tumor development [496], [497], [498], [499], [500].

Interestingly, the absence of cyst formation in NICD;AKT mice with mutant IDH1 suggests a unique *IDH1* mutation influence, potentially disrupting the NOTCH signaling pathway, as indicated by the absence of NICD and its downstream target HES1 in tissue analyses.

Experiments *in vitro* with tumor-derived KRAS;TP53;IDH1 cells have shown distinct behaviors between WT and mutant IDH1 upon overexpression of NICD, suggesting a potential inhibitory interaction with 2-HG accumulation on cell viability and proliferation.

While there are multiple reports of NOTCH signaling pathway relevance to iCCA, including its critical role in the development and progression of the disease by driving the transformation of liver cells into malignant cholangiocytes [501], [502], influencing tumor characteristics, and as such representing a potential target for therapeutic intervention [503], [504], the role of IDH1 mutations in this context remains much less understood.

This broader gap in knowledge necessitates further research to understand the potential interplay between *IDH* mutations, particularly the effects of the interplay between 2-HG and the NOTCH signaling pathway not only in iCCA but perhaps across other tumor types. These findings suggest a complex and nuanced role for *IDH1* mutations in iCCA, with the observed mutual exclusivity between NICD and IDH1 mutant representing a novel discovery.

6. Summary and outlook

In conclusion, this research significantly advances our understanding of *IDH1* mutations in iCCA, shedding light on the molecular mechanisms specific to this kind of tumors and unraveling the complexities of *IDH1* mutations in a broader cancer context. As such, it significantly contributes to currently limited body of knowledge regarding the context-specific emergence of *IDH1* mutations across various tumor entities and their unique contributions to the pathogenesis of iCCA.

Utilizing HTVi, this study elucidated the critical role of 2-HG accumulation in promoting rapid tumor cell proliferation, steering cells towards a more cholangiocytic phenotype, and remodeling the TME. This remodeling fosters both immune evasion — by releasing CCL17 and thus attracting Treg cells — and inflammation by activating neutrophils (**Figure 30**). These insights highlight potential avenues for novel cancer treatment strategies.

Additionally, the novel link between 2-HG accumulation and the accelerated stromal deposition in iCCA, marked by activated fibroblasts and increased fibrosis, presents as another potential therapeutic target. The role of 2-HG as a biomarker, particularly for early detection and diagnosis, further amplifies the impact of this research.

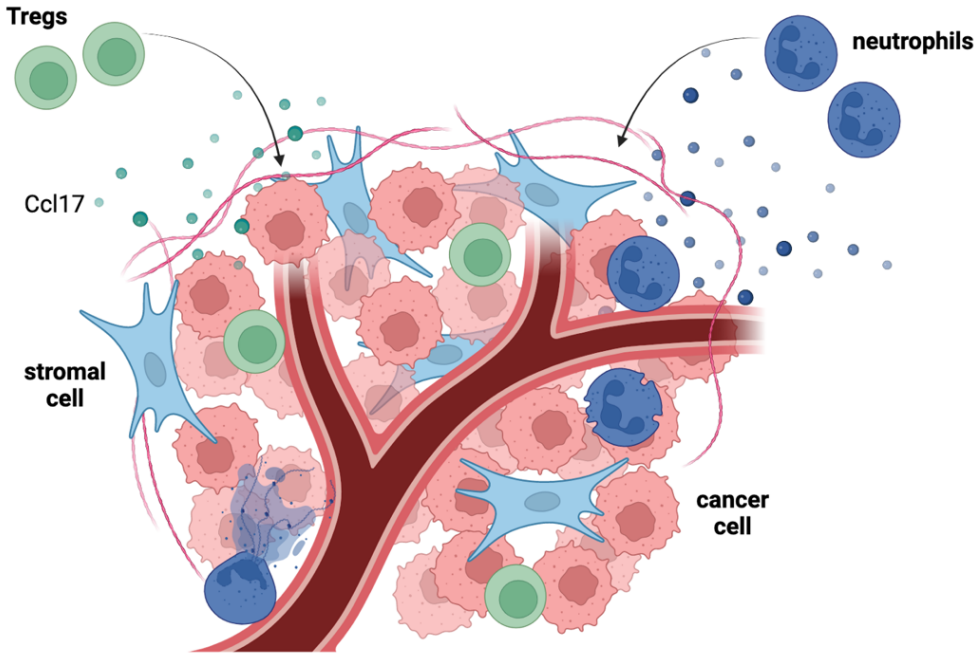

Figure 30. Dynamic changes in the TME stemming from 2-HG accumulation.
Created in Biorender.

Looking forward, this thesis lays a solid foundation for further exploratory studies into *IDH1* mutations and 2-HG's broader implications in iCCA and possibly other cancers. It

underscores the importance of continued innovation in model development, therapeutic targeting, and the strategic use of biomarkers in early cancer detection and treatment.

By acknowledging limitations and proposing future directions, this study not only opens new avenues for investigating *IDH1* mutations and 2-HG in iCCA and beyond, but also makes a profound contribution to the battle against this complex disease.

7. Bibliography

[1] K. Si-Tayeb, F. P. Lemaigre, and S. A. Duncan, "Organogenesis and development of the liver," *Dev. Cell*, vol. 18, no. 2, pp. 175–189, Feb. 2010, doi: 10.1016/j.devcel.2010.01.011.

[2] G. Michalopoulos, "Principles of liver regeneration and growth homeostasis," *Compr Physiol*, vol. 3, pp. 485–513, 2013.

[3] H. J. Chaudhari, M. K. Ravat, V. H. Vaniya, and A. N. Bhedi, "Morphological study of human liver and its surgical importance," *Journal of Clinical and Diagnostic Research*, vol. 11, no. 6, pp. AC09-AC12, 2017, doi: 10.7860/JCDR/2017/24467.10020.

[4] A. J. Knell and W. Hospital, "Liver Function and Failure: The Evolution of Liver Physiology," *J R Coll Physicians Lond*, vol. 14, no. 3, p. 205, 1980.

[5] H. C. Towle, E. N. Kaytor, and H. M. Shih, "REGULATION OF THE EXPRESSION OF LIPOGENIC ENZYME GENES BY CARBOHYDRATE," vol. 17, pp. 405–433, Nov. 2003, doi: 10.1146/ANNUREV.NUTR.17.1.405.

[6] S. J. Pilkis and D. K. Granner, "Molecular physiology of the regulation of hepatic gluconeogenesis and glycolysis," *Annu Rev Physiol*, vol. 54, pp. 885–909, 1992, doi: 10.1146/ANNUREV.PH.54.030192.004321.

[7] I. N. Crispe, "The liver as a lymphoid organ," *Annu Rev Immunol*, vol. 27, pp. 147–163, 2009, doi: 10.1146/ANNUREV.IMMUNOL.021908.132629.

[8] E. Nemeth, A. W. Baird, and C. O'Farrelly, "Microanatomy of the liver immune system," *Semin Immunopathol*, vol. 31, no. 3, pp. 333–343, Sep. 2009, doi: 10.1007/s00281-009-0173-4.

[9] D. M. Grant, "Detoxification pathways in the liver," *J Inherit Metab Dis*, vol. 14, no. 4, pp. 421–430, Jul. 1991, doi: 10.1007/BF01797915.

[10] M. W. Robinson, C. Harmon, and C. O'Farrelly, "Liver immunology and its role in inflammation and homeostasis," *Cell Mol Immunol*, vol. 13, no. 3, pp. 267–276, May 2016, doi: 10.1038/CMI.2016.3.

[11] H. Reinke and G. Asher, "Circadian Clock Control of Liver Metabolic Functions," *Gastroenterology*, vol. 150, no. 3, pp. 574–580, Mar. 2016, doi: 10.1053/j.gastro.2015.11.043.

[12] C. Peralta, M. B. Jiménez-Castro, and J. Gracia-Sancho, "Hepatic ischemia and reperfusion injury: Effects on the liver sinusoidal milieu," *J Hepatol*, vol. 59, no. 5, pp. 1094–1106, Nov. 2013, doi: 10.1016/J.JHEP.2013.06.017.

[13] K. L. Hastings, M. D. Green, B. Gao, P. E. Ganey, R. A. Roth, and G. R. Burleson, "Beyond Metabolism: Role of the Immune System in Hepatic Toxicity," *Int J Toxicol*, vol. 39, no. 2, pp. 151–164, Mar. 2020, doi: 10.1177/1091581819898399/ASSET/IMAGES/LARGE/10.1177_1091581819898399-FIG2.JPEG.

[14] M. W. Robinson, C. Harmon, and C. O'Farrelly, "Liver immunology and its role in inflammation and homeostasis," *Cell Mol Immunol*, vol. 13, no. 3, pp. 267–276, May 2016, doi: 10.1038/CMI.2016.3.

[15] M. Alves-Bezerra and D. E. Cohen, "Triglyceride metabolism in the liver," *Compr Physiol*, vol. 8, no. 1, p. 1, Dec. 2017, doi: 10.1002/CPHY.C170012.

[16] D. H. Ipsen, J. Lykkesfeldt, and P. Tveden-Nyborg, "Molecular mechanisms of hepatic lipid accumulation in non-alcoholic fatty liver disease," *Cellular and Molecular Life Sciences*, vol. 75, no. 18, p. 3313, Sep. 2018, doi: 10.1007/S00018-018-2860-6.

[17] S. J. Pilkis, M. R. El-Maghrabi, and T. H. Claus, "Hormonal regulation of hepatic gluconeogenesis and glycolysis," *Annu Rev Biochem*, vol. 57, pp. 755–783, 1988, doi: 10.1146/ANNUREV.BI.57.070188.003543.

[18] G. Biolo, "Protein Metabolism and Requirements," *Nutrition in Intensive Care Medicine: Beyond Physiology*, vol. 105, pp. 12–20, Oct. 2012, doi: 10.1159/000341545.

[19] Z. Zhou, M. J. Xu, and B. Gao, "Hepatocytes: A key cell type for innate immunity," *Cell Mol Immunol*, vol. 13, no. 3, pp. 301–315, May 2016, doi: 10.1038/CMI.2015.97.

[20] M. Pittiruti, J. H. Siegel, G. Sganga, B. Coleman, C. E. Wiles, and R. Placko, "Determinants of Urea Nitrogen Production in Sepsis: Muscle Catabolism, Total Parenteral Nutrition, and Hepatic Clearance of Amino Acids," *Archives of Surgery*, vol. 124, no. 3, pp. 362–372, Mar. 1989, doi: 10.1001/ARCHSURG.1989.01410030112019.

[21] J. L. Boyer, "Bile Formation and Secretion," *Compr Physiol*, vol. 3, no. 3, p. 1035, 2013, doi: 10.1002/CPHY.C120027.

[22] J. M. Banales, R. C. Huebert, T. Karlsen, M. Strazzabosco, N. F. LaRusso, and G. J. Gores, "Cholangiocyte pathobiology," *Nat Rev Gastroenterol Hepatol*, vol. 16, no. 5, p. 269, May 2019, doi: 10.1038/S41575-019-0125-Y.

[23] W. Y. Lu *et al.*, "Hepatic progenitor cells of biliary origin with liver repopulation capacity," *Nat. Cell Biol.*, vol. 17, no. 8, pp. 971–983, Aug. 2015, doi: 10.1038/ncb3203.
[24] R. V. Guest, L. Boulter, B. J. Dwyer, and S. J. Forbes, "Understanding liver regeneration to bring new insights to the mechanisms driving cholangiocarcinoma," *npj Regenerative Medicine 2017 2:1*, vol. 2, no. 1, pp. 1–8, May 2017, doi: 10.1038/s41536-017-0018-z.
[25] S. Yamada, Y. Yamamoto, M. Nagasawa, A. Hara, T. Kodera, and I. Kojima, "In vitro transdifferentiation of mature hepatocytes into insulin-producing cells," *Endocr J*, vol. 53, no. 6, pp. 789–795, 2006, doi: 10.1507/ENDOCRJ.K06-116.
[26] Y. Nishikawa *et al.*, "Transdifferentiation of mature rat hepatocytes into bile duct-like cells in vitro," *Am J Pathol*, vol. 166, no. 4, pp. 1077–1088, 2005, doi: 10.1016/S0002-9440(10)62328-0.
[27] H. Watanabe *et al.*, "Transdifferentiation into biliary ductular cells of hepatocytes transplanted into the spleen," *Pathology*, vol. 40, no. 3, pp. 272–276, 2008, doi: 10.1080/00313020801911546.
[28] A. Raven *et al.*, "Cholangiocytes act as facultative liver stem cells during impaired hepatocyte regeneration," *Nature 2017 547:7663*, vol. 547, no. 7663, pp. 350–354, Jul. 2017, doi: 10.1038/nature23015.
[29] D. Sia, A. Villanueva, S. L. Friedman, and J. M. Llovet, "Liver Cancer Cell of Origin, Molecular Class, and Effects on Patient Prognosis," *Gastroenterology*, vol. 152, no. 4, pp. 745–761, Mar. 2017, doi: 10.1053/J.GASTRO.2016.11.048.
[30] V. Racanelli and B. Rehermann, "The liver as an immunological organ," *Hepatology*, vol. 43, no. 2 SUPPL. 1, Feb. 2006, doi: 10.1002/HEP.21060.
[31] I. N. Crispe, "Immune tolerance in liver disease," *Hepatology*, vol. 60, no. 6, pp. 2109–2117, Dec. 2014, doi: 10.1002/HEP.27254.
[32] F. Heymann and F. Tacke, "Immunology in the liver-from homeostasis to disease," *Nat Rev Gastroenterol Hepatol*, vol. 13, no. 2, pp. 88–110, Feb. 2016, doi: 10.1038/NRGASTRO.2015.200.
[33] J. Poisson *et al.*, "Liver sinusoidal endothelial cells: Physiology and role in liver diseases," *J Hepatol*, vol. 66, no. 1, pp. 212–227, Jan. 2017, doi: 10.1016/J.JHEP.2016.07.009.
[34] S. Shetty, P. F. Lalor, and D. H. Adams, "Liver sinusoidal endothelial cells — gatekeepers of hepatic immunity," *Nat Rev Gastroenterol Hepatol*, vol. 15, no. 9, pp. 555–567, Sep. 2018, doi: 10.1038/S41575-018-0020-Y.
[35] M. Siwicki *et al.*, "Resident Kupffer cells and neutrophils drive liver toxicity in cancer immunotherapy," *Sci Immunol*, vol. 6, no. 61, pp. 643–655, Jul. 2021, doi: 10.1126/SCIIMMUNOL.ABI7083/SUPPL_FILE/SCIIMMUNOL.ABI7083_TABLES_S1_TO_S8.ZIP.
[36] C. L. Zimmer *et al.*, "A biliary immune landscape map of primary sclerosing cholangitis reveals a dominant network of neutrophils and tissue-resident T cells," *Sci Transl Med*, vol. 13, no. 599, p. 3107, Jun. 2021, doi: 10.1126/SCITRANSLMED.ABB3107/SUPPL_FILE/SCITRANSLMED.ABB3107_SM.PDF.
[37] S. L. Zhou *et al.*, "Tumor-Associated Neutrophils Recruit Macrophages and T-Regulatory Cells to Promote Progression of Hepatocellular Carcinoma and Resistance to Sorafenib," *Gastroenterology*, vol. 150, no. 7, pp. 1646-1658.e17, Jun. 2016, doi: 10.1053/J.GASTRO.2016.02.040.
[38] M. Schneider *et al.*, "Neutrophils suppress mucosal-associated invariant T cells in humans," *Eur J Immunol*, vol. 50, no. 5, pp. 643–655, May 2020, doi: 10.1002/EJI.201948394.
[39] I. N. Crispe, "Hepatic T cells and liver tolerance," *Nat Rev Immunol*, vol. 3, no. 1, pp. 51–62, Jan. 2003, doi: 10.1038/NRI981.
[40] E. Schrumpf *et al.*, "The biliary epithelium presents antigens to and activates natural killer T cells," *Hepatology*, vol. 62, no. 4, pp. 1249–1259, Oct. 2015, doi: 10.1002/HEP.27840.
[41] U. P. Zmrzljak and D. Rozman, "Circadian regulation of the hepatic endobiotic and xenobitoic detoxification pathways: The time matters," *Chem Res Toxicol*, vol. 25, no. 4, pp. 811–824, Apr. 2012, doi: 10.1021/TX200538R/ASSET/IMAGES/MEDIUM/TX-2011-00538R_0005.GIF.
[42] G. Michalopolous, "Terminating hepatocyte proliferation during liver regeneration: The roles of two members of the same family (CCAAT-enhancer-binding protein alpha and beta) with opposing actions," *Hepatology*, vol. 61, no. 1, pp. 32–34, Jan. 2015, doi: 10.1002/HEP.27329.
[43] D. C. Mastellos, R. A. DeAngelis, and J. D. Lambris, "Inducing and Characterizing Liver Regeneration in Mice: Reliable Models, Essential 'Readouts' and Critical Perspectives," *Curr Protoc Mouse Biol*, vol. 3, no. 3, pp. 141–170, Oct. 2013, doi: 10.1002/9780470942390.MO130087.
[44] S. K. Asrani, H. Devarbhavi, J. Eaton, and P. S. Kamath, "Burden of liver diseases in the world," *J Hepatol*, vol. 70, no. 1, pp. 151–171, Jan. 2019, doi: 10.1016/J.JHEP.2018.09.014.
[45] R. Bataller and D. A. Brenner, "Liver fibrosis," *Journal of Clinical Investigation*, vol. 115, no. 2, pp. 209–218, 2005, doi: 10.1172/JCI24282.

[46] W. T. London and K. A. Mcglynn, "Liver Cancer," *Liver cancer. Cancer epidemiology and prevention.*, vol. 3, pp. 763–786, Sep. 2006, doi: 10.1093/acprof:oso/9780195149616.003.0039.

[47] S. Caruso *et al.*, "Analysis of Liver Cancer Cell Lines Identifies Agents With Likely Efficacy Against Hepatocellular Carcinoma and Markers of Response.," *Gastroenterology*, vol. 157, no. 3, pp. 760–776, Sep. 2019, doi: 10.1053/J.GASTRO.2019.05.001.

[48] W. Cao *et al.*, "Modeling liver cancer and therapy responsiveness using organoids derived from primary mouse liver tumors," *Carcinogenesis*, vol. 40, no. 1, pp. 145–154, Mar. 2019, doi: 10.1093/CARCIN/BGY129.

[49] S. Y. Yim *et al.*, "Integrated genomic comparison of mouse models reveals their clinical resemblance to human liver cancer," *Molecular Cancer Research*, vol. 16, no. 11, pp. 1713–1723, Nov. 2018, doi: 10.1158/1541-7786.MCR-18-0313/81839/AM/INTEGRATED-GENOMIC-COMPARISON-OF-MOUSE-MODELS.

[50] T. Y. Doktorova *et al.*, "Transcriptomic responses generated by hepatocarcinogens in a battery of liver-based in vitro models.," *Carcinogenesis*, vol. 34 6, no. 6, pp. 1393–1402, Jun. 2013, doi: 10.1093/CARCIN/BGT054.

[51] G. S. van Tienderen, B. G. Koerkamp, J. N. M. Ijzermans, L. J. W. van der Laan, and M. M. A. Verstegen, "Recreating Tumour Complexity in a Dish: Organoid Models to Study Liver Cancer Cells and their Extracellular Environment," *Cancers (Basel)*, vol. 11, no. 11, Nov. 2019, doi: 10.3390/CANCERS11111706.

[52] A. Saborowski *et al.*, "Murine Liver Organoids as a Genetically Flexible System to Study Liver Cancer In Vivo and In Vitro," *Hepatol Commun*, vol. 3, no. 3, pp. 423–436, Mar. 2019, doi: 10.1002/HEP4.1312.

[53] J. L. Leiting *et al.*, "Biliary tract cancer patient-derived xenografts: Surgeon impact on individualized medicine," *JHEP Reports*, vol. 2, no. 2, Apr. 2020, doi: 10.1016/J.JHEPR.2020.100068.

[54] Z. Y. Li, S. Ni, X. Yang, N. Kiviat, and A. Lieber, "Xenograft models for liver metastasis: Relationship between tumor morphology and adenovirus vector transduction," *Molecular Therapy*, vol. 9, no. 5, pp. 650–657, May 2004, doi: 10.1016/j.ymthe.2004.01.021.

[55] L. D. Shultz, N. Goodwin, F. Ishikawa, V. Hosur, B. L. Lyons, and D. L. Greiner, "Human cancer growth and therapy in immunodeficient mouse models.," *Cold Spring Harb Protoc*, vol. 2014 7, no. 7, pp. 694–708, Jul. 2014, doi: 10.1101/PDB.TOP073585.

[56] B. J. Drapkin *et al.*, "Genomic and Functional Fidelity of Small Cell Lung Cancer Patient-Derived Xenografts.," *Cancer Discov*, vol. 8 5, no. 5, pp. 600–615, May 2018, doi: 10.1158/2159-8290.CD-17-0935.

[57] F. Reyal *et al.*, "Molecular profiling of patient-derived breast cancer xenografts," *Breast Cancer Res*, vol. 14, no. 1, Jan. 2012, doi: 10.1186/BCR3095.

[58] A. M. Moyer *et al.*, "Spontaneous murine tumors in the development of patient-derived xenografts: a potential pitfall," *Oncotarget*, vol. 10, no. 39, pp. 3924–3930, 2019, doi: 10.18632/ONCOTARGET.27001.

[59] D. F. Calvisi *et al.*, "Criteria for preclinical models of cholangiocarcinoma: scientific and medical relevance," *Nature Reviews Gastroenterology & Hepatology 2023 20:7*, vol. 20, no. 7, pp. 462–480, Feb. 2023, doi: 10.1038/s41575-022-00739-y.

[60] S. K. Saha, C. A. Parachoniak, and N. Bardeesy, "IDH mutations in liver cell plasticity and biliary cancer," *Cell Cycle*, vol. 13, no. 20, pp. 3176–3182, Oct. 2014, doi: 10.4161/15384101.2014.965054.

[61] A. Velez-Delgado *et al.*, "Extrinsic KRAS signaling shapes the pancreatic microenvironment through fibroblast reprogramming," *bioRxiv*, p. 2021.08.26.457660, Aug. 2021, doi: 10.1101/2021.08.26.457660.

[62] L. J. Bayne *et al.*, "Tumor-Derived Granulocyte-Macrophage Colony-Stimulating Factor Regulates Myeloid Inflammation and T Cell Immunity in Pancreatic Cancer," *Cancer Cell*, vol. 21, no. 6, pp. 822–835, Jun. 2012, doi: 10.1016/j.ccr.2012.04.025.

[63] W. Zhang *et al.*, "Downstream of mutant KRAS, the transcription regulator YAP is essential for neoplastic progression to pancreatic ductal adenocarcinoma," *Sci Signal*, vol. 7, no. 324, May 2014, doi: 10.1126/SCISIGNAL.2005049.

[64] D. D. Shi *et al.*, "De novo pyrimidine synthesis is a targetable vulnerability in IDH mutant glioma," *Cancer Cell*, vol. 40, no. 9, pp. 939-956.e16, Sep. 2022, doi: 10.1016/J.CCELL.2022.07.011.

[65] L. Zhao *et al.*, "Chronic inflammation aggravates metabolic disorders of hepatic fatty acids in high-fat diet-induced obese mice," *Scientific Reports 2015 5:1*, vol. 5, no. 1, pp. 1–12, May 2015, doi: 10.1038/srep10222.

[66] V. H. I. Fengler *et al.*, "Susceptibility of Different Mouse Wild Type Strains to Develop Diet-Induced NAFLD/AFLD-Associated Liver Disease," *PLoS One*, vol. 11, no. 5, p. e0155163, May 2016, doi: 10.1371/JOURNAL.PONE.0155163.

[67] G. Kanuri *et al.*, "Moderate alcohol consumption diminishes the development of non-alcoholic fatty liver disease (NAFLD) in ob/ob mice," *Eur J Nutr*, vol. 55, no. 3, pp. 1153–1164, Apr. 2016, doi: 10.1007/S00394-015-0929-7/FIGURES/4.

[68] O. Disson *et al.*, "Impaired Clearance of Virus-Infected Hepatocytes in Transgenic Mice Expressing the Hepatitis C Virus Polyprotein," *Gastroenterology*, vol. 126, no. 3, pp. 859–872, Mar. 2004, doi: 10.1053/j.gastro.2003.12.005.

[69] M. L. Washburn *et al.*, "A humanized mouse model to study hepatitis C virus infection, immune response, and liver disease," *Gastroenterology*, vol. 140, no. 4, pp. 1334–1344, Apr. 2011, doi: 10.1053/j.gastro.2011.01.001.

[70] W. Xue *et al.*, "CRISPR-mediated direct mutation of cancer genes in the mouse liver," *Nature*, vol. 514, no. 7522, pp. 380–384, Oct. 2014, doi: 10.1038/NATURE13589.

[71] H. L. Ju, K. H. Han, J. D. Lee, and S. W. Ro, "Transgenic mouse models generated by hydrodynamic transfection for genetic studies of liver cancer and preclinical testing of anti-cancer therapy," *Int J Cancer*, vol. 138, no. 7, pp. 1601–1608, Apr. 2016, doi: 10.1002/IJC.29703.

[72] T. Takayama, M. Ukawa, Y. Kanazawa, H. Ando, T. Shimizu, and T. Ishida, "Hydrodynamic Tail Vein Injection as a Simple Tool for Yielding Extended Transgene Expression in Solid Tumors," *Biol Pharm Bull*, vol. 39, no. 9, pp. 1555–1558, 2016, doi: 10.1248/BPB.B16-00283.

[73] R. Yeikilis *et al.*, "Hydrodynamics based transfection in normal and fibrotic rats," *World J Gastroenterol*, vol. 12, no. 38, pp. 6149–6155, Oct. 2006, doi: 10.3748/wjg.v12.i38.6149.

[74] S. Kameda *et al.*, "Hydrodynamics-based transfer of PCR-amplified DNA fragments into rat liver," *Biochem Biophys Res Commun*, vol. 309, no. 4, pp. 929–936, Oct. 2003, doi: 10.1016/J.BBRC.2003.08.087.

[75] J. Li, Q. Yao, and D. Liu, "Hydrodynamic cell delivery for simultaneous establishment of tumor growth in mouse lung, liver and kidney," *Cancer Biol Ther*, vol. 12, no. 8, pp. 737–741, Oct. 2011, doi: 10.4161/CBT.12.8.16442.

[76] P. Limani *et al.*, "Selective portal vein injection for the design of syngeneic models of liver malignancy," *Am J Physiol Gastrointest Liver Physiol*, vol. 310, no. 9, pp. G682–G688, May 2016, doi: 10.1152/AJPGI.00209.2015/SUPPL_FILE/MOVIE1.MOV.

[77] G. Sawyer, M. Rela, M. Davenport, M. Whitehorne, X. Zhang, and J. Fabre, "Hydrodynamic Gene Delivery to the Liver: Theoretical and Practical Issues for Clinical Application," *Curr Gene Ther*, vol. 9, no. 2, pp. 128–135, Apr. 2009, doi: 10.2174/156652309787909535.

[78] R. M. Pascale, M. M. Simile, G. Peitta, M. A. Seddaiu, F. Feo, and D. F. Calvisi, "Experimental Models to Define the Genetic Predisposition to Liver Cancer," *Cancers 2019, Vol. 11, Page 1450*, vol. 11, no. 10, p. 1450, Sep. 2019, doi: 10.3390/CANCERS11101450.

[79] D. F. Calvisi, V. M. Factor, S. Ladu, E. A. Conner, and S. S. Thorgeirsson, "Disruption of β-Catenin Pathway or Genomic Instability Define Two Distinct Categories of Liver Cancer in Transgenic Mice," *Gastroenterology*, vol. 126, no. 5, pp. 1374–1386, May 2004, doi: 10.1053/j.gastro.2004.02.014.

[80] N. Razumilava and G. J. Gores, "Cholangiocarcinoma," *The Lancet*, vol. 383, no. 9935, pp. 2168–2179, 2014, doi: 10.1016/S0140-6736(13)61903-0.

[81] J. M. Llovet *et al.*, "Hepatocellular carcinoma," *Nature Reviews Disease Primers 2021 7:1*, vol. 7, no. 1, pp. 1–28, Jan. 2021, doi: 10.1038/s41572-020-00240-3.

[82] D. Sia, A. Villanueva, S. L. Friedman, and J. M. Llovet, "Liver Cancer Cell of Origin, Molecular Class, and Effects on Patient Prognosis," *Gastroenterology*, vol. 152, no. 4, pp. 745–761, Mar. 2017, doi: 10.1053/J.GASTRO.2016.11.048.

[83] J. Yang *et al.*, "The burden of primary liver cancer caused by specific etiologies from 1990 to 2019 at the global, regional, and national levels," *Cancer Med*, vol. 11, no. 5, p. 1357, Mar. 2022, doi: 10.1002/CAM4.4530.

[84] P. Dasgupta, C. Henshaw, D. R. Youlden, P. J. Clark, J. F. Aitken, and P. D. Baade, "Global Trends in Incidence Rates of Primary Adult Liver Cancers: A Systematic Review and Meta-Analysis," *Front Oncol*, vol. 10, p. 171, Feb. 2020, doi: 10.3389/FONC.2020.00171.

[85] P. Konyn, A. Ahmed, and D. Kim, "Current epidemiology in hepatocellular carcinoma," vol. 15, no. 11, pp. 1295–1307, 2021, doi: 10.1080/17474124.2021.1991792.

[86] R. El-Diwany, T. M. Pawlik, and A. Ejaz, "Intrahepatic Cholangiocarcinoma," *Surg Oncol Clin N Am*, vol. 28, no. 4, pp. 587–599, Oct. 2019, doi: 10.1016/J.SOC.2019.06.002.

[87] I. Endo *et al.*, "Intrahepatic cholangiocarcinoma: rising frequency, improved survival, and determinants of outcome after resection," *Ann Surg*, vol. 248, no. 1, pp. 84–96, Jul. 2008, doi: 10.1097/sla.0b013e318176c4d3.

[88] M. J. Olnes and R. Erlich, "A review and update on cholangiocarcinoma," *Oncology*, vol. 66, no. 3, pp. 167–179, 2004, doi: 10.1159/000077991.

[89] P. L. Labib, G. Goodchild, and S. P. Pereira, "Molecular Pathogenesis of Cholangiocarcinoma," *BMC Cancer*, vol. 19, no. 1, Feb. 2019, doi: 10.1186/S12885-019-5391-0.

[90] R. Sahu, P. Sharma, and A. Kumar, "An Insight into Cholangiocarcinoma and Recent Advances in its Treatment," *J Gastrointest Cancer*, vol. 54, no. 1, pp. 213–226, Mar. 2023, doi: 10.1007/S12029-021-00728-5.

[91] S. Sekiya and A. Suzuki, "Intrahepatic cholangiocarcinoma can arise from Notch-mediated conversion of hepatocytes," *J Clin Invest*, vol. 122, no. 11, pp. 3914–3918, Nov. 2012, doi: 10.1172/JCI63065.

[92] R. V. Guest *et al.*, "Cell lineage tracing reveals a biliary origin of intrahepatic cholangiocarcinoma," *Cancer Res*, vol. 74, no. 4, pp. 1005–1010, Feb. 2014, doi: 10.1158/0008-5472.CAN-13-1911.

[93] B. Fan *et al.*, "Cholangiocarcinomas can originate from hepatocytes in mice," *J Clin Invest*, vol. 122, no. 8, pp. 2911–2915, Aug. 2012, doi: 10.1172/JCI63212.

[94] G. F. Zhang, L. Qiu, S. L. Yang, J. C. Wu, and T. J. Liu, "Wnt/β-catenin signaling as an emerging potential key pharmacological target in cholangiocarcinoma," *Biosci Rep*, vol. 40, no. 3, p. 20193353, Mar. 2020, doi: 10.1042/BSR20193353/222119.

[95] X. Adhoute *et al.*, "Intrahepatic Cholangiocarcinoma and Hepatocellular Carcinoma: Real-life Data on Liver Disease, Treatment and Prognosis," *J Clin Transl Hepatol*, vol. 11, no. 5, p. 1106, Oct. 2023, doi: 10.14218/JCTH.2022.00141.

[96] J. M. Banales *et al.*, "Cholangiocarcinoma 2020: the next horizon in mechanisms and management," *Nature Reviews Gastroenterology & Hepatology 2020 17:9*, vol. 17, no. 9, pp. 557–588, Jun. 2020, doi: 10.1038/s41575-020-0310-z.

[97] S. Kubo *et al.*, "Liver Cancer Study Group of Japan Clinical Practice Guidelines for Intrahepatic Cholangiocarcinoma," *Liver Cancer*, vol. 11, no. 4, pp. 290–314, Jul. 2022, doi: 10.1159/000522403.

[98] D. Ogawa *et al.*, "Multiple cholangiocarcinomas in the intrahepatic and extrahepatic biliary tree due to dichloromethane exposure: a case report," *Surgical Case Reports 2020 6:1*, vol. 6, no. 1, pp. 1–6, Apr. 2020, doi: 10.1186/S40792-020-00842-9.

[99] T. S. Gerber *et al.*, "N-Cadherin Distinguishes Intrahepatic Cholangiocarcinoma from Liver Metastases of Ductal Adenocarcinoma of the Pancreas," *Cancers (Basel)*, vol. 14, no. 13, p. 3091, Jul. 2022, doi: 10.3390/CANCERS14133091/S1.

[100] J. S. Voss *et al.*, "Molecular profiling of cholangiocarcinoma shows potential for targeted therapy treatment decisions," *Hum. Pathol.*, vol. 44, no. 7, pp. 1216–1222, Jul. 2013, doi: 10.1016/j.humpath.2012.11.006.

[101] I. Endo *et al.*, "Intrahepatic cholangiocarcinoma: Rising frequency, improved survival, and determinants of outcome after resection," *Ann Surg*, vol. 248, no. 1, pp. 84–96, Jul. 2008, doi: 10.1097/SLA.0B013E318176C4D3.

[102] S. S. Jackson, A. A. Florio, K. A. McGlynn, and J. L. Petrick, "Challenges in elucidating cholangiocarcinoma etiology," *Hepatobiliary Surg Nutr*, vol. 9, no. 4, pp. 53739–53539, Aug. 2020, doi: 10.21037/HBSN.2020.02.03.

[103] Y. Chawla and A. Duseja, "Intrahepatic stones: Is it a lifestyle disease?," *J Gastroenterol Hepatol*, vol. 23, no. 7pt1, pp. 998–999, Jul. 2008, doi: 10.1111/J.1440-1746.2008.05516.X.

[104] C. R. Churi *et al.*, "Mutation profiling in cholangiocarcinoma: prognostic and therapeutic implications," *PLoS One*, vol. 9, no. 12, p. e115383, Dec. 2014, doi: 10.1371/journal.pone.0115383.

[105] M. A. Lowery *et al.*, "Comprehensive molecular profiling of intrahepatic and extrahepatic cholangiocarcinomas: Potential targets for intervention," *Clinical Cancer Research*, vol. 24, no. 17, pp. 4154–4161, Sep. 2018, doi: 10.1158/1078-0432.CCR-18-0078.

[106] T. M. Welzel *et al.*, "Risk Factors for Intrahepatic and Extrahepatic Cholangiocarcinoma in the United States: A Population-Based Case-Control Study," *Clinical Gastroenterology and Hepatology*, vol. 5, no. 10, pp. 1221–1228, Oct. 2007, doi: 10.1016/j.cgh.2007.05.020.

[107] W. C. Palmer and T. Patel, "Are common factors involved in the pathogenesis of primary liver cancers? A meta-analysis of risk factors for intrahepatic cholangiocarcinoma," *J Hepatol*, vol. 57, no. 1, pp. 69–76, Jul. 2012, doi: 10.1016/j.jhep.2012.02.022.

[108] N. F. Esnaola, J. E. Meyer, A. Karachristos, J. L. Maranki, E. R. Camp, and C. S. Denlinger, "Evaluation and management of intrahepatic and extrahepatic cholangiocarcinoma," *Cancer*, vol. 122, no. 9, pp. 1349–1369, May 2016, doi: 10.1002/cncr.29692.

[109] D. Ogawa *et al.*, "Multiple cholangiocarcinomas in the intrahepatic and extrahepatic biliary tree due to dichloromethane exposure: a case report," *Surgical Case Reports 2020 6:1*, vol. 6, no. 1, pp. 1–6, Apr. 2020, doi: 10.1186/S40792-020-00842-9.

[110] F. Bartsch, J. Baumgart, M. Hoppe-Lotichius, I. Schmidtmann, S. Heinrich, and H. Lang, "Visceral infiltration of intrahepatic cholangiocarcinoma is most prognostic after curative resection - Retrospective cohort study of 102 consecutive liver resections from a single center.," *International journal of surgery*, vol. 55, pp. 193–200, Jul. 2018, doi: 10.1016/J.IJSU.2018.05.027.

[111] M. Wei, L. Lü, P. Lin, Z. Chen, Z. Quan, and Z. Tang, "Multiple cellular origins and molecular evolution of intrahepatic cholangiocarcinoma.," *Cancer Lett*, vol. 379 2, no. 2, pp. 253–261, Sep. 2016, doi: 10.1016/J.CANLET.2016.02.038.

[112] M. Yamamoto and S. I. Ariizumi, "Surgical outcomes of intrahepatic cholangiocarcinoma," *Surg Today*, vol. 41, no. 7, pp. 896–902, Jul. 2011, doi: 10.1007/S00595-011-4517-Z.

[113] D. Sia, V. Tovar, A. Moeini, and J. M. Llovet, "Intrahepatic cholangiocarcinoma: pathogenesis and rationale for molecular therapies," *Oncogene*, vol. 32, no. 41, pp. 4861–4870, Oct. 2013, doi: 10.1038/onc.2012.617.

[114] Y. Tsou, R. Wu, C. Hung, and C. Lee, "Intrahepatic sarcomatoid cholangiocarcinoma: clinical analysis of seven cases during a 15-year period.," *Chang Gung Med J*, vol. 31 6.

[115] S. -M Sheen-Chen, F. -F Chou, and H. -L Eng, "Intrahepatic cholangiocarcinoma in hepatolithiasis: A frequently overlooked disease," *J Surg Oncol*, vol. 47, no. 2, pp. 131–135, Jun. 1991, doi: 10.1002/JSO.2930470213.

[116] S. Y. Lee and D. Cherqui, "Operative management of cholangiocarcinoma," *Semin Liver Dis*, vol. 33, no. 3, pp. 248–261, 2013, doi: 10.1055/S-0033-1351784/ID/JR00713-22/BIB.

[117] M. Gunaydin *et al.*, "Different techniques for biliary diversion in progressive familial intrahepatic cholestasis," *J Pediatr Surg*, vol. 51, no. 3, pp. 386–389, Mar. 2016, doi: 10.1016/j.jpedsurg.2015.08.011.

[118] J. Adeva, "Current development and future perspective of IDH1 inhibitors in cholangiocarcinoma," *Liver Cancer International*, vol. 3, no. 1, pp. 17–31, Feb. 2022, doi: 10.1002/LCI2.43.

[119] N. Wang, A. Huang, B. Kuang, Y. Xiao, Y. Xiao, and H. Ma, "Progress in Radiotherapy for Cholangiocarcinoma," *Front Oncol*, vol. 12, Apr. 2022, doi: 10.3389/FONC.2022.868034.

[120] W. Chen, Z. Hu, J. Song, Y. Wu, B. Zhang, and L. Zhang, "The state of therapy modalities in clinic for biliary tract cancer," *Frontiers in Bioscience - Landmark*, vol. 27, no. 6, p. 185, Jun. 2022, doi: 10.31083/J.FBL2706185/02614C76CBD5A13AC4EE6AF87EA66AE3.PDF.

[121] J. Valle *et al.*, "Cisplatin plus gemcitabine versus gemcitabine for biliary tract cancer," *N. Engl. J. Med.*, vol. 362, no. 14, pp. 1273–1281, Apr. 2010, doi: 10.1056/nejmoa0908721.

[122] A. Pellino *et al.*, "Precision medicine in cholangiocarcinoma," *Transl Gastroenterol Hepatol*, vol. 3, no. July, Jul. 2018, doi: 10.21037/TGH.2018.07.02.

[123] Z. G. Yuan, T. M. Zeng, and C. J. Tao, "Current and emerging immunotherapeutic approaches for biliary tract cancers," *Hepatobiliary and Pancreatic Diseases International*, vol. 21, no. 5, pp. 440–449, Oct. 2022, doi: 10.1016/j.hbpd.2022.08.015.

[124] G. Frega *et al.*, "Potentially actionable mutations in intrahepatic cholangiocarcinoma," *Annals of Oncology*, vol. 30, pp. vii19–vii20, Nov. 2019, doi: 10.1093/ANNONC/MDZ413.069.

[125] S. Rizvi, S. A. Khan, C. L. Hallemeier, R. K. Kelley, and G. J. Gores, "Cholangiocarcinoma-evolving concepts and therapeutic strategies," *Nat Rev Clin Oncol*, vol. 15, no. 2, pp. 95–111, Feb. 2018, doi: 10.1038/NRCLINONC.2017.157.

[126] G. K. Bonney, R. A. Craven, R. Prasad, A. F. Melcher, P. J. Selby, and R. E. Banks, "Circulating markers of biliary malignancy: opportunities in proteomics ?," *Lancet Oncol.*, vol. 2, no. 2, pp. 149–158, Feb. 2008, doi: 10.1016/s1470-2045(08)70027-5.

[127] A. Bergquist and E. Von Seth, "Epidemiology of cholangiocarcinoma," *Best Pract Res Clin Gastroenterol*, vol. 29, no. 2, pp. 221–232, Apr. 2015, doi: 10.1016/j.bpg.2015.02.003.

[128] A. Jusakul *et al.*, "Whole-genome and epigenomic landscapes of etiologically distinct subtypes of cholangiocarcinoma," *Cancer Discov*, vol. 7, no. 10, pp. 1116–1135, Oct. 2017, doi: 10.1158/2159-8290.CD-17-0368.

[129] X. Y. Wang *et al.*, "Driver mutations of intrahepatic cholangiocarcinoma shape clinically relevant genomic clusters with distinct molecular features and therapeutic vulnerabilities," *Theranostics*, vol. 12, no. 1, pp. 260–276, 2022, doi: 10.7150/THNO.63417.

[130] C. R. Churi *et al.*, "Mutation Profiling in Cholangiocarcinoma: Prognostic and Therapeutic Implications," *PLoS One*, vol. 9, no. 12, p. e115383, Dec. 2014, doi: 10.1371/JOURNAL.PONE.0115383.

[131] M. Niger *et al.*, "Platinum sensitivity in patients with IDH1/2 mutated vs wild-type intrahepatic cholangiocarcinoma: A propensity score-based study," *Int J Cancer*, vol. 151, no. 8, pp. 1310–1320, Oct. 2022, doi: 10.1002/IJC.34182.

[132] C. J. Pirozzi and H. Yan, "The implications of IDH mutations for cancer development and therapy," *Nature Reviews Clinical Oncology 2021 18:10*, vol. 18, no. 10, pp. 645–661, Jun. 2021, doi: 10.1038/s41571-021-00521-0.

[133] D. R. Borger *et al.*, "Frequent mutation of isocitrate dehydrogenase (IDH)1 and IDH2 in cholangiocarcinoma identified through broad-based tumor genotyping," *Oncologist*, vol. 17, no. 1, pp. 72–79, Jan. 2012, doi: 10.1634/theoncologist.2011-0386.

[134] A. R. Grassian, R. Pagliarini, and D. Y. Chiang, "Mutations of isocitrate dehydrogenase 1 and 2 in intrahepatic cholangiocarcinoma," *Curr Opin Gastroenterol*, vol. 30, no. 3, pp. 295–302, 2014, doi: 10.1097/MOG.0000000000000050.

[135] L. Corrigan and M. Lowery, "Ivosidenib for the treatment of isocitrate dehydrogenase-1 mutant cholangiocarcinoma," *Expert Rev Gastroenterol Hepatol*, vol. 15, no. 5, pp. 475–481, 2021, doi: 10.1080/17474124.2021.1915765.

[136] T. Imamura *et al.*, "Molecular characterization-based multi-omics analyses in primary liver cancer using the Japanese version of the genome atlas," *J Hepatobiliary Pancreat Sci*, vol. 30, no. 3, pp. 269–282, Mar. 2023, doi: 10.1002/JHBP.1223.

[137] Y. Jiao *et al.*, "Exome sequencing identifies frequent inactivating mutations in BAP1, ARID1A and PBRM1 in intrahepatic cholangiocarcinomas," *Nat Genet*, vol. 45, no. 12, pp. 1470–1473, Dec. 2013, doi: 10.1038/ng.2813.

[138] G. Kendre, K. Murugesan, T. Brummer, O. Segatto, A. Saborowski, and A. Vogel, "Charting co-mutation patterns associated with actionable drivers in intrahepatic cholangiocarcinoma," *J Hepatol*, vol. 78, no. 3, pp. 614–626, Mar. 2023, doi: 10.1016/j.jhep.2022.11.030.

[139] J. Andrici *et al.*, "Loss of BAP1 expression occurs frequently in intrahepatic Cholangiocarcinoma," *Medicine (Baltimore)*, vol. 95, no. 2, Jan. 2016, doi: 10.1097/md.0000000000002491.

[140] B. Ma *et al.*, "Distinct clinical and prognostic implication of IDH1/2 mutation and other most frequent mutations in large duct and small duct subtypes of intrahepatic cholangiocarcinoma," *BMC Cancer*, vol. 20, no. 1, pp. 1–12, Apr. 2020, doi: 10.1186/S12885-020-06804-6/FIGURES/6.

[141] Y. Arai *et al.*, "Fibroblast growth factor receptor 2 tyrosine kinase fusions define a unique molecular subtype of cholangiocarcinoma," *Hepatology*, vol. 59, no. 4, pp. 1427–1434, Apr. 2014, doi: 10.1002/HEP.26890.

[142] J. E. Berchuck *et al.*, "The clinical landscape of cell-free DNA alterations in 1671 patients with advanced biliary tract cancer," *Annals of Oncology*, vol. 33, no. 12, pp. 1269–1283, Dec. 2022, doi: 10.1016/J.ANNONC.2022.09.150.

[143] A. Mahipal, S. H. Tella, A. Kommalapati, D. Anaya, and R. Kim, "FGFR2 genomic aberrations: Achilles heel in the management of advanced cholangiocarcinoma," *Cancer Treat Rev*, vol. 78, pp. 1–7, Aug. 2019, doi: 10.1016/J.CTRV.2019.06.003.

[144] T. Boerner *et al.*, "Genetic Determinants of Outcome in Intrahepatic Cholangiocarcinoma," *Hepatology*, vol. 74, no. 3, pp. 1429–1444, Sep. 2021, doi: 10.1002/HEP.31829.

[145] D. T. Cheng *et al.*, "Memorial Sloan Kettering-Integrated Mutation Profiling of Actionable Cancer Targets (MSK-IMPACT): A Hybridization Capture-Based Next-Generation Sequencing Clinical Assay for Solid Tumor Molecular Oncology," *J Mol Diagn*, vol. 17, no. 3, p. 251, May 2015, doi: 10.1016/J.JMOLDX.2014.12.006.

[146] P. Wang *et al.*, "Mutations in Isocitrate Dehydrogenase 1 and 2 Occur Frequently in Intrahepatic Cholangiocarcinomas and Share Hypermethylation Targets with Glioblastomas," *Oncogene*, vol. 32, no. 25, p. 3091, Jun. 2013, doi: 10.1038/ONC.2012.315.

[147] M. Mut *et al.*, "Extracellular-Vesicle-Based Cancer Panels Diagnose Glioblastomas with High Sensitivity and Specificity," *Cancers (Basel)*, vol. 15, no. 15, Aug. 2023, doi: 10.3390/CANCERS15153782.

[148] M. Capuozzo *et al.*, "Evolution of Treatment in Advanced Cholangiocarcinoma: Old and New towards Precision Oncology," *Int J Mol Sci*, vol. 23, no. 23, Dec. 2022, doi: 10.3390/IJMS232315124.

[149] N. Holzapfel *et al.*, "Whole-genome sequencing of 20 cholangiocarcinoma cases reveals unique profiles in patients with cirrhosis and primary sclerosing cholangitis," *J Gastrointest Oncol*, vol. 14, no. 1, pp. 379–389, Feb. 2023, doi: 10.21037/JGO-22-676/COIF).

[150] M. A. Lowery *et al.*, "Comprehensive Molecular Profiling of Intrahepatic and Extrahepatic Cholangiocarcinomas: Potential Targets for Intervention," *Clin Cancer Res*, vol. 24, no. 17, pp. 4154–4161, Sep. 2018, doi: 10.1158/1078-0432.CCR-18-0078.

[151] D. B. Hewitt, H. Aziz, Z. J. Brown, and T. M. Pawlik, "Role of genetic testing in hepatic, pancreatic, and biliary cancers," *Surg Oncol*, vol. 44, Sep. 2022, doi: 10.1016/J.SURONC.2022.101844.
[152] J. S. Damrauer *et al.*, "Genomic characterization of rare molecular subclasses of hepatocellular carcinoma," *Commun Biol*, vol. 4, no. 1, Dec. 2021, doi: 10.1038/S42003-021-02674-1.
[153] L. Dang *et al.*, "Cancer-associated IDH1 mutations produce 2-hydroxyglutarate," *Nature*, vol. 462, no. 7274, pp. 739–744, Dec. 2009, doi: 10.1038/nature08617.
[154] H. Al-Khallaf, "Isocitrate dehydrogenases in physiology and cancer: Biochemical and molecular insight," *Cell Biosci*, vol. 7, no. 1, pp. 1–18, Aug. 2017, doi: 10.1186/S13578-017-0165-3/FIGURES/1.
[155] M. G. Badur *et al.*, "Oncogenic R132 IDH1 Mutations Limit NADPH for De Novo Lipogenesis through (D)2-Hydroxyglutarate Production in Fibrosarcoma Cells," *Cell Rep*, vol. 25, no. 4, p. 1018, Oct. 2018, doi: 10.1016/J.CELREP.2018.09.074.
[156] J. A. Losman and W. G. Kaelin, "What a difference a hydroxyl makes: mutant IDH, (R)-2-hydroxyglutarate, and cancer," *Genes Dev.*, vol. 27, no. 8, pp. 836–852, Apr. 2013, doi: 10.1101/gad.217406.113.
[157] W. Xu *et al.*, "Oncometabolite 2-hydroxyglutarate is a competitive inhibitor of α-ketoglutarate-dependent dioxygenases," *Cancer Cell*, vol. 19, no. 1, pp. 17–30, Jan. 2011, doi: 10.1016/j.ccr.2010.12.014.
[158] D. L. Nelson and M. M. Cox, "Lehninger Biochemie," 2001, doi: 10.1007/978-3-662-08289-8.
[159] J. M. Berg, J. L. Tymoczko, G. J. Gatto, and L. Stryer, "Stryer Biochemie," *Stryer Biochemie*, 2018, doi: 10.1007/978-3-662-54620-8.
[160] A. S. McKenney and R. L. Levine, "Isocitrate dehydrogenase mutations in leukemia," *J Clin Invest*, vol. 123, no. 9, pp. 3672–3677, Sep. 2013, doi: 10.1172/jci67266.
[161] H. Yan *et al.*, "IDH1 and IDH2 mutations in gliomas," *N. Engl. J. Med.*, vol. 360, no. 8, pp. 765–773, Feb. 2009, doi: 10.1056/nejmoa0808710.
[162] C. Hartmann *et al.*, "Type and frequency of IDH1 and IDH2 mutations are related to astrocytic and oligodendroglial differentiation and age: a study of 1,010 diffuse gliomas," *Acta Neuropathol.*, vol. 118, no. 4, pp. 469–474, 2009, doi: 10.1007/s00401-009-0561-9.
[163] T. Watanabe, S. Nobusawa, P. Kleihues, and H. Ohgaki, "IDH1 mutations are early events in the development of astrocytomas and oligodendrogliomas," *Am. J. Pathol.*, vol. 174, no. 4, pp. 1149–1153, 2009, doi: 10.2353/ajpath.2009.080958.
[164] D. Rohle *et al.*, "An Inhibitor of Mutant IDH1 Delays Growth and Promotes Differentiation of Glioma Cells," *Science*, vol. 340, no. 6132, p. 626, May 2013, doi: 10.1126/SCIENCE.1236062.
[165] M. C. Garrett *et al.*, "HDAC1 and HDAC6 are essential for driving growth in IDH1 mutant glioma," *Sci Rep*, vol. 13, no. 1, Dec. 2023, doi: 10.1038/S41598-023-33889-3.
[166] S. Haddock *et al.*, "Phenotypic and molecular states of IDH1 mutation-induced CD24-positive glioma stem-like cells," *Neoplasia*, vol. 28, Jun. 2022, doi: 10.1016/J.NEO.2022.100790.
[167] C. Lu *et al.*, "IDH mutation impairs histone demethylation and results in a block to cell differentiation," *Nature*, vol. 483, no. 7390, pp. 474–478, Mar. 2012, doi: 10.1038/nature10860.
[168] H. Zhu *et al.*, "IDH1 R132H Mutation Enhances Cell Migration by Activating AKT-mTOR Signaling Pathway, but Sensitizes Cells to 5-FU Treatment as NADPH and GSH Are Reduced," *PLoS One*, vol. 12, no. 1, p. e0169038, Jan. 2017, doi: 10.1371/JOURNAL.PONE.0169038.
[169] B. R. Kipp *et al.*, "Isocitrate dehydrogenase 1 and 2 mutations in cholangiocarcinoma," *Hum Pathol*, vol. 43, no. 10, pp. 1552–1558, Oct. 2012, doi: 10.1016/J.HUMPATH.2011.12.007.
[170] A. N. Boscoe, C. Rolland, and R. K. Kelley, "Frequency and prognostic significance of isocitrate dehydrogenase 1 mutations in cholangiocarcinoma: a systematic literature review," *J. Gastrointest. Oncol.*, vol. 10, no. 4, pp. 751–765, 2019, doi: 10.21037/jgo.2019.03.10.
[171] L. Goyal *et al.*, "Prognosis and Clinicopathologic features of patients with advanced stage Isocitrate dehydrogenase (IDH) mutant and IDH wild-type intrahepatic Cholangiocarcinoma," *Oncologist*, vol. 20, no. 9, pp. 1019–1027, Sep. 2015, doi: 10.1634/theoncologist.2015-0210.
[172] A. V. Belikov, A. D. Vyatkin, and S. V. Leonov, "Novel Driver Strength Index highlights important cancer genes in TCGA PanCanAtlas patients," *PeerJ*, vol. 10, Aug. 2022, doi: 10.7717/PEERJ.13860.
[173] P. Wang *et al.*, "Mutations in isocitrate dehydrogenase 1 and 2 occur frequently in intrahepatic cholangiocarcinomas and share hypermethylation targets with glioblastomas," *Oncogene*, vol. 32, no. 25, pp. 3091–3100, Jun. 2013, doi: 10.1038/onc.2012.315.
[174] R. J. Molenaar *et al.*, "Radioprotection of IDH1-mutated cancer cells by the IDH1-mutant inhibitor AGI-5198," *Cancer Res*, vol. 75, no. 22, pp. 4790–4802, Nov. 2015, doi: 10.1158/0008-5472.CAN-14-3603/651832/AM/RADIOPROTECTION-OF-IDH1-MUTATED-CANCER-CELLS-BY.
[175] Y. Zhu and L. N. Kwong, "IDH1 Inhibition Reawakens the Immune Response against Cholangiocarcinoma," *Cancer Discov*, vol. 12, no. 3, pp. 604–605, Mar. 2022, doi: 10.1158/2159-8290.CD-21-1643.

[176] G. Marcucci *et al.*, "IDH1 and IDH2 gene mutations identify novel molecular subsets within de novo cytogenetically normal acute myeloid leukemia: a Cancer and Leukemia Group B study," *J. Clin. Oncol.*, vol. 28, no. 14, pp. 2348–2355, May 2010, doi: 10.1200/jco.2009.27.3730.

[177] E. R. Mardis *et al.*, "Recurring mutations found by sequencing an acute myeloid leukemia genome," *N. Engl. J. Med.*, vol. 361, no. 11, pp. 1058–1066, Sep. 2009, doi: 10.1056/nejmoa0903840.

[178] S. Zarnegar-Lumley *et al.*, "Characteristics and prognostic impact of IDH mutations in AML: a COG, SWOG, and ECOG analysis," *Blood Adv*, vol. 7, no. 19, Oct. 2023, doi: 10.1182/BLOODADVANCES.2022008282.

[179] C. D. DiNardo *et al.*, "A phase 1 study of IDH305 in patients with IDH1R132-mutant acute myeloid leukemia or myelodysplastic syndrome," *J Cancer Res Clin Oncol*, vol. 149, no. 3, pp. 1145–1158, Mar. 2023, doi: 10.1007/S00432-022-03983-6.

[180] G. G. Zhu *et al.*, "Genomic profiling identifies association of IDH1/IDH2 mutation with longer relapse-free and metastasis-free survival in high-grade chondrosarcoma," *Clinical Cancer Research*, vol. 26, no. 2, pp. 419–427, Jan. 2020, doi: 10.1158/1078-0432.CCR-18-4212/74935/AM/GENOMIC-PROFILING-IDENTIFIES-ASSOCIATION-OF-IDH1.

[181] S. Chen *et al.*, "Diagnostic utility of IDH1/2 mutations to distinguish dedifferentiated chondrosarcoma from undifferentiated pleomorphic sarcoma of bone," *Hum Pathol*, vol. 65, pp. 239–246, Jul. 2017, doi: 10.1016/J.HUMPATH.2017.05.015.

[182] L. Li *et al.*, "Mutant IDH1 Depletion Downregulates Integrins and Impairs Chondrosarcoma Growth," *Cancers 2020, Vol. 12, Page 141*, vol. 12, no. 1, p. 141, Jan. 2020, doi: 10.3390/CANCERS12010141.

[183] M. F. Amary *et al.*, "IDH1 and IDH2 mutations are frequent events in central chondrosarcoma and central and periosteal chondromas but not in other mesenchymal tumours," *J Pathol*, vol. 224, no. 3, pp. 334–343, Jul. 2011, doi: 10.1002/PATH.2913.

[184] M. Nakagawa *et al.*, "Selective inhibition of mutant IDH1 by DS-1001b ameliorates aberrant histone modifications and impairs tumor activity in chondrosarcoma," *Oncogene 2019 38:42*, vol. 38, no. 42, pp. 6835–6849, Aug. 2019, doi: 10.1038/s41388-019-0929-9.

[185] H. Zhang *et al.*, "Distinct Roles of Glutamine Metabolism in Benign and Malignant Cartilage Tumors With IDH Mutations," *J Bone Miner Res*, vol. 37, no. 5, pp. 983–996, May 2022, doi: 10.1002/JBMR.4532.

[186] S. K. Saha *et al.*, "Mutant IDH inhibits HNF-4α to block hepatocyte differentiation and promote biliary cancer," *Nature*, vol. 513, no. 7516, pp. 110–114, Sep. 2014, doi: 10.1038/nature13441.

[187] M.-J. Wu *et al.*, "Abstract 1810: The mutant IDH1 inhibitor ivosidenib promotes tumor cell differentiation and anti-tumor immunity in intrahepatic cholangiocarcinoma," *Cancer Res*, vol. 80, no. 16_Supplement, pp. 1810–1810, Aug. 2020, doi: 10.1158/1538-7445.AM2020-1810.

[188] Z. Turkalp, J. Karamchandani, S. Das, S. Labatt Brain, K. Research Centre, and L. Ka Shing, "IDH Mutation in Glioma: New Insights and Promises for the Future," *JAMA Neurol*, vol. 71, no. 10, pp. 1319–1325, Oct. 2014, doi: 10.1001/JAMANEUROL.2014.1205.

[189] F. G. Schaap, P. J. French, and J. V. M. G. Bovée, "Mutations in the isocitrate dehydrogenase genes IDH1 and IDH2 in tumors," *Adv Anat Pathol*, vol. 20, no. 1, pp. 32–38, Jan. 2013, doi: 10.1097/PAP.0B013E31827B654D.

[190] E. Hansen *et al.*, "AG-120, an Oral, Selective, First-in-Class, Potent Inhibitor of Mutant IDH1, Reduces Intracellular 2HG and Induces Cellular Differentiation in TF-1 R132H Cells and Primary Human IDH1 Mutant AML Patient Samples Treated Ex Vivo," *Blood*, vol. 124, no. 21, pp. 3734–3734, Dec. 2014, doi: 10.1182/BLOOD.V124.21.3734.3734.

[191] Z. J. Reitman, S. A. Sinenko, E. P. Spana, and H. Yan, "Genetic dissection of leukemia-associated IDH1 and IDH2 mutants and D-2-hydroxyglutarate in Drosophila," *Blood*, vol. 125, no. 2, pp. 336–345, Jan. 2015, doi: 10.1182/BLOOD-2014-05-577940.

[192] D. Krell, P. Mulholland, A. E. Frampton, J. Krell, J. Stebbing, and C. Bardella, "IDH mutations in tumorigenesis and their potential role as novel therapeutic targets," vol. 9, no. 12, pp. 1923–1935, Dec. 2013, doi: 10.2217/FON.13.143.

[193] D. Sia *et al.*, "Integrative molecular analysis of intrahepatic cholangiocarcinoma reveals 2 classes that have different outcomes," *Gastroenterology*, vol. 144, no. 4, pp. 829–840, 2013, doi: 10.1053/j.gastro.2013.01.001.

[194] P. F. Przytycki and M. Singh, "Differential analysis between somatic mutation and germline variation profiles reveals cancer-related genes," *Genome Med*, vol. 9, no. 1, pp. 1–11, Aug. 2017, doi: 10.1186/S13073-017-0465-6/FIGURES/4.

[195] H. Tan, J. Bao, and X. Zhou, "Genome-wide mutational spectra analysis reveals significant cancer-specific heterogeneity," *Scientific Reports 2015 5:1*, vol. 5, no. 1, pp. 1–14, Jul. 2015, doi: 10.1038/srep12566.

[196] S. Gross *et al.*, "Cancer-associated metabolite 2-hydroxyglutarate accumulates in acute myelogenous leukemia with isocitrate dehydrogenase 1 and 2 mutations," *Journal of Experimental Medicine*, vol. 207, no. 2, pp. 339–344, Feb. 2010, doi: 10.1084/JEM.20092506.

[197] M. R. Gilbert *et al.*, "Autophagy and oxidative stress in gliomas with IDH1 mutations," *Acta Neuropathol*, vol. 127, no. 2, pp. 221–233, Feb. 2014, doi: 10.1007/S00401-013-1194-6/FIGURES/5.

[198] M. Kranendijk *et al.*, "IDH2 mutations in patients with D-2-hydroxyglutaric aciduria," *Science (1979)*, vol. 330, no. 6002, p. 336, Oct. 2010, doi: 10.1126/SCIENCE.1192632/SUPPL_FILE/KRANENDIJK.SOM.PDF.

[199] C. L. Green, C. M. Evans, R. K. Hills, A. K. Burnett, D. C. Linch, and R. E. Gale, "The prognostic significance of IDH1 mutations in younger adult patients with acute myeloid leukemia is dependent on FLT3/ITD status," *Blood*, vol. 116, no. 15, pp. 2779–2782, Oct. 2010, doi: 10.1182/BLOOD-2010-02-270926.

[200] Z. J. Reitman, S. A. Sinenko, E. P. Spana, and H. Yan, "Genetic dissection of leukemia-associated IDH1 and IDH2 mutants and D-2-hydroxyglutarate in Drosophila," *Blood*, vol. 125, no. 2, pp. 336–345, Jan. 2015, doi: 10.1182/BLOOD-2014-05-577940.

[201] S. A. M. Van Lith, R. Molenaar, C. J. F. Van Noorden, and W. P. J. Leenders, "Tumor cells in search for glutamate: an alternative explanation for increased invasiveness of IDH1 mutant gliomas," *Neuro Oncol*, vol. 16, no. 12, pp. 1669–1670, Dec. 2014, doi: 10.1093/NEUONC/NOU152.

[202] J. Leca, J. Fortin, and T. W. Mak, "Illuminating the cross-talk between tumor metabolism and immunity in IDH-mutated cancers," *Curr Opin Biotechnol*, vol. 68, pp. 181–185, Apr. 2021, doi: 10.1016/J.COPBIO.2020.11.013.

[203] A. Kayabolen, E. Yilmaz, and T. Bagci-Onder, "IDH Mutations in Glioma: Double-Edged Sword in Clinical Applications?," *Biomedicines 2021, Vol. 9, Page 799*, vol. 9, no. 7, p. 799, Jul. 2021, doi: 10.3390/BIOMEDICINES9070799.

[204] T. C. A. Johannessen *et al.*, "Rapid Conversion of Mutant IDH1 from Driver to Passenger in a Model of Human Gliomagenesis," *Mol Cancer Res*, vol. 14, no. 10, pp. 976–983, Oct. 2016, doi: 10.1158/1541-7786.MCR-16-0141.

[205] S. Babakoohi, R. G. Lapidus, R. Faramand, E. A. Sausville, and A. Emadi, "Comparative analysis of methods for detecting Isocitrate dehydrogenase 1 and 2 mutations and their metabolic consequence, 2-Hydroxyglutarate, in different neoplasms," *Appl Immunohistochem Mol Morphol*, vol. 25, no. 5, pp. 334–337, 2017, doi: 10.1097/pai.0000000000000342.

[206] M. F. Amary *et al.*, "IDH1 and IDH2 mutations are frequent events in central chondrosarcoma and central and periosteal chondromas but not in other mesenchymal tumours," *J. Pathol.*, vol. 224, no. 3, pp. 334–343, Jul. 2011, doi: 10.1002/path.2913.

[207] J. Popovici-Muller *et al.*, "Discovery of AG-120 (Ivosidenib): a first-in-class mutant IDH1 inhibitor for the treatment of IDH1 mutant cancers," *ACS Med Chem Lett*, vol. 9, no. 4, pp. 300–305, Apr. 2018, doi: 10.1021/acsmedchemlett.7b00421.

[208] E. Aguado-Fraile *et al.*, "Abstract 2275: Detection of IDH1 mutations in plasma cell-free circulating tumor DNA (ctDNA) from patients with cholangiocarcinoma," *Cancer Res*, vol. 79, no. 13_Supplement, pp. 2275–2275, Jul. 2019, doi: 10.1158/1538-7445.AM2019-2275.

[209] J. K. Mito *et al.*, "Immunohistochemical detection and molecular characterization of IDH-mutant sinonasal undifferentiated carcinomas," *Am. J. Surg. Pathol.*, vol. 42, no. 8, pp. 1067–1075, Aug. 2018, doi: 10.1097/pas.0000000000001064.

[210] S. Raineri and J. Mellor, "IDH1: Linking Metabolism and Epigenetics," *Front Genet*, vol. 9, Oct. 2018, doi: 10.3389/FGENE.2018.00493.

[211] S. Zhao *et al.*, "Glioma-derived mutations in IDH1 dominantly inhibit IDH1 catalytic activity and induce HIF-1α," *Science (1979)*, vol. 324, no. 5924, pp. 261–265, Apr. 2009, doi: 10.1126/SCIENCE.1170944/SUPPL_FILE/ZHAO_SOM.PDF.

[212] D. Golub *et al.*, "Mutant isocitrate dehydrogenase inhibitors as targeted cancer therapeutics," *Front Oncol*, vol. 9, no. MAY, p. 461713, May 2019, doi: 10.3389/FONC.2019.00417/BIBTEX.

[213] P. Koivunen *et al.*, "Transformation by the (R)-enantiomer of 2-hydroxyglutarate linked to EGLN activation," *Nature*, vol. 483, no. 7390, pp. 484–488, Mar. 2012, doi: 10.1038/NATURE10898.

[214] M. Tarrado-Castellarnau, P. de Atauri, and M. Cascante, "Oncogenic regulation of tumor metabolic reprogramming," *Oncotarget*, vol. 7, no. 38, p. 62726, Sep. 2016, doi: 10.18632/ONCOTARGET.10911.

[215] X. Bai *et al.*, "Ten-Eleven Translocation 1 Promotes Malignant Progression of Cholangiocarcinoma With Wild-Type Isocitrate Dehydrogenase 1," *Hepatology*, vol. 73, no. 5, pp. 1747–1763, May 2021, doi: 10.1002/HEP.31486.

[216] S. Ito *et al.*, "Tet proteins can convert 5-methylcytosine to 5-formylcytosine and 5-carboxylcytosine," *Science (1979)*, vol. 333, no. 6047, pp. 1300–1303, Sep. 2011, doi: 10.1126/SCIENCE.1210597/SUPPL_FILE/ITO.SOM.PDF.

[217] A. M. Intlekofer *et al.*, "Hypoxia Induces Production of L-2-Hydroxyglutarate.," *Cell Metab*, vol. 22 2, no. 2, pp. 304–311, Aug. 2015, doi: 10.1016/J.CMET.2015.06.023.

[218] M. R. Shait Mohammed, F. Alzahrani, S. Hosawi, H. Choudhry, and M. I. Khan, "Profiling the Effect of Targeting Wild Isocitrate Dehydrogenase 1 (IDH1) on the Cellular Metabolome of Leukemic Cells," *Int J Mol Sci*, vol. 23, no. 12, Jun. 2022, doi: 10.3390/IJMS23126653.

[219] J. M. Hair *et al.*, "BRCA1 role in the mitigation of radiotoxicity and chromosomal instability through repair of clustered DNA lesions," *Chem Biol Interact*, vol. 188, no. 2, pp. 350–358, Nov. 2010, doi: 10.1016/J.CBI.2010.03.046.

[220] R. Kumareswaran, O. Ludkovski, A. Meng, J. Sykes, M. Pintilie, and R. G. Bristow, "Chronic hypoxia compromises repair of DNA double-strand breaks to drive genetic instability," *J Cell Sci*, vol. 125, no. 1, pp. 189–199, Jan. 2012, doi: 10.1242/JCS.092262.

[221] H. Huang *et al.*, "Abnormal Cytokinesis after X-Irradiation in Tumor Cells that Override the G2 DNA Damage Checkpoint," *Cancer Res*, vol. 68, no. 10, pp. 3724–3732, May 2008, doi: 10.1158/0008-5472.CAN-08-0479.

[222] G. E. Dodson, Y. Shi, and R. S. Tibbetts, "DNA replication defects, spontaneous DNA damage, and ATM-dependent checkpoint activation in replication protein A-deficient cells," *J Biol Chem*, vol. 279, no. 32, pp. 34010–34014, Aug. 2004, doi: 10.1074/JBC.C400242200.

[223] H. Li, S. E. Zimmerman, and U. Weyemi, "Genomic instability and metabolism in cancer," *Int Rev Cell Mol Biol*, vol. 364, pp. 241–265, Jan. 2021, doi: 10.1016/BS.IRCMB.2021.05.004.

[224] K. A. Jansen, A. J. Licup, A. Sharma, R. Rens, F. C. MacKintosh, and G. H. Koenderink, "The Role of Network Architecture in Collagen Mechanics," *Biophys J*, vol. 114, no. 11, pp. 2665–2678, Jun. 2018, doi: 10.1016/j.bpj.2018.04.043.

[225] P. Rappu, A. M. Salo, J. Myllyharju, and J. Heino, "Role of prolyl hydroxylation in the molecular interactions of collagens," *Essays Biochem*, vol. 63, no. 3, pp. 325–335, Sep. 2019, doi: 10.1042/EBC20180053.

[226] A. Veß *et al.*, "A dual phenotype of MDA-MB-468 cancer cells reveals mutual regulation of tensin3 and adhesion plasticity," *J Cell Sci*, vol. 130, no. 13, pp. 2172–2184, Jul. 2017, doi: 10.1242/JCS.200899.

[227] J. Koh *et al.*, "IDH2 mutation in gliomas including novel mutation," *Neuropathology*, vol. 35, no. 3, pp. 236–244, Jun. 2015, doi: 10.1111/NEUP.12187.

[228] S. Pusch *et al.*, "D-2-Hydroxyglutarate producing neo-enzymatic activity inversely correlates with frequency of the type of isocitrate dehydrogenase 1 mutations found in glioma," *Acta Neuropathol Commun*, vol. 2, no. 1, Jan. 2014, doi: 10.1186/2051-5960-2-19.

[229] A. Tefferi *et al.*, "IDH1 and IDH2 mutation studies in 1473 patients with chronic-, fibrotic- or blast-phase essential thrombocythemia, polycythemia vera or myelofibrosis," *Leukemia*, vol. 24, no. 7, pp. 1302–1309, 2010, doi: 10.1038/leu.2010.113.

[230] R. Longuespée *et al.*, "Rapid detection of 2-hydroxyglutarate in frozen sections of IDH mutant tumors by MALDI-TOF mass spectrometry," *Acta Neuropathol Commun*, vol. 6, no. 1, p. 21, Mar. 2018, doi: 10.1186/S40478-018-0523-3.

[231] T. Schumacher *et al.*, "A vaccine targeting mutant IDH1 induces antitumour immunity," *Nature*, vol. 512, no. 7514, pp. 324–327, Aug. 2014, doi: 10.1038/NATURE13387.

[232] T. Avsar, T. B. Kose, M. D. Oksal, G. Turan, and T. Kilic, "IDH1 mutation activates mTOR signaling pathway, promotes cell proliferation and invasion in glioma cells," *Mol Biol Rep*, vol. 49, no. 10, pp. 9241–9249, Oct. 2022, doi: 10.1007/S11033-022-07750-1.

[233] M. J. Kwon *et al.*, "Mutated IDH1 is a favorable prognostic factor for type 2 gliomatosis cerebri," *Brain Pathology*, vol. 22, no. 3, pp. 307–317, May 2012, doi: 10.1111/J.1750-3639.2011.00532.X.

[234] C. Peraldo-Neia *et al.*, "Assessment of a High Sensitivity Method for Identification of IDH1 R132x Mutations in Tumors and Plasma of Intrahepatic Cholangiocarcinoma Patients," *Cancers 2019, Vol. 11, Page 454*, vol. 11, no. 4, p. 454, Mar. 2019, doi: 10.3390/CANCERS11040454.

[235] H. Alkhatabi *et al.*, "Investigation of Isocitrate Dehydrogenase 1 and 2 Mutations in Acute Leukemia Patients in Saudi Arabia," *Genes (Basel)*, vol. 12, no. 12, Dec. 2021, doi: 10.3390/GENES12121963.

[236] P. S. Ward *et al.*, "The potential for isocitrate dehydrogenase mutations to produce 2-hydroxyglutarate depends on allele specificity and subcellular compartmentalization," *Journal of Biological Chemistry*, vol. 288, no. 6, pp. 3804–3815, Feb. 2013, doi: 10.1074/jbc.M112.435495.

[237] V. K. Gupta *et al.*, "Hypoxia-driven oncometabolite L-2HG maintains stemness-differentiation balance and facilitates immune evasion in pancreatic cancer," *Cancer Res*, vol. 81, no. 15, pp. 4001–4013, Aug. 2021,

doi: 10.1158/0008-5472.CAN-20-2562/673673/AM/HYPOXIA-DRIVEN-ONCOMETABOLITE-L-2HG-MAINTAINS.

[238] H. Colvin *et al.*, "Oncometabolite D-2-Hydroxyglurate Directly Induces Epithelial-Mesenchymal Transition and is Associated with Distant Metastasis in Colorectal Cancer," *Scientific Reports 2016 6:1*, vol. 6, no. 1, pp. 1–11, Nov. 2016, doi: 10.1038/srep36289.

[239] C. B. Thompson *et al.*, "Abstract SY43-01: Stereochemistry matters: L-2HG as a tumor response to hypoxia," *Cancer Res*, vol. 75, no. 15_Supplement, pp. SY43-01, Aug. 2015, doi: 10.1158/1538-7445.AM2015-SY43-01.

[240] G. Notarangelo *et al.*, "Oncometabolite D-2HG alters T cell metabolism to impair CD8+ T cell function," *Science (1979)*, vol. 377, no. 6614, pp. 1519–1529, Sep. 2022, doi: 10.1126/SCIENCE.ABJ5104/SUPPL_FILE/SCIENCE.ABJ5104_MDAR_REPRODUCIBILITY_CHECKLIST.PDF.

[241] G. Brinkley *et al.*, "Teleological role of L-2-hydroxyglutarate dehydrogenase in the kidney," *DMM Disease Models and Mechanisms*, vol. 13, no. 11, Nov. 2020, doi: 10.1242/DMM.045898/267220/AM/TELEOLOGICAL-ROLE-OF-L-2-HYDROXYGLUTARATE.

[242] A. Vaziri-Gohar *et al.*, "Limited nutrient availability in the tumor microenvironment renders pancreatic tumors sensitive to allosteric IDH1 inhibitors," *Nat Cancer*, vol. 3, no. 7, pp. 852–865, Jul. 2022, doi: 10.1038/S43018-022-00393-Y.

[243] P. S. Ward *et al.*, "The potential for isocitrate dehydrogenase mutations to produce 2-hydroxyglutarate depends on allele specificity and subcellular compartmentalization," *Journal of Biological Chemistry*, vol. 288, no. 6, pp. 3804–3815, Feb. 2013, doi: 10.1074/jbc.M112.435495.

[244] W. Tian *et al.*, "Recent advances of IDH1 mutant inhibitor in cancer therapy," *Front Pharmacol*, vol. 13, Aug. 2022, doi: 10.3389/FPHAR.2022.982424.

[245] A. Chaturvedi *et al.*, "Synergistic activity of IDH1 inhibitor BAY1436032 with azacitidine in IDH1 mutant acute myeloid leukemia," *Haematologica*, vol. 106, no. 2, pp. 565–573, Feb. 2021, doi: 10.3324/HAEMATOL.2019.236992.

[246] P. Xu, G. Hu, C. Luo, and Z. Liang, "DNA methyltransferase inhibitors: an updated patent review (2012-2015)," *Expert Opin Ther Pat*, vol. 26, no. 9, pp. 1017–1030, Sep. 2016, doi: 10.1080/13543776.2016.1209488.

[247] T. Sato *et al.*, "Transcriptional Selectivity of Epigenetic Therapy in Cancer.," *Cancer Res*, vol. 77 2, no. 2, pp. 470–481, Jan. 2017, doi: 10.1158/0008-5472.CAN-16-0834.

[248] K. Agrawal, V. Das, P. Vyas, and M. Hajdúch, "Nucleosidic DNA demethylating epigenetic drugs – A comprehensive review from discovery to clinic," *Pharmacol Ther*, vol. 188, pp. 45–79, Aug. 2018, doi: 10.1016/J.PHARMTHERA.2018.02.006.

[249] G. Karpel-Massler, T. T. T. Nguyen, E. Shang, and M. D. Siegelin, "Novel IDH1-Targeted Glioma Therapies.," *CNS Drugs*, vol. 33, no. 12, pp. 1155–1166, Dec. 2019, doi: 10.1007/S40263-019-00684-6.

[250] D. R. Wahl *et al.*, "Glioblastoma Therapy Can be Augmented by Targeting IDH1-mediated NADPH Biosynthesis," *Cancer Res*, vol. 77, no. 4, p. 960, Feb. 2017, doi: 10.1158/0008-5472.CAN-16-2008.

[251] Y. Liu *et al.*, "Targeting IDH1-Mutated Malignancies with NRF2 Blockade," *JNCI: Journal of the National Cancer Institute*, vol. 111, no. 10, pp. 1033–1041, Oct. 2019, doi: 10.1093/JNCI/DJY230.

[252] E. Bergaggio and R. Piva, "Wild-Type IDH Enzymes as Actionable Targets for Cancer Therapy," *Cancers (Basel)*, vol. 11, no. 4, Apr. 2019, doi: 10.3390/CANCERS11040563.

[253] R. Ma and C. H. Yun, "Crystal structures of pan-IDH inhibitor AG-881 in complex with mutant human IDH1 and IDH2," *Biochem Biophys Res Commun*, vol. 503, no. 4, pp. 2912–2917, Sep. 2018, doi: 10.1016/J.BBRC.2018.08.068.

[254] M. Thamim, A. K. Agrahari, P. Gupta, and K. Thirumoorthy, "Rational Computational Approaches in Drug Discovery: Potential Inhibitors for Allosteric Regulation of Mutant Isocitrate Dehydrogenase-1 Enzyme in Cancers," *Molecules*, vol. 28, no. 5, Mar. 2023, doi: 10.3390/MOLECULES28052315.

[255] C. C. Lin *et al.*, "IDH mutations are closely associated with mutations of DNMT3A, ASXL1 and SRSF2 in patients with myelodysplastic syndromes and are stable during disease evolution," *Am J Hematol*, vol. 89, no. 2, pp. 137–144, Feb. 2014, doi: 10.1002/AJH.23596.

[256] L. Li *et al.*, "Treatment with a Small Molecule Mutant IDH1 Inhibitor Suppresses Tumorigenic Activity and Decreases Production of the Oncometabolite 2-Hydroxyglutarate in Human Chondrosarcoma Cells," *PLoS One*, vol. 10, no. 9, p. e0133813, Sep. 2015, doi: 10.1371/JOURNAL.PONE.0133813.

[257] T. Schumacher *et al.*, "A vaccine targeting mutant IDH1 induces antitumour immunity," *Nature*, vol. 512, no. 7514, pp. 324–327, Aug. 2014, doi: 10.1038/NATURE13387.

[258] M. C. McCabe *et al.*, "Evaluation and Refinement of Sample Preparation Methods for Extracellular Matrix Proteome Coverage," *Mol Cell Proteomics*, vol. 20, 2021, doi: 10.1016/J.MCPRO.2021.100079.

[259] A. Shevchenko, H. Tomas, J. Havliš, J. V. Olsen, and M. Mann, "In-gel digestion for mass spectrometric characterization of proteins and proteomes," *Nature Protocols 2007 1:6*, vol. 1, no. 6, pp. 2856–2860, Jan. 2007, doi: 10.1038/nprot.2006.468.

[260] S. Tyanova, T. Temu, and J. Cox, "The MaxQuant computational platform for mass spectrometry-based shotgun proteomics," *Nat Protoc*, vol. 11, no. 12, pp. 2301–2319, Dec. 2016, doi: 10.1038/NPROT.2016.136.

[261] J. Cox, M. Y. Hein, C. A. Luber, I. Paron, N. Nagaraj, and M. Mann, "Accurate Proteome-wide Label-free Quantification by Delayed Normalization and Maximal Peptide Ratio Extraction, Termed MaxLFQ," *Mol Cell Proteomics*, vol. 13, no. 9, p. 2513, Sep. 2014, doi: 10.1074/MCP.M113.031591.

[262] M. R. O'Dell *et al.*, "Kras(G12D) and p53 mutation cause primary intrahepatic cholangiocarcinoma," *Cancer Res.*, vol. 72, no. 6, pp. 1557–1567, Mar. 2012, doi: 10.1158/0008-5472.can-11-3596.

[263] A. N. Boscoe, C. Rolland, and R. K. Kelley, "Frequency and prognostic significance of isocitrate dehydrogenase 1 mutations in cholangiocarcinoma: a systematic literature review," *J Gastrointest Oncol*, vol. 10, no. 4, pp. 751–765, 2019, doi: 10.21037/JGO.2019.03.10.

[264] H. L. Ju, K. H. Han, J. D. Lee, and S. W. Ro, "Transgenic mouse models generated by hydrodynamic transfection for genetic studies of liver cancer and preclinical testing of anti-cancer therapy," *Int J Cancer*, vol. 138, no. 7, pp. 1601–1608, Apr. 2016, doi: 10.1002/IJC.29703.

[265] I. Elmaci, M. A. Altinoz, R. Sari, and F. H. Bolukbasi, "Phosphorylated Histone H3 (PHH3) as a Novel Cell Proliferation Marker and Prognosticator for Meningeal Tumors: A Short Review," *Appl Immunohistochem Mol Morphol*, vol. 26, no. 9, pp. 627–631, Oct. 2018, doi: 10.1097/PAI.0000000000000499.

[266] S. Fukushima *et al.*, "Sensitivity and usefulness of anti-phosphohistone-H3 antibody immunostaining for counting mitotic figures in meningioma cases," *Brain Tumor Pathol*, vol. 26, no. 2, pp. 51–57, Oct. 2009, doi: 10.1007/s10014-009-0249-9.

[267] M. Karlsson and S. Björnsson, "Quantitation of proteoglycans in biological fluids using Alcian blue," *Methods Mol Biol*, vol. 171, pp. 159–173, 2001, doi: 10.1385/1-59259-209-0:159.

[268] Y. Y. Dan *et al.*, "Isolation of multipotent progenitor cells from human fetal liver capable of differentiating into liver and mesenchymal lineages," *Proc Natl Acad Sci U S A*, vol. 103, no. 26, pp. 9912–9917, Jun. 2006, doi: 10.1073/PNAS.0603824103.

[269] Y. Kawaguchi, "Sox9 and programming of liver and pancreatic progenitors," *J Clin Invest*, vol. 123, no. 5, pp. 1881–1886, May 2013, doi: 10.1172/JCI66022.

[270] C. Walesky and U. Apte, "Role of Hepatocyte Nuclear Factor 4α (HNF4α) in Cell Proliferation and Cancer," *Gene Expr*, vol. 16, no. 3, p. 101, 2015, doi: 10.3727/105221615X14181438356292.

[271] M. Ehrlich and M. Lacey, "DNA methylation and differentiation: silencing, upregulation and modulation of gene expression.," *Epigenomics*, vol. 5 5, no. 5, pp. 553–68, Oct. 2013, doi: 10.2217/EPI.13.43.

[272] A. G. Porter and R. U. Jänicke, "Emerging roles of caspase-3 in apoptosis," *Cell Death & Differentiation 1999 6:2*, vol. 6, no. 2, pp. 99–104, Jan. 1999, doi: 10.1038/sj.cdd.4400476.

[273] M. E. Figueroa *et al.*, "Leukemic IDH1 and IDH2 mutations result in a hypermethylation phenotype, disrupt TET2 function, and impair hematopoietic differentiation," *Cancer Cell*, vol. 18, no. 6, pp. 553–567, Dec. 2010, doi: 10.1016/j.ccr.2010.11.015.

[274] S. Shelar *et al.*, "Biochemical and Epigenetic Insights into L-2-Hydroxyglutarate, a Potential Therapeutic Target in Renal Cancer," *Clin Cancer Res*, vol. 24, no. 24, p. 6433, Dec. 2018, doi: 10.1158/1078-0432.CCR-18-1727.

[275] M. Kusi *et al.*, "2-Hydroxyglutarate destabilizes chromatin regulatory landscape and lineage fidelity to promote cellular heterogeneity," *Cell Rep*, vol. 38, no. 2, p. 110220, Jan. 2022, doi: 10.1016/J.CELREP.2021.110220.

[276] A. R. Cutter DiPiazza, N. Taneja, J. Dhakshnamoorthy, D. Wheeler, S. Holla, and S. I. S. Grewal, "Spreading and epigenetic inheritance of heterochromatin require a critical density of histone H3 lysine 9 tri-methylation," *Proc Natl Acad Sci U S A*, vol. 118, no. 22, p. e2100699118, Jun. 2021, doi: 10.1073/PNAS.2100699118/SUPPL_FILE/PNAS.2100699118.SAPP.PDF.

[277] V. A. Stepanik and P. J. Harte, "A mutation in the E(Z) methyltransferase that increases trimethylation of histone H3 lysine 27 and causes inappropriate silencing of active Polycomb target genes," *Dev Biol*, vol. 364, no. 2, pp. 249–258, Apr. 2012, doi: 10.1016/J.YDBIO.2011.12.007.

[278] M. S. Levine and A. J. Holland, "The impact of mitotic errors on cell proliferation and tumorigenesis," *Genes Dev*, vol. 32, no. 9–10, pp. 620–638, May 2018, doi: 10.1101/GAD.314351.118.

[279] P. Thiru *et al.*, "Kinetochore genes are coordinately up-regulated in human tumors as part of a FoxM1-related cell division program," *Mol Biol Cell*, vol. 25, no. 13, pp. 1983–1994, Jul. 2014, doi: 10.1091/MBC.E14-03-0837/ASSET/IMAGES/LARGE/1983FIG7.JPEG.

[280] C. H. Bassing *et al.*, "Histone H2AX: A dosage-dependent suppressor of oncogenic translocations and tumors," *Cell*, vol. 114, no. 3, pp. 359–370, Aug. 2003, doi: 10.1016/S0092-8674(03)00566-X.
[281] F. Petitprez *et al.*, "The murine Microenvironment Cell Population counter method to estimate abundance of tissue-infiltrating immune and stromal cell populations in murine samples using gene expression," *Genome Med*, vol. 12, no. 1, pp. 1–15, Oct. 2020, doi: 10.1186/S13073-020-00783-W/FIGURES/6.
[282] K. Goldring, G. E. Jones, C. A. Sewry, and D. J. Watt, "The muscle-specific marker desmin is expressed in a proportion of human dermal fibroblasts after their exposure to galectin-1," *Neuromuscular Disorders*, vol. 12, no. 2, pp. 183–186, Feb. 2002, doi: 10.1016/S0960-8966(01)00280-2.
[283] L. Chadli *et al.*, "Identification of regulators of the myofibroblast phenotype of primary dermal fibroblasts from early diffuse systemic sclerosis patients," *Sci Rep*, vol. 9, no. 1, Dec. 2019, doi: 10.1038/S41598-019-41153-W.
[284] B. R. De Young, H. F. Frierson, M. N. Ly, D. Smith, and P. E. Swanson, "CD31 Immunoreactivity in Carcinomas and Mesotheliomas," *Am J Clin Pathol*, vol. 110, no. 3, pp. 374–377, Sep. 1998, doi: 10.1093/AJCP/110.3.374.
[285] M. A. Haber, A. Iranmahboob, C. Thomas, M. Liu, A. Najjar, and D. Zagzag, "ERG is a novel and reliable marker for endothelial cells in central nervous system tumors," *Clin Neuropathol*, vol. 34, no. 3, pp. 117–127, 2015, doi: 10.5414/NP300817.
[286] M. C. McCabe *et al.*, "Evaluation and Refinement of Sample Preparation Methods for Extracellular Matrix Proteome Coverage," *Mol Cell Proteomics*, vol. 20, 2021, doi: 10.1016/J.MCPRO.2021.100079.
[287] J. D. Hood and D. A. Cheresh, "Role of integrins in cell invasion and migration," *Nature Reviews Cancer 2002 2:2*, vol. 2, no. 2, pp. 91–100, 2002, doi: 10.1038/nrc727.
[288] H. Yousefi *et al.*, "Understanding the role of integrins in breast cancer invasion, metastasis, angiogenesis, and drug resistance," *Oncogene*, vol. 40, no. 6, pp. 1043–1063, Feb. 2021, doi: 10.1038/S41388-020-01588-2.
[289] D. A. Simon Davis and C. R. Parish, "Heparan sulfate: A ubiquitous glycosaminoglycan with multiple roles in immunity," *Front Immunol*, vol. 4, no. DEC, p. 72098, Dec. 2013, doi: 10.3389/FIMMU.2013.00470/BIBTEX.
[290] I. Häuselmann and L. Borsig, "Altered tumor-cell glycosylation promotes metastasis," *Front Oncol*, vol. 4, 2014, doi: 10.3389/FONC.2014.00028.
[291] M. Gonzalez-Aparicio and C. Alfaro, "Influence of interleukin-8 and neutrophil extracellular trap (NET) formation in the tumor microenvironment: Is there a pathogenic role?," *J Immunol Res*, vol. 2019, 2019, doi: 10.1155/2019/6252138.
[292] J. Pardo, M. M. Simon, and C. J. Froelich, "Granzyme A is a proinflammatory protease.," *Blood*, vol. 114 18, no. 18, pp. 3968; author reply 3969-70, Oct. 2009, doi: 10.1182/BLOOD-2009-07-231027.
[293] M. Germann *et al.*, "Neutrophils suppress tumor-infiltrating T cells in colon cancer via matrix metalloproteinase-mediated activation of TGFβ," *EMBO Mol Med*, vol. 12, no. 1, p. e10681, Jan. 2020, doi: 10.15252/EMMM.201910681.
[294] B. G. Yipp and P. Kubes, "Antibodies against neutrophil LY6G do not inhibit leukocyte recruitment in mice in vivo.," *Blood*, vol. 121 1, no. 1, pp. 241–2, Jan. 2013, doi: 10.1182/BLOOD-2012-09-454348.
[295] Z.-Q. Lin, T. Kondo, Y. Ishida, T. Takayasu, and N. Mukaida, "Essential involvement of IL-6 in the skin wound-healing process as evidenced by delayed wound healing in IL-6-deficient mice," *J Leukoc Biol*, vol. 73, no. 6, pp. 713–721, Jun. 2003, doi: 10.1189/JLB.0802397.
[296] L. A. Murray *et al.*, "Targeting interleukin-13 with tralokinumab attenuates lung fibrosis and epithelial damage in a humanized SCID idiopathic pulmonary fibrosis model.," *Am J Respir Cell Mol Biol*, vol. 50 5, no. 5, pp. 985–994, 2014, doi: 10.1165/RCMB.2013-0342OC.
[297] N. Nishida *et al.*, "Non-Inflamed Tumor Microenvironment and Methylation/Downregulation of Antigen-Presenting Machineries in Cholangiocarcinoma," *Cancers (Basel)*, vol. 15, no. 8, Apr. 2023, doi: 10.3390/CANCERS15082379.
[298] M. C. W. Westergaard *et al.*, "Changes in the Tumor Immune Microenvironment during Disease Progression in Patients with Ovarian Cancer," *Cancers 2020, Vol. 12, Page 3828*, vol. 12, no. 12, p. 3828, Dec. 2020, doi: 10.3390/CANCERS12123828.
[299] E. Reeves and E. James, "Antigen processing and immune regulation in the response to tumours," *Immunology*, vol. 150, no. 1, pp. 16–24, Jan. 2017, doi: 10.1111/IMM.12675.
[300] R. E. Wawman, H. Bartlett, and Y. H. Oo, "Regulatory T cell metabolism in the hepatic microenvironment," *Front Immunol*, vol. 8, no. DEC, Jan. 2018, doi: 10.3389/FIMMU.2017.01889.
[301] H. Yagi *et al.*, "Crucial role of FOXP3 in the development and function of human CD25+CD4+ regulatory T cells," *Int Immunol*, vol. 16, no. 11, pp. 1643–1656, Nov. 2004, doi: 10.1093/INTIMM/DXH165.

[302] H. Loo Yau *et al.*, "DNA hypomethylating agents increase activation and cytolytic activity of CD8+ T cells.," *Mol Cell*, vol. 81, no. 7, pp. 1469-1483.e8, Apr. 2021, doi: 10.1016/J.MOLCEL.2021.01.038.

[303] I. C. Nicholson *et al.*, "PI16 is expressed by a subset of human memory Treg with enhanced migration to CCL17 and CCL20," *Cell Immunol*, vol. 275, no. 1–2, pp. 12–18, Jan. 2012, doi: 10.1016/J.CELLIMM.2012.04.002.

[304] Y. Mizukami *et al.*, "CCL17 and CCL22 chemokines within tumor microenvironment are related to accumulation of Foxp3+ regulatory T cells in gastric cancer," *Int J Cancer*, vol. 122, no. 10, pp. 2286–2293, May 2008, doi: 10.1002/IJC.23392.

[305] C. Nepal *et al.*, "Genomic perturbations reveal distinct regulatory networks in intrahepatic cholangiocarcinoma," *Hepatology*, vol. 68, no. 3, pp. 949–963, Sep. 2018, doi: 10.1002/HEP.29764/SUPPINFO.

[306] D. Sia, A. Villanueva, S. L. Friedman, and J. M. Llovet, "Liver Cancer Cell of Origin, Molecular Class, and Effects on Patient Prognosis," *Gastroenterology*, vol. 152, no. 4, pp. 745–761, Mar. 2017, doi: 10.1053/J.GASTRO.2016.11.048.

[307] Z. H. Liu, X. M. Dai, and B. Du, "Hes1: a key role in stemness, metastasis and multidrug resistance," *Cancer Biol Ther*, vol. 16, no. 3, pp. 353–359, Mar. 2015, doi: 10.1080/15384047.2015.1016662.

[308] S. K. Saha *et al.*, "Isocitrate dehydrogenase mutations confer Dasatinib hypersensitivity and SRC dependence in intrahepatic Cholangiocarcinoma," *Cancer Discov*, vol. 6, no. 7, pp. 727–739, Jul. 2016, doi: 10.1158/2159-8290.cd-15-1442.

[309] H. Fujiwara *et al.*, "Isocitrate dehydrogenase 1 mutation sensitizes intrahepatic cholangiocarcinoma to the BET inhibitor JQ1," *Cancer Sci*, vol. 109, no. 11, p. 3602, Nov. 2018, doi: 10.1111/CAS.13784.

[310] J. A. Brinkman, S. C. Fausch, J. S. Weber, and W. M. Kast, "Peptide-based vaccines for cancer immunotherapy," *Expert Opin Biol Ther*, vol. 4, no. 2, pp. 181–198, Feb. 2004, doi: 10.1517/14712598.4.2.181.

[311] M. S. Bijker, C. J. M. Melief, R. Offringa, and S. H. Van Der Burg, "Design and development of synthetic peptide vaccines: past, present and future," *Expert Rev Vaccines*, vol. 6, no. 4, pp. 591–603, Aug. 2007, doi: 10.1586/14760584.6.4.591.

[312] M. Platten *et al.*, "A vaccine targeting mutant IDH1 in newly diagnosed glioma," *Nature 2021 592:7854*, vol. 592, no. 7854, pp. 463–468, Mar. 2021, doi: 10.1038/s41586-021-03363-z.

[313] E. Van Doorn, H. Liu, A. Huckriede, and E. Hak, "Safety and tolerability evaluation of the use of Montanide ISA^{TM}51 as vaccine adjuvant: A systematic review," *Hum Vaccin Immunother*, vol. 12, no. 1, pp. 159–169, Jan. 2016, doi: 10.1080/21645515.2015.1071455.

[314] K. S. Lang *et al.*, "Immunoprivileged status of the liver is controlled by Toll-like receptor 3 signaling," *Journal of Clinical Investigation*, vol. 116, no. 9, p. 2456, Sep. 2006, doi: 10.1172/JCI28349.

[315] J. V. Forrester, H. Xu, T. Lambe, and R. Cornall, "Immune privilege or privileged immunity?," *Mucosal Immunology 2008 1:5*, vol. 1, no. 5, pp. 372–381, Jul. 2008, doi: 10.1038/mi.2008.27.

[316] W. Xu *et al.*, "Oncometabolite 2-hydroxyglutarate is a competitive inhibitor of α-ketoglutarate-dependent dioxygenases," *Cancer Cell*, vol. 19, no. 1, pp. 17–30, Jan. 2011, doi: 10.1016/j.ccr.2010.12.014.

[317] A. Saharia, "Changing Landscape of Cholangiocarcinoma," *Nov Approaches Cancer Study*, vol. 4, no. 2, Mar. 2020, doi: 10.31031/NACS.2020.04.000584.

[318] K. Obama *et al.*, "Genome-wide analysis of gene expression in human intrahepatic cholangiocarcinoma," *Hepatology*, vol. 41, no. 6, pp. 1339–1348, Jun. 2005, doi: 10.1002/HEP.20718.

[319] Y. H. Shaib, H. B. El-Serag, J. A. Davila, R. Morgan, and K. A. Mcglynn, "Risk factors of intrahepatic cholangiocarcinoma in the United States: a case-control study," *Gastroenterology*, vol. 128, no. 3, pp. 620–626, 2005, doi: 10.1053/j.gastro.2004.12.048.

[320] B. Gumustop and G. P. Aithal, "Striking trends in the cholangiocarcinoma incidence and mortality in the United States of America 1979–1998," *Gastroenterology*, vol. 120, no. 5, p. A257, Apr. 2001, doi: 10.1016/S0016-5085(08)81270-X.

[321] H. Duygu Saatcioglu *et al.*, "552 Characteristics of the tumor microenvironment in IDH1-mutated cholangiocarcinoma patients from ClarIDHy trial," *Regular and Young Investigator Award Abstracts*, pp. A576–A577, Nov. 2022, doi: 10.1136/JITC-2022-SITC2022.0552.

[322] C. L. Lee *et al.*, "Serum concentrations of oncometabolite, 2-hydroxyglutarate (2HG), as biomarkers for isocitrate dehydrogenase (IDH1/2) mutations in cholangiocarcinoma (ICCA).," vol. 40, no. 16_suppl, pp. 3049–3049, Jun. 2022, doi: 10.1200/JCO.2022.40.16_SUPPL.3049.

[323] Y. L. Zheng *et al.*, "Less Efficient G2-M Checkpoint Is Associated with an Increased Risk of Lung Cancer in African Americans," *Cancer Res*, vol. 65, no. 20, pp. 9566–9573, Oct. 2005, doi: 10.1158/0008-5472.CAN-05-1003.

[324] B. Goeppert *et al.*, "Integrative Analysis Defines Distinct Prognostic Subgroups of Intrahepatic Cholangiocarcinoma," *Hepatology*, vol. 69, no. 5, pp. 2091–2106, May 2019, doi: 10.1002/HEP.30493.
[325] K. Lee *et al.*, "Intrahepatic cholangiocarcinomas with IDH1/2 mutation-associated hypermethylation at selective genes and their clinicopathological features," *Scientific Reports 2020 10:1*, vol. 10, no. 1, pp. 1–10, Sep. 2020, doi: 10.1038/s41598-020-72810-0.
[326] C. H. Lee *et al.*, "Cancer related gene alterations can be detected with next-generation sequencing analysis of bile in diffusely infiltrating type cholangiocarcinoma," *Exp Mol Pathol*, vol. 101, no. 1, pp. 150–156, Aug. 2016, doi: 10.1016/J.YEXMP.2016.07.010.
[327] J. H. Lee *et al.*, "IDH1 R132C mutation is detected in clear cell hepatocellular carcinoma by pyrosequencing," *World J Surg Oncol*, vol. 15, no. 1, Apr. 2017, doi: 10.1186/S12957-017-1144-1.
[328] M. Javle *et al.*, "Biliary cancer: Utility of next-generation sequencing for clinical management," *Cancer*, vol. 122, no. 24, pp. 3838–3847, Dec. 2016, doi: 10.1002/CNCR.30254.
[329] A. Ruzzenente *et al.*, "Cholangiocarcinoma Heterogeneity Revealed by Multigene Mutational Profiling: Clinical and Prognostic Relevance in Surgically Resected Patients," *Ann Surg Oncol*, vol. 23, no. 5, pp. 1699–1707, May 2016, doi: 10.1245/S10434-015-5046-6.
[330] H. Winter *et al.*, "Circulating tumour DNA and oncometabolites in patients with intrahepatic cholangiocarcinoma," *Annals of Oncology*, vol. 28, pp. vii10–vii11, Oct. 2017, doi: 10.1093/annonc/mdx508.024.
[331] R. J. Molenaar, T. Radivoyevitch, J. P. Maciejewski, C. J. F. van Noorden, and F. E. Bleeker, "The driver and passenger effects of isocitrate dehydrogenase 1 and 2 mutations in oncogenesis and survival prolongation," *Biochimica et Biophysica Acta (BBA) - Reviews on Cancer*, vol. 1846, no. 2, pp. 326–341, Dec. 2014, doi: 10.1016/J.BBCAN.2014.05.004.
[332] W. Chan-On *et al.*, "Exome sequencing identifies distinct mutational patterns in liver fluke-related and non-infection-related bile duct cancers," *Nat Genet*, vol. 45, no. 12, pp. 1474–1478, Dec. 2013, doi: 10.1038/NG.2806.
[333] M. Nakagawa *et al.*, "Prognostic impact of IDH mutations in chondrosarcoma.," *J Orthop Sci*, vol. 27, no. 6, pp. 1315–1322, Nov. 2022, doi: 10.1016/J.JOS.2021.07.024.
[334] I. Lugowska *et al.*, "IDH1/2 Mutations Predict Shorter Survival in Chondrosarcoma," *J Cancer*, vol. 9, no. 6, pp. 998–1005, 2018, doi: 10.7150/JCA.22915.
[335] M. C. Y. De Wit, H. G. De Bruin, W. Eijkenboom, P. A. E. Sillevis Smitt, and M. J. Van Den Bent, "Immediate post-radiotherapy changes in malignant glioma can mimic tumor progression," *Neurology*, vol. 63, no. 3, pp. 535–537, Aug. 2004, doi: 10.1212/01.WNL.0000133398.11870.9A.
[336] K. Ichimura *et al.*, "IDH1 mutations are present in the majority of common adult gliomas but rare in primary glioblastomas," *Neuro Oncol*, vol. 11, no. 4, pp. 341–347, Aug. 2009, doi: 10.1215/15228517-2009-025.
[337] Q. Songtao *et al.*, "IDH mutations predict longer survival and response to temozolomide in secondary glioblastoma," *Wiley Online LibraryQ SongTao, Y Lei, G Si, D YanQing, H HuiXia, Z XueLin, W LanXiao, Y FeiCancer science, 2012•Wiley Online Library*, vol. 103, no. 2, pp. 269–273, Feb. 2012, doi: 10.1111/j.1349-7006.2011.02134.x.
[338] N. Sabha *et al.*, "Analysis of IDH mutation, 1p/19q deletion, and PTEN loss delineates prognosis in clinical low-grade diffuse gliomas," *Neuro Oncol*, vol. 16, no. 7, pp. 914–923, 2014, doi: 10.1093/NEUONC/NOT299.
[339] H. Sun *et al.*, "Prognostic significance of IDH mutation in adult low-grade gliomas: A meta-analysis," *J Neurooncol*, vol. 113, no. 2, pp. 277–284, Jun. 2013, doi: 10.1007/S11060-013-1107-5.
[340] P. Yang *et al.*, "IDH mutation and MGMT promoter methylation in glioblastoma: Results of a prospective registry," *Oncotarget*, vol. 6, no. 38, pp. 40896–40906, 2015, doi: 10.18632/ONCOTARGET.5683.
[341] M. A. Lewandowska *et al.*, "An analysis of the prognostic value of IDH1 (isocitrate dehydrogenase 1) mutation in Polish glioma patients," *Mol Diagn Ther*, vol. 18, no. 1, pp. 45–53, Feb. 2014, doi: 10.1007/S40291-013-0050-7.
[342] P. Zou *et al.*, "IDH1/IDH2 Mutations Define the Prognosis and Molecular Profiles of Patients with Gliomas: A Meta-Analysis," *PLoS One*, vol. 8, no. 7, Jul. 2013, doi: 10.1371/JOURNAL.PONE.0068782.
[343] Y. Dai, X. Ning, G. Han, and W. Li, "Assessment of the Association between Isocitrate Dehydrogenase 1 Mutation and Mortality Risk of Glioblastoma Patients," *Mol Neurobiol*, vol. 53, no. 3, pp. 1501–1508, Apr. 2016, doi: 10.1007/S12035-015-9104-7.
[344] R. J. Molenaar *et al.*, "The combination of IDH1 mutations and MGMT methylation status predicts survival in glioblastoma better than either IDH1 or MGMT alone," *Neuro Oncol*, vol. 16, no. 9, pp. 1263–1273, 2014, doi: 10.1093/NEUONC/NOU005.

[345] S. Choi, Y. Yu, M. R. Grimmer, M. Wahl, S. M. Chang, and J. F. Costello, "Temozolomide-associated hypermutation in gliomas," *Neuro Oncol*, vol. 20, no. 10, pp. 1300–1309, Sep. 2018, doi: 10.1093/NEUONC/NOY016.

[346] A. R. Grassian, R. Pagliarini, and D. Y. Chiang, "Mutations of isocitrate dehydrogenase 1 and 2 in intrahepatic cholangiocarcinoma," *Curr Opin Gastroenterol*, vol. 30, no. 3, pp. 295–302, 2014, doi: 10.1097/MOG.0000000000000050.

[347] T. C. A. Johannessen *et al.*, "Rapid conversion of mutant IDH1 from driver to passenger in a model of human gliomagenesis," *Molecular Cancer Research*, vol. 14, no. 10, pp. 976–983, Oct. 2016, doi: 10.1158/1541-7786.MCR-16-0141/176168/AM/RAPID-CONVERSION-OF-MUTANT-IDH1-FROM-DRIVER-TO.

[348] A. R. Grassian, R. Pagliarini, and D. Y. Chiang, "Mutations of isocitrate dehydrogenase 1 and 2 in intrahepatic cholangiocarcinoma," *Curr Opin Gastroenterol*, vol. 30, no. 3, pp. 295–302, 2014, doi: 10.1097/MOG.0000000000000050.

[349] P. Wang *et al.*, "Mutations in isocitrate dehydrogenase 1 and 2 occur frequently in intrahepatic cholangiocarcinomas and share hypermethylation targets with glioblastomas," *Oncogene*, vol. 32, no. 25, pp. 3091–3100, Jun. 2013, doi: 10.1038/ONC.2012.315.

[350] L. A. Salas, K. C. Johnson, D. C. Koestler, D. E. O'Sullivan, and B. C. Christensen, "Integrative epigenetic and genetic pan-cancer somatic alteration portraits," *Epigenetics*, vol. 12, no. 7, pp. 561–574, Jul. 2017, doi: 10.1080/15592294.2017.1319043.

[351] T. Ushijima, T. Nakajima, and T. Maekita, "DNA methylation as a marker for the past and future," *J Gastroenterol*, vol. 41, no. 5, pp. 401–407, May 2006, doi: 10.1007/S00535-006-1846-6/METRICS.

[352] I. Keshet, J. Lieman-Hurwitz, and H. Cedar, "DNA methylation affects the formation of active chromatin," *Cell*, vol. 44, no. 4, pp. 535–543, Feb. 1986, doi: 10.1016/0092-8674(86)90263-1.

[353] A. Catteau and J. R. Morris, "BRCA1 methylation: a significant role in tumour development?," *Semin Cancer Biol*, vol. 12 5, no. 5, pp. 359–371, 2002, doi: 10.1016/S1044-579X(02)00056-1.

[354] J. G. Herman and S. B. Baylin, "Gene silencing in cancer in association with promoter hypermethylation.," *N Engl J Med*, vol. 349 21, no. 21, pp. 2042–54, Nov. 2003, doi: 10.1056/NEJMRA023075.

[355] A. Lujambio *et al.*, "A microRNA DNA methylation signature for human cancer metastasis," *Proceedings of the National Academy of Sciences*, vol. 105, no. 36, pp. 13556–13561, Sep. 2008, doi: 10.1073/PNAS.0803055105.

[356] E. M. Kennedy *et al.*, "An integrated -omics analysis of the epigenetic landscape of gene expression in human blood cells," *BMC Genomics*, vol. 19, no. 1, Jun. 2018, doi: 10.1186/S12864-018-4842-3.

[357] J. Li *et al.*, "Guide Positioning Sequencing identifies aberrant DNA methylation patterns that alter cell identity and tumor-immune surveillance networks," *Genome Res*, vol. 29, no. 2, pp. 270–280, Feb. 2019, doi: 10.1101/GR.240606.118.

[358] S. Lou *et al.*, "Whole-genome bisulfite sequencing of multiple individuals reveals complementary roles of promoter and gene body methylation in transcriptional regulation," *Genome Biol*, vol. 15, no. 7, Jul. 2014, doi: 10.1186/S13059-014-0408-0.

[359] A. Teissandier and D. Bourc'his, "Gene body DNA methylation conspires with H3K36me3 to preclude aberrant transcription," *EMBO J*, vol. 36, no. 11, pp. 1471–1473, Jun. 2017, doi: 10.15252/EMBJ.201796812.

[360] D. Jjingo, A. B. Conley, S. V. Yi, V. V. Lunyak, and I. King Jordan, "On the presence and role of human gene-body DNA methylation," *Oncotarget*, vol. 3, no. 4, pp. 462–474, 2012, doi: 10.18632/ONCOTARGET.497.

[361] A. K. Maunakea *et al.*, "Conserved Role of Intragenic DNA Methylation in Regulating Alternative Promoters," *Nature*, vol. 466, no. 7303, pp. 253–257, Jul. 2010, doi: 10.1038/NATURE09165.

[362] C. Lu *et al.*, "IDH mutation impairs histone demethylation and results in a block to cell differentiation," *Nature*, vol. 483, no. 7390, pp. 474–478, Mar. 2012, doi: 10.1038/NATURE10860.

[363] J. Huang, J. Yu, L. Tu, N. Huang, H. Li, and Y. Luo, "Isocitrate Dehydrogenase Mutations in Glioma: From Basic Discovery to Therapeutics Development," *Front Oncol*, vol. 9, no. JUN, 2019, doi: 10.3389/FONC.2019.00506.

[364] S. Choe *et al.*, "Molecular mechanisms mediating relapse following ivosidenib monotherapy in IDH1-mutant relapsed or refractory AML.," *Blood Adv*, vol. 4 9, no. 9, pp. 1894–1905, May 2020, doi: 10.1182/BLOODADVANCES.2020001503.

[365] D. F. Tschaharganeh *et al.*, "p53 dependent Nestin regulation links tumor suppression to cellular plasticity in liver cancer," *Cell*, vol. 158, no. 3, p. 579, Jul. 2014, doi: 10.1016/J.CELL.2014.05.051.

[366] S. Sekiya and A. Suzuki, "Hepatocytes, Rather than Cholangiocytes, Can Be the Major Source of Primitive Ductules in the Chronically Injured Mouse Liver," *Am J Pathol*, vol. 184, no. 5, pp. 1468–1478, May 2014, doi: 10.1016/J.AJPATH.2014.01.005.

[367] Y. Zong *et al.*, "Notch signaling controls liver development by regulating biliary differentiation," *Development*, vol. 136, no. 10, pp. 1727–1739, May 2009, doi: 10.1242/DEV.029140.

[368] G. K. Michalopoulos, L. Barua, and W. C. Bowen, "Transdifferentiation of Rat Hepatocytes Into Biliary Cells After Bile Duct Ligation and Toxic Biliary Injury," *Hepatology*, vol. 41, no. 3, p. 535, Mar. 2005, doi: 10.1002/HEP.20600.

[369] R. S. Berger *et al.*, "Degradation of D-2-hydroxyglutarate in the presence of isocitrate dehydrogenase mutations," *Scientific Reports 2019 9:1*, vol. 9, no. 1, pp. 1–11, May 2019, doi: 10.1038/s41598-019-43891-3.

[370] H. Yang, D. Ye, K. L. Guan, and Y. Xiong, "IDH1 and IDH2 Mutations in Tumorigenesis: Mechanistic Insights and Clinical Perspectives," *Clinical Cancer Research*, vol. 18, no. 20, pp. 5562–5571, Oct. 2012, doi: 10.1158/1078-0432.CCR-12-1773.

[371] Z. Yang *et al.*, "2-HG Inhibits Necroptosis by Stimulating DNMT1-Dependent Hypermethylation of the RIP3 Promoter.," *Cell Rep*, vol. 19 9, no. 9, pp. 1846–1857, May 2017, doi: 10.1016/J.CELREP.2017.05.012.

[372] Y. Jin *et al.*, "Mutant IDH1 Dysregulates the Differentiation of Mesenchymal Stem Cells in Association with Gene-Specific Histone Modifications to Cartilage- and Bone-Related Genes," *PLoS One*, vol. 10, no. 7, p. e0131998, Jul. 2015, doi: 10.1371/JOURNAL.PONE.0131998.

[373] G. K. Patel, N. Chugh, and M. Tripathi, "Neuroendocrine Differentiation of Prostate Cancer—An Intriguing Example of Tumor Evolution at Play," *Cancers 2019, Vol. 11, Page 1405*, vol. 11, no. 10, p. 1405, Sep. 2019, doi: 10.3390/CANCERS11101405.

[374] N. Rajbhandari *et al.*, "Tracing tumor evolution and subtype specification in pancreatic cancer," Aug. 2021, doi: 10.21203/RS.3.RS-101578/V1.

[375] S. Ali, D. Hamam, X. Liu, and J. J. Lebrun, "Terminal differentiation and anti-tumorigenic effects of prolactin in breast cancer," *Front Endocrinol (Lausanne)*, vol. 13, p. 993570, Sep. 2022, doi: 10.3389/FENDO.2022.993570/BIBTEX.

[376] H. Raskov, A. Orhan, S. Gaggar, and I. Gögenur, "Cancer-Associated Fibroblasts and Tumor-Associated Macrophages in Cancer and Cancer Immunotherapy," *Front Oncol*, vol. 11, p. 668731, May 2021, doi: 10.3389/FONC.2021.668731/BIBTEX.

[377] A. Kameyama, R. Nishijima, and K. Yamakoshi, "Bmi-1 regulates mucin levels and mucin O-glycosylation in the submandibular gland of mice," *PLoS One*, vol. 16, no. 1, Jan. 2021, doi: 10.1371/JOURNAL.PONE.0245607.

[378] J. Wei, M. Hu, K. Huang, S. Lin, and H. Du, "Roles of Proteoglycans and Glycosaminoglycans in Cancer Development and Progression," *Int J Mol Sci*, vol. 21, no. 17, pp. 1–28, Sep. 2020, doi: 10.3390/IJMS21175983.

[379] K. L. Carraway, V. P. Ramsauer, B. Haq, and C. A. Carothers Carraway, "Cell signaling through membrane mucins," *BioEssays*, vol. 25, no. 1, pp. 66–71, Jan. 2003, doi: 10.1002/BIES.10201.

[380] N. Thompson and W. Wakarchuk, "O-glycosylation and its role in therapeutic proteins," *Biosci Rep*, vol. 42, no. 10, Oct. 2022, doi: 10.1042/BSR20220094/231919.

[381] C. K. Payne, S. A. Jones, C. Chen, and X. Zhuang, "Internalization and Trafficking of Cell Surface Proteoglycans and Proteoglycan-Binding Ligands," *Traffic*, vol. 8, no. 4, pp. 389–401, Apr. 2007, doi: 10.1111/J.1600-0854.2007.00540.X.

[382] I. S. Reynolds, M. Fichtner, D. A. McNamara, E. W. Kay, J. H. M. Prehn, and J. P. Burke, "Mucin glycoproteins block apoptosis; promote invasion, proliferation, and migration; and cause chemoresistance through diverse pathways in epithelial cancers," *Cancer and Metastasis Reviews 2019 38:1*, vol. 38, no. 1, pp. 237–257, Jan. 2019, doi: 10.1007/S10555-019-09781-W.

[383] H. Läubli and L. Borsig, "Altered Cell Adhesion and Glycosylation Promote Cancer Immune Suppression and Metastasis," *Front Immunol*, vol. 10, p. 484841, Sep. 2019, doi: 10.3389/FIMMU.2019.02120/BIBTEX.

[384] J. G. Rodrigues *et al.*, "Glycosylation in cancer: Selected roles in tumour progression, immune modulation and metastasis," *Cell Immunol*, vol. 333, pp. 46–57, Nov. 2018, doi: 10.1016/J.CELLIMM.2018.03.007.

[385] I. Häuselmann and L. Borsig, "Altered tumor-cell glycosylation promotes metastasis," *Front Oncol*, vol. 4, 2014, doi: 10.3389/FONC.2014.00028.

[386] S. Mereiter, M. Balmaña, D. Campos, J. Gomes, and C. A. Reis, "Glycosylation in the Era of Cancer-Targeted Therapy: Where Are We Heading?," *Cancer Cell*, vol. 36, no. 1, pp. 6–16, Jul. 2019, doi: 10.1016/J.CCELL.2019.06.006.

[387] P. M. Drake *et al.*, "Sweetening the Pot: Adding Glycosylation to the Biomarker Discovery Equation," *Clin Chem*, vol. 56, no. 2, pp. 223–236, Feb. 2010, doi: 10.1373/CLINCHEM.2009.136333.

[388] D. Sobral, R. Francisco, L. Duro, P. A. Videira, and A. R. Grosso, "Concerted Regulation of Glycosylation Factors Sustains Tissue Identity and Function," *Biomedicines*, vol. 10, no. 8, Aug. 2022, doi: 10.3390/BIOMEDICINES10081805.

[389] G. Tzanakakis, M. Neagu, A. Tsatsakis, and D. Nikitovic, "Proteoglycans and immunobiology of cancer-therapeutic implications," *Front Immunol*, vol. 10, no. APR, 2019, doi: 10.3389/fimmu.2019.00875.

[390] L. Gasimli, R. J. Linhardt, and J. S. Dordick, "Proteoglycans in stem cells," *Biotechnol Appl Biochem*, vol. 59, no. 2, pp. 65–76, Mar. 2012, doi: 10.1002/BAB.1002.

[391] C. E. Ament *et al.*, "Aberrant fucosylation sustains the NOTCH and EGFR/NF-κB pathways and has a prognostic value in human intrahepatic cholangiocarcinoma," *Hepatology*, vol. 78, no. 6, pp. 1742–1754, Dec. 2023, doi: 10.1097/HEP.0000000000000322.

[392] A. Terunuma *et al.*, "MYC-driven accumulation of 2-hydroxyglutarate is associated with breast cancer prognosis.," *J Clin Invest*, vol. 124 1, no. 1, pp. 398–412, Jan. 2014, doi: 10.1172/JCI71180.

[393] L. Salamanca-Cardona *et al.*, "In Vivo Imaging of Glutamine Metabolism to the Oncometabolite 2-Hydroxyglutarate in IDH1/2 Mutant Tumors.," *Cell Metab*, vol. 26 6, no. 6, pp. 830–8413, Dec. 2017, doi: 10.1016/J.CMET.2017.10.001.

[394] C. Yong, G. D. Stewart, and C. Frezza, "Oncometabolites in renal cancer," *Nat Rev Nephrol*, vol. 16, no. 3, pp. 156–172, Mar. 2020, doi: 10.1038/S41581-019-0210-Z.

[395] R. M. Phillips, C. Lam, H. Wang, and P. T. Tran, "Bittersweet tumor development and progression: Emerging roles of epithelial plasticity glycosylations," *Adv Cancer Res*, vol. 142, pp. 23–62, Jan. 2019, doi: 10.1016/BS.ACR.2019.01.002.

[396] N. N. Pavlova and C. B. Thompson, "The Emerging Hallmarks of Cancer Metabolism.," *Cell Metab*, vol. 23 1, no. 1, pp. 27–47, Jan. 2016, doi: 10.1016/J.CMET.2015.12.006.

[397] P. Chaiyawat, P. Netsirisawan, J. Svasti, and V. Champattanachai, "Aberrant O-GlcNAcylated Proteins: New Perspectives in Breast and Colorectal Cancer," *Front Endocrinol (Lausanne)*, vol. 5, no. NOV, 2014, doi: 10.3389/FENDO.2014.00193.

[398] M. C. Lucena *et al.*, "Epithelial Mesenchymal Transition Induces Aberrant Glycosylation through Hexosamine Biosynthetic Pathway Activation*," *J Biol Chem*, vol. 291, no. 25, pp. 12917–12929, Jun. 2016, doi: 10.1074/JBC.M116.729236.

[399] J. M. Simmons, T. A. Müller, and R. P. Hausinger, "Fe(II)/alpha-ketoglutarate hydroxylases involved in nucleobase, nucleoside, nucleotide, and chromatin metabolism.," *Dalton transactions*, vol. 38, no. 38, pp. 5132–42, 2008, doi: 10.1039/B803512A.

[400] S. Jia *et al.*, "A fully active catalytic domain of bovine aspartyl (asparaginyl) beta-hydroxylase expressed in Escherichia coli: characterization and evidence for the identification of an active-site region in vertebrate alpha-ketoglutarate-dependent dioxygenases.," *Proc Natl Acad Sci U S A*, vol. 91 15, no. 15, pp. 7227–31, Jul. 1994, doi: 10.1073/PNAS.91.15.7227.

[401] A. R. Grassian *et al.*, "IDH1 mutations alter citric acid cycle metabolism and increase dependence on oxidative mitochondrial metabolism.," *Cancer Res*, vol. 74 12, no. 12, pp. 3317–31, Jun. 2014, doi: 10.1158/0008-5472.CAN-14-0772-T.

[402] H. Fujiwara *et al.*, "Mutant IDH1 confers resistance to energy stress in normal biliary cells through PFKP-induced aerobic glycolysis and AMPK activation," *Sci Rep*, vol. 9, no. 1, Dec. 2019, doi: 10.1038/S41598-019-55211-W.

[403] S. J. Gelman *et al.*, "Consumption of NADPH for 2-HG Synthesis Increases Pentose Phosphate Pathway Flux and Sensitizes Cells to Oxidative Stress," *Cell Rep*, vol. 22, no. 2, pp. 512–522, 2018, doi: 10.1016/J.CELREP.2017.12.050.

[404] Z. J. Reitman *et al.*, "Cancer-associated Isocitrate Dehydrogenase 1 (IDH1) R132H Mutation and d-2-Hydroxyglutarate Stimulate Glutamine Metabolism under Hypoxia*," *J Biol Chem*, vol. 289, no. 34, pp. 23318–23328, 2014, doi: 10.1074/JBC.M114.575183.

[405] W. Lv, Y. Tan, X. Zhou, Q. Zhang, J. Zhang, and Y. Wu, "Landscape of prognosis and immunotherapy responsiveness under tumor glycosylation-related lncRNA patterns in breast cancer," *Front Immunol*, vol. 13, p. 989928, Sep. 2022, doi: 10.3389/FIMMU.2022.989928/BIBTEX.

[406] V. Vitiazeva *et al.*, "The O-Linked Glycome and Blood Group Antigens ABO on Mucin-Type Glycoproteins in Mucinous and Serous Epithelial Ovarian Tumors," *PLoS One*, vol. 10, no. 6, Jun. 2015, doi: 10.1371/JOURNAL.PONE.0130197.

[407] D. Virág *et al.*, "Altered Glycosylation of Human Alpha-1-Acid Glycoprotein as a Biomarker for Malignant Melanoma," *Molecules 2021, Vol. 26, Page 6003*, vol. 26, no. 19, p. 6003, Oct. 2021, doi: 10.3390/MOLECULES26196003.
[408] S. L. Friedman, "Mechanisms of hepatic fibrogenesis.," *Gastroenterology*, vol. 134 6, no. 6, pp. 1655–69, 2008, doi: 10.1053/J.GASTRO.2008.03.003.
[409] C. Y. Jing *et al.*, "Hepatic stellate cells promote intrahepatic cholangiocarcinoma progression via NR4A2/osteopontin/Wnt signaling axis," *Oncogene 2021 40:16*, vol. 40, no. 16, pp. 2910–2922, Mar. 2021, doi: 10.1038/s41388-021-01705-9.
[410] H. Okabe *et al.*, "Abstract 1013: Hepatic stellate cells promote progression of cholangiocarcinoma in vitro and in vivo," *Cancer Res*, vol. 70, no. 8_Supplement, pp. 1013–1013, Apr. 2010, doi: 10.1158/1538-7445.AM10-1013.
[411] M. Mikula, V. Proell, A. N. M. Fischer, and W. Mikulits, "Activated hepatic stellate cells induce tumor progression of neoplastic hepatocytes in a TGF-β dependent fashion," *J Cell Physiol*, vol. 209, no. 2, pp. 560–567, Nov. 2006, doi: 10.1002/JCP.20772.
[412] R. A. Itou *et al.*, "Immunohistochemical characterization of cancer-associated fibroblasts at the primary sites and in the metastatic lymph nodes of human intrahepatic cholangiocarcinoma," *Hum Pathol*, vol. 83, pp. 77–89, Jan. 2019, doi: 10.1016/J.HUMPATH.2018.08.016.
[413] R. Yang *et al.*, "MiR-206 suppresses the deterioration of intrahepatic cholangiocarcinoma and promotes sensitivity to chemotherapy by inhibiting interactions with stromal CAFs," *Int J Biol Sci*, vol. 18, no. 1, pp. 43–64, 2022, doi: 10.7150/IJBS.62602.
[414] M. Sha *et al.*, "Isolation of cancer-associated fibroblasts and its promotion to the progression of intrahepatic cholangiocarcinoma," *Cancer Med*, vol. 7, no. 9, pp. 4665–4677, Sep. 2018, doi: 10.1002/CAM4.1704.
[415] E. Milani, M. Strazzabosco, L. Fabris, and M. Cadamuro, "Molecular Pathogenesis: From Inflammation and Cholestasis to a Microenvironment-Driven Tumor," *Intrahepatic Cholangiocarcinoma*, pp. 167–182, 2019, doi: 10.1007/978-3-030-22258-1_12.
[416] H. El Mourabit, E. Loeuillard, S. Lemoinne, A. Cadoret, and C. Housset, "Culture Model of Rat Portal Myofibroblasts," *Front Physiol*, vol. 7, no. MAR, Mar. 2016, doi: 10.3389/FPHYS.2016.00120.
[417] V. M. Weaver, "The glycocalyx in tumor progression and metastasis," *The FASEB Journal*, vol. 36, no. S1, May 2022, doi: 10.1096/FASEBJ.2022.36.S1.0I189.
[418] C. Dou *et al.*, "P300 Acetyltransferase Mediates Stiffness-Induced Activation of Hepatic Stellate Cells Into Tumor-Promoting Myofibroblasts.," *Gastroenterology*, vol. 154 8, no. 8, pp. 2209–222114, Jun. 2018, doi: 10.1053/J.GASTRO.2018.02.015.
[419] Y. Li, I. Lua, S. W. French, and K. Asahina, "Role of TGF-β signaling in differentiation of mesothelial cells to vitamin A-poor hepatic stellate cells in liver fibrosis.," *Am J Physiol Gastrointest Liver Physiol*, vol. 310 4, no. 4, pp. 262–72, Feb. 2016, doi: 10.1152/AJPGI.00257.2015.
[420] P. Wang *et al.*, "Mutations in isocitrate dehydrogenase 1 and 2 occur frequently in intrahepatic cholangiocarcinomas and share hypermethylation targets with glioblastomas," *Oncogene*, vol. 32, no. 25, pp. 3091–3100, Jun. 2013, doi: 10.1038/onc.2012.315.
[421] H. Jiang, S. Hegde, and D. G. DeNardo, "Tumor-associated fibrosis as a regulator of tumor immunity and response to immunotherapy," *Cancer Immunology, Immunotherapy*, vol. 66, no. 8, pp. 1037–1048, Aug. 2017, doi: 10.1007/S00262-017-2003-1.
[422] D. R. Borger *et al.*, "Frequent mutation of isocitrate dehydrogenase (IDH)1 and IDH2 in cholangiocarcinoma identified through broad-based tumor genotyping.," *Oncologist*, vol. 17 1, no. 1, pp. 72–9, Jan. 2012, doi: 10.1634/THEONCOLOGIST.2011-0386.
[423] C. Kaltenmeier, H. O. Yazdani, K. Morder, D. A. Geller, R. L. Simmons, and S. Tohme, "Neutrophil Extracellular Traps Promote T Cell Exhaustion in the Tumor Microenvironment," *Front Immunol*, vol. 12, Nov. 2021, doi: 10.3389/FIMMU.2021.785222.
[424] Q. Fang, A. M. Stehr, E. Naschberger, J. Knopf, M. Herrmann, and M. Stürzl, "No NETs no TIME: Crosstalk between neutrophil extracellular traps and the tumor immune microenvironment," *Front Immunol*, vol. 13, Dec. 2022, doi: 10.3389/FIMMU.2022.1075260.
[425] U. Demkow, "Neutrophil Extracellular Traps (NETs) in Cancer Invasion, Evasion and Metastasis," *Cancers (Basel)*, vol. 13, no. 17, Sep. 2021, doi: 10.3390/CANCERS13174495.
[426] L. Cristinziano *et al.*, "Neutrophil Extracellular Traps in Cancer.," *Semin Cancer Biol*, vol. 79, pp. 91–104, Feb. 2022, doi: 10.1016/J.SEMCANCER.2021.07.011.
[427] J. Cools-Lartigue *et al.*, "Neutrophil extracellular traps sequester circulating tumor cells and promote metastasis.," *J Clin Invest*, vol. 123, no. 8, pp. 3446–3458, Aug. 2013, doi: 10.1172/JCI67484.

[428] M. Terabe *et al.*, "NKT cell–mediated repression of tumor immunosurveillance by IL-13 and the IL-4R–STAT6 pathway," *Nature Immunology 2000 1:6*, vol. 1, no. 6, pp. 515–520, 2000, doi: 10.1038/82771.

[429] Z. L. Hay, D. Kim, A. L. Silva, and J. E. Slansky, "The impact of the tumor microenvironment on granzyme production by CD8 T cells," *The Journal of Immunology*, vol. 204, no. 1_Supplement, pp. 242.24-242.24, May 2020, doi: 10.4049/JIMMUNOL.204.SUPP.242.24.

[430] M. K. Ruhland *et al.*, "Stromal senescence establishes an immunosuppressive microenvironment that drives tumorigenesis," *Nature Communications 2016 7:1*, vol. 7, no. 1, pp. 1–18, Jun. 2016, doi: 10.1038/ncomms11762.

[431] M. Pinzani, P. Gentilini, and E. A. Hanna, "Phenotypical modulation of liver fat-storing cells by retinoids. Influence on unstimulated and growth factor-induced cell proliferation.," *J Hepatol*, vol. 14 2–3, no. 2–3, pp. 211–20, 1992, doi: 10.1016/0168-8278(92)90160-Q.

[432] M. Sasaki *et al.*, "D-2-hydroxyglutarate produced by mutant IDH1 perturbs collagen maturation and basement membrane function.," *Genes Dev*, vol. 26 18, no. 18, pp. 2038–49, Sep. 2012, doi: 10.1101/GAD.198200.112.

[433] Y. Chen *et al.*, "Lysyl hydroxylase 2 is secreted by tumor cells and can modify collagen in the extracellular space," *Journal of Biological Chemistry*, vol. 291, no. 50, pp. 25799–25808, Dec. 2016, doi: 10.1074/jbc.M116.759803.

[434] Z. Zhang, W. Zhao, X. Yang, and H. Han, "Abstract 3902: Liver cancer stem cells initiate extracellular matrix remodeling," *Cancer Res*, vol. 74, no. 19_Supplement, pp. 3902–3902, Oct. 2014, doi: 10.1158/1538-7445.AM2014-3902.

[435] Y. Zhu *et al.*, "Interplay between Extracellular Matrix and Neutrophils in Diseases," *J Immunol Res*, vol. 2021, 2021, doi: 10.1155/2021/8243378.

[436] J. S. Graham, A. N. Vomund, C. L. Phillips, and M. Grandbois, "Structural changes in human type I collagen fibrils investigated by force spectroscopy.," *Exp Cell Res*, vol. 299 2, no. 2, pp. 335–342, Oct. 2004, doi: 10.1016/J.YEXCR.2004.05.022.

[437] M. Romero-López *et al.*, "Recapitulating the human tumor microenvironment: Colon tumor-derived extracellular matrix promotes angiogenesis and tumor cell growth.," *Biomaterials*, vol. 116, pp. 118–129, Feb. 2017, doi: 10.1016/J.BIOMATERIALS.2016.11.034.

[438] G. A. Meyer and R. L. Lieber, "Elucidation of extracellular matrix mechanics from muscle fibers and fiber bundles.," *J Biomech*, vol. 44 4, no. 4, pp. 771–773, Feb. 2011, doi: 10.1016/J.JBIOMECH.2010.10.044.

[439] X. J. Ma, S. Dahiya, E. Richardson, M. Erlander, and D. C. Sgroi, "Gene expression profiling of the tumor microenvironment during breast cancer progression," *Breast Cancer Research*, vol. 11, no. 1, pp. 1–18, Feb. 2009, doi: 10.1186/BCR2222/FIGURES/6.

[440] I. I. Verginadis *et al.*, "Abstract 3178: A stromal integrated stress response activates perivascular cancer-associated fibroblasts to drive angiogenesis and tumor progression," *Cancer Res*, vol. 82, no. 12_Supplement, pp. 3178–3178, Jun. 2022, doi: 10.1158/1538-7445.AM2022-3178.

[441] K. Shiga, M. Hara, T. Nagasaki, T. Sato, H. Takahashi, and H. Takeyama, "Cancer-Associated Fibroblasts: Their Characteristics and Their Roles in Tumor Growth," *Cancers (Basel)*, vol. 7, no. 4, pp. 2443–2458, Dec. 2015, doi: 10.3390/CANCERS7040902.

[442] M. Zhang *et al.*, "Single cell transcriptomic architecture and intercellular crosstalk of human intrahepatic cholangiocarcinoma.," *J Hepatol*, vol. 73, no. 5, pp. 1118–1130, Nov. 2020, doi: 10.1016/J.JHEP.2020.05.039.

[443] N. M. Amankulor *et al.*, "Mutant IDH1 regulates the tumor-associated immune system in gliomas," *Genes Dev*, vol. 31, no. 8, pp. 774–786, Apr. 2017, doi: 10.1101/GAD.294991.116.

[444] T. Cejalvo *et al.*, "Immune Profiling of Gliomas Reveals a Connection with IDH1/2 Mutations, Tau Function and the Vascular Phenotype," *Cancers (Basel)*, vol. 12, no. 11, pp. 1–18, Nov. 2020, doi: 10.3390/CANCERS12113230.

[445] M. Fauskanger, O. A. W. Haabeth, F. M. Skjeldal, B. Bogen, and A. A. Tveita, "Tumor Killing by CD4+ T Cells Is Mediated via Induction of Inducible Nitric Oxide Synthase-Dependent Macrophage Cytotoxicity," *Front Immunol*, vol. 9, no. JUL, Jul. 2018, doi: 10.3389/FIMMU.2018.01684.

[446] T. Accogli, M. Bruchard, and F. Végran, "Modulation of CD4 T Cell Response According to Tumor Cytokine Microenvironment," *Cancers (Basel)*, vol. 13, no. 3, pp. 1–21, Feb. 2021, doi: 10.3390/CANCERS13030373.

[447] D. Y. Oh *et al.*, "Intratumoral CD4+ T Cells Mediate Anti-tumor Cytotoxicity in Human Bladder Cancer," *Cell*, vol. 181, no. 7, pp. 1612–162513, Jun. 2020, doi: 10.1016/J.CELL.2020.05.017.

[448] T. Čaval, F. Alisson-Silva, and F. Schwarz, "Roles of glycosylation at the cancer cell surface: opportunities for large scale glycoproteomics," *Theranostics*, vol. 13, no. 8, p. 2605, 2023, doi: 10.7150/THNO.81760.

[449] S. Hakomori, “Glycosylation defining cancer malignancy: New wine in an old bottle,” *Proc Natl Acad Sci U S A*, vol. 99, no. 16, pp. 10231–10233, Aug. 2002, doi: 10.1073/PNAS.172380699.
[450] L. Oliveira-Ferrer, K. Legler, and K. Milde-Langosch, “Role of protein glycosylation in cancer metastasis.,” *Semin Cancer Biol*, vol. 44, pp. 141–152, Jun. 2017, doi: 10.1016/J.SEMCANCER.2017.03.002.
[451] K. B. Chandler, C. E. Costello, and N. Rahimi, “Glycosylation in the Tumor Microenvironment: Implications for Tumor Angiogenesis and Metastasis,” *Cells*, vol. 8, no. 6, Jun. 2019, doi: 10.3390/CELLS8060544.
[452] J. Gomes, S. Mereiter, A. Magalhães, and C. A. Reis, “Early GalNAc O-Glycosylation: Pushing the Tumor Boundaries.,” *Cancer Cell*, vol. 32 5, no. 5, pp. 544–545, Nov. 2017, doi: 10.1016/J.CCELL.2017.10.010.
[453] G. Kohanbash, S. Shrivastav, B. Ahn, Y. Hou, J. Costello, and H. Okada, “IDH mutation-induced suppression of type-1 anti-glioma immune response,” *J Immunother Cancer*, vol. 3, no. S2, pp. 271–271, Dec. 2015, doi: 10.1186/2051-1426-3-S2-P271.
[454] M. C. Martin Soberón *et al.*, “Study of tumor infiltrating immune CELLS and vasculature in human gliomas: Differences in IDH1/2 mutant versus IDH1/2WT tumors.,” *Journal of Clinical Oncology*, vol. 37, no. 15_suppl, pp. 2030–2030, May 2019, doi: 10.1200/JCO.2019.37.15_SUPPL.2030.
[455] L. Galluzzi and G. Kroemer, “Potent immunosuppressive effects of the oncometabolite R-2-hydroxyglutarate,” *Oncoimmunology*, vol. 7, no. 12, Dec. 2018, doi: 10.1080/2162402X.2018.1528815.
[456] L. Bunse *et al.*, “Suppression of antitumor T cell immunity by the oncometabolite (R)-2-hydroxyglutarate,” *Nat Med*, vol. 24, no. 8, pp. 1192–1203, Aug. 2018, doi: 10.1038/S41591-018-0095-6.
[457] L. G. Richardson *et al.*, “IDH-mutant gliomas harbor fewer regulatory T cells in humans and mice,” *Oncoimmunology*, vol. 9, no. 1, Jan. 2020, doi: 10.1080/2162402X.2020.1806662.
[458] F. Ren *et al.*, “The R132H mutation in IDH1 promotes the recruitment of NK cells through CX3CL1/CX3CR1 chemotaxis and is correlated with a better prognosis in gliomas,” *Immunol Cell Biol*, vol. 97, no. 5, pp. 457–469, May 2019, doi: 10.1111/IMCB.12225.
[459] Q. Wang *et al.*, “Tumor Evolution of Glioma-Intrinsic Gene Expression Subtypes Associates with Immunological Changes in the Microenvironment.,” *Cancer Cell*, vol. 32 1, no. 1, pp. 42–566, Jul. 2017, doi: 10.1016/J.CCELL.2017.06.003.
[460] L. G. Richardson, J. J. Miller, Y. Kitagawa, H. Wakimoto, B. D. Choi, and W. T. Curry, “Implications of IDH mutations on immunotherapeutic strategies for malignant glioma.,” *Neurosurg Focus*, vol. 52 2, no. 2, Feb. 2022, doi: 10.3171/2021.11.FOCUS21604.
[461] A. Pellerino and F. Franchino, “OS11.1 Temozolomide (TMZ) 1 week on/1 week off as initial treatment for high risk low grade oligodendroglial tumors: a phase II AINO (Italian Association for Neuro-Oncology) study,” *Neuro Oncol*, vol. 19, no. suppl_3, pp. iii21–iii21, Apr. 2017, doi: 10.1093/NEUONC/NOX036.072.
[462] A. Picca and G. Finocchiaro, “Deciphering diffuse glioma immune microenvironment as a key to improving immunotherapy results,” *Curr Opin Oncol*, vol. 34, no. 6, pp. 653–660, Nov. 2022, doi: 10.1097/CCO.0000000000000895.
[463] X. A. M. H. van Dierendonck, K. E. de Goede, and J. Van den Bossche, “IDH-Mutant Brain Tumors Hit the Achilles’ Heel of Macrophages with R-2-Hydroxyglutarate.,” *Trends Cancer*, vol. 7, no. 8, pp. 666–667, Aug. 2021, doi: 10.1016/J.TRECAN.2021.06.003.
[464] G. Bindea *et al.*, “Spatiotemporal dynamics of intratumoral immune cells reveal the immune landscape in human cancer.,” *Immunity*, vol. 39 4, no. 4, pp. 782–95, Oct. 2013, doi: 10.1016/J.IMMUNI.2013.10.003.
[465] L. Mu *et al.*, “The IDH1 Mutation-Induced Oncometabolite, 2-Hydroxyglutarate, May Affect DNA Methylation and Expression of PD-L1 in Gliomas,” *Front Mol Neurosci*, vol. 11, Mar. 2018, doi: 10.3389/FNMOL.2018.00082.
[466] J. Haas *et al.*, “Specific recruitment of regulatory T cells into the CSF in lymphomatous and carcinomatous meningitis.,” *Blood*, vol. 111 2, no. 2, pp. 761–6, Jan. 2008, doi: 10.1182/BLOOD-2007-08-104877.
[467] H. Lou *et al.*, “Frequency, Suppressive Capacity, Recruitment and Induction Mechanisms of Regulatory T Cells in Sinonasal Squamous Cell Carcinoma and Nasal Inverted Papilloma,” *PLoS One*, vol. 10, no. 5, May 2015, doi: 10.1371/JOURNAL.PONE.0126463.
[468] B. Ruf, B. Heinrich, and T. F. Greten, “Immunobiology and immunotherapy of HCC: spotlight on innate and innate-like immune cells,” *Cellular & Molecular Immunology 2020 18:1*, vol. 18, no. 1, pp. 112–127, Nov. 2020, doi: 10.1038/s41423-020-00572-w.
[469] S. Rizvi, J. Wang, and A. B. El-Khoueiry, “Liver Cancer Immunity,” *Hepatology*, vol. 73, no. S1, pp. 86–103, Jan. 2021, doi: 10.1002/HEP.31416.
[470] K. He *et al.*, “Novel Use of Low-Dose Radiotherapy to Modulate the Tumor Microenvironment of Liver Metastases,” *Front Immunol*, vol. 12, p. 812210, Dec. 2021, doi: 10.3389/FIMMU.2021.812210/BIBTEX.

[471] T. F. Greten, C. W. Lai, G. Li, and K. F. Staveley-O'Carroll, "Targeted and Immune-Based Therapies for Hepatocellular Carcinoma," *Gastroenterology*, vol. 156, no. 2, pp. 510–524, Jan. 2019, doi: 10.1053/J.GASTRO.2018.09.051.

[472] A. B. El-Khoueiry *et al.*, "Nivolumab in patients with advanced hepatocellular carcinoma (CheckMate 040): an open-label, non-comparative, phase 1/2 dose escalation and expansion trial," *Lancet*, vol. 389, no. 10088, pp. 2492–2502, Jun. 2017, doi: 10.1016/S0140-6736(17)31046-2.

[473] V. K. Gupta *et al.*, "Hypoxia-driven oncometabolite L-2HG maintains stemness-differentiation balance and facilitates immune evasion in pancreatic cancer," *Cancer Res*, vol. 81, no. 15, pp. 4001–4013, Aug. 2021, doi: 10.1158/0008-5472.CAN-20-2562/673673/AM/HYPOXIA-DRIVEN-ONCOMETABOLITE-L-2HG-MAINTAINS.

[474] G. Kohanbash *et al.*, "Isocitrate dehydrogenase mutations suppress STAT1 and CD8+ T cell accumulation in gliomas," *J Clin Invest*, vol. 127, no. 4, pp. 1425–1437, Apr. 2017, doi: 10.1172/JCI90644.

[475] Y. Zhu and L. N. Kwong, "IDH1 Inhibition Reawakens the Immune Response against Cholangiocarcinoma," *Cancer Discov*, vol. 12, no. 3, pp. 604–605, Mar. 2022, doi: 10.1158/2159-8290.CD-21-1643.

[476] M. D. Muzumdar *et al.*, "Survival of pancreatic cancer cells lacking KRAS function," *Nat Commun*, vol. 8, no. 1, Dec. 2017, doi: 10.1038/S41467-017-00942-5.

[477] K. Kawada, K. Toda, and Y. Sakai, "Targeting metabolic reprogramming in KRAS-driven cancers," *Int J Clin Oncol*, vol. 22, no. 4, pp. 651–659, Aug. 2017, doi: 10.1007/S10147-017-1156-4.

[478] A. J. Levine *et al.*, "The 1993 Walter Hubert Lecture: the role of the p53 tumour-suppressor gene in tumorigenesis.," *Br J Cancer*, vol. 69, no. 3, pp. 409–416, 1994, doi: 10.1038/BJC.1994.76.

[479] C. D. DiNardo *et al.*, " Durable Remissions with Ivosidenib in IDH1 -Mutated Relapsed or Refractory AML," *New England Journal of Medicine*, vol. 378, no. 25, pp. 2386–2398, Jun. 2018, doi: 10.1056/NEJMOA1716984/SUPPL_FILE/NEJMOA1716984_DISCLOSURES.PDF.

[480] W. Huang, N. Li, Y. Zhang, X. Wang, M. Yin, and Q. Y. Lei, "AHCYL1 senses SAH to inhibit autophagy through interaction with PIK3C3 in an MTORC1-independent manner," *Autophagy*, vol. 18, no. 2, pp. 309–319, 2022, doi: 10.1080/15548627.2021.1924038.

[481] L. Mainsiouw, M. E. Ryan, S. Hafizi, and J. C. Fleming, "The molecular and clinical role of Tensin 1/2/3 in cancer," *J Cell Mol Med*, vol. 27, no. 13, pp. 1763–1774, Jul. 2023, doi: 10.1111/JCMM.17714.

[482] I. W.-Y. Cheuk, M. T. Siu, J. C.-W. Ho, J. Chen, V. Y. Shin, and A. Kwong, "ITGAV targeting as a therapeutic approach for treatment of metastatic breast cancer," *Am J Cancer Res*, vol. 10, no. 1, p. 211, 2020.

[483] S. Wang, J. Xie, J. Li, F. Liu, X. Wu, and Z. Wang, "Cisplatin suppresses the growth and proliferation of breast and cervical cancer cell lines by inhibiting integrin β5-mediated glycolysis," *Am J Cancer Res*, vol. 6, no. 5, p. 1108, 2016.

[484] D. S. Chulpanova, K. V. Kitaeva, C. S. Rutland, A. A. Rizvanov, and V. V. Solovyeva, "Mouse Tumor Models for Advanced Cancer Immunotherapy," *Int J Mol Sci*, vol. 21, no. 11, pp. 1–15, Jun. 2020, doi: 10.3390/IJMS21114118.

[485] Y. Zhou *et al.*, "Experimental mouse models for translational human cancer research," *Front Immunol*, vol. 14, 2023, doi: 10.3389/FIMMU.2023.1095388/PDF.

[486] T. M. Errington, A. Denis, N. Perfito, E. Iorns, and B. A. Nosek, "Challenges for assessing replicability in preclinical cancer biology," *Elife*, vol. 10, Dec. 2021, doi: 10.7554/ELIFE.67995.

[487] X. Lu *et al.*, "YAP Accelerates Notch-Driven Cholangiocarcinogenesis via mTORC1 in Mice," *Am J Pathol*, vol. 191, no. 9, p. 1651, Sep. 2021, doi: 10.1016/J.AJPATH.2021.05.017.

[488] G. F. Hoyne, M. J. Dallman, B. R. Champion, and J. R. Lamb, "Notch signalling in the regulation of peripheral immunity," *Immunol Rev*, vol. 182, pp. 215–227, 2001, doi: 10.1034/J.1600-065X.2001.1820118.X.

[489] J. Lewis, "Notch signalling: A short cut to the nucleus," *Nature*, vol. 393, no. 6683, pp. 304–305, May 1998, doi: 10.1038/30597.

[490] D. A. Ross and T. Kadesch, "The Notch Intracellular Domain Can Function as a Coactivator for LEF-1," *Mol Cell Biol*, vol. 21, no. 22, pp. 7537–7544, Nov. 2001, doi: 10.1128/MCB.21.22.7537-7544.2001.

[491] B. Gil-García and V. Baladrón, "The complex role of NOTCH receptors and their ligands in the development of hepatoblastoma, cholangiocarcinoma and hepatocellular carcinoma," *Biol Cell*, vol. 108, no. 2, pp. 29–40, Feb. 2016, doi: 10.1111/BOC.201500029.

[492] A. Briot and M. L. Iruela-Arispe, "Blockade of specific NOTCH ligands: a new promising approach in cancer therapy.," *Cancer Discov*, vol. 5 2, no. 2, pp. 112–114, Feb. 2015, doi: 10.1158/2159-8290.CD-14-1501.

[493] S. X. Tan *et al.*, "Amplification and Demultiplexing in Insulin-regulated Akt Protein Kinase Pathway in Adipocytes*," *J Biol Chem*, vol. 287, no. 9, pp. 6128–6138, Feb. 2012, doi: 10.1074/JBC.M111.318238.

[494] A. Khwaja, "Apoptosis: Akt is more than just a Bad kinase," *Nature*, vol. 401, no. 6748, pp. 33–34, Sep. 1999, doi: 10.1038/43354.

[495] R. M. Adam *et al.*, “Cholesterol sensitivity of endogenous and myristoylated Akt.,” *Cancer Res*, vol. 67 13, no. 13, pp. 6238–6246, Jul. 2007, doi: 10.1158/0008-5472.CAN-07-0288.
[496] C. Liu *et al.*, “Suppression of YAP/TAZ-Notch1-NICD axis by bromodomain and extraterminal protein inhibition impairs liver regeneration,” *Theranostics*, vol. 9, no. 13, pp. 3840–3852, 2019, doi: 10.7150/THNO.33370.
[497] S. M. Jarrett *et al.*, “Extension of the Notch intracellular domain ankyrin repeat stack by NRARP promotes feedback inhibition of Notch signaling,” *Sci Signal*, vol. 12, no. 606, Nov. 2019, doi: 10.1126/SCISIGNAL.AAY2369.
[498] A. Takahashi *et al.*, “Incidence of intrahepatic biliary cysts in biliary atresia after hepatic portoenterostomy and associated histopathologic findings in the liver and porta hepatis at diagnosis.,” *J Pediatr Surg*, vol. 34 9, no. 9, pp. 1364–1368, 1999, doi: 10.1016/S0022-3468(99)90012-X.
[499] K. Okuda, Y. Kanda, Y. Fukuyama, H. Musha, and T. Sumikoshi, “Hepatic vascular anomalies in nonparasitic cysts of the liver.,” *Acta Hepatogastroenterol (Stuttg)*, vol. 23 2.
[500] E. Waanders *et al.*, “Cysts of PRKCSH mutated polycystic liver disease patients lack hepatocystin but express Sec63p,” *Histochem Cell Biol*, vol. 129, no. 3, pp. 301–310, 2008, doi: 10.1007/S00418-008-0381-3.
[501] S. Sekiya and A. Suzuki, “Intrahepatic cholangiocarcinoma can arise from Notch-mediated conversion of hepatocytes,” *J Clin Invest*, vol. 122, no. 11, pp. 3914–3918, Nov. 2012, doi: 10.1172/JCI63065.
[502] B. Rauff, A. Malik, Y. A. Bhatti, S. A. Chudhary, I. Qadri, and S. Rafiq, “Notch signalling pathway in development of cholangiocarcinoma,” vol. 12, no. 9, pp. 957–974, Sep. 2020, doi: 10.4251/WJGO.V12.I9.957.
[503] S. Gruttadauria *et al.*, “Liver transplantation for unresectable intrahepatic cholangiocarcinoma: The role of sequencing genetic profiling,” *Cancers (Basel)*, vol. 13, no. 23, p. 6049, Dec. 2021, doi: 10.3390/CANCERS13236049/S1.
[504] L. Che *et al.*, “Jagged 1 is a major Notch ligand along cholangiocarcinoma development in mice and humans,” *Oncogenesis 2016 5:12*, vol. 5, no. 12, pp. e274–e274, Dec. 2016, doi: 10.1038/oncsis.2016.73.

8. Acknowledgments

Embarking on this PhD journey at the DKFZ in Heidelberg has been one of the most transformative periods of my life. Reflecting on these years, I realize the profound impact of the support and camaraderie I've been fortunate to experience. This dissertation is not just a testament to my academic pursuit but a monument to the invaluable contributions of those who stood by me throughout this adventure.

Firstly, I extend my deepest gratitude to Prof. Dr. Darjus Felix Tschaharganeh, for not only welcoming me into your lab but also entrusting me with a project that both challenged and excited me. Your guidance has been a cornerstone of my professional development, and for that, I am eternally grateful.

To my collaborators, thank you for your invaluable contributions and for the spirit of teamwork that made our joint efforts not only successful but also enjoyable. Your expertise and insights have significantly enriched my research experience.

I must take a moment to express my wholehearted appreciation for every member of the AG Tschaharganeh team, both past and present. Your collective wisdom, encouragement, and kind, steadfast support have been nothing short of transformative for me. The camaraderie within our group hasn't just been motivational; it's been like the ultimate group hug— warm, comforting, and reliably present whenever I've stumbled, metaphorically (and occasionally, quite literally). Each of you has touched my heart in such profound ways, contributing to my growth with every shared experiment, every coffee break giggle, and even those moments when my 'brilliant' ideas weren't so... brilliant.

Additionally, the AG Tschaharganeh is of course not alone on our floor, and I'm equally thankful for the entire community on the 2nd floor of Pathology. Your collaboration, shared knowledge, and friendly faces have greatly enriched my daily work life. It's been a privilege to share this space with such a dynamic and supportive group of scientists and professionals.

To my beloved friends in Germany, who have become the family I chose (or perhaps who chose me despite my occasional tendency to be the human equivalent of a walking, talking bloopers reel). Your support has been the solid ground beneath my feet. Whether we met amid the nerve-wracking excitement of PhD selections, collaborated in the trenches of the PhD council or Helmholtz Juniors' activities, danced our hearts out or drowned our sorrows at DKFZ events, each memory shines brightly in my mind. Your friendship has been my lighthouse in the foggy chaos of PhD life. Your ability to turn even the most mundane days into adventures and to laugh with me (and at me, let's be real) has been a source of endless joy.

And then there's my support network back in Poland. Your constant encouragement and understanding have been a source of strength, reminding me that true friendship knows no borders. Your faith in my abilities has been a source of constant inspiration.

Moreover, I owe a heartfelt thank you to my friends around the world, beyond Poland and Germany. Your friendship has been a source of joy and support, lighting up my journey from afar. Despite the miles, our virtual chats and visits made me feel closer to home,

wherever I was. Your encouragement, laughter, and warmth across continents have been crucial. You've made the world feel smaller and infinitely warmer—thank you for being my global village.

As for my family—my bedrock and beacon—especially my mother and grandmother. It has been both an honor and a joy to follow in your academic footsteps. To my entire family, your unconditional love, unwavering belief in my dreams, and the values you've instilled in me have been the guiding compass through this PhD odyssey.

And to everyone who has been part of this journey, in any capacity: your support has been the cornerstone of my achievements. If I have inadvertently omitted anyone, I ask for your forgiveness, knowing that my gratitude extends to you as well.

This dissertation is not merely the culmination of my academic work; it is a tapestry woven from all the love, laughter, and wisdom you have all shared with me. From the depths of my grateful heart: thank you. Let us raise a glass to this journey we've shared and to the adventures that lie ahead.